Adsorption and Conformation Change of Short Helical Peptides on Silica and Aluminosilicate Surfaces

by
Michael J. Read
B.S., Mechanical Engineering
University of Colorado at Boulder, 1997

SUBMITTED TO THE DEPARTMENT OF MATERIALS SCIENCE AND ENGINEERING IN PARTIAL FULFILLMENT OF THE REQUIREMENTS FOR THE DEGREE OF

DOCTOR OF PHILOSOPHY IN MATERIALS SCIENCE AND ENGINEERING
AT THE
MASSACHUSETTS INSTITUTE OF TECHNOLOGY

February 19, 2002
[June 2002]

Signature of Author: Michael Read
Department of Materials Science and Engineering
February 19, 2002

Certified by:
Sandra L. Burkett
Assistant Professor of Chemistry
Amherst College
Thesis Supervisor

Certified by:
Anne M. Mayes
Professor of Polymer Physics
MacVicar Faculty Fellow
Thesis Supervisor

Accepted by:
Harry L. Tuller
Professor of Ceramics and Electronic Materials
Chair, Departmental Committee on Graduate Students

To my parents, David and Susan, with thanks

Acknowledgements

I would like to express my most sincere gratitude to my thesis coadvisors, Professors Sandra Burkett and Anne Mayes, who made this work possible. Over the last four years, since entrusting me with the germ of this project, Prof. Burkett has spent an incalculable amount of time answering questions, examining results, and posing detailed insights and questions of her own. I will always remember the importance she attaches to the logic and organization of scientific arguments, as well as clear communication. Prof. Mayes has welcomed me to her group, and on many occasions has taken the time to brainstorm with me over interesting results, and their theoretical meaning. The result for me has invariably been a better understanding of the data and its interpretation. Both coadvisors have provided indispensable support and advice on many occasions, ranging from practice sessions for my first conference presentation, to their detailed reading of the present document, and I owe my accomplishments during this time to them.

Within this document, it will be evident how much I owe to the work of Dr. Shuguang Zhang. He provided unflagging excitement and optimism for my work, as well as access to his ideas and his equipment, both of which influenced the course of this research in many ways. Professor Paul Laibinis has contributed time and insights over the entire course of this work, particularly to some of its most challenging aspects. I am very grateful for his thoughts and guidance. I hold the greatest respect and admiration for all four professors; each has contributed to this work in different but important ways.

I have been fortunate to share friendships with several great thinkers, some of whom I met during my years at MIT, and others from previous years. Richard Holman is a man of many talents; I will miss our near-daily coffee runs and conversations on all topics imaginable. His photographic skills resurrected the micrograph which appears on p. 155. Jim Yurko has been a source of good advice and perspective, and the reminder that there's always a party happening somewhere. It's been a long time since cramming for those first exams, but we made it! Yoritaka Sakakura, Michael Day and Mahesh Mahanthappa provided alternating support and harassment from the world outside MIT.

Claire Fujii has been a source of love and perspective, while enduring the seemingly interminable writing of this document. Thanks for believing that I would finish this, back when I was mumbling about starting to write it.

I have been privileged to be a member, or hanger-on, of multiple research groups at MIT. Sincerest thanks to Team Mayes group members, past and present. In particular, Stella Park provided in-depth conversations which had an enormous impact on large parts of this work. Thanks to members of the Cima group, who offered their resources without reservation. Malinda Tupper, Ryan Kershner, and Sherry Morrisette are exceptional in their energy, intelligence, and friendliness; best of luck to all of you. Others from MIT (in no particular order) include Doug Twisselmann, Steven Murray, Doug Matson, Catherine Bishop, Hartmut Rudmann, and Chris Henry. Thanks also to Monica Rixman, Julien Guiu, and the many other officemates who have been supportive and understanding during various periods of my time here; I appreciated you the most during stressful times, when I was at my most disagreeable.

All students at MIT are fortunate to have the support of people who help do the actual work; these people were especially important to me. Bernie Brown was always

willing to lend his time and expertise to me, and fixed the spectrometer multiple times during my time here. Jeff Simpson and Mark Wahl are responsible for a remarkable spectroscopy lab, in terms of both equipment and technical assistance. They would never put it this way, but they train the people later referred to as experts. Thanks to Anthony Garratt-Reed for help with microscopy. Lenny Rigione, Libby Shaw, and John Centorino provided training and analysis on a variety of important techniques. Barbara Layne and Cathy Bruce provided indispensable solutions to many problems. MIT was unfortunate to lose the services of Alison Park and Leila Ripley, who have moved on to bigger and better things, but in their time here they also provided great assistance.

Finally, I'd like to thank my parents, who believe implicitly in the value of education. My father was wisely circumspect when describing the process of getting a Ph.D., at least until I was already established here; the importance which he attaches to this achievement gives it new meaning. My mother sent endless care packages, messages, and prayers. To both of you, with love and thanks.

This work was supported by funding from the National Science Foundation under Grant No. DMR-9996338.

Adsorption and Conformation Change of Short Helical Peptides on Silica and Aluminosilicate Surfaces

by

Michael J. Read

Submitted to the Department of Materials Science and Engineering on February 19, 2002 in Partial Fulfillment of the Requirements for the Degree of Doctor of Philosophy in Materials Science and Engineering

Abstract

Motivated by the challenges in understanding important features of protein adsorption, the interactions between α-helical peptides and a carefully selected set of model surfaces were studied. The peptide sequences contained three blocks of two to five residues each, with the side chains of the N-terminal and C-terminal blocks having negative and positive charges, respectively, and the central block having uncharged side chains. The conformation of a variety of such peptides was studied in solution by circular dichroism (CD) and ^{1}H nuclear magnetic resonance (NMR) spectroscopy, in order to characterize the degree of α-helicity in solution, as a function of temperature, pH, and chemical denaturant (urea) concentration. Intramolecular electrostatic interactions arising from the charged side chains, together with the central block of α-helix-forming alanine residues, were found to stabilize α-helicity. These interactions were balanced by the natural tendency toward disordered structures, which resulted in fractional α-helicities between 25% and 50% when in solution.

Adsorption isotherms for the peptide Ac-DDDDAAYAARRRR-Am on amorphous colloidal silica nanoparticles were studied in detail. A greater amount of peptide was adsorbed at basic pH than at neutral pH. The was fit with Langmuir and Frumkin isotherms, and the free energy, enthalpy, and entropy of adsorption were calculated. The enthalpy of adsorption at pH 9 (-17 kJ mol^{-1}) was consistent with calculations of the electrostatic interaction between the screened silica surface charge and the dipolar charge distribution on the peptide arising from the charged side chains. The entropy of adsorption at pH 9 (15 J mol^{-1} K^{-1}) arose in part from conformational changes which were observed in the CD and NMR spectra of adsorbed molecules. Solution ^{1}H NMR spectra of peptide adsorbed to colloidal silica resolved resonances from aspartate and alanine, but not from arginine; this was shown to arise from selective immobilization of positively-charged arginine side chains due to electrostatic interactions with the negatively-charged silica, which resulted in a specific orientation of the peptide on the surface. Conformationally-sensitive resonances from aspartate and alanine residues displayed peak shifts characteristic of reduced α-helicity. The CD spectra of adsorbed peptides also indicated a decrease in α-helicity. Taken together, these measurements supported the view that loss of α-helicity of adsorbed molecules propagates

from the arginine terminus, which is directly adjacent to the surface, into the alanine and arginine segments, which extend into solution.

Because conformational changes have important implications for the functionality of adsorbed molecules, the extent of α-helicity loss was measured quantitatively as a function of temperature and pH for the peptide Ac-DDDDAAAARRRRR-Am. At neutral pH, the α-helicity of adsorbed peptides decreased with increasing temperature, much like the behavior observed for peptides in solution. In contrast, at basic pH, the α-helicity of adsorbed peptides increased with increasing temperature. These results were interpreted using a statistical model based on modifications to existing theories of the helix–coil transition to include residue-specific electrostatic interactions between the surface and charged peptide side chains. At basic pH these interactions are stronger, and their temperature dependence dominates, resulting in a net increase in α-helicity. Adsorption to charged oxide surfaces thus results in a new conformation dictated by the electrostatic forces exerted on the adsorbed molecule, and which contains decreased levels of α-helicity in favor of a more coiled structure. Functionality of the adsorbed peptide Ac-AAAAAAAARRRR-Am in a proteolysis reaction, catalyzed by the enzyme thermolysin, was also investigated. The observed shift in the distribution of proteolysis sites toward the N-terminus of adsorbed molecules was interpreted in terms of the above adsorption mechanism.

Surface morphology, nanoscale topology, and chemical composition were varied systematically through hydrothermal synthesis of microporous crystalline silicates and aluminosilicates (zeolites), which allowed the effects of these characteristics on peptide adsorption to be investigated. Among the siliceous substrates studied, the crystalline form (sodalite) adsorbed more peptide than the amorphous colloidal silica. The adsorbed amount was modulated by the introduction of tetrahedral aluminum sites into the framework, increasing at low aluminum concentrations (Si/Al = 20) but decreasing at higher concentrations (Si/Al = 5). Changes in surface composition and nanoscale topology influenced the pH dependence of adsorption as well, with stronger adsorption observed on colloidal faujasite at neutral pH relative to basic pH.

Adsorption of short α-helical peptides to model oxide surfaces thus represents a powerful model system for study of questions pertinent to protein adsorption and surface engineering, such as the mechanism of conformational changes in adsorbed molecules, and the dependence of the adsorption process on surface characteristics. Future progress in these fields will require development of a predictive theory, using detailed information supplied by model systems such as the one considered here.

Thesis Supervisor: Sandra L. Burkett
Title: Assistant Professor of Chemistry, Amherst College

Thesis Supervisor: Anne M. Mayes
Title: Professor of Polymer Physics
MacVicar Faculty Fellow

Contents

Figures

Tables

Chapter I. Introduction

1. Introduction and Outline

Surface properties are among the most important features of biomaterials. Materials used to repair the human body are increasingly selected based on interactions with a wide range of biological components including blood, cells, and extracellular matrix. Processes that affect the course of the repair depend on properties of both the material and the biological system. For example, certain plastics have long been rejected for blood-contacting applications because of the presence of surface groups associated with complement activation [1], but the mechanism is only partly understood. Coatings of nonspecifically-adsorbed adhesion proteins as well as grafted bioactive peptides modulate cell adhesion and migration in a systematic way by binding cell-surface receptors; optimization of these interactions leads to control over cell adhesion and migration processes [2]. Biomineralization is controlled by proteins that direct nucleation and growth of a variety of nanocrystalline materials, including calcite, hydroxyapatite, or amorphous silica, and an understanding of this process is desired for novel materials synthesis strategies [3,4]. Biosurface engineering, or the creation and characterization of material surfaces that interact with biological systems to produce desired biological responses, is a primary goal of biomaterials research.

In each of the examples above, functional groups present on the material surface exert forces on the surrounding biological system by forming noncovalent interactions with incipient proteins. Proteins play an enormous variety of roles in the body, acting as the structural backbone of cells and extracellular matrix, as informational signals relayed between cells or across cell walls, and as chemical regulators that catalyze a wide variety of reactions. Protein molecules have surfaces with precisely-defined arrangements of chemical groups that allow them to participate in complex biological processes through molecular recognition. The variety of surface topologies which proteins may form ensures that nearly any surface will adsorb some proteins spontaneously. Because a large number of different proteins are present in blood in varying amounts, they are among the first molecules to contact implanted materials [5,6]. Surface functional groups and their arrangement in the nanoscale topology of the material surface have dramatic effects on amount, orientation, and conformation of

adsorbed proteins. For these reasons, adsorption and conformational change of proteins on biomaterial surfaces are widely considered to be one of the most important mechanisms controlling interactions between biomaterials and the surrounding biological system. Since surface functional groups and nanoscale topology can increasingly be controlled due to advances in self-assembly and nanotechnology, biosurface engineering is expected to dramatically improve biomaterial performance.

This promise has not yet been fulfilled, in part because of the difficulty of predicting how specific surface properties affect protein adsorption and conformational change. Beyond the most basic principles, the physical chemistry governing protein adsorption to solid surfaces is not well understood. Research into protein adsorption, in general, has focused on surfaces with disparate properties and on biomolecules too complex to be characterized effectively on surfaces. While many material surfaces have been studied for their biological properties, the constant creation of new surfaces and the variety of environments in which biomaterials are expected to perform make detailed predictive information on the type, orientation, and conformation of adsorbed proteins a necessity. In Section I.2, selected areas of the literature on protein adsorption are reviewed in order to illustrate what types of information about adsorbed proteins can be obtained using current experimental techniques, how the properties of the adsorbed protein layer affect the interactions between biomaterials and the surrounding biological system, and how these interactions are currently being applied in bioengineering.

Chapters II through V of this work address the need for predictive understanding of protein adsorption, starting with a model system carefully formulated to allow detailed characterization of adsorbates and substrates, yet retaining basic features relevant to protein adsorption. In Chapter II, a class of short peptides is introduced for use as adsorbates, and characterized in solution using a variety of spectroscopic techniques. These molecules have significant α-helicity when in aqueous solution and a dipolar distribution of charge within the molecule. Thorough characterization of adsorbate properties relevant to adsorption is carried out to provide as much information as possible for use in interpreting the behavior of these molecules on the surface.

In Chapter III, these molecules are adsorbed to amorphous colloidal silica particles, a system chosen for its relative simplicity [7], as well as for the availability of other closely-

related model surfaces, as described below. The amount, orientation, and conformation of adsorbed molecules are studied using spectroscopic techniques, and these properties are linked to specific properties of the material surface. Thermodynamic parameters of adsorption are measured experimentally and used, in combination with knowledge of molecular structure in solution, to formulate a model of adsorption. The combination of well-characterized adsorbate and substrates is shown to lead to a powerful model system for studying questions related to protein adsorption.

In Chapter IV, the model system of short α-helical peptides on colloidal silica is used to answer questions about the retention of functionality by adsorbed molecules. The molecular structure on the surface is studied as a function of adsorption conditions and surface properties. Finally, the ability of adsorbed molecules to participate in a model biological reaction is studied, and the influence of adsorption on this reaction is evaluated. Such studies provide the basis for moving beyond quantitative characterization of protein adsorption processes toward a study of functionality of molecules at interfaces.

In Chapter V, the complexity of the system is increased in a systematic way, in order to explore the effect of surface chemistry and structure on adsorbed molecules. Zeolites, or microporous aluminosilicates, are synthesized to provide varying compositions within the same crystal structure, or different crystal structures with similar compositions, depending on synthesis parameters which are readily controlled. This has been previously shown to provide control over model protein adsorption [8]. Information from the model system is used to study the effects of surface chemistry and topology on adsorbed molecules independently, and to explore the possibilities of introducing novel surface chemical properties in a controlled manner.

2. Current Understanding of Protein and Peptide Adsorption

Protein and Peptide Structure and Properties

Proteins and peptides are unbranched heteropolymers of α-L-amino acids differentiated by side chains at the α-carbon [9]. With the exception of proline (not studied

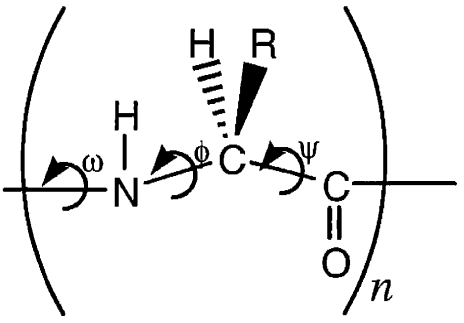

Figure I-1. Monomer unit (residue) of a peptide chain.

here), the monomer unit, or residue, has the form shown in Figure I-1. These biopolymers are structured on several different levels. The primary structure is a sequential listing of residue types along the backbone, by convention running from N-terminus to C-terminus. The peptides used in the present work are composed primarily of only four of the twenty different amino acid types common in nature. Hereafter, primary structure is assumed to be either known from existing literature or intentionally specified during synthesis.

Each residue of a peptide chain has two variable dihedral angles, ϕ and ψ, in addition to the fixed peptide bond angle ω. Secondary structures are repeating patterns of backbone conformations such as α-helix and β-sheet, usually containing four to twenty residues. Ubiquitous within proteins in solution, these secondary structures act as building blocks for the formation of the dense, highly-specific tertiary structure which excludes solvent and is ordered over the entire molecule.[1] The spontaneous process by which an unfolded peptide chain reaches this native conformation is not completely understood, and is known as the "protein folding problem."

Folded proteins in aqueous solution sequester hydrophobic side chains in the core, where they are protected from the solvent by a shell of hydrophilic side chains [10-12]. Dehydration of hydrophobic side chains provides the primary driving force to counteract the large barrier to folding which arises from the much lower conformational entropy of the folded state. Additional stabilization is provided by favorable electrostatic contacts that arise from regular secondary structures as well as from specific interactions among side chain and backbone chemical groups. Thus, most common tertiary structures arise from a large number of cooperative interactions and resist unfolding ("denaturation") even when individual

[1] Post-translational modification and folding chaperones are beyond the scope of this work.

residues are substituted, though such point mutations may dramatically change the thermodynamic stability of a particular fold. The formation of quaternary structures, by self-assembly of proteins into ordered macromolecular structures, relies on the heirarchical organization of these molecules.

Many variations in the primary structure of proteins, for example those encountered in analogous molecules from different species, have little effect on the secondary, tertiary, and quaternary structures of these molecules [9]. In contrast, small variations in primary structure strongly affect the local predisposition toward secondary structure in smaller peptides. α-Helix [13], β-sheet [14], and a variety of turns [15] have been reported for short peptides. These are consistently found to depend strongly on the primary structure. For example, in model α-helical peptides, favorable intramolecular electrostatic interactions arising from charged side chains are frequently used to stabilize α-helicity [16]. In contrast, polypeptides lacking such specific interactions follow the entropic bias toward a "random coil" conformation,[2] in which the average dihedral angles follow local torsional energetics, independent of surrounding residues [17].

Characterization and Modeling of Adsorbed Proteins and Peptides

A vast body of literature exists on the adsorption of proteins to surfaces [18-23]. Many methods have been used to characterize the important general features of the adsorption process, primarily: kinetics of diffusion, adsorption, and conformation change in which important processes occur on timescales ranging from seconds to days; the type and amount of adsorbed protein and the reversibility of adsorption; orientation of molecules on the surface; alteration of tertiary, secondary, and occasionally primary structure of proteins on the surface; and the distribution of these properties within the adsorbed layer. Experimental relations between such physicochemical features of adsorption and the bioactivity and functionality of the protein on the surface are an important component of such studies. These methods and the results they have provided are surveyed in this section. Since the remainder

[2] In this work, the terms "random coil" and "coil" will both be used to denote coiled structures. The latter term will be used for structures which are non-ordered, but do not necessarily satisfy the condition for "random coil" structures defined above.

of this work focuses on adsorbed peptides, particular attention is paid to such studies where possible. However, despite the importance of peptides in studies of protein folding, few studies have been made of the conformational behavior of peptides at interfaces.

Protein adsorption studies naturally benefit greatly from the enormous amount of conformational information available for proteins in solution. However, in general, the powerful spectroscopic techniques which provide such information not only lack surface-sensitive analogues, but are inapplicable to adsorbed molecules except in very special circumstances. This is the primary reason why the understanding of the structures of adsorbed proteins lags behind that of proteins in solution. The low number of surface sites relative to bulk material requires sensitive methods or maximization of surface area through minimization of particle size. Solid–liquid interfaces interfere with many experimental techniques and preclude the use of high-vacuum spectroscopic techniques. Crystallography, historically the most powerful technique for examining protein structure, is not applicable to adsorbed layers, which lack the necessary long-range order.

Adsorption isotherms are used to quantify the adsorbed amount as a function of solution concentration and can be measured precisely through ellipsometry [24], UV absorption [25], radiolabeling methods [26], and molecular recognition by immobilized antibodies (ELISA) [27]. Typically, the adsorbed amount approaches its terminal value within minutes or sometimes seconds, but smaller changes continue to occur over a period of several hours. Historically, isotherms have provided some of the first indications of the complexity of protein adsorption [28]: irreversibility upon dilution, plateaus and other features not captured by simple models, and strong dependence on experimental conditions. Such characteristics are generally attributed to adsorption-induced changes in the intramolecular and intermolecular interactions in the surface layer. In some cases, the shape of the isotherm reveals the number of cooperative contacts made with the surface [29]. Systematic variations in surface properties (for example, gradients in surface energy on functionalized polymer surfaces [30,31]), typically link surface hydrophobicity to larger adsorbed amounts of many model proteins. Interestingly, however, the hydrophilic end of one such "wettability gradient" surface adsorbed somewhat more protein from a plasma solution (containing more than 200 different proteins) than the hydrophobic end, with dramatic consequences for the number and appearance of adsorbed platelet cells [32].

Systematic variations of surface and protein charge demonstrate the importance of favorable electrostatic interactions [33]. Increases in the equilibration time and temperature generally lead to greater adsorbed amounts and irreversibility of adsorption, while increasing ionic strength [34] and increasing surfactant concentration [35,36] typically decrease adsorption.

Circular dichroism (CD) spectroscopy is the primary method for measuring secondary structures of proteins in solution. Distinct spectral features have been assigned to α-helical and β-strand structures [37], and the secondary structures of adsorbed molecules can be monitored either in transparent colloidal suspensions or in stacks of transparent plates [38]. Adsorption-induced changes in secondary structure can be quantified for general model proteins [39], for a variety of point mutations within the same model protein [40], and as a function of colloid material [41]. In general, the degree of α-helical secondary structure in proteins decreases upon adsorption to silica surfaces; this represents the most direct experimental link between adsorption and conformation change. Certain proteins demonstrate permanent structural alterations upon adsorption and desorption from surfaces [42]. The degree of conformational change depends on the stability of adsorbing proteins, the relative importance of electrostatic and hydrophobic interactions in stabilizing the protein structure, and properties of the nanoparticle surface. Interestingly, the degree of α-helical secondary structure detected by CD increases upon adsorption to fluorocarbon surfaces [43,44]. However, CD is not surface-selective, and in the absence of additional information, this technique cannot be used to assign α-helicity losses to specific α-helical regions of the protein.

Nuclear magnetic resonance (NMR) spectroscopy is the only experimental method to provide detailed, site-specific information on the conformations of proteins in their native state (i.e., aqueous solutions). It has been successfully applied to adsorbed molecules on a much more limited basis using solid-state methods [45]. Peptide fragments of statherin have been studied on hydroxyapatite in order to elucidate the mechanism of specific binding [46,47]. For these and other conformational studies on surfaces, special equipment and expensive isotopic labeling is required. In addition, although ^{1}H nuclei are central to NMR of proteins in solution, these nuclei are not useful for studying adsorbed molecules because the separation of chemical shifts is relatively small compared to typical peak widths in the solid state, and because many of the well-known pulse sequences cannot be applied.

Use of these well-developed techniques has been confined to special circumstances where information on the adsorbed state could be "stored" in the protein through H/D exchange methods, then retrieved during analysis of molecules in solution after desorption from the surface by ion-exchange [48].

Total internal reflectance (TIR) spectroscopic techniques, in which a solid substrate is used as a waveguide, have been widely applied to study conformations of adsorbed proteins as well as the distribution of orientations present in molecules comprising the adsorbed layer. Surface selectivity is provided by the exponential decay of the radiation at the surface of the waveguide, which samples only the region within a few micrometers of the surface. Orientational information is provided by differential absorption of polarized light in reflection absorbance spectroscopy (RAS). The chemical groups probed by optical and near-UV absorption and fluorescence of proteins are limited for the most part to heme groups and to three amino acid types (phenylalanine, tyrosine, and tryptophan), making these spectroscopic techniques useful probes of orientation as well as the local conformation of certain areas of the molecule. For example, total internal reflection fluorescence (TIRF) was used to show that lysozyme adsorbs in specific and coverage-dependent orientations on silica [49]. Non-random and surface-dependent molecular orientation of heme-containing proteins was observed on a coated optical waveguide [50].

In contrast to optical and near-UV techniques, infrared spectroscopy is sensitive to secondary structure and bonding [51,52], although only a few materials are suitable for use as wave guides. For example, relatively small time-dependent changes in the conformationally-sensitive amide I vibrational band on a one-day timescale were found in ribonuclease A adsorbed to germanium [53]. These changes were associated with a decrease in elutability from the surface. A wider variety of surfaces may be studied by coating thin films onto the wave guide. Fibrinogen adsorbed to polyurethanes was examined by this technique [54]. Self-assembled monolayers of α-helical peptides were studied using FTIR-RAS at gold interfaces [55]. Adsorption of oligo-lysine (n = 2-5) and poly-lysine (n = 169) was reported to depend on the electrostatic attraction of these molecules to a negatively-charged titania substrate, and changes were observed in the coordination of backbone carbonyl groups with surface groups [56]. However, FTIR peaks of proteins often cannot be assigned to specific

regions of the molecule; conformationally-sensitive peaks tend to be broad; and the strong absorption bands of water severely hinder peak measurement in some regions [57].

Scanning probe microscopy (SPM), in conjunction with molecular modeling [58], has recently become a powerful tool for exploring the forced unfolding of specific protein structures in individual molecules [59]. This technique is often applied in conjunction with recent advances in chemical functionalization and patterning of surfaces in order to examine adsorption processes on well-defined surfaces [60,61]. Forced unraveling of poly-lysine helices on gold surfaces has been studied by atomic force microscopy (AFM) [62]. In addition, arrays of lysozyme observed by scanning tunneling microscopy (STM) [63] appeared to have both spatial periodicity and orientational specificity.

Given the available experimental information for adsorbed proteins, only a basic picture of the adsorption process can be formulated. Protein adsorption to surfaces, like protein folding in solution, is driven by electrostatic and hydrophobic interactions. Adsorbing proteins reoptimize their conformations according to the array of chemical groups presented by the surface. These principles lead to a basic distinction between protein adsorption on hydrophobic surfaces, which is thought to be driven by reduction of hydrophobic surface area through exposure of hydrophobic side chains to the surface, and on hydrophilic surfaces, which is thought to result from the overlap of electrostatic fields surrounding the surface and protein, as well as from specific electrostatic interactions between surface and protein functional groups. Because hydrophobic side chains are sequestered in the protein core in aqueous solution, protein adsorption to hydrophobic surfaces is generally thought to be associated with a greater extent of structural change and irreversibility than adsorption to hydrophilic surfaces. The specificity of the adsorbed conformation is not well understood; although ordered adsorption has been observed for certain systems [63], the presence of such order is likely to depend strongly on the degree of reversibility of the adsorption process.

The above is not a sufficiently detailed picture to allow practical predictive modeling of protein adsorption processes. The available techniques do not constitute a sufficient set of methods for characterizing the properties of adsorbed proteins. Few studies provide information on the specificity of adsorption and on the number of adsorption mechanisms acting. Fewer still provide any site-specific conformational information, and those that do are for very specific model systems. Thus, in contrast to the protein folding problem in solution,

there does not exist a set of experimental data for protein adsorption against which a predictive theory can be formulated and tested. A new approach is needed to provide quantitative information on the basic processes that drive adsorption and conformation change.

Technological Significance of Adsorbed Proteins

Proteins play central roles as the functional elements in any natural or biologically-inspired application. When proteins are immobilized at interfaces in active devices, the conformation and orientation of small parts of the molecule may greatly influence the performance of the device, but these properties depend on the physical chemistry of the adsorption and immobilization process in a complex way. Different applications present unique challenges in controlling this process. For example, biosensors and devices based on functional proteins require economically-practical methods to immobilize enzymes while retaining their bioactivity in the non-native environment. In contrast, surfaces used in tissue engineering to control cell adhesion, differentiation, spreading, and signaling must be fabricated economically with an optimal concentration and distribution of ligand groups. A description of some selected technical applications of adsorbed proteins follows, to illustrate the impact that could be made by advances in this field.

Chemical sensors transduce chemical concentrations in solution into electronic signals. Properties of certain functional proteins can be exploited for biosensing, such as the ability to catalyze electron-transfer reactions dependent on the presence of peroxides (or a variety of substrates specifically recognized by oxidases) [64]. Specific and reversible conformational changes can signal the binding of maltose or other analyte species [65]. Redox enzymes form the anode and cathode of a device recently demonstrated to run on energy collected from nutrients in blood [66], providing a way to power miniaturized implant devices. Enzymes and antibodies are also immobilized on surfaces [67] for use in chromatographic [68], catalytic [69], and immunological [70] applications, often in conjunction with recent advances in surface patterning and functionalization techniques [71]. Control over the conformation and orientation of immobilized proteins is provided by residue-

specific grafting chemistry, but this does not always lead to the expected increase in bioactivity relative to nonspecifically-adsorbed proteins [72,73]. The ability to control the orientation and conformation of immobilized patterned proteins will form the basis for future biosensors used in manufacturing processes, diagnostics, and security applications.

Adsorbed plasma proteins have been shown to modulate platelet cell adhesion in a surface-dependent fashion. Plasma proteins increased the number of cells adsorbed to a hydrophobic surface, but decreased the number adsorbed to a hydrophilic surface [32]. The time dependence of the amount and type of adsorbed plasma has been explained as a function of different kinetic timescales for transport and adhesion of different proteins to the surface, but little is known about the conformations of proteins, which may influence bioactivity. Short peptides such as the well-known RGD cell-adhesion sequence are used as surface signals on scaffolds to direct cell adhesion, tissue regeneration and wound healing responses. Though these processes are often remarkably independent of RGD conformation, differences in surface fabrication technique can lead to large differences in the amount and activity of immobilized proteins and peptides [61].

Future progress in these and other advanced areas such as biomimetics will depend on the ability to order molecules such as proteins at many different types of interfaces while retaining functionality. Advances in understanding the general driving forces of protein adsorption and conformation change, and their use in modeling specific processes, will greatly increase the practicality of developing and manufacturing such devices. Such understanding must be obtained from simplified systems which combine effective characterization through a variety of experimental techniques with systematic variations to demonstrate the effects of adsorbate and substrate parameters. The purpose of this work is to contribute to this understanding by examining a model system.

Chapter II. Characterization of DAR-Type Peptides in Solution

1. Introduction

Purpose of Solution Characterization

DAR-type peptides are so-named because their sequence consists of contiguous blocks of aspartate (D), alanine (A), and arginine (R) residues. Specific peptides are abbreviated *n*DAR*m*, with *n* equal to the number of D and R residues and *m* equal to the number of A residues. All peptides have N-terminal acetyl (Ac) and C-terminal amide (Am) caps unless otherwise noted; thus the sequence Ac-DDDDAAAAARRRR-Am is abbreviated 4DAR5, and the sequence Ac-DDDDDAAAARRRRR-Am is abbreviated 5DAR4. Related peptides are abbreviated based on descriptive modifications to these formulas. Important properties of the amino acids used in this work are listed in Table II-I, and the peptides studied in detail are listed in Table II-II.

Knowledge of the structures of these molecules in solution is essential to a study of the conformational changes occurring upon adsorption. Powerful chemical and spectroscopic techniques are available for characterizing conformation in solution at a variety of levels, making this task much easier than for the adsorbed structure. Because of the novel nature of the peptides in this study, characterization serves two purposes: to contribute to the knowledge of the structures of short α-helical peptides in solution, and to allow a more detailed comparison between molecular structures in the solution and adsorbed states than has previously been possible for biomolecules. In the remainder of this introductory section, the general features of peptide α-helix formation and its measurement by CD spectroscopy are discussed. Sections II.2 and II.3 describe CD spectroscopic characterization of a variety of DAR-type peptides, providing insights into the basis for their solution structures. Section II.4 extends this characterization using a variety of site-specific conformational measures from 1D and 2D ^{1}H NMR spectroscopy of peptides in solution.

Table II-I. Properties of selected amino acids.

Residue	*Abbrev.*	*Side chain*$^{(charge)}$	*Side chain* pK_a *[9]*
Alanine	A	$-CH_3$	n/a
Arginine	R	$-CH_2-CH_2-CH_2-NH-C(NH_2)_2^+$	12
Aspartate	D	$-CH_2-COO^-$	4
Tyrosine	Y	$-CH_2-C_6H_4-OH$	10

Table II-II. Solution properties of DAR-type α-helical peptides. *Values of $-[\theta]_{222}$ are given in units of deg cm^2 dmol^{-1}. †The value of $-[\theta]_{222}$ at 25 °C is taken to be the measure of the α-helicity of the peptide. ‡Temperature at which $-[\theta]_{222}$ declines to 50% of the value it has at 4 °C. Fractional α-helicities are calculated using Equation (II-2).

Name	*MW*	*Sequence*	$-[\theta]_{222}$* *(25 °C)*†	$-[\theta]_{222}$* *(90 °C)*	$-[\theta]_{222}$* *6 M urea (25 °C)*	$T_{50\%}$‡ *(°C)*
2DAR8	1170	Ac D_2 A_8 R_2 Am	13,200	5,500	7,300	49
3DAR6	1299	Ac D_3 A_6 R_3 Am	12,200	5,900	7,500	59
4DAR2	1286	Ac D_4 A_2 R_4 Am	8,700	5,600	5,000	> 90
4DAR3	1357	Ac D_4 A_3 R_4 Am	11,100	6,200	4,400	77
4DAR5	1500	Ac D_4 A_5 R_4 Am	16,500	8,200	9,900	64
4DAYAR5	1592	Ac D_4 A_2 Y A_2 R_4 Am	7,300	6,000	3,400	> 90
5DAR4	1700	Ac D_5 A_4 R_5 Am	9,800	5,000	5,600	60
4AAR4	1252	Ac A_8 R_4 Am	10,600	3,700	2,500	37
4DAK3	1245	Ac D_4 A_3 K_4 Am	6,200	3,100	2,600	57
4EAR3	1413	Ac E_4 A_3 R_4 Am	11,700	8,600	5,600	> 90
4EAK3	1301	Ac E_4 A_3 K_4 Am	7,600	5,100	1,200	54
4^+DAR4	1585	Ac D_4 A_4 R_5 Am	9,000	4,500	n/m	53

Definition of α-Helicity and the Helix-Coil Transition

The backbone dihedral angles (ϕ and ψ) of any given residue may occupy a variety of different conformations, dictated by the steric restrictions imposed by the side chain and neighboring residues. About one third of these fall within the range of α-helicity, shown by the oval in Figure II-1. This region represents the set of conformations which are observed for residues residing in α-helical secondary structures in proteins. Pauling's idealized α-helix

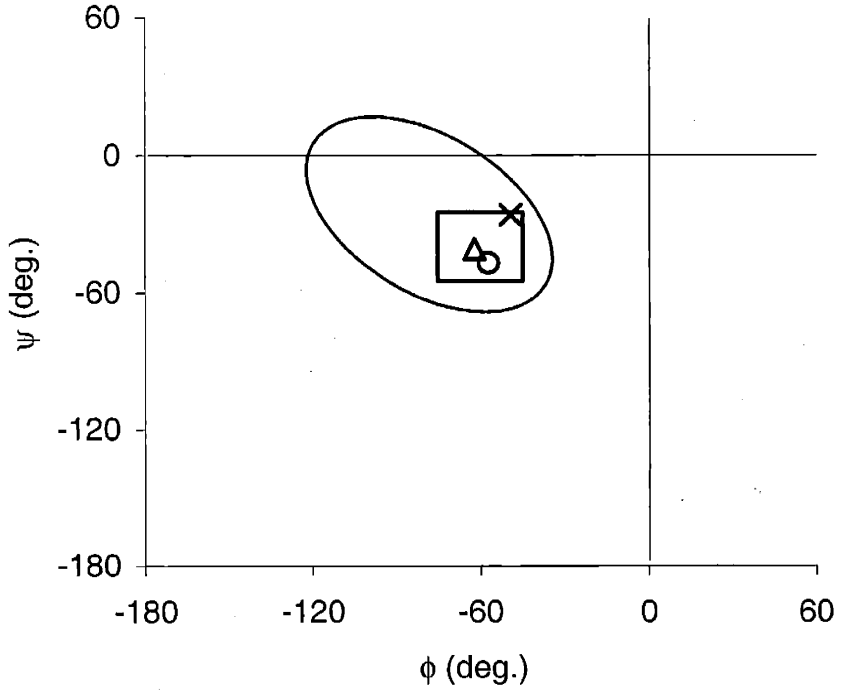

Figure II-1. Map of residue conformations observed in regular protein secondary structures. Oval: conformers commonly observed in proteins [74]. (○) Classical α-helix [75] ($\phi = -57°$, $\psi = -47°$); (△) Native protein α-helix [9] ($\phi = -62°$, $\psi = -41°$); (box) Standard region of α-helicity [76] ($\phi = -60° \pm 15°$, $\psi = -40° \pm 15°$); (×) 3_{10} helix [9] ($\phi = -49°$, $\psi = -26°$).

is shown as a single point on this figure. This set of α-helical conformations will form the basis for the definition of α-helicity in this study. Other important types of ordered secondary structures are also shown on this diagram. The 3_{10} helix, a more tightly-wound conformation, will be discussed in detail later; it is most often observed in very short segments at the end of α-helices, or in peptides containing C^{α}-tetrasubstituted residues.

CD signals measure the differential absorption of electronic transitions with respect to left- and right-circularly polarized light, which arise as a result of the chirality of the L-amino acids comprising the chain. Each α-carbon in a peptide chain (with the exception of glycine) is chiral; this results in an asymmetry in the environment of the peptide bonds within the chain. The ordered secondary structures, such as α-helix and β-strand, impose qualitatively different asymmetries on the environment of the peptide bond chromophores, giving rise to distinct CD spectra. The α-helix, for example, is associated with a strong negative peak at 222 nm. Despite the importance of CD spectroscopy for characterizing secondary structures,

particularly α-helicity of proteins and peptides, a complete theoretical understanding of the origin of the peak at 222 nm is lacking. Originally observed to correlate strongly with the number of α-helical residues in protein structures as determined independently from crystal structures [77], this peak is now known to result from the n-π* transition of the backbone carbonyl chromophore. This transition has no electronic dipole transition moment (EDTM) in the isolated chromophore and therefore is forbidden in symmetric molecules. In α-helices, however, the n–π* transition may couple with electronic transitions in the surrounding backbone chromophores resulting in the introduction of an EDTM, and thus a peak is observed [78-80]. The intensity of the peak at 222 nm, therefore, is primarily related to orientational order in surrounding residues, although both intramolecular and solvent hydrogen bonds are likely to be important as well. Because the number of dihedral angles that separate the interacting chromophores is rather small, orientational order must be associated with confinement of the intervening dihedral angles to a relatively small set of conformations, and these are the α-helical conformations measured by CD.

Two other methods for defining α-helicity are commonly used, depending on the analytical method or application, and are noted here for completeness. Hydrogen bonding between backbone carbonyl oxygen atoms and backbone amide protons located four residues further along the chain toward the C-terminus forms the basis for all idealized α-helical structures. This pattern of hydrogen bonding, illustrated in Figure II-2, leads to distinct NMR spectral characteristics which can be used to identify α-helicity. Any contiguous set of residues that display this hydrogen bond, which is characterized by separations of about 0.2 nm between the proton and oxygen and nearly linear alignments of the N–H···O group [9], is considered to be α-helical. Finally, the positions of α-carbons found from x-ray crystal structures of proteins can also be used to delineate α-helix boundaries [81]. The definitions of α-helicity based on hydrogen bonding or α-carbon positions regard α-helicity as a feature of different groups within the same molecule. However, for practical purposes, they, along with the definition based on CD spectral intensity at 222 nm, refer to a similar set of conformers and are therefore largely equivalent.

Because the bulk of the work in this study was done using CD spectroscopy, the fractional α-helicity of peptides will be calculated from the normalized intensity of the

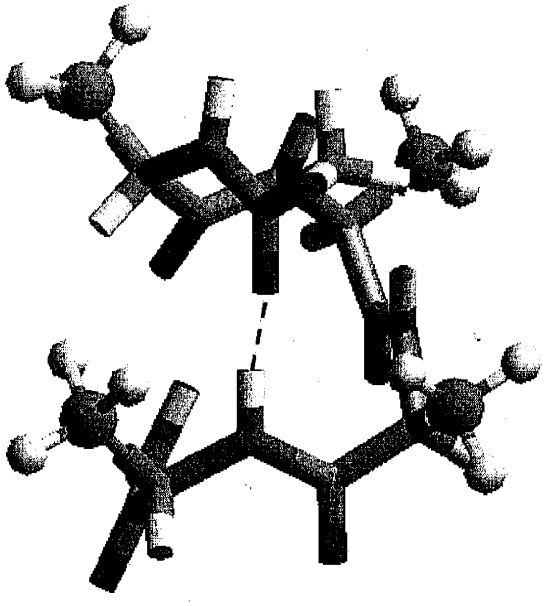

Figure II-2. α-Helical hydrogen bond (- - -) produced for the dihedral angles (ϕ = -62°, ψ = -41°). The molecule shown is a capped tetraalanine oligopeptide (alanine-β groups are rendered as spheres to distinguish them from the peptide backbone). Molecular visualization was produced with Cerius2 (Accelrys).

negative CD signal at 222 nm. This is measured by normalizing R_{222}, the raw CD signal intensity at 222 nm, by the number of residues in the peptide N, peptide concentration c, and measurement pathlength l, to yield the specific α-helicity:

$$[\theta]_{222} = \frac{R_{222}}{clN} \qquad \textbf{(II-1)}$$

For convenience, it can be shown that the quantities in the above equation may be used in the following typical units: R_{222}, mdeg; c, mol L^{-1}; l, mm; $[\theta]_{222}$, deg cm^2 $dmol^{-1}$.

Fractional α-helicity is the specific α-helicity relative to that of an ideal α-helix of the same length:

$$f_{Hel} = \frac{[\theta]_{222}}{[\theta]^{\infty}_{222}(1-k/N)+100 \cdot T} \qquad \textbf{(II-2)}$$

where values of $[\theta]^{\infty}_{222}$ = -40,000 deg cm^2 dmol^{-1} and k = 3 will be used in this work [82,83]. N is the number of residues in the α-helix, and T is the temperature. For peptides with aromatic residues, an additional term is added to the denominator in Equation (II-2) to correct for the observed interaction with the spectrum of the α-helix [84]; this affects the calculation for 4DAYAR5 only. Because larger magnitudes of the CD peak are associated with more α-helical conformations, the α-helicity will hereafter be referred to as $-[\theta]_{222}$. The above assumes that the contribution of the coiled structure to $-[\theta]_{222}$ can be neglected, and in general this is the case. For example, $-[\theta]_{222}$ for α-helical 4DAYAR5 in solution at 4 °C is 8,500 deg cm^2 dmol^{-1}, whereas $-[\theta]_{222}$ for coiled structures is estimated as 540 deg cm^2 dmol^{-1} [83]. Complications due to the length dependence in Equation (II-2) will be avoided for the comparisons made in this work since the peptides studied all have essentially the same length.

α-Helicity of Peptides

α-Helicity has been widely studied in peptides with both natural and designed sequences. The former are fragments of model proteins, typically α-helical termini, obtained either from peptide synthesis or proteolysis from parent proteins [85-87]. The best known of these is the C-peptide of ribonuclease, a 13-residue peptide produced by proteolysis, which has specific interactions that contribute to α-helicity [88]. One advantage of natural sequences is their sequence heterogeneity: most of the 20 naturally-occurring amino acids are common in protein helices. However, these natural sequences frequently fail to display α-helicity in solution. Adoption of secondary structure often relies on stabilization provided by the context of a folded tertiary structure.

Design of short α-helical peptides has often been successful with very simple sequences [13,16]. Many examples, such as Ac-A(EAAK)AGY-Am, use only two or three amino acid types, in a repeating sequence [89]. These are usually alanine-based because of the high frequency with which alanine is observed in protein α-helices. In the above example, charged side chains are introduced at four-residue intervals to provide solubility, specific electrostatic interactions stabilizing α-helicity, and favorable interactions with the net

dipole moment of the molecule. Early studies on such peptides established a basic paradigm of α-helix design: (i) selection of residues with high α-helix-forming propensity, and (ii) introduction of specific intramolecular interactions that stabilize α-helicity.

Both natural and synthetic sequences show a variety of common behaviors. α-Helicity decreases as temperature increases. Chemical denaturants such as urea or guanidine produce a decrease in α-helicity, whereas trifluoroethanol increases α-helicity. The degree of α-helicity depends strongly on the charge state of side chains, and therefore on the solution pH. Finally, when the α-helical structure is destabilized chemically or thermally, a gradual transition is observed rather than a sharp, sigmoidal, cooperative transition characteristic of protein unfolding. Formation of secondary structure in peptides thus must be qualitatively different from protein folding, for which a cooperatively-folded hydrophobic core stabilizes a single, well-defined structure and limits conformational fluctuations [10-12,90,91].

2. CD Studies of DAR-Type Peptides I: Sequence and Solution Properties

Introduction

DAR-type peptides are a robust family of helices, within which large variations in sequence may be made while maintaining a high degree of α-helicity, so long as the underlying charge pattern is maintained. The quantitative dependence of α-helicity on sequence, including variations in the relative number of terminal charges and length of the central alanine block, residue-type substitution, and sequence reversal will be described in this section and used to elucidate the mechanism for α-helix formation in these molecules.

Peptide concentration must be measured in order to normalize the CD signal and produce the specific α-helicity according to Equation (II-1). When a chromophore such as tyrosine is present, the absorbance A from the sample across a pathlength l may be measured by UV spectroscopy, and the concentration c calculated using ε, the known molar extinction coefficient, according to the Beer-Lambert law:

$$c = \frac{A}{\varepsilon l}$$

(II-3)

For peptides without chromophores, quantitative amino acid analysis (AAA) or colorimetric assays are common. AAA involves hydrolysis of the peptide into its component amino acids using strong acid and high temperatures (typically 6N HCl and 110-160 °C), derivatization with the hydrophobic chromophore phenylisothiocyanate (PITC), and chromatographic separation. Each residue type is measured, thus providing a check on the identity of the peptide and an estimate of the experimental error as well as a value for the total peptide concentration. The bicinchoninic acid (BCA) assay is a highly sensitive colorimetric test for the presence of proteins and peptides, which is noted here for completeness. Although the spectrophotometric response is linear for a variety of proteins [92], the dependence on concentration was found to be highly nonlinear for the peptides and concentration ranges of interest here, and thus ineffective for quantitative concentration measurements.

Experimental: Measurement of CD Spectra

Peptides were obtained in crude form from Research Genetics or synthesized on a Rainin peptide synthesizer using standard Fmoc chemistry. For synthesized peptides (4DAYAR5, 4AAR4) Fmoc-coupled amino acids were obtained from Anaspec Inc. Where necessary, peptides were purified using reverse-phase gradient HPLC on a C18 preparative-scale column. Typically, lyophilized peptide was dissolved in 9/1 v/v water/acetonitrile containing 0.1 volume% trifluoroacetic acid, and injected onto the column with the solvent running at 10 ml min^{-1} at this concentration. A concentration gradient was then applied, typically increasing the concentration of acetonitrile by 0.5 % min^{-1}. Elution of the peptides was detected by UV absorbance at 280 nm (4DAYAR5) or 220 nm (other peptides) and typically occurred after 12 min, at acetonitrile concentrations of approximately 12-15%. The peptide was then recovered by lyophilization.

CD spectra were taken in 1 mm pathlength quartz cells (Starna) on an Aviv 520 spectrometer. Typical spectra were measured between 190 and 250 nm, at 1 nm intervals, using a minimum averaging time of 2 s per data point. A baseline spectrum of Milli-Q

purified water, which exhibited low absorbance relative to the peptide CD signals, was subtracted from all spectra. Between measurements, the cell was rinsed with deionized water. The maximum amount of rinse fluid remaining in the cell after vigorous shaking and drying with compressed air was 0.01 ml. For the typical sample volume of 0.3 ml this amount is negligible; however, it could make a detectable difference in the CD signal for the minimum sample volume of 0.15 ml. When small sample volumes were used in sensitive quantitative experiments, the cell was first rinsed with approximately 0.025 ml of sample in order to minimize the dilution effect of residual fluid.

Whatever the anticipated use of a peptide sample, the fraction used for CD spectroscopy was dissolved in phosphate buffer or other pH-neutral buffer, since peptide samples dissolved in pure water typically lowered the pH due to the presence of residual trifluoroacetic acid (TFA) introduced during peptide synthesis as well as purification. Phosphate buffer was made using the monobasic and dibasic sodium salts ($NaH_2PO_4 \cdot H_2O$, Mallinckrodt; Na_2HPO_4, EM) and adjusted to the desired pH with small amounts of sodium hydroxide or aqueous hydrochloric acid (Mallinckrodt). Measurement of CD spectra of DAR-type peptides in pure water at pH below 5 produced erroneously low signals at 222 nm due to protonation of aspartate side chains.

Destabilization of α-helicity was studied in urea/water solutions. The transparency of these solutions was limited at wavelengths less than 215 nm. This appeared to be due to impurities present in the urea (EM industries), since recrystallization of urea from toluene led to a significant decrease in UV absorbance in this range. However, since this process introduced small amounts of toluene into the urea, and treatment with a 0.22 μm syringe filter (Millipore) also failed to remove the impurities, the urea was used as received. Fresh 7 M solutions were diluted with buffer to the desired concentrations, and spectra were collected between 215-250 nm.

Concentration Dependence of α-Helicity

Interactions between peptides in solution often lead to conformation changes, which are manifest in a concentration dependence of the CD spectrum. CD spectra of DAR-type α-helical peptides are independent of concentration, which is evidence that these molecules

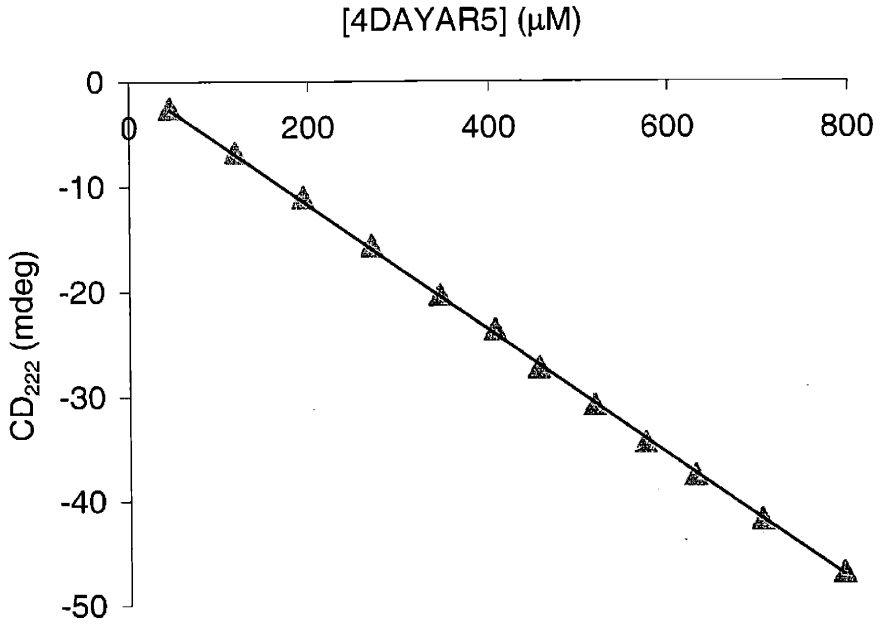

Figure II-3. CD signal intensity at 222 nm of 4DAYAR5 as a function of concentration.

are monomeric in solution. Independence of the specific α-helicity of 4DAYAR5 ($-[\theta]_{222}$) from concentration is equivalent to a linear relation between concentration and CD signal intensity, as shown in Figure II-3. Related peptides, including 2DAR8, 3DAR6, 4DAR3, 5DAR4, and 4^{+}DAR4, were analyzed at two concentrations, typically 400 and 800 μM, and no dependence of α-helicity on concentration was found below a concentration of about 1 mM. The peptide 4DAR4, not studied here, has been examined by Zhang and coworkers using equilibrium ultracentrifugation and shown to be monomeric in solution [93] in this concentration range.

A concentration-dependent shift to a β-strand structure is observed at peptide concentrations above about 1 mM. Some distortion is observed in the β spectrum, including a shoulder at 212 nm. β-strand structures are clearly differentiated from α-helices, showing a single negative peak at 216 nm, but the number of peptides aggregated into β-sheets is not easily discerned spectroscopically. Figure II-4 shows the CD spectrum of the β form of 4DAR5 as well as the spectrum of the α-helical structure obtained upon dilution with buffer. Such concentration-dependent transitions are likely to result from aggregation in solution, but no differences were observed in the optical transparency between the two samples. This may indicate that any aggregates are extremely small. It is interesting to note that these peptides

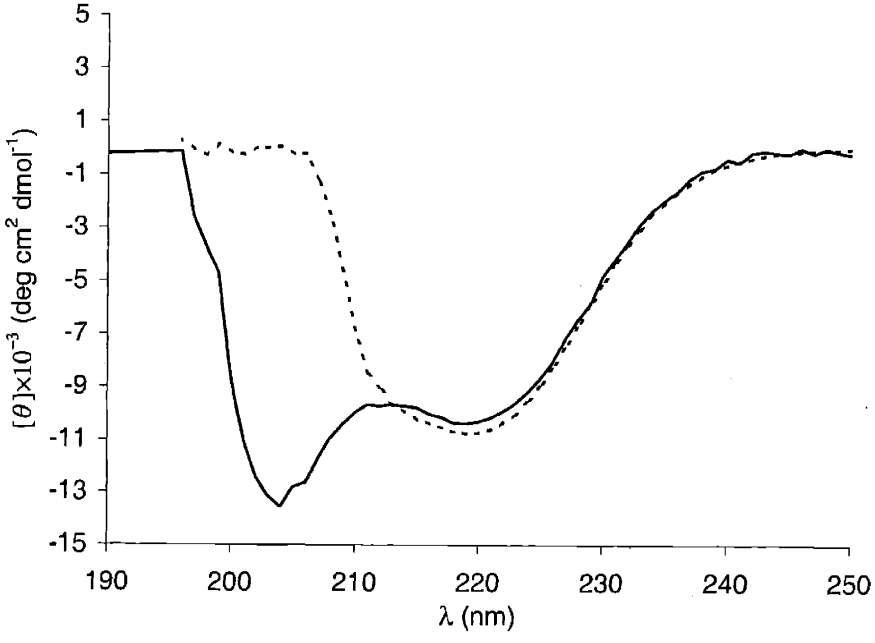

Figure II-4. Specific CD spectra of the α-helical and β-strand forms of 4DAR5. Spectra were taken at pH 8 at (- - -) 1.4 mM (2.2 mg ml^{-1}); and (——) 349 μM (0.56 mg ml^{-1}). The latter sample was obtained from the former by dilution with buffer.

bear no net charge and possess "self-complimentary" dipolar charge distributions, and thus the aggregated state may resemble stacks of molecules in alternating orientations [94].

Effect of Segment Length

Zhang and coworkers [94] have explored α-helicity as a function of the number of alanine residues in DAR-type peptides. In these studies, the number of charged side chains was kept constant, and the peptide chain length was varied. A longer alanine segment was generally associated with an increase in α-helicity: $-[\theta]_{222}$ increased with the length of the central alanine segment.

As shown in Table II-II, replacement of alanines with charged side chains while holding the total length of the peptide constant does not lead to dramatic changes in the α-helicity of a peptide with a given length. Variation of the number of anionic and cationic residues on both the N- and C-termini between two and five, while holding the total length of the peptide constant, does not significantly change $-[\theta]_{222}$. This, combined with the

observation that addition of alanine residues to the central segment (i.e., increasing the length of the chain) increases the specific α-helicity of the peptide, indicates that chain length is the most important factor controlling the α-helicity of DAR-type peptides.

Effect of Residue Type and Capping

Replacement of aspartate by glutamate does not significantly alter α-helicity, while replacement of arginine by lysine significantly decreases α-helicity. Interestingly, this contrasts with statistical data on the occurrence of these residue types within protein α-helices [76]. Aspartate occurs much more frequently than glutamate at the N-terminal residue of protein α-helices, while lysine and arginine occur with nearly identical frequency. Many scales of α-helix-forming propensities of individual amino acids based on host–guest studies [95] ascribe greater α-helix-forming tendencies to arginine and glutamate relative to lysine and aspartate, respectively. Since the arginine side chain is longer than that of lysine, and the glutamate side chain is longer than that of aspartate, this has been interpreted as an effect of chain length [96]. As noted above, the factors that stabilize α-helicity in peptides differ from those in proteins, and neither one is necessarily represented by the statistical occurrence of residue types in these structures. For example, long, charged side chains may tend to stabilize α-helicity in short peptides more effectively than short side chains with the same charge, since they may more readily form "capping" hydrogen bonds with backbone peptide groups at α-helix termini, which otherwise are not hydrogen bonded in short peptides. This preference may be suppressed in proteins since the tertiary structure provides alternative ways to satisfy the need for terminal hydrogen bonds, and packing longer side chains into specific structures carries a higher entropic penalty. This is a possible explanation for the effectiveness of arginine in stabilizing α-helicity in DAR-type peptides relative to lysine; the α-helicity may be less sensitive to the choice of aspartate or glutamate for the N-terminal residues because of the lower intrinsic α-helicity of these residues.

Substitution of alanine by tyrosine (which allows concentration to be precisely measured by UV absorbance) leads to decreased α-helicity, as would be expected from the large difference in the relative inherent α-helix-forming propensities of these two amino

acids [82,97]. Though these propensities neglect interactions with other residues in the peptide (as was discussed above), the difference between the values for alanine and tyrosine probably reflects real differences in conformational preferences between these residues due to the bulky tyrosine side chain. The presence of the aromatic chromophore may have an additional effect on the CD spectrum, independent of the associated conformational changes [98]. Although the physical basis for this interaction is not completely understood, the suggested [99] quantitative correction for this effect has been employed here.

Removal of the N-terminal acetyl and C-terminal amide capping groups results in the replacement of these hydrogen-bonding groups with positive and negative charges, respectively, at the termini. These charges interact unfavorably with the peptide dipole and significantly destabilize the α-helix. Figure II-5 shows the reduced α-helicity of the uncapped version of 3DAR6 relative to the capped version, as evidenced by the decreased magnitude of the negative peak at 222 nm.

Effect of Block Order

Placement of negatively-charged aspartates at the C-terminus and positively-charged arginines at the N-terminus significantly decreases the specific α-helicity of the peptides. Other helix-forming sequences are also sensitive to the identity of charged groups, with negative N-terminal and positive C-terminal groups favoring α-helical structures [88]. Such charge configurations provide favorable interactions with the overall α-helix dipole, and may also interact more specifically with terminal backbone groups for which the α-helix structure does not provide hydrogen bonding. Such side chain-backbone interactions have previously been observed in a "capping box," where certain residues act as hydrogen bond acceptors for the amide protons of backbone peptide groups, thus stabilizing the formation of α-helical structures [76].

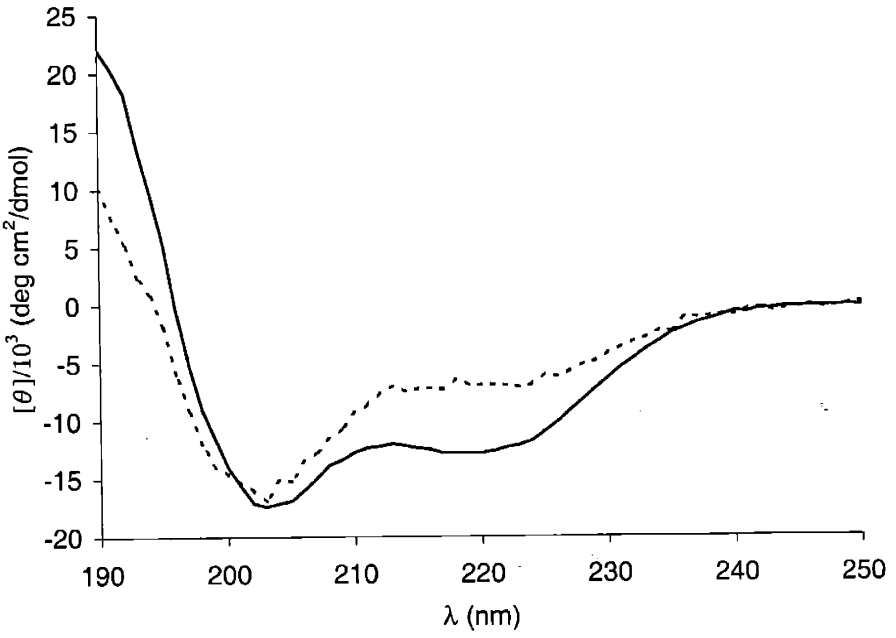

Figure II-5. Specific CD spectra of capped and uncapped peptide in 4 mM phosphate buffer at pH 7, 25 °C: (- - -) H^+-DDDAAAAAAARRR-O^-; (——) Ac-DDDAAAAAAARRR-Am (3DAR6).

Basis for α-Helicity of DAR-Type Peptides

DAR-type peptides, which are unique in being built from blocks of identical residues, combine many of the factors known to stabilize α-helicity of short peptides. Residues with high α-helix-forming propensities are used in all three segments [76]. The charged residues interact with the overall α-helix dipole in the proper orientation, with negative charges placed at the N-terminal segment and positive charges at the C-terminal segment.

Charged residues adjacent to the alanine segment are sufficiently close in some of the DAR-type peptides to form a salt bridge; however, direct interaction between these residues does not appear to be a primary factor in determining α-helicity. Some of the peptides studied here, such as 2DAR8 and 3DAR6, have high values of α-helicity despite the fact that the long alanine segment prevents direct interaction of oppositely-charged residues. Similarly, the large magnitude of the dipolar charge distribution produces a potential that tends to minimize the average end-to-end distance of the molecule, favoring α-helicity. In 4DAR5, for example, the average distance between oppositely-charged side chains decreases from about 2 nm in the random-coil conformation to about 1 nm in the α-helix conformation.

However, the α-helicity is not systematically reduced when the number of charges on the termini is reduced. Either this energy is unimportant for the stabilization of α-helicity, or its removal is compensated by the addition of α-helix-forming alanine residues.

The model for α-helicity of DAR-type peptides in solution is thus based on favorable interactions between the charged termini and the α-helix dipole, which reinforces the natural propensity of the alanine segment to form an α-helical conformation. α-Helicity propagates toward the termini, modulated by solvent and thermal conditions.

3. CD Studies of DAR-Type Peptides II: Thermal and Chemical Destabilization of α-Helicity in Solution

Temperature Dependence of α-Helicity

The temperature dependence of α-helicity in peptides arises from the entropic component of the free energy. α-Helical conformations are relatively low in entropy, and thus are disfavored at elevated temperatures. Figure II-6(a) shows the changing CD spectrum of 5DAR4 as a function of temperature. The spectrum gradually becomes more characteristic of a random-coil conformation. Similar spectra were observed for all the DAR-type peptides investigated, and have been observed by other authors in studies of a wide range of short α-helical peptides [89].

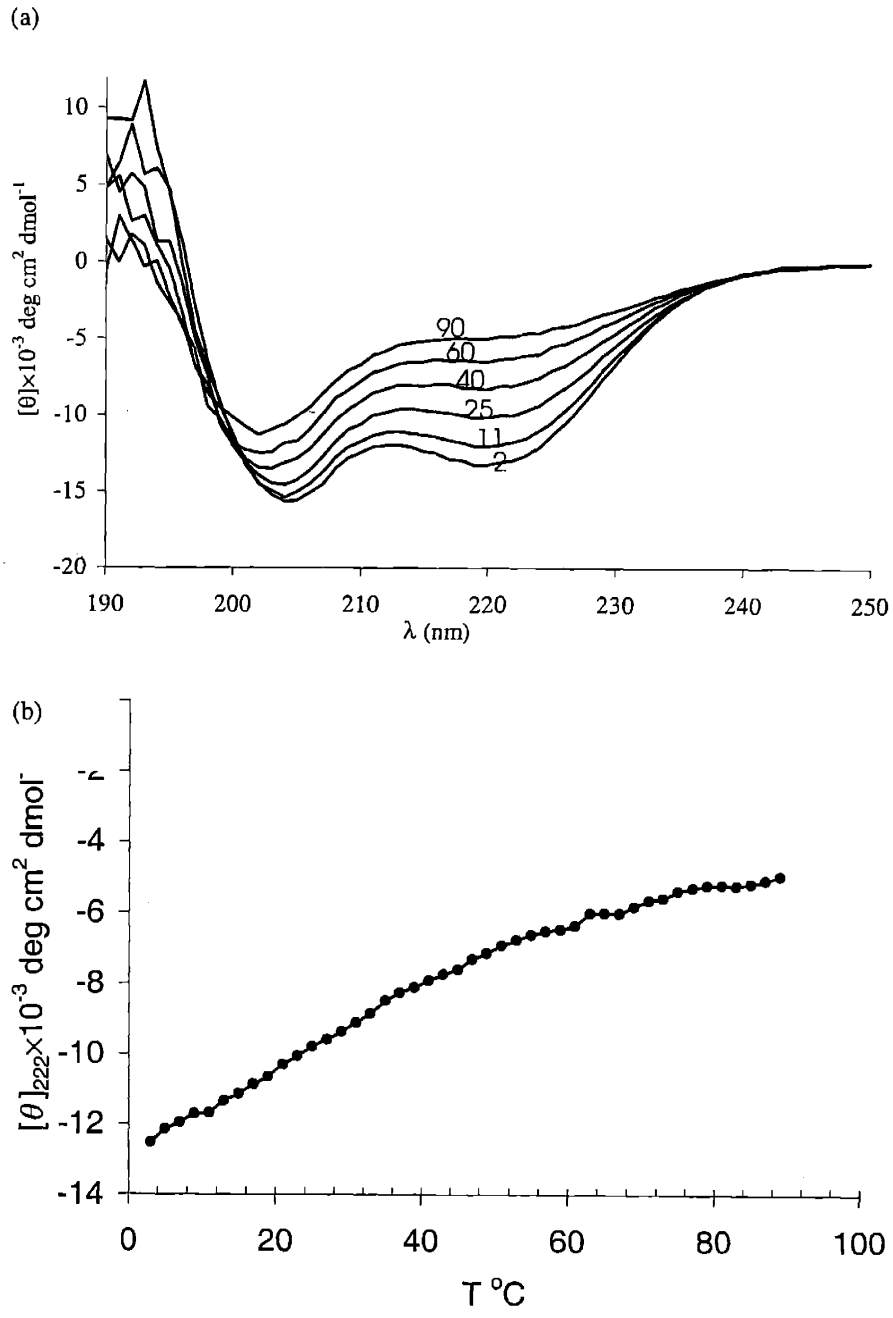

Figure II-6. Temperature dependence of the CD spectra of 5DAR4. (a) CD spectra of 5DAR4 (266 μM, 0.45 mg ml^{-1}) in 10 mM phosphate buffer, pH 8.3 with the temperature indicated in °C. (b) Trace of the specific α-helicity of 5DAR4 as a function of temperature.

The quantitative dependence of the peptide α-helicity on temperature varies between peptides. A wide variety of peptides, including 2DAR8, 3DAR6, 4DAYAR5, and 5DAR4, have α-helicities between –5,000 and –6,000 deg cm^2 dmol^{-1} at 90 °C, even though their α-helicity values at 25 °C vary widely. Figure II-6(b) shows a trace of the loss of α-helicity

from 5DAR4 with increasing temperature. A cooperative transition would give rise to a sigmoidal dependence on temperature, but none is observed. Cooperative transitions are often observed for proteins, but not for short peptides [82], although it is important to note that sigmoidal behavior in α-helicity as a function of temperature may be observed for the conformation change of individual residues even when the transition as a whole is not cooperative [100].

Solvent Dependence of α-Helicity

α-Helicity of 4DAR*m*-type peptides has previously been studied [94] as a function of ionic strength in order to evaluate the importance of electrostatic stabilization of secondary structure. It was found that α-helicity generally decreases by about 7% for an increase of 100 mM in ionic strength, probably due to screening of charge interactions. This value represents a considerably higher sensitivity than the Ac-Y$(AEAAKA)_2$F-Am α-helical peptides [101], which are also stabilized by intramolecular electrostatic interactions. Increased sensitivity of α-helicity in DAR-type peptides to ionic strength probably results from the higher fraction of charged residues relative to other helix-forming sequences.

Addition of urea decreases the α-helix content of all DAR-type peptides studied, as shown in Figure II-7. Urea is a better choice than guanidine hydrochloride for studies of secondary structure in peptides, since a substantial fraction of the denaturing action of guanidine hydrochloride has been shown to arise from its effect on solution ionic strength [101]. As with temperature, no cooperativity is observed in the transition from α-helix to random-coil structure. Loss of protein secondary and tertiary structure due to chemical denaturants may arise partly from favorable interactions with hydrophobic side chains normally buried in the protein core. However, these agents are just as effective in destabilizing secondary structure in peptides, which possess no hydrophobic core. Instead, chemical denaturants may interact favorably with the peptide group, which would also tend to destabilize α-helicity [102]. Trifluoroethanol (TFE) was previously found to stabilize α-helicity in all DAR-type peptides studied [94]. Stabilization of α-helicity by TFE probably

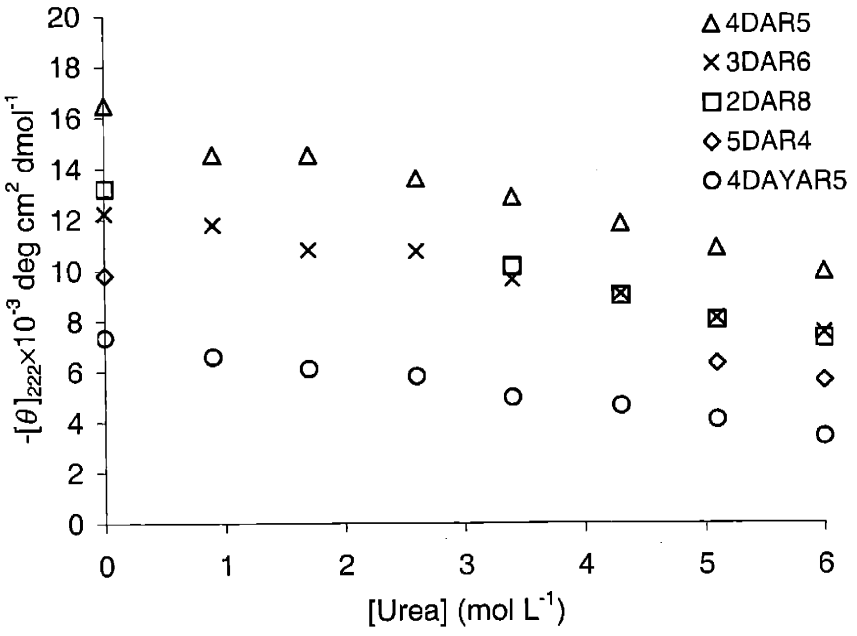

Figure II-7. Specific CD signal at 222 nm for different peptides as a function of increasing urea concentration in 10 mM phosphate buffer, pH 7.

results from the reduction in intermolecular hydrogen bonds formed between peptide and solvent [103].

As shown in Figure II-8, secondary structure is destabilized at low pH, due to titration of the charged aspartate side chains. The α-helicity declines by more than 40% of its maximum value, but this does not mean that the α-helicity is concentrated in the N-terminus of the peptide. Instead, removal of the negative charge on the N-terminus probably destabilizes α-helicity in the alanine and arginine segments. The charged termini were shown in Section II.2 to be important in stabilizing α-helicity through interactions with the net α-helix dipole; removal of this effect would be expected to decrease α-helicity over the entire length of the molecule. In addition, there is some evidence [84] that uncharged aspartate residues provide less favorable capping interactions[3] which are important in stabilizing the N-terminus of an α-helix; therefore, removal of the aspartate charges would destabilize α-helicity in the alanine segment as well because of the increased difficulty of initiating the α-helix.

[3] Capping interactions were defined previously, in Section II.2, as the ability of sidechains to hydrogen bond with backbone peptide groups at helix termini, which are not otherwise hydrogen bonded in short peptides.

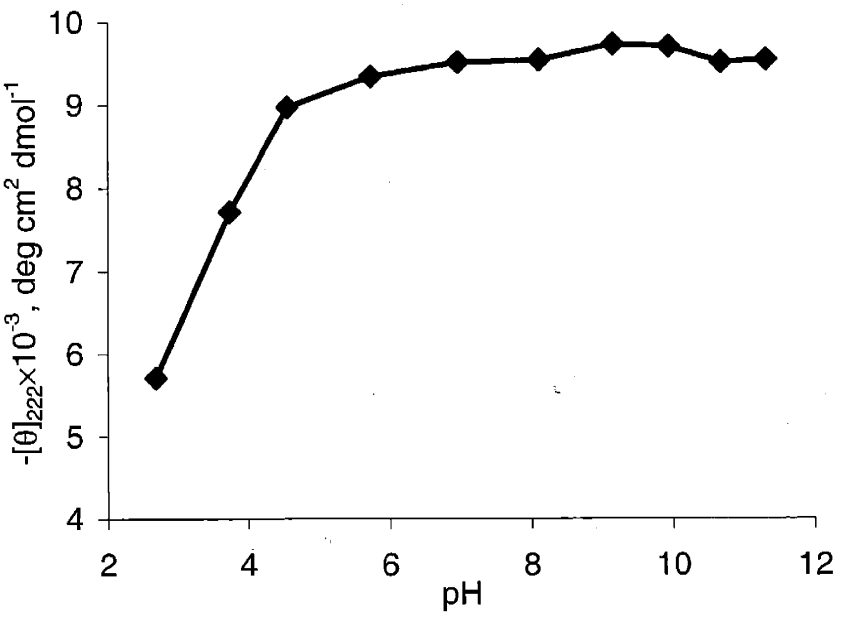

Figure II-8. Specific CD signal at 222 nm for 5DAR4 as a function of pH.

4. Characterization of Peptide Conformation by Solution ^{1}H NMR

Introduction to Conformational Measurements from Solution ^{1}H NMR

Nuclear magnetic resonance (NMR) has become one of the most powerful methods for characterizing the structures of biomolecules in solution. Application of this technique to short peptides uses essentially the same principles which have become standard for protein characterization, but benefits from the relative simplicity of the spectra. In this section, the conformational information available from solution ^{1}H NMR is summarized, and the spectroscopic properties of one particular DAR-type peptide, 4DAR5, are presented.

Designations of protons in DAR-type peptides are shown in Figure II-9. Individual amide resonances are assigned to a specific residue type using 2D TOCSY (total correlation spectroscopy), which produces cross peaks between protons in the same spin system (i.e., belonging to the same residue). Individual amide resonances are further indexed to their position in the sequence using 2D NOESY (nuclear Overhauser effect spectroscopy) to elucidate spatial connectivities.

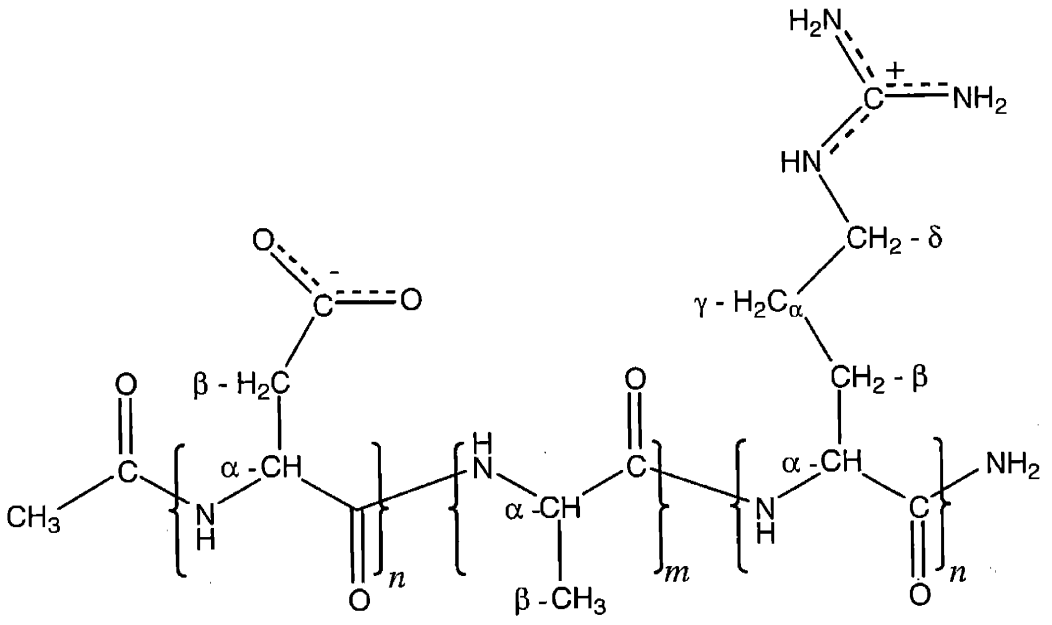

Figure II-9. Designations of ^{1}H nuclei in DAR-type peptides.

The amide (NH; 7.7 – 8.6 ppm) and alpha (αH; 4.0 – 4.5 ppm) proton resonances contain a wealth of conformational information. NH resonances (except for those from glycine and proline) are split into doublets by the α proton, with the value of the scalar coupling ($^3J_{HN\alpha}$; the splitting of the doublet, in Hz) related to the dihedral angle ϕ of the residue [104]. Surveys of crystallographic and NMR data from a variety of proteins have also shown that the chemical shift of the αH resonance is strongly correlated with the conformation of the residue; these correlations have formed the basis for identification of regions of ordered secondary structure in proteins. Although many factors influence the chemical shift [105], including the identity of adjacent residues [106] and the position of the residue within an α-helix [107], trends can often be compared for particular residues within the same molecule. For example, trends associated with changes in solvent can provide information on the resulting changes in secondary structure [105]. The chemical shift of αH resonances in α-helical secondary structures tends to be upfield of the chemical shift averaged over all conformations, while in β-strand structures the αH resonances are typically found downfield of the average. Finally, the exchange rate of NH protons with deuterium from deuterated solvent is influenced by temperature, pH, and, most importantly, the extent of hydrogen bonding. When applied to proteins, H/D exchange of the NH protons reveals regions of either strong hydrogen bonding associated with secondary structures, or

sequestration from solvent in the hydrophobic core [108,109]. Applied to peptides, it is a good indicator of α-helicity [110,111], though isotopic labeling is sometimes required to resolve individual NH signals [112].

2D NOESY NMR produces additional conformational information by measuring the distance between protons which are, on average, within 0.6 nm in the solution structure. Certain connectivities are characteristic of particular secondary structures [113]; these are summarized in Table II-III. Briefly, through-space connectivities between NH protons on adjacent residues (NH_i–NH_{i+1}), and between the αH of one residue and the NH of the following residue (αH_i–NH_{i+1}), are present in all peptide NOESY spectra of sufficient signal-to-noise ratios, and are usually used to assign the peptide sequence. Certain sets of cross peaks between protons on nonadjacent residues are characteristic of different helical structures, with αH_i–NH_{i+4} observed for α-helix only and αH_i–NH_{i+2} observed for the 3_{10} helix only. In general, complete sets of connectivities are not observed [105], for several reasons. Conformational flexibility reduces signal strength; through-space cross peaks decrease sharply with distance; and weak peaks can easily be obscured by nearby strong ones.

The different conformational measures available from solution ^{1}H NMR provide complementary measures of peptide conformation. When combined with other measurements such as CD, they provide valuable site-specific information on the localization of α-helicity within peptides and proteins. α-Helicity of a peptide molecule has already been defined by the experimentally-measurable CD signal as in Equation (II-2). The basis for this definition is the observed close correlation between $-[\theta]_{222}$ and the number of α-helical residues in the molecules determined independently by crystallography. α-Helicity is defined for an individual residue as the average population of α-helical conformers, represented by the dihedral angle values (ϕ and ψ) within the α-helical conformation space shown in Figure II-1. The NMR signals used in this work will be those which are also closely associated with the population of α-helical conformers, allowing the observation of α-helicity in individual residues.

Table II-III. Solution ^{1}H NOESY cross peaks characteristic of helical secondary structures of proteins [113].

Cross peak	*α-helix*	*3_{10} helix*
NH_i–NH_{i+1}	strong	strong
αH_i–NH_{i+1}	medium	medium
NH_i–NH_{i+2}	weak	weak
αH_i–NH_{i+2}	none	weak
αH_i–NH_{i+3}	medium	medium
αH_i–NH_{i+4}	medium	none

Experimental: Measurement of ^{1}H NMR Spectra

HPLC-purified 4DAR5 or 5DAR4 was dissolved separately in 9/1 v/v H_2O/D_2O. Peptide concentrations were typically 1.3 mg ml^{-1}, and samples were typically buffered with 10 mM phosphate buffer. Spectra were referenced to either trimethylsilane (TMS; $\delta = 0$ ppm), dissolved in $CDCl_3$ in an internal standard tube (Aldrich), or to 3-(trimethylsilyl)propionic-*2,2,3,3-d*$_4$ acid (TSP; $\delta = -0.063$ ppm from TMS in $CDCl_3$ [107]). All spectra were taken on a Varian Unity Inova with 500 MHz ^{1}H frequency, with presaturation of the solvent peak at 4.8 ppm. NOESY spectra were taken with a mixing time of 300 ms, while TOCSY spectra had a mixing time of 80 ms. For 2D spectra of samples in D_2O, the carrier frequency was set to approximately 3.6 ppm while in H_2O it was set to 5 ppm, to avoid interference with peptide signals.

For NH exchange experiments, HPLC-purified 4DAR5 was dissolved in chilled D_2O (5 °C) buffered with 10 mM sodium acetate-d_3 adjusted to pH* 4.43[4] with DCl. The sample was inserted immediately into the NMR spectrometer, thermostatted at 5 °C, and analyzed.

Results

Solution ^{1}H NMR spectra of peptides in solution reveals resonances from the backbone and sidechain protons of each residue. In D_2O, the backbone αH signals are resolved between 4.0 and 4.5 ppm, aliphatic sidechain resonances are resolved between 1.0 and 3.5 ppm, and the aromatic protons on the tyrosine residue appear between 6.8 and

[4] pH* is the glass-electrode pH meter reading, uncorrected for isotope effects (pD = pH* + 0.4).

7.2 ppm. Other signals are not resolved due to H/D exchange with the solvent. In H_2O/D_2O, the exchangeable protons are observed: these are the backbone NH protons between 7.7 and 8.6 ppm, the guanido protons of the arginine sidechains between 6.5 and 7.4 ppm, and the C-terminal amide protons between 7.4 and 7.5 ppm.

Figure II-10 shows the 1D and 2D ^{1}H NMR spectra of 4DAR5 at 5 °C. Figure II-11 shows the conformational information derived from individual αH and NH proton peaks in spectra of 4DAR5, while Figure II-12 shows connectivities resolved in 2D NOESY spectra. These spectra display quite similar trends between the various conformational markers. Aspartate NH protons display the largest $^3J_{HN\alpha}$-couplings, while alanine has the smallest $^3J_{HN\alpha}$-couplings, and those for arginine are in between. $^3J_{HN\alpha}$-couplings provide reliable information on the value of the backbone dihedral angle ϕ; smaller values of $^3J_{HN\alpha}$ correspond to smaller values of ϕ, and thus higher α-helicity values [104]. Thus, the $^3J_{HN\alpha}$-couplings indicate that the average population of α-helical conformers is greater for alanine residues than for arginine and aspartate. On average, arginine residues are more α-helical than aspartate residues. Concentration of α-helicity in the center of molecules has been observed for other peptides [105], and is thought to arise from the greater ease of forming cooperative secondary structure.

Trends in the αH signals are similar to those observed for the scalar couplings, with the highest α-helicities localized in the alanine residues. However, indicates significant α-helicity in all three segments of the 4DAR5 molecule, including the aspartate residues. Scalar couplings and αH peak shifts may give somewhat complementary information on the α-helicity in these residues. For example, the aspartate residues may reside in a distorted helical conformation in order to allow the favorable α-helix-capping interactions described in Section II.3. Average positions of the αH signals as a function of temperature are shown in Figure II-13. Interestingly, the aspartate αH peak shift is relatively insensitive to elevated temperatures, while the alanine and arginine peaks shift downfield. Recalling that downfield αH peak shifts are associated with losses of α-helicity, this indicates that the decrease in α-helicity observed for peptides at elevated temperature is associated with a shift toward more coiled conformations within the arginine and alanine segments.

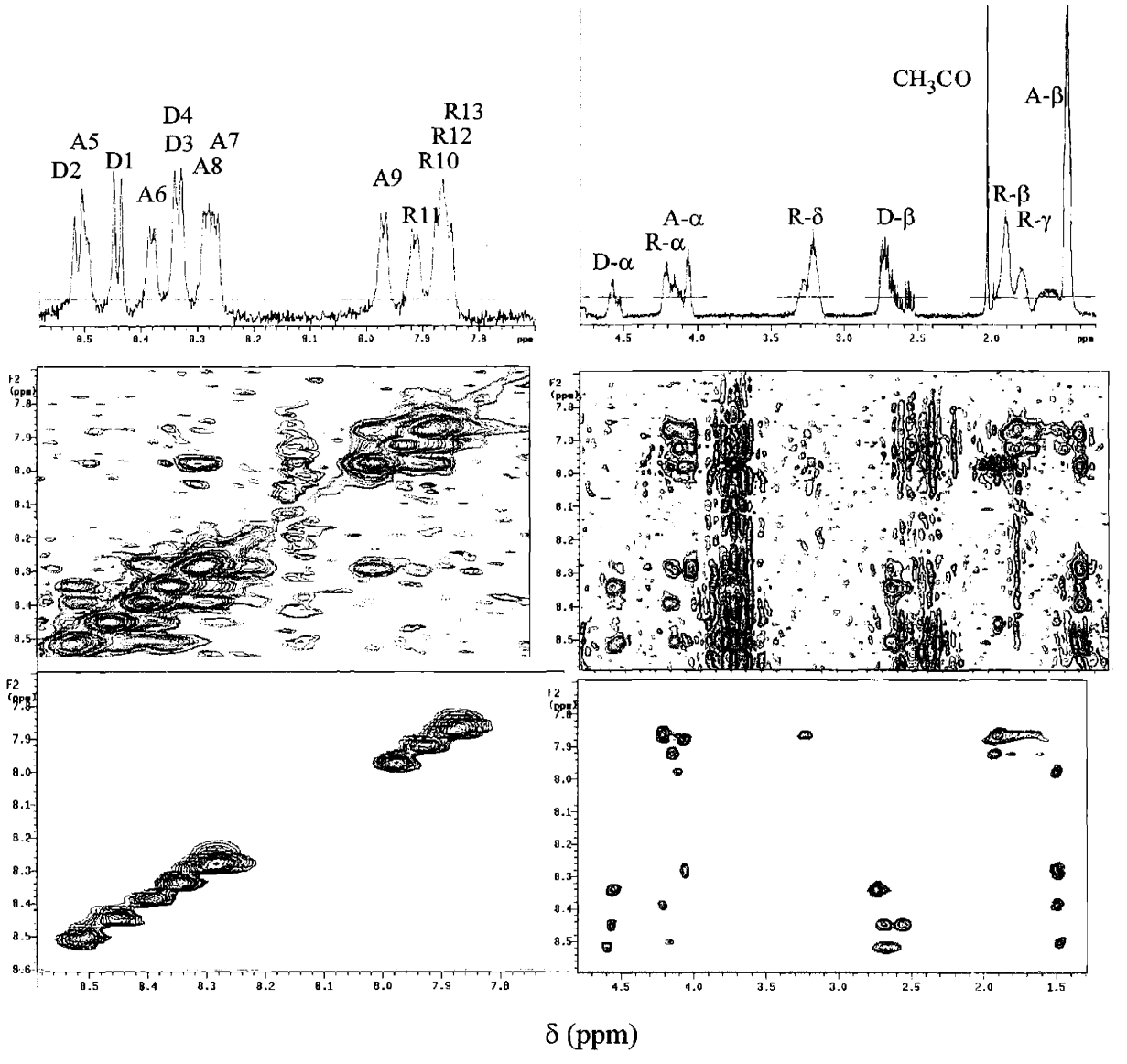

Figure II-10. **^{1}H solution NMR spectra of 4DAR5 in 9/1 v/v H_2O/D_2O (5 °C, phosphate buffer, pH 7.5). The NH (left column) and sidechain (right column) regions of the 1D spectrum (top panels) are projected down to show NOESY (middle panels) and TOCSY (bottom panels) crosspeaks. Peaks are referenced to TSP (δ = 0 ppm).**

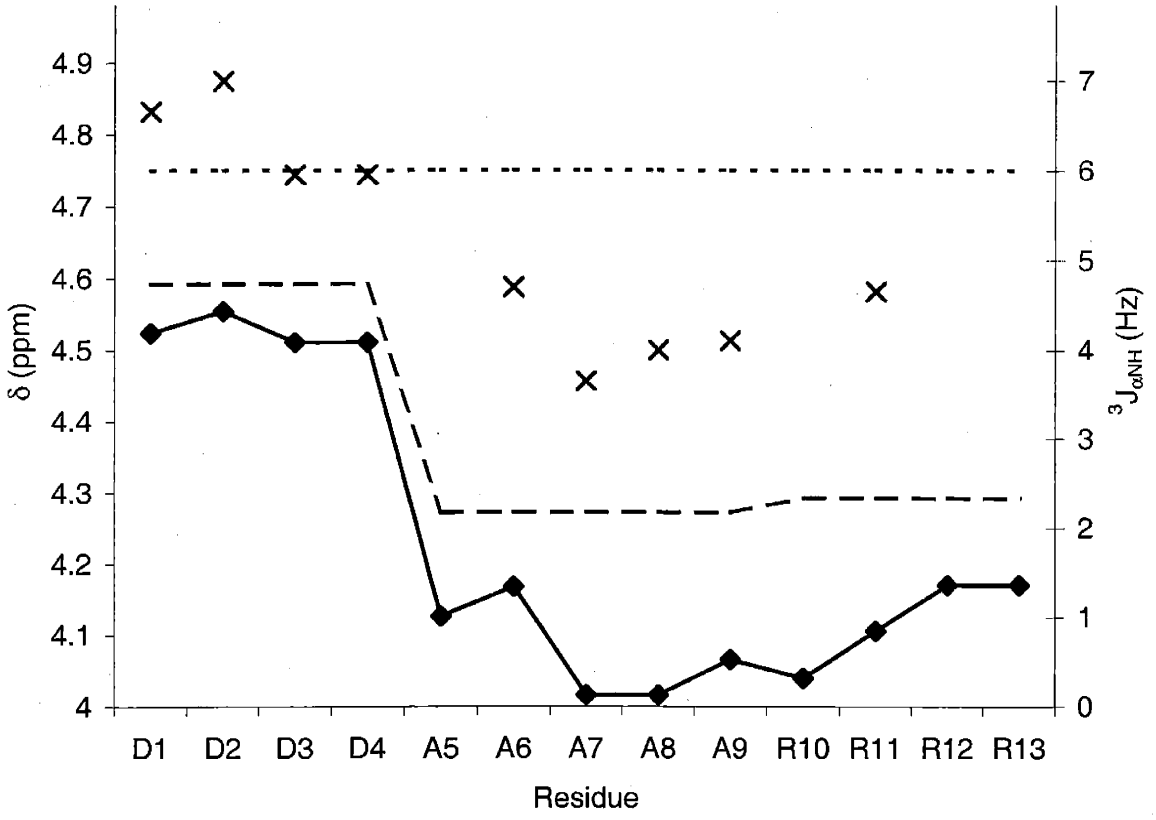

Figure II-11. Conformational information from ^{1}H solution NMR signals, same conditions as Figure II-10. Left axis: α-^{1}H peak shifts (◆) relative to the random-coil values (– – –) [114]. Right axis: $^3J_{HN\alpha}$ (×) relative to the helix–coil boundary (- - -). α-Helical and coil regions of J-coupling values are separated by the dashed line.

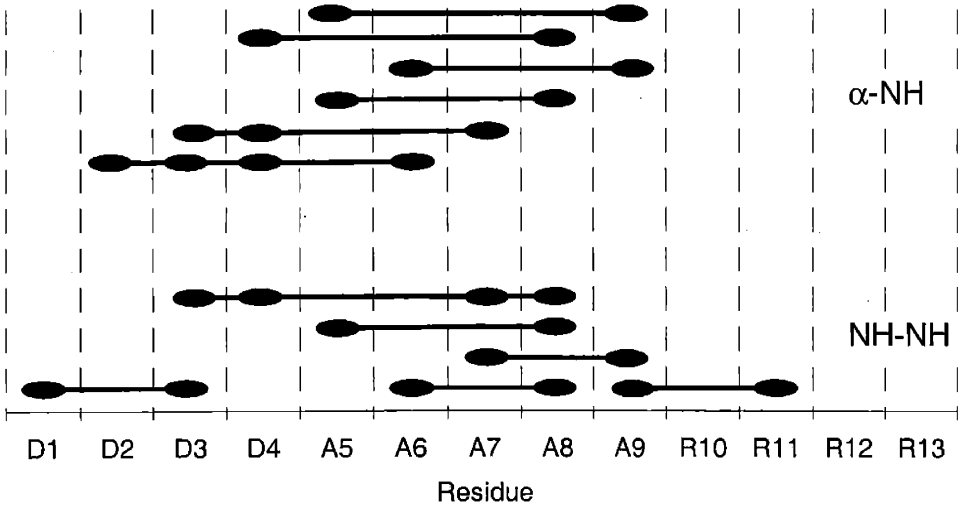

Figure II-12. Through-space connectivities observed in ^{1}H NOESY spectra of 4DAR5, same conditions as Figure II-10.

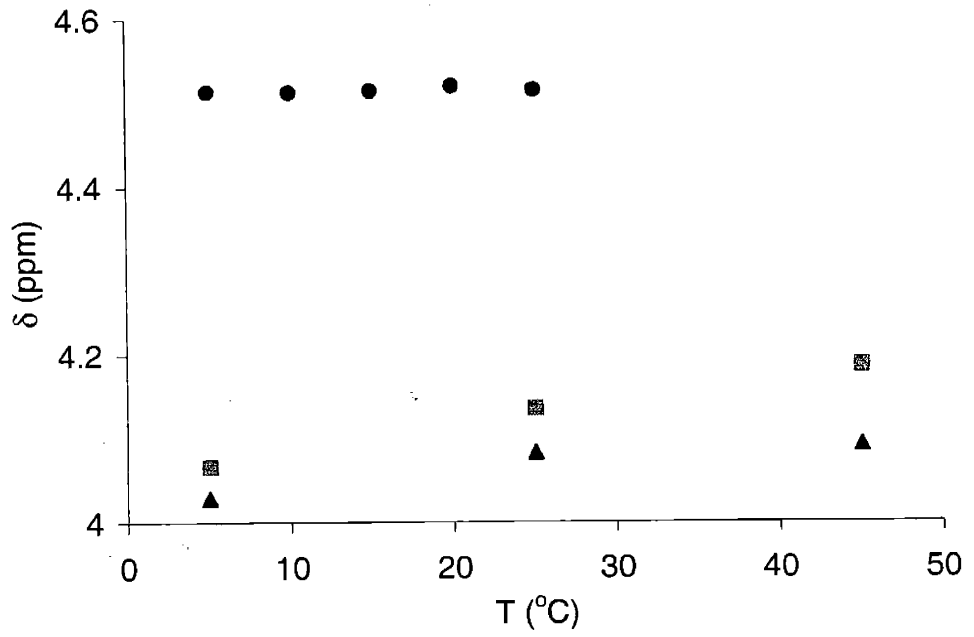

Figure II-13. Dependence of average αH peak position on temperature for ● aspartate αH; ■ alanine αH; ▲ arginine αH multiplets. Peak positions represent the average location of αH-NH cross peaks measured by TOCSY. The typical width of the αH multiplets is 0.1 ppm.

The NH peaks are visible in Figure II-10. Their positions are shifted progressively upfield from the residues at the peptide N-terminus to those at the C-terminus, a trend which has been observed previously [115]. This shift has been explained as a consequence of the electric dipole that arises in α-helical structures from the alignment of sequential peptide groups, each of which carries a dipole of about 3.5 D (Debye units) [9]. This correlation indicates that the absolute value of the chemical shift of the NH signals is probably not significant. In fact, predicting the α-helicity using the NH chemical shifts produces no correlation with the more reliable data from $^{3}J_{HN\alpha}$-coupling. The resonances of the aspartate residues are slightly downfield of the average, while those for alanine are shifted significantly downfield and those for arginine are shifted significantly upfield. It is noted that all signals are well within the range reported for a variety of proteins, and that the conformation dependence of these chemical shifts is probably masked by the dependence of this parameter on the surrounding electrostatic field and other parameters.

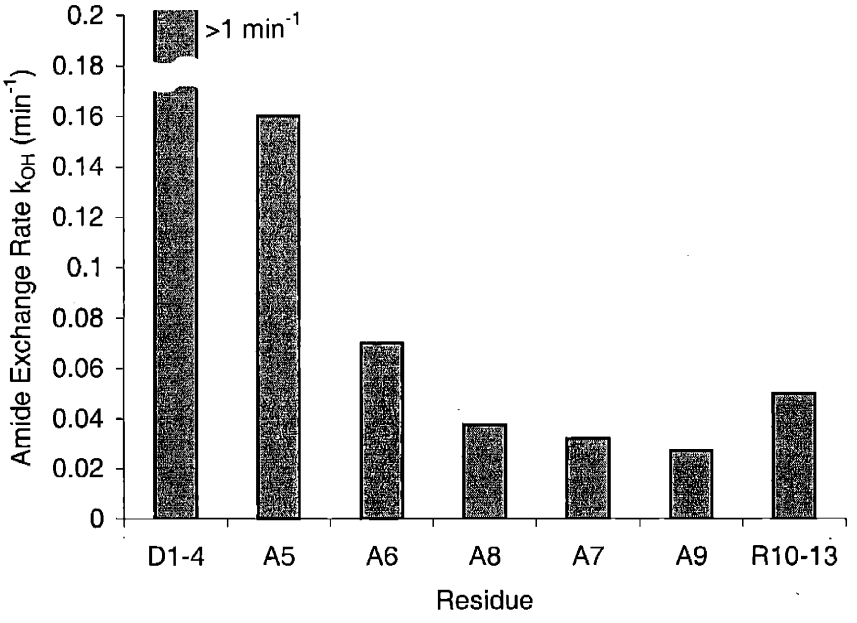

Figure II-14. Exchange rate of NH protons of 4DAR5 in 10 mM acetate buffer in D_2O, pH* 4.43, 5 °C.

The high levels of α-helicity in the alanine and arginine segments, which was discussed above based on αH peak shifts and $^3J_{HN\alpha}$-couplings, are supported by NH exchange data. This data indicates that NH protons in the arginine segment are protected from base-catalyzed exchange with the deuterated solvent at 25 °C. Figure II-14 shows the measured NH exchange rate as a function of position in the peptide sequence. Residues in the aspartate segment are completely exchanged within the initiation time of the experiment (2.5 min), while those at the C-terminal end of the alanine segment exchange most slowly. Protons of the N-terminal aspartate segment of 4DAR5 cannot participate in hydrogen bonds even in perfectly α-helical peptides. Therefore, the exchange rates of aspartate residues contain little conformational information. However, the arginine exchange rates may be roughly compared to the alanine exchange rates: if the C-terminus were significantly less α-helical than the alanine terminus, the NH proton exchange rate would be expected to be significantly larger in the arginine segment. The absence of such a large increase indicates that the alanine and arginine segments are α-helical; as demonstrated by αH peak shifts, the aspartate segment also appears to be α-helical, but this cannot be shown by the exchange experiment.

5. Conclusions

Limits to the Characterization of Solution Conformation, and Type of Helicity Present

Due to bond vibrations and interactions with solvent molecules, peptides in solution are in a constant state of conformational variation. Spectroscopic measurements give a view of the conformation which is averaged over the set of molecules visible to the technique, as well as over the period of time during which the signal is generated. Thus, for example, CD shows a percentage of α-helicity averaged over all the peptide residues in the sample as well as the time during which light intensity is measured, whereas 1D solution ^{1}H NMR signals are site-specific but averaged over the relaxation time of the nuclear spins, and 2D solution ^{1}H NMR signals are subject to complicated dynamical averaging. Statistical mechanics, along with molecular dynamics simulations, may provide details of the distribution of conformations in solution.

An important example of the limitations of some of the experimental techniques used in characterizing peptide conformation in solution is the uncertainty regarding the importance of 3_{10} helix structure in short helical peptides in aqueous solvent. Knowledge of the type of helix being studied is fundamental for the characterization of DAR-type peptides, and this topic will be explored in detail here. CD spectra of 3_{10} helices are distinguished from those of α-helices mainly by relative peak magnitudes [37,116]. Both have negative peaks at 207 nm (assigned to the amide π–π* transition), and at 222 nm (amide *n*–π*), but the ratio $[\theta]_{222} / [\theta]_{207}$ is 0.4 for the 3_{10} helix and about 1.0 for α-helix. The α-helix has a strong positive peak at 190 nm (amide *n*–π*), while the 3_{10} helix does not have a peak at this wavelength. The coil spectrum, in contrast, has only a strong negative peak at 198 nm. Spectra of partially α-helical peptides could therefore be consistent with a substantial amount of 3_{10} helix structure, since this latter element contributes no unique peaks but shifts the relative intensities of existing peaks.

Literature references on 3_{10} helices deal mainly with peptides containing non-natural C^{α}-tetra-substituted residues [116,117]. There is some question whether significant amounts of 3_{10} helix are formed in the absence of such residues. The primary evidence for the population of 3_{10} conformers in short peptides is the observation in some NMR spectra [118]

of both αH_i–NH_{i+2} (3_{10}) and αH_i–NH_{i+4} (α) helical cross peaks. Cross peaks representing these multiple conformations may be interpreted in two different ways. Most references attribute the cross peaks to β-turn [119,120], or alternatively to "either 3_{10} helix or nascent helical turns" [118,121]. A "nascent helix" is defined as "an ensemble of turnlike structures that interconvert via extended-chain forms" [121]. These turns, like the 3_{10} helix, have short αH_i–NH_{i+2} distances and therefore can account for the observation of these cross peaks. In this view, $-[\theta]_{222}$ is attributed solely to α-helicity, with no significant contribution from 3_{10} helical structures, except at the ends of α-helices where they may be stabilized.

In contrast, it has been argued [122] that "nascent helix" and 3_{10} helix are intermediates in the α-helix–random-coil transition. This picture would seem to require that the isodichroic point ubiquitous in CD helix–coil transitions actually be a fortuitous coincidence of the CD spectra of all four possible states. Adherents of the latter viewpoint neglect the turn states and use the $[\theta]_{222}$ / $[\theta]_{207}$ ratios given above to assign relative weights to 3_{10} and α-helix [123]. This approach leads to very large 3_{10} helix contents in short helical peptides. However, since increasing temperature decreases the magnitude of the negative peak at 222 nm, this would indicate that 3_{10} helix dominates at high temperatures, when the opposite would be expected for a low-entropy structure. In addition, X-ray structural data for proteins indicate that 3_{10} helices are rarely observed for natural amino acids, except sometimes as the final turn of an α-helix [9]. Therefore, while a 3_{10} helix could conceivably be the source of some CD signal intensity in short helical peptides that have a predominantly α-helical structure, it is not itself the dominant structure.

Taken together, the available data indicates that, although the experimental techniques used here do not differentiate well between α-helix and 3_{10} helix, the latter structure is not highly populated in DAR-type peptides, since (1) they do not contain non-natural C^{α}-tetrasubstituted amino acids; and (2) the CD spectra as well as weak αH_i–NH_{i+2} NOESY cross peaks are consistent with an α-helix–random-coil transition. A small amount of 3_{10} structure is possible, and would be a natural result of the partially coiled nature of the α-helical peptides studied here.

Basis for α-Helicity in DAR-Type Peptides

There are other important factors that influence the conformation of peptides in solution which are not well understood. These include the effects of hydration, which has been implicated as a major factor in determining the α-helix-forming propensities of individual residues [124], as well as the state of coions and counterions surrounding the peptide. These factors may be important in understanding the solution structure of the peptide, as well as its adsorption behavior in more detail.

Like other short peptides, the helix–coil transition of these peptides is not cooperative. Cooperative transitions are observed to have a sigmoidal decrease in secondary structure with increasing temperature or chemical denaturant concentration, while for these peptides this dependence is gradual. This represents an important qualitative difference between proteins and the model peptides studied here, but does not detract from the significance of insights which these molecules may yield into structure formation in solution and adsorbed to surfaces. The other factors determining conformation in proteins, which include hydrogen bonding and conformational entropy, also determine the conformations of peptides [13,125]. Cooperative transitions are an emergent property of long peptide helices; this can be seen clearly in systematic studies of peptides with repeating sequences [103]. Therefore the trends observed in the adsorption behavior of peptides, lacking a cooperative folding transition, are still indicative of important factors in the adsorption of proteins. Clearly a very interesting area of future work would be the development of simple model systems that contain the cooperative folding transitions which these peptides lack.

DAR-type peptides represent a novel class of short α-helical peptides, in which strong α-helicity is retained over wide sequence variations within the generic sequence pattern. α-Helicity is primarily concentrated within the alanine segment. Aspartate and arginine residues at the N- and C-termini provide increased solubility as well as capping interactions [84] which stabilize α-helicity. Both the arginine, and to a lesser extent the aspartate segments, have significant amounts of α-helicity.

Chapter III. Adsorption of DAR-Type α-Helical Peptides to Colloidal Silica

1. Introduction

Adsorption of DAR-type α-helical peptides to colloidal silica surfaces shares many of the most important features of nonspecific protein adsorption processes, yet represents a sufficiently simple system for detailed characterization of adsorbate and substrate. The purpose of this chapter is to develop this system as a model for studying the interesting features of protein adsorption. Multiple experimental methods including adsorption isotherms and CD and NMR spectroscopy will be used to provide detailed information on the amount, conformation, and orientation of adsorbed molecules.

Silica is a useful model surface. Although published data is available for all of the properties relevant here [126], the most important properties are measured in Section III.2 in order to verify surface characterization. Peptides adsorbed to silica can be studied by nearly all of the techniques discussed in Chapter I.2, and a selection of these are applied in subsequent sections of this chapter. Adsorption isotherms of 4DAYAR5 on amorphous colloidal silica are characterized as a function of pH in Section III.3, providing the first indications of the importantse of electrostatic driving forces for adsorption. In Section III.4, the temperature dependence of the isotherm at pH 9 is used to derive valuable thermodynamic information, and in Section III.5 the isotherm technique is extended to characterize the adsorption at pH 9 for a variety of peptides. CD spectroscopy is extremely useful for studying this system because of the strong signals obtained, and because these signals are more easily localized to α-helical regions within the small peptides; CD studies of the helix–coil transition which occurs when DAR-type peptides adsorb to colloidal silica are described in Section III.6. Finally, solution ^{1}H NMR provides a remarkable amount of information on the conformation and orientation of adsorbed molecules, as shown in Section III.7. Simultaneous application of these three techniques produces a wealth of information rare in the long-established field of protein adsorption and conformation change; the results are a cohesive model of adsorption, described in Section III.8.

2. Surface Chemistry of Colloidal Silica

Introduction

Amorphous colloidal silica possesses one of the most widely-studied model oxide surfaces [126]. At neutral and basic pH, silica interacts with ions primarily through electrostatic forces generated by its strong negative surface charge. Adsorption of charged species therefore depends strongly on ionic valence. Additional variation is seen between cations with the same valence, and for monovalent cations this has been shown to depend on the hydrated radius of the cation [127]. To minimize complications from specific adsorption in this study, sodium is the predominant cationic counterion in solution.

Three varieties of anionic colloidal silica were used in this study, due to varying requirements for adsorption and spectroscopic experiments. In general, Ludox HS (12 nm diameter particles) was used when a high surface area was required to drive adsorption to completion, or when UV-transparency was necessary for precise CD studies. Ludox TM (22 nm diameter) was selected for experiments which required both UV-transparency and separation by centrifugation. Because separation of Ludox TM requires prolonged centrifugation at high speeds, Snowtex ZL (74 nm diameter) was used for more convenient sedimentation by centrifugation. Properties of these colloids are listed in Table III-I.

From the standpoint of peptide adsorption studies, the most important properties of colloidal silica suspensions are particle size, monodispersity, specific surface area, composition, surface charge, and zeta potential. Surface area of the colloidal silica suspensions used is available from the manufacturers' specifications. Measurements of the other properties are presented in this section; in all cases the data are consistent with those previously published [126].

Experimental: Characterization of Colloidal Silica

Titration of colloidal silica was performed by adding known masses of HNO_3 or KOH to a stirred suspension. Masses of titrant were measured to 10^{-4} g upon removal from the containers, and pH was allowed to equilibrate between measurements until no further change was evident, a period of one or two minutes. Titration behavior of the aqueous solvent for the

Table III-I. Varieties of colloidal silica used in adsorption studies (data from manufacturers' specifications). †Calculated from the particle size assuming a density of 2.2 g cm^{-2} [128].

Colloidal Silica	*Source*	*Diameter (nm)*	*Surface Area (m^2 g^{-1})*
Ludox HS	Aldrich (DuPont product)	12	220
Ludox TM	Aldrich (DuPont product)	22	140
Snowtex ZL	Nissan Chemical Co.	74	37†

colloidal particles, which contained sodium cations and other dispersants, was studied after separating the liquid phase from the particles using an Amicon YM-50 filter. The 50,000 g mol^{-1} protein molecular weight cutoff for these filters corresponds to a pore diameter of approximately 9 nm, using a density for folded proteins of 0.75 g cm^{-3} [9]. Therefore these filters retain colloidal silica particles but allow the solvent to be removed and replaced with deionized or deuterated water. The titration behavior of the solvent was found to be identical to that of water, and therefore no correction was necessary.

Measurements of zeta potential as a function of pH were obtained from the electrokinetic sonic amplitude (ESA) of the colloidal particles. Briefly, this technique applies an oscillating electrical field to an aqueous solution of charged colloidal particles, which interacts with the electrical double layer to produce particle vibrations. The resulting acoustic signal depends on the magnitude of the surface charge, as well as the particle size and density. This measurement was performed on a commercial apparatus (Matek SSP-1) according to the manufacturer's specifications.

For solution ^1H NMR of colloidal suspensions, the aqueous solvent was exchanged for deuterium oxide (99.9 atom % D; Cambridge Isotope Laboratories). Deuteration of Ludox HS and Ludox TM was performed by repeated dilution of 1 g of Ludox solution with 5 g of D_2O and reconcentration over an Amicon YM-50 filter. Three rinses with D_2O removed 98% of the H_2O content.

For adsorption isotherms and CD measurements, dispersants such as sodium cations must be removed. In both cases, this was done for Ludox HS and Ludox TM by repeated dilutions of 1 g of Ludox solution with 15 mL Millipore Milli-Q purified water, followed by reconcentration using the Amicon filter. Purification of Snowtex ZL was done by centrifugation and resuspension. At typical centrifugation speeds (2000 rcf), Snowtex ZL particles sediment on the side of the Amicon YM-50 filter before all the solvent has passed

through the filter. These sedimented particles were resuspended in deionized water, providing the purified colloidal solution.

Final silica concentrations were determined by evaporating water from a known mass of the colloidal solution in a drying oven and weighing the remaining silica (typically about 10 wt% from 50 - 100 mg of colloid solution; note that 10 mM buffer contributes 0.1 wt% and therefore is negligible in this measurement). When this procedure was applied to undiluted Ludox TM solutions, the result was in good agreement with the manufacturer's specifications for solids content.

Results

Silica is uncharged at pH 3, and has an increasingly negative zeta potential and surface charge at higher pH conditions. Approximately 10% of silanol groups have pK_a values less than 9, and 90% have pK_a values of approximately 9 [126]. Titration of anionic colloidal silica (Ludox HS) with nitric acid indicates a surface charge density of approximately 0.54 $Si–O^-$ groups per square nanometer, or approximately one $Si–O^-$ group per 1.8 nm^2, at pH 9 and ionic strength of 0.35. Figure III-1 shows surface charge and zeta potential data as a function of pH.

Suspensions of Ludox HS or Ludox TM used for peptide adsorption do not interfere with characterization of the adsorbed peptides by spectroscopic techniques. Some light scattering occurs in the wavelength range of interest for peptide characterization by CD measurements, but silica particles do not contribute to the differential absorbance of circularly-polarized light. Surface hydroxyl groups are not observed by ^1H NMR ($\approx$ 5 ppm) due to static line broadening.

Monodispersity of the silica suspensions is important to the interpretation of results in subsequent sections. Ludox TM suspensions were examined to determine whether a significant fraction of particles could exist between 5 and 9 nm in diameter. Such small particles could be retained during purification but fail to sediment during adsorption experiments. No such fraction exists, as indicated by the negligible silica signal observed by transmission IR of filtrate from Ludox TM (data not shown) and by TEM of dried samples of Ludox TM, as shown in Figure III-2.

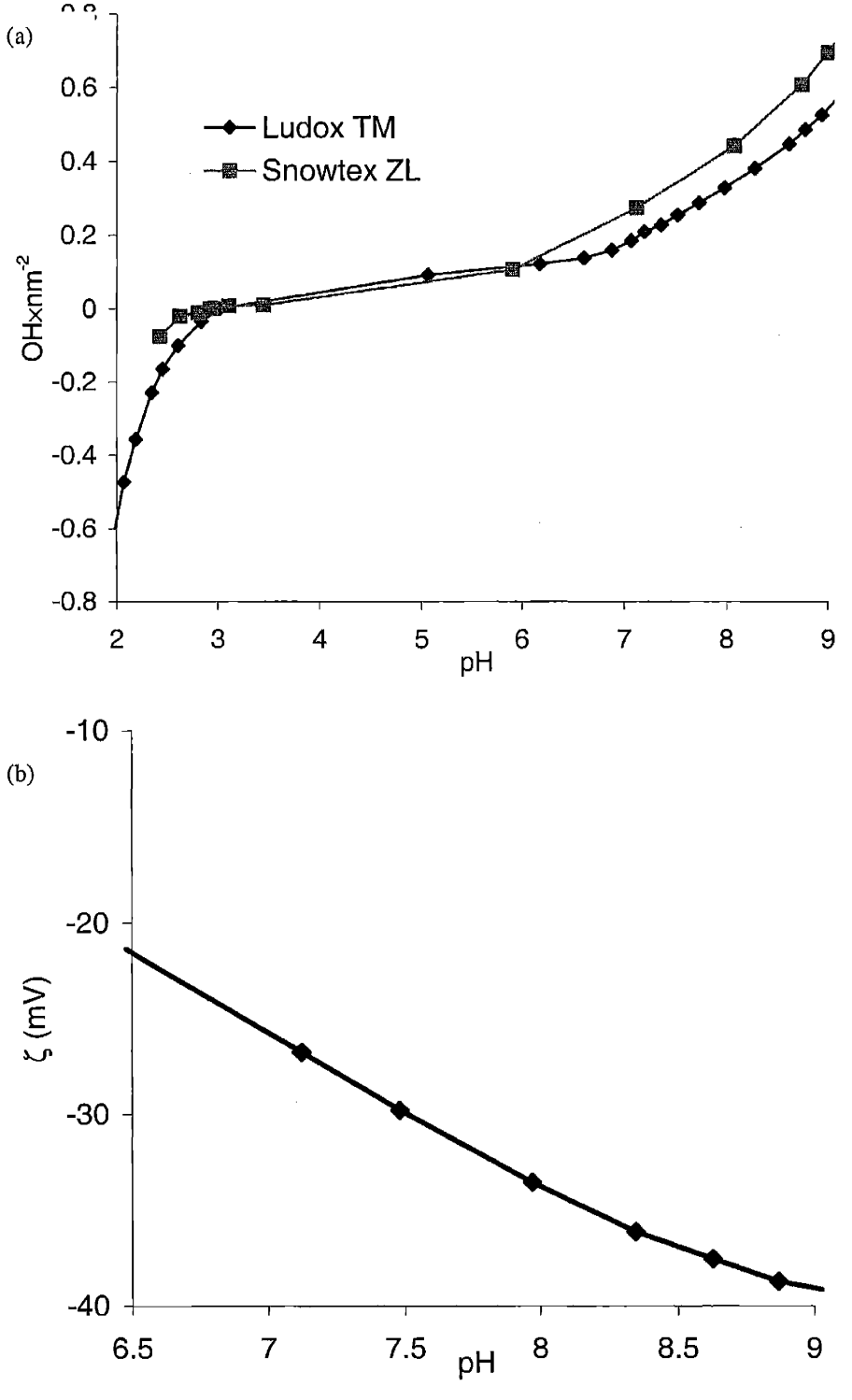

Figure III-1. Electrostatic properties of the colloidal silica surface. (a) surface charge of colloidal silica samples measured by titration with HCl and NaOH; (b) zeta potential of Ludox TM measured by ESA.

(a)

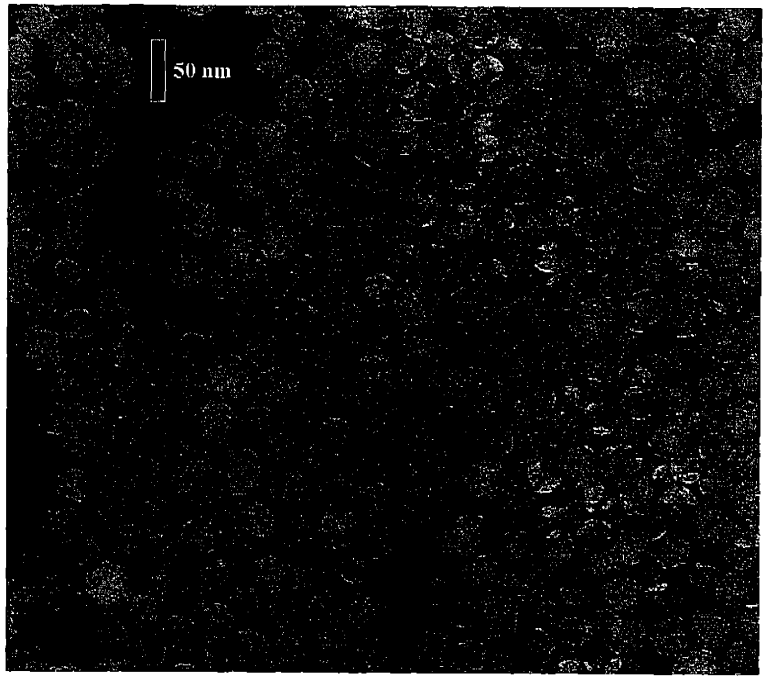

(b)

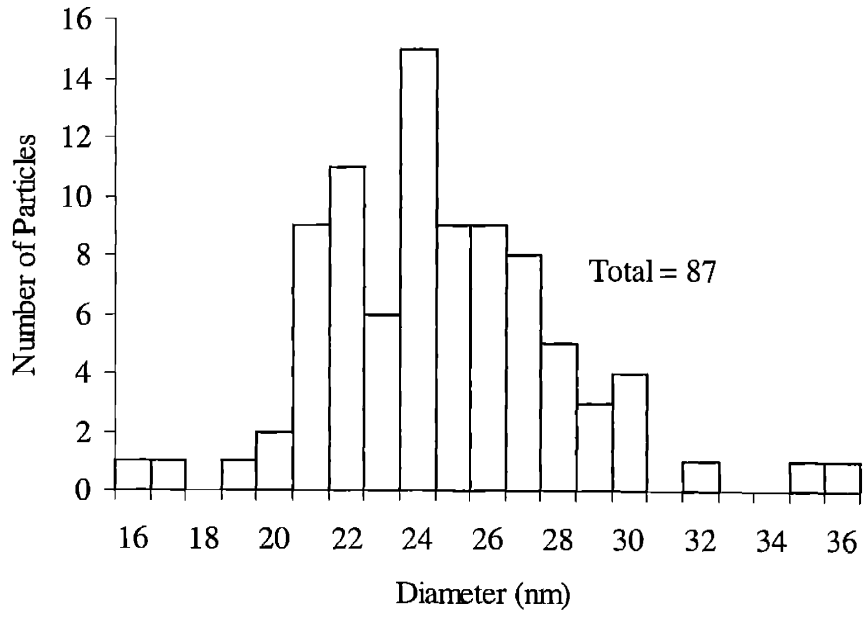

Figure III-2. Ludox TM colloidal silica: (a) TEM micrograph; (b) histogram of Ludox TM particle sizes based on micrograph (a).

3. Adsorption Isotherms I: Dependence on pH

Introduction: Basic Isotherm Models

A simple model for the interaction between molecules in solution and a finite number of identical adsorption sites leads to the Langmuir isotherm [129], which expresses the surface coverage (Γ) as a function of free adsorbate concentration:

$$\Gamma = \Gamma_{max} \frac{K_{eq} c}{1 + K_{eq} c} \qquad \textbf{(III-1)}$$

In this formulation, c is the concentration of peptide in solution (not adsorbed to the surface), Γ_{max} is the plateau surface coverage, and K_{eq} is the equilibrium constant for peptide adsorption to the surface. This well-known model is based upon three key assumptions. First, adsorption must be thermodynamically reversible; that is, the ascending and descending adsorption isotherms must coincide. Second, the energy of adsorption must be independent of surface coverage, which precludes lateral interactions between adsorbed molecules. Third, all adsorbed molecules must occupy the same area on the surface.

Most or all of the assumptions of the Langmuir model are known to be invalid for proteins adsorbing at liquid–gas, liquid–liquid, and liquid–solid interfaces. In addition, the interfacial behavior of proteins and surfactants frequently displays multiple plateaus, multilayer adsorption, and irreversibility in the adsorbed amount, features not predicted by the Langmuir model. Permanent conformation changes, which result in the formation of large numbers of surface contacts, bind proteins cooperatively and irreversibly to surfaces. Free energies cannot be calculated from adsorption isotherms measured for irreversible processes.

Therefore, much effort has been devoted to formulating models that allow interactions between adsorbed molecules (such as the Frumkin isotherm described below), time- and surface coverage-dependent conformational changes [130,131], and partial or complete irreversibility of adsorption [132,133]. Irreversibility and conformational change have long been thought to account for observed "steps" in adsorption isotherms that are not accounted for by experimental error; these are well established from literature on protein adsorption, although they are frequently associated with complicated or irreproducible

behavior [28,33,134-136]. Models for reversible adsorption behavior have been formulated in the context of the thermodynamics of surfactant adsorption, in which interactions between adsorbed molecules are manifested as first-order phase transitions [137], although there is continuing dissent on the precise nature of the transitions observed experimentally [138].

A simple modification to the Langmuir isotherm allows the energy of adsorption to vary with fractional surface coverage ($\theta = \Gamma/\Gamma_{max}$) [139]:

$$\Delta G_\theta^0 = \Delta G_{\theta=0}^0 - 2\alpha\theta \qquad \textbf{(III-2)}$$

This produces the Frumkin isotherm:

$$\Gamma = \Gamma_{max} \frac{K_{eq}c}{1+K_{eq}c} e^{2\alpha\theta} \qquad \textbf{(III-3)}$$

in which α is a parameter representing the attraction between adsorbed molecules. The Langmuir isotherm is thus a special case of the Frumkin isotherm for which $\alpha = 0$.

In this chapter, adsorption of DAR-type peptides to colloidal silica is shown to be a reversible equilibrium process. Adsorption isotherms are compared with Langmuir and Frumkin isotherms. Fitting to these theoretical models allows calculation of the adsorption equilibrium constant K_{eq}, which is related to the strength of the electrostatic interaction between the surface and the peptide. Reasons for remaining deviations from the theoretical forms are discussed.

Experimental: Measurement of Adsorption Isotherms

Adsorption isotherms of HPLC-purified 4DAYAR5 were measured for Ludox TM and Snowtex ZL colloidal SiO_2 using a sedimentation technique. The experimental parameters were selected to maximize the accuracy and concentration range of the experiment. pH was adjusted with NaOH and HCl. Ionic strength was calculated according to [129]

$$I = \frac{1}{2}\sum_i m_i z_i^2 \qquad \textbf{(III-4)}$$

where m_i is the molar concentration of species i with valence z_i.

Solids were purified by ultrafiltration and resuspended in deionized H_2O as described in Section III.2. The initial concentration of 4DAYAR5 was determined using the UV absorbance of tyrosine at 274 nm (ε_{274} = 1,405 M^{-1} cm^{-1}) [140]. The peptide solution was diluted with known volumes of buffer and colloidal silica solution to give the desired range of concentrations of peptide and colloid. Because of the difficulty of sedimenting Ludox TM particles, few data points were collected; the ease of sedimentation of Snowtex ZL facilitated collection of much more highly-resolved isotherms. Ludox TM particles were sedimented using a Sorvall RC-5B refrigerated centrifuge operating at 25,000 relative centripetal force (rcf) for 2.5 hours. Snowtex ZL particles were sedimented using a microcentrifuge (VWR) operating at 3,600 rcf for 0.5 hours. Isotherm temperatures were measured from tubes containing deionized water that were centrifuged with the isotherm samples. Centrifugation results in a significant increase in temperature from the nominal equilibration temperature.

The supernatant was removed immediately and the UV absorbance measurements were repeated to find the concentration of peptide remaining in solution. The amount of adsorbed peptide was determined by difference. Difference methods based on the peak height at 274 nm sometimes produce erroneous results due to small changes in baseline arising from the sensitivity of the 4DAYAR5 absorption spectrum to pH (due to titration of the tyrosine side chain, pKa = 10 [9]); small amounts of colloidal particles remaining in solution, and drift in the baseline of the UV spectrophotometer. Therefore, data points were also evaluated using spectral subtraction. A standard UV absorbance spectrum S_{std} was subtracted from the measured spectrum S_{meas} to produce the subtracted spectrum S_{sub} defined by

$$S_{sub} = S_{meas} - \chi S_{std} \qquad \textbf{(III-5)}$$

Here, χ is the subtraction coefficient: when S_{sub} displays no UV absorbance peak, χ gives the concentration of 4DAYAR5 in the measured spectrum relative to the standard spectrum. The value of χ was optimized using the numerical solver contained in a commercial software package (Microsoft Excel) such that E, the least-squares deviation between the subtracted spectrum S_{sub} and a straight line (L; obtained from linear regression), was minimized:

$$E = \sum_{i=260\,\mathrm{nm}}^{i=320\,\mathrm{nm}} \left(S_{sub} - L(x_i)\right)^2$$

(III-6)

This procedure reproducibly and objectively produces subtracted spectra which eliminate the peptide peak at 274 nm despite sloping baselines. For the Snowtex ZL isotherms, spectral subtraction produced results nearly identical to the simple difference method, but with decreased scatter, thus validating this method for future use. For both methods, uncertainty was evaluated for individual data points using the larger of either the scatter of the data points or the signal-to-noise ratio of the subtracted spectrum.

In addition to the isotherm at 36 °C, isotherms were measured at 20 °C and 60 °C after equilibrating the samples (and the centrifuge) in a refrigerator or drying oven, respectively. As before, temperatures were measured from tubes containing deionized water, which were centrifuged with the isotherm samples. For these temperature-dependent studies, isotherm samples were equilibrated for at least 1 hour, then centrifuged at the same rcf at all temperatures. These samples were adversely affected by sloping baselines in the absorbance spectra of 4DAYAR5. Therefore, they were also analyzed using the spectral subtraction method described above. Spectral subtraction greatly improved data quality, as measured by increased agreement with the room-temperature high-resolution isotherm taken under identical conditions.

Adsorption experiments were performed for several other peptides at pH 9 in 10 mM borate buffer. In general, DAR-type peptides that do not have the tyrosine chromophore are not conveniently quantified by UV absorbance spectroscopy. The only absorbance occurs at 200 nm, which overlaps with that of common buffer salts containing chloride, potassium, or nitrate ions. Instead, because the CD signal at 222 nm at 25 °C is proportional to peptide concentration (Chapter II.2), this peak was used as a quantitative measure of peptide concentration.

Adsorption isotherms were measured by suspending peptides (as received from Research Genetics) in 10 mM borate buffer. The concentration of each peptide solution was measured by CD, then the solutions were combined with known weights of a colloidal solution of purified Snowtex ZL and buffer, and equilibrated. The solid with adsorbed

peptide was then removed by centrifugation, and the remaining concentration of peptide was found from the difference.

Fitting of adsorption isotherm data points to equations of the Langmuir or Frumkin types (Equations (III-1) and (III-3), respectively) was done numerically using a commercial software package (Microsoft Excel or Mathematica). The sum of weighted residuals (i.e., deviations between the data points and fitting function, Equation (III-7) below), was minimized with respect to the fitting parameters; care was taken to ensure that the values presented correspond to global minima in the residuals. Because the adsorbed amount (Γ) is an implicit variable in the Frumkin isotherm, the Frumkin equation was solved numerically during the fitting process using the implementation of the secant method in the Mathematica software.

$NaH_2PO_4 \cdot H_2O$, NaOH, tris hydrochloride ($NH_2C(CH_2OH)_3 \cdot HCl$), HCl (37 wt%), and HNO_3 (69 wt%) were used as received from Mallinckrodt. Na_2HPO_4 (EM Industries), $Na_2B_4O_7 \cdot 10\,H_2O$ (A.C.S. Reagent, Aldrich), and tris base ($NH_2C(CH_2OH)_3$, Boehringer Mannheim) were used as received from the suppliers.

Results

Isotherms for the adsorption of 4DAYAR5 to Ludox TM colloidal silica at pH 7–9 with an equilibration temperature of 4 °C (data in Figure III-3; parameters in Table III-II) were fit to equations of the Langmuir type. Peptide adsorption was found to be reversible with respect to dilution. Fitting was done using the method of weighted least squares [141], in which the isotherm parameters Γ_{max} and K_{eq} in Equation (III-1) were found which minimize the sum of weighted residuals (R), where:

$$R = \sum_i \left[\frac{\Gamma_i - \Gamma(c_i)}{\delta\Gamma_i} \right]^2 \qquad \textbf{(III-7)}$$

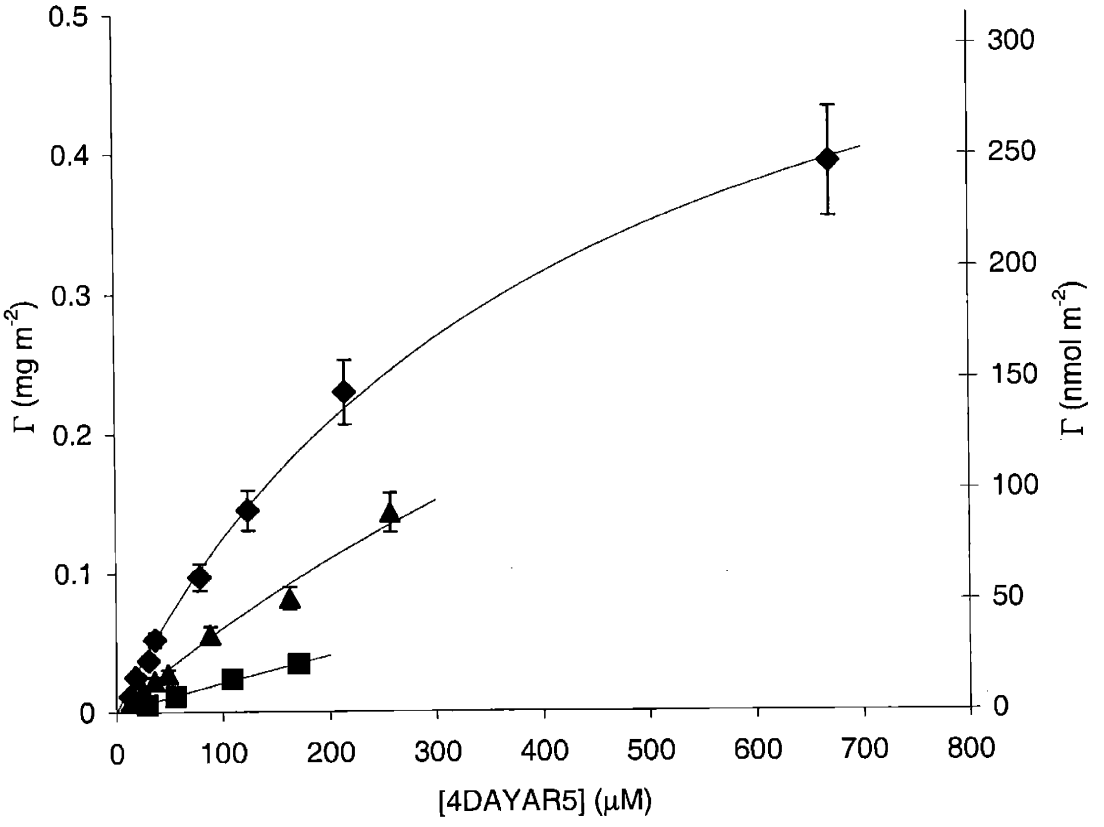

Figure III-3. Adsorption isotherms of 4DAYAR5 on Ludox TM, as a function of pH, in 5 mM phosphate buffer at an equilibration temperature of 4 °C: (■) pH 7, 5 wt% SiO_2; (▲) pH 8, 2.3 wt% SiO_2; (◆) pH 9, 2.3 wt% SiO_2. Fitting parameters are given in Table III-II.

Table III-II. Experimental and fitting parameters for adsorption isotherms of 4DAYAR5 on Ludox TM at an equilibration temperature of 4 °C.

pH	*Buffer*	*Ionic Strength*	*SiO_2 wt%*	K_{eq} (M^{-1})	Γ_{max} (mg m^{-2})
7	5 mM phosphate	0.018 M	5.0	333	0.64
8	5 mM phosphate	0.018 M	2.3	1028	0.64
9	5 mM phosphate	0.018 M	2.3	2385	0.64

Here, i is an index which is summed over the experimental data points for peptide concentration and adsorbed amount (c_i, Γ_i), each of which has an associated uncertainty ($\delta\Gamma_i$). $\Gamma(c_i)$ is the Langmuir isotherm function evaluated at c_i. The maximum surface coverage is accurately measurable only at pH 9, so this parameter was held constant in fitting data obtained at lower pH values. Given the quality of fit obtained with the Langmuir model,

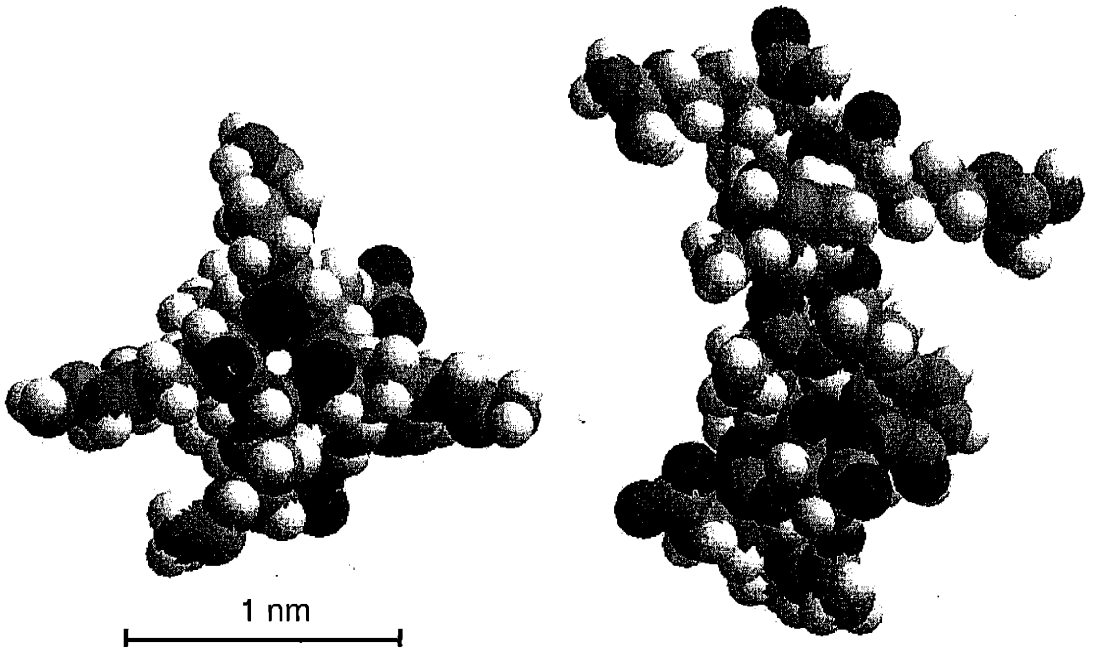

Figure III-4. Ideal α-helix model of 4DAYAR5 produced using Cerius2 (Accelrys) and visualized using a spacefilling model (Shapely color coding). α-Helix angles are $\phi = -62°$, $\psi = -45°$. The molecule is shown with the α-helix axis perpendicular to the page (left); and with the α-helix axis aligned vertically within the page (right). The scale bar is 1 nm.

fitting this data to a more complex isotherm equation is not justified. An extrapolated monolayer coverage of 0.64 mg m^{-2} (400 nmol m^{-2}) is observed, which corresponds to approximately one peptide molecule per 4 nm^2. For perspective, Figure III-4 shows the space-filling model of the ideal α-helical peptide; a steric dimension of approximately 4 nm^2 is consistent with a variety of orientations of the adsorbed α-helical peptide relative to the surface.

Data for the amount of 4DAYAR5 adsorbed reversibly to Snowtex ZL colloidal silica at pH 7–9 with an equilibration temperature of 25 °C (data in Figure III-5, parameters in Table III-III) were fit, using the weighted-least-squares method described above, to equations of the Langmuir and Frumkin types to facilitate comparison. In this case, the Frumkin model provides a better fit. However, certain combinations of parameters of the Frumkin equation may be widely varied while producing essentially the same curve, making precise specification of parameters difficult unless the previous extrapolated monolayer coverage of 0.64 mg m^{-2} (400 nmol m^{-2}) was retained in the Frumkin fits.

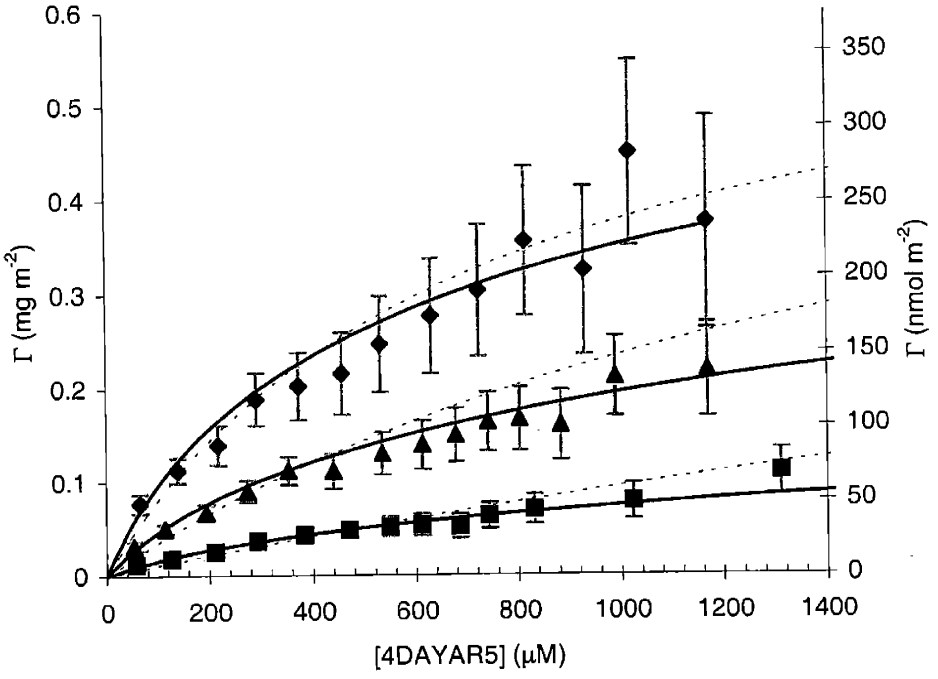

Figure III-5. Adsorption isotherms of 4DAYAR5 on Snowtex ZL, as a function of pH, in 10 mM buffer at an equilibration temperature of 25 °C: (■) pH 7, phosphate buffer, 6.48 wt% SiO_2; (▲) pH 8, tris buffer, 2.94 wt% SiO_2; (◆) pH 9, borate buffer, 1.32 wt% SiO_2. Data points are fit with Langmuir (dashed) and Frumkin (solid) equations. Parameters are given in Table III-III.

Table III-III. Experimental and fitting parameters for adsorption isotherms of 4DAYAR5 on Snowtex ZL at an equilibration temperature of 25 °C. For Langmuir and Frumkin fits, Γ_{max} was held constant at 0.64 mg m^{-2}.

pH	*Buffer*	*Ionic strength*	*SiO_2 wt%*	*T (°C)*	*Langmuir*	*Frumkin*	
					K_{eq} (M^{-1})	*K_{eq} (M^{-1})*	α
7	phosphate	0.035 M	6.48	36	173	302	-3.6
8	tris	0.035 M	2.94	36	577	927	-1.2
9	borate	0.035 M	1.32	36	1432	2002	-0.46

Adsorption isotherms were fit with the Langmuir ($\alpha = 0$) or Frumkin ($\alpha \neq 0$) models under the assumption that the plateau surface coverage, Γ_{max}, is independent of temperature, pH, and fitting method. This parameter is thought to be determined mainly by the steric exclusion of adsorbed molecules. Though some variation in the effective area of adsorbed molecules is possible depending on adsorption conditions, this effect should be relatively small compared to the large changes observed in K_{eq}. Specification of the surface area allows trends in K_{eq} to be examined with confidence, since trends in the relative values of K_{eq} are not

sensitive to the value adopted for Γ_{max}. To a first approximation, the magnitude of the K_{eq} values derived from Equation (III-3) are inversely proportional to the value selected for Γ_{max}. Thus, errors in the value of Γ_{max} introduce a relatively uniform scaling factor into the derived values of K_{eq}. This scaling factor has little effect on the relative free energy values calculated, although it adds uncertainty to the absolute values of the free energy terms.

A large amount of scatter was observed in data points at concentrations of 4DAYAR5 above 800 μM. These points were not used in calculations of isotherm fitting parameters, though this made little practical difference in the resulting values because of the large error bars associated with these points.

Adsorption isotherms based on only a few data points can appear to follow the Langmuir form, when in fact deviations from the Langmuir form are found when a large number of data points are collected to provide higher resolution. Since any isotherm for reversible adsorption reduces to the Langmuir isotherm under sufficiently stringent assumptions, models such as the Frumkin approximation produce similar curves in physical situations which are closely equivalent to the idealized Langmuir model. Distinguishing between these models, or obtaining accurate fitting parameters, is quite difficult in the presence of limited data points and experimental uncertainty. To provide standardization to the isotherms presented in this work, calculations are done using parameters from Langmuir fits to adsorption data on Snowtex ZL particles, and a value of $\Gamma_{max} = 0.64$ mg m^{-2} is used for the monolayer coverage of 4DAYAR5.

A number of important observations can be made from these adsorption isotherms, which are not qualitatively affected by any of the issues discussed above. First, as the pH is raised from 7 to 9, the equilibrium constant for adsorption increases. This behavior is attributed to the increased negative surface charge on the colloidal silica substrate due to deprotonation of silanol groups at higher pH. The strong pH dependence of the adsorption process, combined with the insensitivity of the peptide α-helical structure to pH within this range, suggest that the adsorption is driven by electrostatic interactions between the peptide and the surface, with the fraction of adsorbed molecules controlled by the substrate surface charge. The driving forces for adsorption are discussed in detail in subsequent sections.

Frumkin fitting parameters for adsorption to Snowtex ZL exhibit trends in adsorption affinities similar to those observed for the Langmuir fits, but with a relatively strong repulsive

($\alpha < 0$) interaction between adsorbed molecules. Significantly negative values of α are to be expected for peptide molecules adsorbed in similar orientations, which would be repelled by the relatively long-range electrostatic interactions between the charged side chains. The repulsion may decrease with increasing pH because of increased screening due to stronger (more negative) surface charge associated with a larger number of adsorbed counterions. Typical values of α from the recent literature include -1.9 for monovalent dicarborbollylcobaltate(III) anions at the organic–aqueous solvent interface [142], +4 to +5 for ionic surfactants on ferrihydrite [143], and +2 to +10 for anionic molybdate species on alumina [144].

Although the pH-dependent isotherms on Snowtex ZL at 25 °C and on Ludox TM at 4 °C demonstrate similar trends, the differences between the two are significant relative to the experimental error. In Section III.4, adsorption affinity will be shown to decrease with increasing temperature; this temperature factor alone accounts for much of the difference between these two sets of isotherms. It is also interesting to note that the isotherms for adsorption to Ludox TM appear to follow the Langmuir model more closely than those for adsorption to the larger Snowtex ZL particles, possibly because the increased surface curvature of the Ludox TM particles suppresses repulsive interactions between adsorbed molecules by increasing the effective distance between them. This hypothesis is supported by the observation that application of the Frumkin model (incorporating repulsive interactions) to the data available for Ludox TM decreases the quality of the fit. In other words, although higher-quality isotherms on Ludox TM would be required for a definitive conclusion regarding which set of isotherms is more appropriate, the available information indicates that 4DAYAR5 adsorbed to Ludox TM follows the Frumkin model with no detectable interactions between adsorbate (i.e., the Langmuir model), but that lateral interactions are detected for the adsorption of 4DAYAR5 to Snowtex ZL.

The deviations from the Frumkin fit appear to follow a regular pattern. This consists of a small plateau, points lying at or slightly below the fit, at peptide concentrations between 400 and 700 μM, depending on pH. At higher concentrations (above 800 - 1000 μM, depending on pH) the deviations from the model become large and positive. The intermediate deviations are on the order of the experimental error, while the latter deviations are significant. Both sets could arise from oversimplification of the interactions between

adsorbed molecules. At high concentrations the average distance between peptides decreases, and their interaction may become attractive due to van der Waals or hydrophobic interactions, as amply demonstrated by the helix–strand transition observed for these peptides in solution, as mentioned in Chapter II. The simple form of the adsorption energy given in Equation (III-2) cannot account for this complex distance dependence. The simple treatment of attractive interactions in the Frumkin model can cause a rapid increase in the adsorption isotherm at a concentration that is controlled by the fitting parameters, and the model of Minton [131] in particular predicts more general deviations from the Langmuir form arising from orientation and association of adsorbed molecules.

Conclusions

Isotherms for the adsorption of 4DAYAR5 to two different types of colloidal silica indicate the importance of electrostatic charge in the adsorption of DAR-type peptides to colloidal silica. A greater extent of adsorption occurs at higher pH, and is associated with a more negatively-charged surface. The importance of surface charge will be supported and expanded in the following sections. There is evidence for interactions between adsorbed molecules, since the Frumkin isotherm provides a better fit to the adsorption isotherm of 4DAYAR5 on Snowtex ZL than the Langmuir isotherm. The dipolar charge distribution on DAR-type peptides could give rise to a repulsive interaction between similarly-oriented adsorbed molecules, accounting for the observed negative values of the Frumkin constant (α).

4. Adsorption Isotherms II: Thermodynamics of Peptide Adsorption

Introduction: Fitting Thermodynamic Parameters

Measurement of adsorption isotherms at a variety of temperatures gives an estimate of the thermodynamic parameters for the adsorption process. With suitable assumptions, these results can be used to calculate the free energy, enthalpy, and entropy of adsorption. In the

reversible process discussed here, these thermodynamic parameters govern the amount adsorbed and provide insight into the mechanism of adsorption.

The equilibrium constant for adsorption may be derived from either the Langmuir or Frumkin isotherm, and is directly related to ΔG_{ads}, the free energy of adsorption:

$$\Delta G_{ads} = \Delta H_{ads} - T\Delta S_{ads} = -RT \ln K_{eq} \qquad \textbf{(III-8)}$$

where T is the temperature and R is the ideal gas constant, 8.314 J mol^{-1} K^{-1}. The temperature dependence of the adsorption free energy is related to the enthalpy of adsorption (ΔH_{ads}), through the van't Hoff equation [129] in the form:

$$\left(\frac{\partial \ln K_{eq}}{\partial\left(T^{-1}\right)}\right)_{\theta} = -\frac{\Delta H_{ads}}{R} \qquad \textbf{(III-9)}$$

The above equations apply only to reversible adsorption, although the energy of adsorption is allowed to vary with surface coverage (θ) as in the Frumkin model. Under the more restrictive Langmuir model, the enthalpy of adsorption is independent of surface coverage; in this case the derivative in Equation (III-9) becomes a total derivative. For irreversible adsorption, which is generally observed for proteins, isotherms may be fit with the Langmuir model, but the binding constants obtained can only be taken as a qualitative measure of adsorption affinity. Estimates of the minimum error involved in treating protein adsorption as a reversible process [18] have shown that in some cases the thermodynamic parameters such as ΔG_{ads} derived from these fits are significantly in error. In this case, ΔH_{ads} and $(\Delta C_p)_{ads}$ are the only thermodynamic parameters available, since they may be determined directly through isothermal titration microcalorimetry [21,25,33]. For a model protein at a charged interface, ΔH_{ads} ranges from 50-1000 kJ mol^{-1}, and varies substantially within this range with surface coverage and solution pH. Such variations indicate that interactions among adsorbed molecules as well as electrostatic effects contribute significantly to the driving force for protein adsorption.

Changes in $(\Delta C_p)_{ads}$ are thought to reflect hydrophobic and other entropic effects[145]. Estimates of the entropic driving force for protein adsorption are derived from the increased

number of conformations Ω_2 accessible to the backbone dihedral angles in the random-coil conformation relative to the number of accessible conformations Ω_1 in regular secondary structures (α-helix or β-strand):

$$\Delta S_{conf} = RT \ln(\Omega_2 / \Omega_1)$$

(III-10)

If the number of accessible conformations increases by a factor of four [145], this contributes 3.5 kJ mol^{-1} per residue to the driving force for adsorption.

In this section, the reversible adsorption isotherms of 4DAYAR5 on Snowtex ZL colloidal silica are fit to Langmuir and Frumkin adsorption isotherms, and the resulting equilibrium constants are used to derive thermodynamic parameters and to gain insights into the driving force for adsorption.

Results

Adsorption isotherms are shown as a function of temperature in Figure III-6. These represent reversible equilibria between peptides in solution and in the adsorbed state. As in Section III.3, they are fit with the Langmuir model in order to obtain an estimate of the equilibrium constant for adsorption. As noted previously, use of the same monolayer coverage (Γ_{max}) and the simple Langmuir model to fit the data ensures that the K_{eq} values extracted from these isotherms represent the correct trend in the data. Uncertainties in the values for K_{eq} are due mainly to the relatively small number of data points available for each isotherm, as well as to the interactions between adsorbed molecules not accounted for by the Langmuir model. The importance of these effects will be assessed by comparison with the Frumkin model.

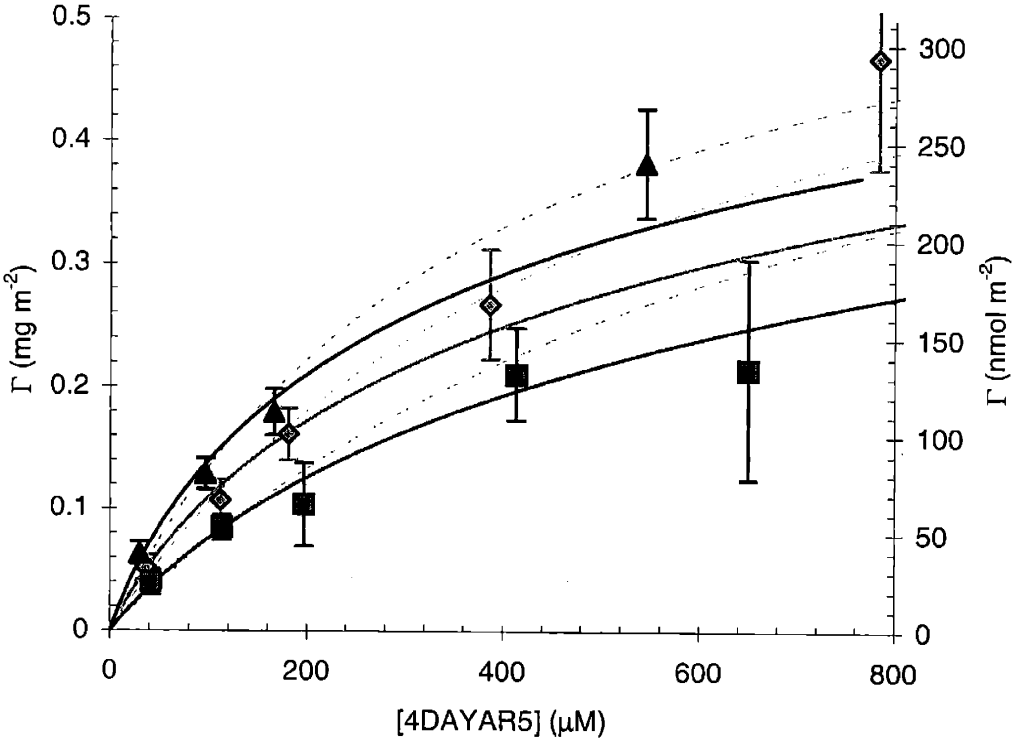

Figure III-6. Adsorption isotherms of 4DAYAR5 on Snowtex ZL at a variety of equilibration temperatures: 45 °C (□); 25 °C (◇); 4 °C (△). Isotherms are fit with Langmuir (dashed) and Frumkin (solid) models using the weighted-least-squares method. Centrifugation parameters are given in Table III-IV.

The equilibrium constants (K_{eq}), measured from the adsorption isotherms, can be used to create the van't Hoff plot shown in Figure III-7. Adsorption parameters resulting from least-squares fits are tabulated in Table III-IV. As is clear from the isotherm data, desorption is a thermally-activated process, with significantly higher adsorption affinities at lower temperatures. The slope of this line gives the enthalpy of adsorption, (ΔH_{ads} = –15 kJ mol^{-1}) at pH 9. Use of the fitting parameters from Frumkin isotherms increases the value of ΔH_{ads} by 2 kJ mol^{-1}. It must be noted that the isotherm data points are consistent with a broad range of equilibrium constants, as indicated by the error bars; the resulting uncertainty in ΔH_{ads} is large (4 kJ mol^{-1}), but this is an upper limit on the uncertainty. In either case, this molar value is much smaller than generally found for proteins, but the enthalpy of adsorption per residue, -1.1 kJ mol^{-1} per residue, is comparable. For example, at the fractional surface coverage θ = 0.5 (this fractional surface coverage is selected as a reference for the literature data only), lysozyme is reported to have ΔH_{ads} values of –1.2, –2.7, and –4.65 kJ mol^{-1} per residue on

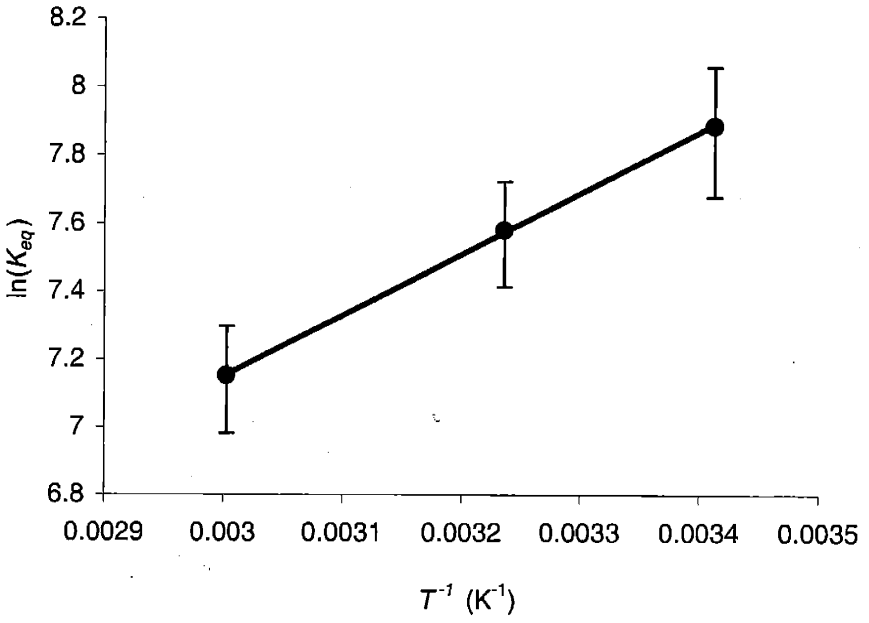

Figure III-7. Temperature dependence of the equilibrium constant for adsorption to Snowtex ZL at pH 9. The error bars indicate the range of equilibrium constants with which the isotherm data is consistent, giving an upper limit on the uncertainty in the resulting thermodynamic parameters.

Table III-IV. Temperature Dependence of adsorption parameters. All fits use $\Gamma_{max} = 0.64$ mg m^{-2}; Frumkin fits use $\alpha = -0.46$ (see Section III.3). Free energies are calculated based on the Langmuir fits.

Equilibration Temperature (°C)	*Centrifugation Temperature (°C)*	*Langmuir Fit K_{eq} (L mol^{-1})*	*ΔG_{ads} (kJ mol^{-1})*	*Frumkin Fit K_{eq} (L mol^{-1})*
4	20	2660	-19.2	3620
25	36	1959	-19.5	2539
45	60	1276	-19.8	1551

negatively-charged polystyrene (pH 7.0), positively-charged polystyrene (pH 7.0), and negatively-charged hematite (pH 9.5) respectively [25].

The enthalpic component of the driving force for peptide adsorption represents a sum of several subprocesses, including those suggested in previous studies of protein adsorption [146]: electrostatic interactions between charged side chains and the silica surface, structural changes in adsorbed molecules, transfer of ions (protons as well as electrolytes) to and from the surface, and changes in the hydration state of the peptide and the surface. Early work on albumin adsorbed to polystyrene latex [146] examined the different components of ΔH_{ads} and showed that the magnitudes of these competing factors can be large relative to the

overall measured enthalpy of adsorption. Driving forces which favor and oppose adsorption offset each other to produce the measured value.

The entropic component of adsorption ($T\Delta S_{ads}$) may be determined in two different ways from Equation (III-8), either by producing individual data points for each temperature studied or by fitting a single value from the temperature dependence of the calculated values of ΔG_{ads}. These give essentially the same result; the latter method gives $\Delta S_{ads} = 14.6$ J mol^{-1} K^{-1} $\equiv$ 1.1 J mol^{-1} K^{-1} per residue. The measured entropy of adsorption is somewhat more sensitive to curve fitting parameters than the enthalpy of adsorption. For example, if the Frumkin isotherm parameters are used, the calculated entropy of adsorption decreases to 9 J mol^{-1} K^{-1}.

Little data is available for comparison since this calculation generally cannot be done for protein adsorption due to the irreversibility of the process. Using Equation (III-10), a large, positive entropy of adsorption is generally assumed for proteins as a result of conformational changes. Conformational changes are explored in depth in Section III.6; for now it is noted that the entropy of adsorption given above for DAR-type peptides adsorbed to SiO_2 probably includes important contributions from factors other than conformational change, which could either decrease or increase the observed entropy of adsorption. Dehydration of the silica surface could decrease the entropy by forcing surrounding water molecules to compensate for lost hydrogen bonds by ordering; this is often referred to as formation of "ice-like" structure in the near-surface region. Ordered water at a silica-water interface has been observed by sum-frequency spectroscopy [147] and its formation is strongly pH-dependent. By contrast, displacement of small ions from the surface could contribute to an increase in the overall entropy of adsorption.

Conclusions

Adsorption isotherms for 4DAYAR5 at three different temperatures indicate that adsorption is a thermally-activated process. The reversibility of peptide adsorption allows the calculation of quantities that are inaccessible from protein adsorption studies, which makes it possible for the balance of interactions to be explored further.

The enthalpy of adsorption of 4DAYAR5 at pH 9 is -17 ± 4 kJ mol^{-1}. On a per-residue basis, this is roughly comparable to values for protein adsorption [25]. The entropy of adsorption under these same conditions is 14.6 J mol^{-1} K^{-1}. Although there is no good comparison for the entropy term, the value is relatively small, little more than the entropy of α-helix formation of two residues from the random-coil state (11 J mol^{-1} K^{-1}, calculated from Equation (III-10)). The relation of these quantities to the electrostatic driving force and conformational changes associated with peptide adsorption will be discussed in the remainder of this chapter.

5. Adsorption Isotherms III: Dependence on Peptide Sequence

Introduction

Measurement of adsorption isotherms for a variety of DAR-type peptides permits further elucidation of the mechanism of adsorption. Variations within the DAR-type peptides studied here incorporate a series of essentially constant chain lengths, with progressive substitution of charged side chains for alanine residues. Since the overall α-helicity remains on the same order of magnitude for these peptides, this set of molecules provides a systematic increase in the importance of electrostatic interactions, while maintaining the overall robustness of the α-helicity approximately constant. Differences in the equilibrium constant for adsorption therefore provide quantitative measurements of the importance of adding a pair of complementary electrostatic interactions between the peptide and surface, while maintaining no net charge on the peptide.

Finally, the role of a net charge on the peptide in producing complete adsorption is measured. Subsequent experiments will require systems in which the vast majority of peptide is adsorbed in order to eliminate contributions to measurements from molecules in solution.

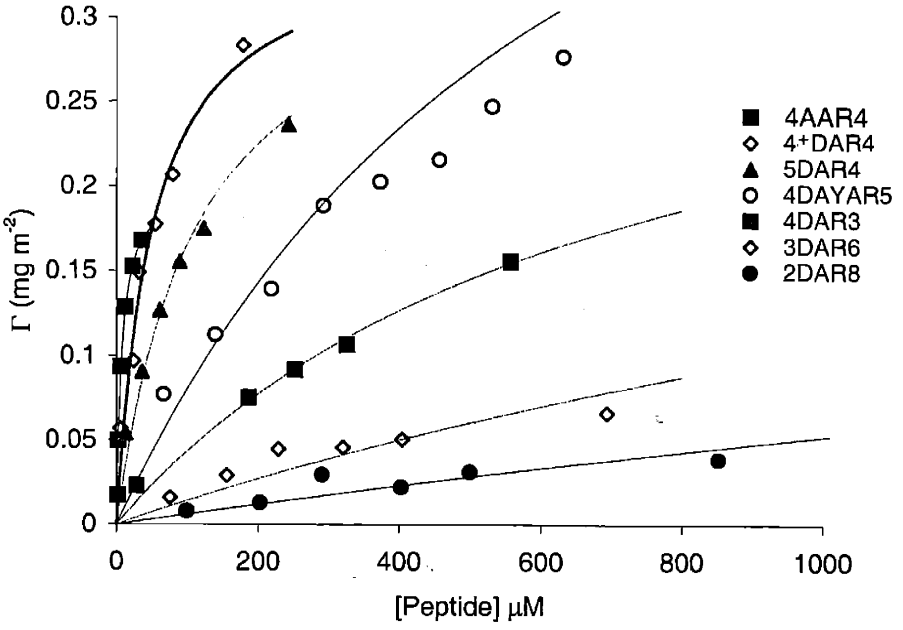

Figure III-8. Adsorption isotherms for peptides of various residue compositions on Snowtex ZL at pH 9 (except 4AAR4; pH 8). All isotherms were fit using the weighted-least-squares method described previously in Section III.3.

Table III-V. Peptides used in adsorption isotherms, and resulting adsorption isotherm parameters. Comparison of free energies of adsorption for various peptides. Adsorption free energy is calculated as: $\Delta G_{ads} = -RT \ln(K_{eq})$. Γ_{max} was fixed for certain peptides as described in the text.

Peptide	K_{eq} ($L\ mol^{-1}$)	Γ_{max} ($mg\ m^{-2}$)	$K_{eq}\Gamma_{max}$	ΔG_{ads} ($kJ\ mol^{-1}$)
2DAR8	176	0.35	62	-13.3
3DAR6	419	0.35	147	-15.5
4DAR3	1422	0.35	498	-18.7
4DAYAR5	1432	0.64	917	-18.7
5DAR4	9011	0.35	3154	-23.4
4^{+}DAR4	20082	0.35	7029	-25.5
4AAR4	147232 (pH 8)	0.20 (pH 8)	29446	-30.6

Results

Adsorption isotherms for various peptides are plotted in Figure III-8, as well as for 4DAYAR5 (measured by UV absorbance) and 4AAR4. Isotherms are fit with the parameters shown in Table III-V. These isotherms appear to display different behavior from peptide to peptide. To demonstrate this, it is noted that the 4DAYAR5 isotherm data points reach as high as 0.43 mg m^{-2}, require a fit with $\Gamma_{max} \geq 0.5$ mg m^{-2}, and deviate substantially from the

Langmuir form. In contrast, the 5DAR4 isotherm appears to follow the Langmuir equation with $\Gamma_{max} = 0.35$ mg m^{-2}; even a small change, to 0.4 mg m^{-2}, significantly decreases the quality of the fit. Both peptides are at the high end of the molecular weight range, making it unlikely that these effects are due solely to molecular weight.

As shown in Section III.3, adsorption isotherms have been measured for 4DAYAR5 with sufficient precision to demonstrate conclusively that the Langmuir isotherm is not followed. The peptides 2DAR8 and 3DAR6 appear to display deviations at similar concentrations of free peptide. Therefore some deviations should be suspected, even for peptides with adsorption behavior in accord with the Langmuir model, such as 4DAR3 and 5DAR4. The limited number of data points available may appear to fit the isotherm, but a higher resolution might reveal deviations. Further investigations of adsorption isotherms of different peptides would be required to fully elucidate these differences, but these questions are beyond the scope of this work.

The following approach was taken for calculation and interpretation of adsorption isotherm fitting parameters, in order to provide standardization and ensure that the proper trends are reflected. Isotherms are plotted with $\Gamma_{max} = 0.35$ mg m^{-2} when the use of this value provides a high-quality fit. For 4AAR4 and 4DAYAR5 this value results in a low-quality fit, and the values used for these two peptides were fit by least-squares and taken from Section III.3, respectively. In actuality, each peptide may have a different value for Γ_{max}; variations in the value of this parameter among peptides could result from differences in the orientational specificity of adsorbed molecules, or in the strength of the interactions between adsorbed molecules. Such differences could be produced by changes in the number of charged sidechains among the peptides studied here. To reduce the impact of the unknown set of Γ_{max} for comparative purposes, the adsorption isotherm parameters are lumped together as the "initial adsorption affinity," $K_{eq} \times \Gamma_{max}$, which is the slope of the isotherm at low surface coverage. The values of the initial adsorption affinity are plotted in Figure III-9 and listed in Table III-V. As described in detail in Section III.3, these values are relatively independent of the choice of the individual values for K_{eq} and Γ_{max}.

Increasing the number of charged amino acid side chains on the peptide termini strongly increases the adsorption affinity. The two peptides that have four charges on each end (4DAR3 and 4DAYAR5) differ by a factor of two, but are closer together compared to

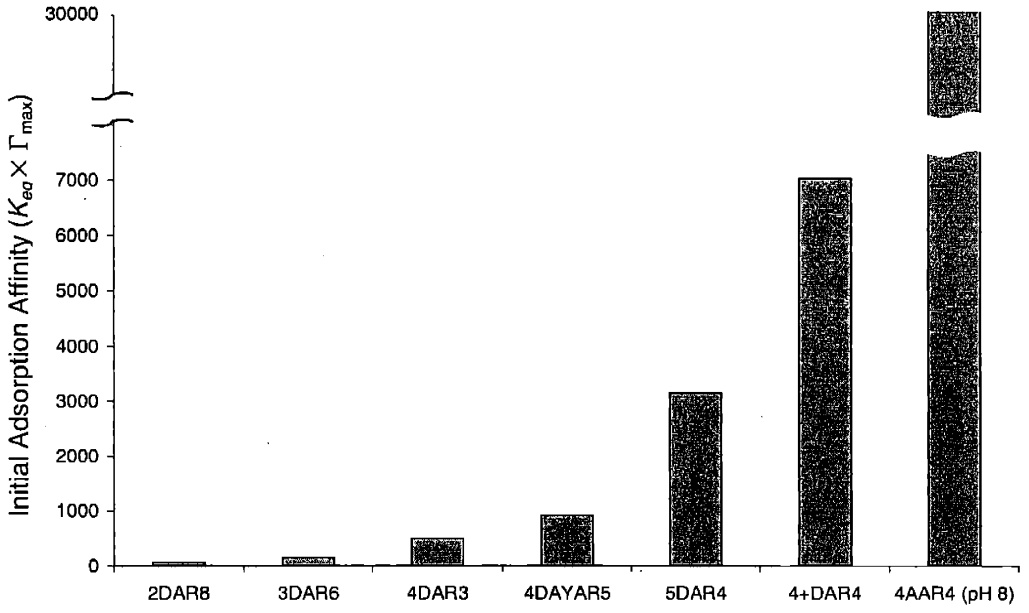

Figure III-9. Initial adsorption affinity $K_{eq} \times \Gamma_{max}$ for adsorption of peptides of various residue compositions on Snowtex ZL at pH 9 (except for AAR, measured at pH 8).

peptides with increasing or decreasing numbers of charged sidechains. The adsorption affinity of decreases by a factor of three when the number of terminal charges is reduced from four (4DAR3) to three (3DAR6), and increases by a factor of three when the number of terminal charges is increased from four (4DAYAR5) to five (5DAR4). As expected, the most dramatic differences in adsorption affinity are made by the addition of net charge. Considering this effect in more detail, the addition of a single arginine (4^+DAR4 vs. 4DAYAR5) increases the adsorption affinity by a factor of three, whereas removing a single aspartate (4^+DAR4 vs. 5DAR4) increases the adsorption affinity by a factor of two.

These trends are dominated by the dependence of the equilibrium constant on the peptide sequence. The magnitude of the difference in the free energy of peptide adsorption becomes progressively greater as more arginine residues are added to the C-terminus of the peptide. This trend provides evidence that arginines contribute to the free energy of peptide adsorption in a cooperative way.

Since adsorption of DAR-type peptides is reversible, ΔG_{ads} can be calculated from the equilibrium constant. However, this calculation is very sensitive to the choice of Langmuir fitting parameters (K_{eq} and Γ_{max}), and, as noted above, there is not a reliable way to get the absolute values of these parameters from the measured isotherms; only their product

$K_{eq} \times \Gamma_{max}$ can be reliably extracted. Comparisons among the values of K_{eq} for the peptides calculated with the same Γ_{max} (2DAR8, 3DAR6, 4DAR3, 5DAR4, and 4^{+}DAR4) are more reliable; these values are given in Table III-V.

Two interesting trends emerge. First, for peptides with no net charge, each additional pair of charged side chains makes a larger contribution to ΔG_{ads}: a third pair (3DAR6) adds -2.2 kJ mol^{-1}, a fourth (4DAR3) adds -3.2 kJ mol^{-1}, and a fifth (5DAR4) adds -4.7 kJ mol^{-1}. Second, when the data for 4^{+}DAR4 and 4AAR4 are examined, it appears that each unit of net charge on the peptide adds about -2 kJ mol^{-1} to ΔG_{ads}. The former trend may indicate some cooperativity in the binding of arginine residues to the surface, where the stabilization due to each additional residue is increased by the residues already adsorbed to the surface. The latter trend may be useful in controlling the binding affinity of reversibly-adsorbed molecules to silica surfaces.

Conclusions

Adsorption isotherms for peptides with different amino acid compositions have been used to quantify the effect of charged side chains on adsorption affinity through calculation of the initial adsorption affinity ($K_{eq} \times \Gamma_{max}$), and the adsorption free energy (ΔG_{ads}). Though these latter values suffer from uncertainty in the values of Γ_{max}, it is clear that the addition of net charge makes a greater difference in ΔG_{ads} than the addition of pairs of oppositely-charged side chains to peptides, maintaining no net charge. It appears that each net charge contributes to an equal extent to the free energy of adsorption; in contrast, the free energy contributed by addition of pairs of complementary charges (maintaining no net charge) appears to increase with the number of charged groups already in the peptide, providing evidence for cooperativity in the mechanism by which cationic arginine sidechains contribute to the free energy of adsorption.

6. CD Studies of Adsorbed Conformation

Introduction

Circular dichroism of adsorbed molecules is possible in two different configurations. First, a multiplate geometry has been described [38] where the light path is passed through several thin quartz plates. This configuration is very versatile, since a wide variety of polymers may be spin-coated into thin transparent layers, and several well-known strategies exist for derivatizing silica to produce well-defined surface functionalities [148,149]. However, the equipment is specialized, and the signal-to-noise ratio is quite low due to the relatively small amount of protein in the interfacial layers. Each additional plate increases the amount of protein in the light path but reduces the intensity of light transmitted.

More conventionally, molecules are adsorbed to ultrafine particles, and the CD spectrum of the resulting liquid suspension is measured. Even the larger Ludox TM particles are sufficiently small that light-scattering does not impair measurement of CD spectra between 190 and 250 nm, although Snowtex ZL particles (74 nm diameter) do scatter light in this range. Direct measurements have been made of the conformation of a variety of adsorbed proteins [39] and single-residue mutants [150,151] as a function of adsorption conditions such as temperature, surface coverage, and pH [42,152].

Other colloidal particles may be used as well, provided that they have no electronic absorbance in the wavelength range of interest. Thus, commercially-available ultrafine polystyrene latexes cannot be used because they are not transparent below 220 nm, but the CD spectra of model proteins adsorbed to colloidal tetrafluoroethylene particles have recently been reported [43,44].

CD signal intensity is proportional to concentration [37], so that with knowledge of the CD spectrum of free molecules and the fraction of adsorbed molecules, the signal can be analyzed to reveal the contributions from each fraction[5]. Since data for the fraction of adsorbed peptide has been provided in previous sections of this chapter (for 4DAYAR5,

[5] This analysis is based on the assumption that the surface does not affect the intrinsic CD spectral properties of adsorbed molecules. In other words, it is assumed that the CD spectrum arising from an adsorbed peptide with a given conformation is identical to that from a molecule in solution with the same conformation. Adsorption to silica may alter the local electrostatic field, but it does not provide any electronic transitions to which the n-π^* transition can couple. Thus the presence of the surface is unlikely to affect the intrinsic CD spectrum of adsorbed molecules.

Section III.3; for other peptides, Section III.5), the CD spectra of adsorbed DAR-type peptides can be measured as a function of pH and compared to those of free peptides. The results are related to the electrostatic model of adsorption developed in previous sections.

Experimental: CD Spectroscopy of Peptide/Colloid Suspensions

CD spectra of colloidal suspensions were measured using the wavelength and averaging parameters described in Chapter II.2. Briefly, CD spectra were measured in 1 mm pathlength cells between 190 and 250 nm, at 1 nm intervals using a minimum averaging time of 2 s per data point. In order to evaluate α-helicity loss in adsorbed molecules, the initial solution concentration of 4DAYAR5 was measured using the known $-[\theta]_{222}$ value, which is an average of the CD signal in the range 221-223 nm. Sample solutions were then prepared with the desired concentrations of peptide and colloid. For CD, weighing samples was not practical, and dilutions were controlled by micropipetting. The same pipette was used for each dilution, and measurements were found to be highly reproducible. Between measurements, the sample cell was rinsed with deionized water, then with 0.025 ml of sample in order to prevent unintended dilution of samples by residual rinse water. The cell was then filled, the CD spectrum measured, and the observed value of $-[\theta]_{222}$ used to calculate the α-helicity remaining in adsorbed molecules according to Equation (III-11).

Measurements were obtained for a variety of DAR-type peptides. Representative results from the peptide 5DAR4 thermostatted at 25 °C are presented here; these samples contained 1.9 wt % Ludox HS, and 215 μM total peptide in solution. In addition, measurements of the α-helicity of 4DAYAR5 on Ludox TM at 4 °C and Ludox HS at 25 °C are presented and compared with the adsorption isotherms in Section III.3. Concentrations of 4DAYAR5 for samples adsorbed to Ludox TM (to be compared with adsorption isotherms on Ludox TM) ranged from 50 to 300 μM total peptide in solution; the silica concentrations used for these samples were 6.5, 2.9, and 1.3 wt % for pH 7, 8, and 9, respectively. Concentrations of 4DAYAR5 for samples adsorbed to Ludox HS ranged from 50 to 1000 μM total peptide in solution; the silica concentrations used for these samples were 2.4 and 0.44 wt % for pH 7 and 9, respectively. This data for Ludox HS was collected for comparison with the adsorption

isotherms on Snowtex ZL, since measurements of CD spectra for peptide adsorbed to Snowtex ZL are not possible due to light scattering. Finally, CD measurements of a variety of peptides were taken with the peptides in solution (no colloid) and in solutions with a high silica content, 6.9 wt% Ludox HS, in 10 mM sodium borate buffer at pH 9. The typical total concentration of peptide in these samples was 0.2 mg ml^{-1} (≈ 150 μM peptide).

Results

In the presence of colloidal silica, the CD spectra of the α-helical peptides studied here display a loss of α-helicity as pH is increased in the range between pH 7–10. In the absence of colloidal silica, the CD spectra of these peptides are independent of pH in this range (Chapter II.3). Increasing pH has been shown to be associated with an increase in the amount of adsorbed peptide; therefore, the observed α-helicity decreases result from the adsorption of peptide to the silica surface. Representative CD spectra of 5DAR4 in solution and adsorbed to silica (pH 6.8–11) are shown in Figure III-10. Some peak intensity remains in the band at 222 nm, partly due to the adsorption equilibrium, in which a certain fraction of the peptide remains in solution, with unperturbed conformations. The new, pronounced negative band at 198 nm that is present in the spectra of adsorbed peptides is evidence of a coiled structure [37]. For the peptide concentrations used in this study, there is no evidence for the β-strand conformation, which would be indicated by an additional characteristic negative band at 215 nm.

As the pH is increased to favor adsorption, an isodichroic point is observed at 202 nm, indicating a shift in the relative populations of the two peptide conformations (α-helical and coiled). An isodichroic point is also observed at 202 nm as temperature is increased; however, the spectral changes differ qualitatively in the relative intensities of the signal at 198 nm [82,88,89]. The different appearance of the spectra of adsorbed molecules relative to spectra of molecules in solution at elevated temperatures indicate that, although both populations have decreased α-helicity relative to molecules in solution at low temperature, the two factors that induce loss of α-helicity result in different conformational tendencies. Thermal destabilization is likely to favor conformations in which dihedral angles are

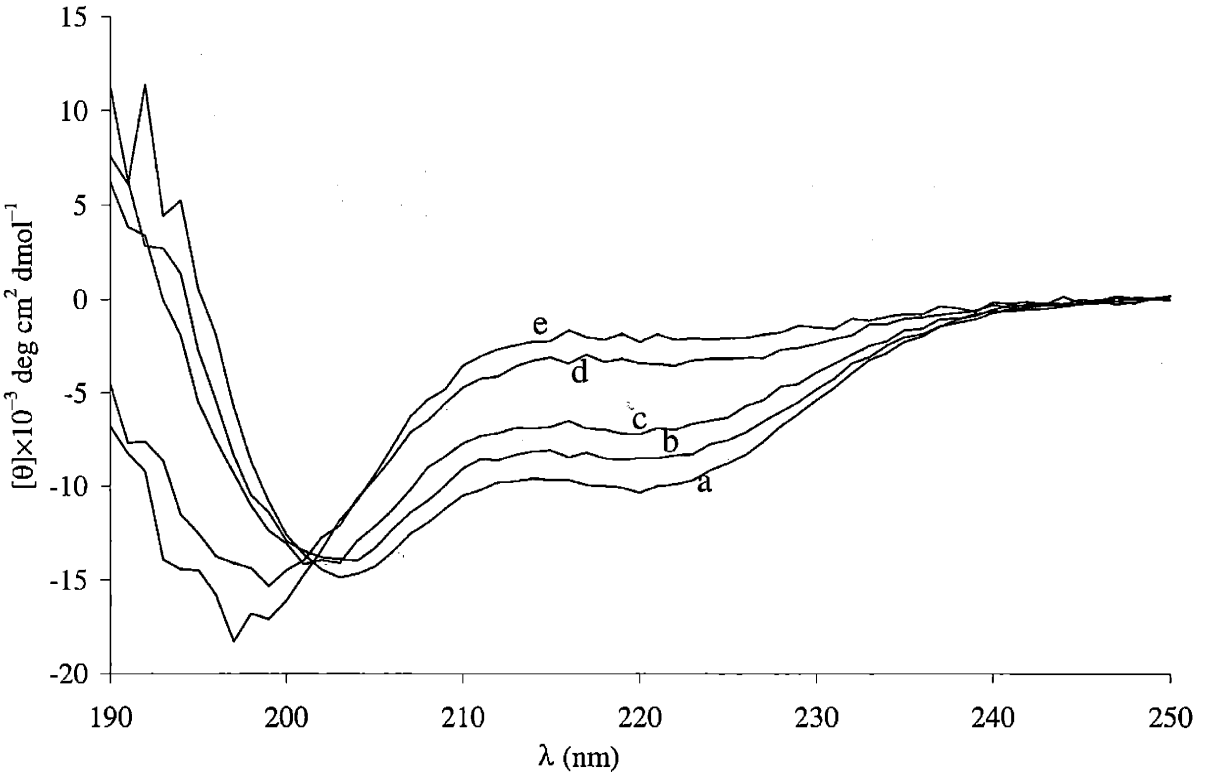

Figure III-10. Progressive changes in CD spectra of 5DAR4 with increasing adsorption to Ludox HS colloidal silica. (a) 215 μM 5DAR4 free in solution; (b) the same peptide concentration with 1.9 wt % Ludox HS, pH 6.8; (c) the same peptide and silica concentrations at pH 7.9; (d) pH 9.2; (e) pH 11.3. Increased pH does not significantly affect the α-helicity of the peptide in the absence of colloid, as shown in Figure II-8.

independent of surrounding residues, referred to as random-coil. The coiled conformations resulting from adsorption to a surface are not the same as those favored by elevated temperatures. Adsorption of DAR-type peptides to a surface thus appears to favor formation of a specific conformation, which has spectral properties distinct from those of the familiar secondary structures.

No time dependence is observed within the time scale of the CD experiment (30 s to 2 h). α-Helicity loss associated with adsorption of DAR-type peptides to colloidal silica particles is observed to be reversible. If adsorption parameters are varied to induce desorption, for example a decrease in the pH of the sample from 9 to 7, the CD signal smoothly reverts from the coiled type to the α-helical type.

Decreased intensity of the peak at 222 nm in the CD spectra indicates that adsorption to colloidal silica induces a conformational change in the peptides, yet it is apparent that both

α-helical and coiled structures are present. Since the fractions of adsorbed (X^{ads}) and non-adsorbed (X^{free}) molecules are known from sedimentation data, the α-helicity of the adsorbed molecules ($-[\theta]_{222}^{ads}$) can be calculated from the measured specific helicity of the molecules in the sample ($-[\theta]_{222}^{meas}$):

$$[\theta]_{222}^{meas} = X^{free}[\theta]_{222}^{free} + X^{ads}[\theta]_{222}^{ads}$$

(III-11)

where $-[\theta]_{222}^{free}$ is the α-helicity of the molecules in solution at the adsorption temperature. This results in the following relation between the fraction of α-helicity retained by adsorbed molecules relative to their α-helicity in solution (φ_{Hel}^{ads}), and the experimentally-measured helicity of the sample relative to the helicity in the absence of colloid (φ_{Hel}^{meas}):

$$\varphi_{Hel}^{meas} \equiv \frac{[\theta]_{222}^{meas}}{[\theta]_{222}^{free}} = X^{free} + X^{ads}\left(\frac{[\theta]_{222}^{ads}}{[\theta]_{222}^{free}}\right) = X^{free} + X^{ads}\left(\frac{f_{Hel}^{ads}}{f_{Hel}^{free}}\right) = X^{free} + X^{ads}\varphi_{Hel}^{ads}$$

(III-12)

In this work, the quantity f_{Hel}^{ads} is the fraction of α-helicity in the molecule (relative to a perfectly α-helical molecule) calculated from CD measurements of $[\theta]_{222}$ using the length-dependent Equation (II-2). In contrast, φ_{Hel}^{ads} denotes a ratio between α-helicity values measured for the same peptide at the same temperature.[6] The subscript indicates whether the ratio is one of α-helicity retained (*Hel*) or lost (*Loss*, used to simplify subsequent equations), and the superscript refers to the population of molecules being measured: adsorbed molecules (*ads*), free in solution (*free*), or all the peptides in the sample (*meas*).

Each CD measurement (φ_{Hel}^{meas}), combined with the free and adsorbed fractions (X^{free} and X^{ads}), thus produces a conformational measurement of adsorbed molecules (φ_{Hel}^{ads}). These two quantities were measured under the same conditions by CD and UV absorbance spectroscopy for adsorption of 4DAYAR5 to Ludox TM, but not for adsorption to Ludox HS

[6] Note that the symbol for ratios of fractional helicity (φ) has a different meaning from the dihedral angle (ϕ).

since, as noted above, these particles are too small to be sedimented conveniently. In order to find the fraction of adsorbed peptide X^{ads} for samples containing 4DAYAR5 and Ludox HS, the adsorption isotherms of this peptide (measured at the same temperature) on Snowtex ZL were used. Values of φ_{Hel}^{ads} can be derived from the adsorption isotherm plot in a simplified way, as shown in Appendix A.

For 4DAYAR5 adsorbed to Ludox TM at 4 °C, the average of three (pH 7) or four (pH 8, 9) measurements between 20 and 271 μM indicated that adsorbed molecules retained 45%, 40%, and 25% of α-helicity at pH 7, 8, and 9, respectively[7]. Adsorbed peptide molecules undergo a partial loss of α-helicity; that is, on average, some residues of the α-helix unwind to a coiled structure, although some α-helical structure (and intensity of the $-[\theta]_{222}$ signal) is retained.

Adsorbed molecules retain less α-helicity when adsorbed at a more basic pH. Increased pH does not significantly affect the α-helicity of the peptide in the absence of colloid, as shown in Figure II-8. This suggests that conformational changes, as well as adsorption in general, are driven by electrostatic interactions between the peptide and surface. At more basic pH values, and, correspondingly, more strongly negative surface charge values, the positively-charged arginine side chains are more strongly attracted to the silica surface, while the negatively-charged aspartate side chains are more strongly repelled from the surface. Thus, a driving force for elongation of the peptide molecule is established, in order to maximize the average distance of the aspartate side chains from the surface while maintaining the arginine side chains fixed at the surface. Recalling that, for peptides in solution, the electrostatic interactions between the side chains promote a smaller end-to-end peptide distance, and that electrostatic interactions clearly have a strong influence on peptide conformation (as demonstrated by the large decrease in α-helicity observed for the corresponding RAD-type peptides relative to the DAR-type peptides; Chapter II.2), it is not surprising that reversal of the electrostatic driving force to promote a longer end-to-end distance of the molecule is associated with conformational changes. Intramolecular interactions are rebalanced such that conformational entropy now pulls the ends of the

[7] Aromatic residues have been shown to affect the CD spectra of helical peptides as mentioned in Chapter II.2 [98], but to the extent that such effects are the same for peptides in solution or adsorbed, they are eliminated by use of the equation for relative helicity loss Equation (III-12).

molecule together, while electrostatic interactions push them apart. Conformational changes in adsorbed molecules will be explored in more detail in Chapter IV.2.

In general, Equation (III-12) allows the conformation of adsorbed molecules to vary with concentration and surface coverage. CD data was collected at a range of peptide concentrations (corresponding to a range of surface coverages), in order to determine whether the conformation of adsorbed molecules depends on surface coverage. For 4DAYAR5 adsorbed to Ludox HS, the α-helicity measurements (φ_{Hel}^{meas}) were analyzed using the adsorbed fraction (X^{ads}) calculated from the isotherms of this peptide on Snowtex ZL as described in detail in Appendix A. The results are shown in Figure III-11. As found from the measurements of 4DAYAR5 conformation on Ludox TM, adsorbed molecules retain less α-helicity at pH 9 than at pH 7. However, the coverage dependence of this data displays interesting trends: adsorbed molecules retain less α-helicity at higher surface coverages at pH 7, whereas at pH 9, higher surface coverages lead to increased α-helicity. This data is fairly sensitive to experimental error since it depends on the difference between two relatively independent sets of spectroscopic measurements. In particular, one would expect the dependence of φ_{Hel}^{meas} on surface coverage to be very small at low surface coverages, where adsorbed molecules are unlikely to interact. The data for adsorption at pH 7 does not follow this trend, possibly indicating that the use of two different types of colloidal silica distorts the trends.

The forces that determine the α-helicity of adsorbed peptides may be quite complex:

- Steric interactions, as well as longer-range electrostatic repulsions between the negatively-charged C-termini of molecules uniformly adsorbed in an "end-on" orientation could favor certain elongated, coiled conformations that have smaller lateral dimensions than α-helices.
- Larger amounts of adsorbed peptide lead to increased ionic strength at the surface, increased screening of surface charge, and a reduction in the electrostatic driving force to separate the aspartate side chains from the surface. This would tend to promote α-helicity gain at higher surface coverage by reducing the electrostatic driving force for elongation of the molecule.

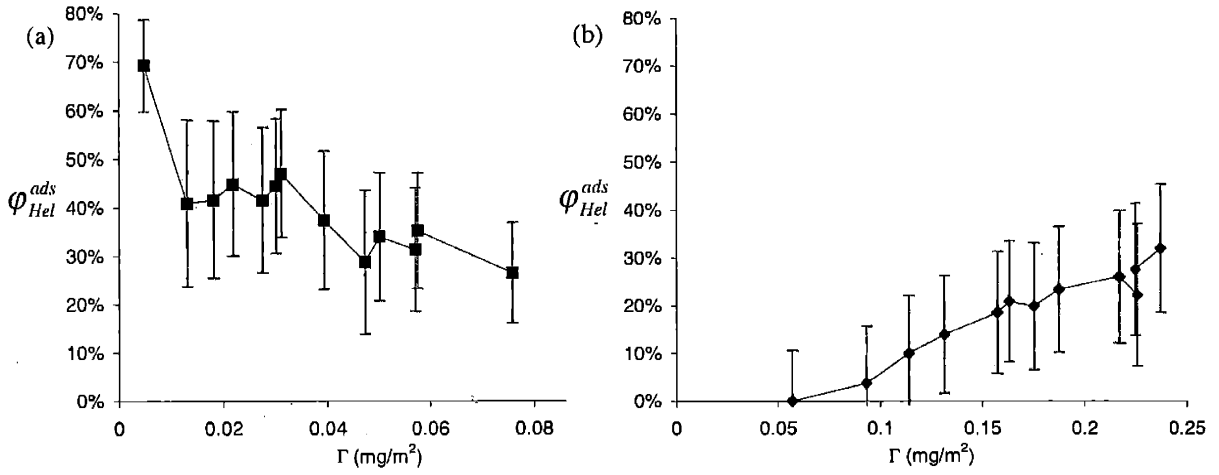

Figure III-11. Percentage of α-helicity retained by adsorbed 4DAYAR5 relative to 4DAYAR5 in solution. Peptide is adsorbed to Ludox HS at 25 °C. (a): (■) 2.4 wt%, pH 7; (b): (◆) 0.44 wt%, pH 9. α-Helicity values were calculated from Equation (III-12) using adsorbed amounts obtained from the adsorption isotherms on Snowtex ZL at 25 °C. A detailed description of this procedure is given in Appendix A.

The first factor may be more important at pH 7, where adsorbed molecules are more α-helical and conformation could be sensitive to steric interactions, while the second factor may dominate at pH 9, where the charge on the surface is higher. This would explain the observed difference in trends.

The DAR-type peptides studied here all display qualitatively similar changes in their CD spectra upon adsorption to anionic colloidal silica, but the extent of α-helicity loss in adsorbed molecules varies (Figure III-12). The loss of α-helicity is strongly correlated with the number of charged side chains at the peptide termini, but not with the actual value of the α-helicity in solution. Measurement of α-helicity loss in adsorbed peptides with varying amounts of α-helicity in solution provides a direct measurement of the relation between the degree of α-helical structure in solution and the resistance of this structure to destabilization resulting from adsorption. Since protein structures that have strong thermodynamic stability are often resistant to conformation changes at interfaces [25,150], it is interesting to determine whether a similar trend is observed for short α-helical peptides. The correlation between the α-helicity in solution of any peptide i listed in Table II-II ($-[\theta]_{222,i}$), and the fraction of α-helicity retained by that peptide upon adsorption ($\varphi_{Hel,i}^{ads}$), plotted in Figure III-12, can be calculated from the standard formula [153]

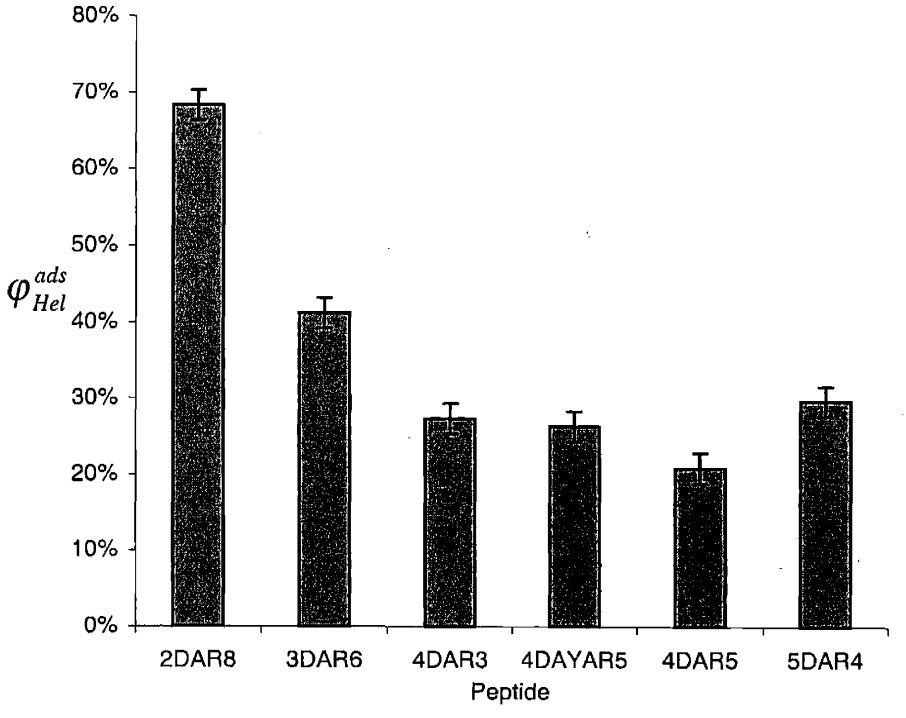

Figure III-12. Percentage of α-helicity retained in peptides of various residue compositions, relative to the α-helicity of the peptide in solution. α-Helicity of peptides adsorbed to Ludox HS colloidal silica at pH 9, in the limit of low surface coverage (less than 0.01 mg m^{-2}), as a percentage of solution α-helicity.

$$\rho_{\theta,\varphi} = \frac{n\sum_{i=1}^{n}\left(-[\theta]_{222,i}\times\varphi_{Hel,i}^{ads}\right)-\left(\sum_{i=1}^{n}-[\theta]_{222,i}\right)\left(\sum_{i=1}^{n}\varphi_{Hel,i}^{ads}\right)}{\sqrt{\left[n\sum_{i=1}^{n}\left([\theta]_{222,i}\right)^2-\left(\sum_{i=1}^{n}-[\theta]_{222,i}\right)^2\right]\left[n\sum_{i=1}^{n}\left(\varphi_{Hel,i}^{ads}\right)^2-\left(\sum_{i=1}^{n}\varphi_{Hel,i}^{ads}\right)^2\right]}}$$

(III-13)

where the sums are calculated over the $n = 6$ peptides shown in Figure III-12. The correlation value $\rho_{\theta,\varphi}$ is only 0.14. This relatively insignificant correlation indicates that, among the molecules studied here, the amount of α-helicity lost upon adsorption is determined mainly by the strength of the electrostatic interactions between the peptide and the surface (governed by the number of charged side chains) and is not strongly dependent on the α-helicity of the molecule in solution. The strength of this interaction is influenced both by the number of charged sidechains in the peptide, and by the pH-dependent surface charge of the colloidal silica, but not by the fractional α-helicity in the molecule.

Conclusions

The CD spectra of peptides adsorbed to ultrafine silica particles provide direct evidence of the conformational changes that occur upon adsorption. Losses of α-helicity observed in the CD spectra of short α-helical peptides in equilibrium with the silica surface can be used, in conjunction with independent data regarding the adsorbed fraction, to determine the α-helicity of the adsorbed molecules. Adsorbed molecules display a partial loss of α-helicity at pH 7, but the fraction of α-helicity lost, and the amount of adsorbed peptide, increase with increasing pH. The fraction of α-helicity lost for adsorbed molecules is determined primarily by the number of charged side chains in the peptide sequence, rather than by the original degree of α-helicity in solution.

7. NMR Studies of Adsorbed Conformation and Orientation

Introduction

NMR studies of proteins at interfaces frequently use specialized solid-state techniques; however, for DAR-type peptides in reversible equilibrium with a surface, a great deal of information can be gained from solution ^{1}H NMR spectra. Some of the information obtained to characterize the conformations of these molecules in solution (Chapter II.4) is also available for adsorbed molecules. In addition, the sensitivity of NMR signals to molecular motions can be exploited to probe the interactions of the peptide molecule with the surface.

An understanding of the effect of motion relative to the magnetic field is central to either solid-state or solution studies of molecules and interfaces. The physics of NMR are described in detail elsewhere [154-156], but a foundation for the concepts relevant to this work is given here. NMR signals arise from the precession of the magnetic moment of a nucleus (with magnetic moment μ and gyromagnetic ratio γ) in an external magnetic field $\bar{B}_0$. This precession occurs for spin I = ½ nuclei at the Larmor frequency,

$$\omega_0 = \gamma B_0$$

(III-14)

For the instrument used in this work (B_0 = 11.7 T), ^{1}H nuclei (γ = 26.75×10^7 rad T^{-1} s^{-1}) precess at a Larmor frequency of 500 MHz. This frequency defines an NMR time scale.

Resolution of a frequency is inversely related to the peak width at half-maximum (FWHM) of the Lorentzian NMR peak, given by [156]:

$$\Delta\nu_{1/2} = \frac{1}{\pi T_2}$$

(III-15)

where T_2 is the transverse relaxation rate. Here it is sufficient to consider the right hand side of this equation to be a measure of how rapidly a signal decays ("relaxes"). For example, broad peaks arise from signals that decay rapidly. If the NMR signal decay is too rapid, the peaks become too broad to be resolved. The typical range of ^{1}H NMR chemical shifts is 10 ppm, or 5 kHz at the magnetic field strength used, such that signals which last less than 0.2 ms broaden into the baseline and are undetectable. Typical frequency separations between ^{1}H NMR chemical shifts range between 0.1 – 1.0 ppm, so that signals must last at least 2 - 20 ms for effective resolution.

The duration of an NMR signal (or its relaxation time) is intimately related to the dynamic motion of precessing nuclei. The mechanisms by which molecular motion translates into signal decay are broadly classified into spin-lattice relaxation and spin-spin relaxation. Spin-spin relaxation dominates when the correlation time of molecular motions (i.e., the time required for random motion to reorient the molecule) is 10^{-8} s or less. Therefore, only this type of relaxation will be considered here, and spin-lattice relaxation can be neglected. Spin-spin relaxation arises from fluctuations in the magnetic field that surrounds a precessing nucleus, which cause a time dependence in the precession frequency. The cumulative effect of small fluctuations in the rotation rate causes the phase of each nucleus to drift relative to the mean transverse magnetization. Treatment of this drift as a random walk leads to the approximation [154,157]

$$\frac{1}{T_2} = \gamma^2 \langle B^2 \rangle \tau_c$$

(III-16)

where $\gamma^2 \langle B^2 \rangle \approx \Delta\omega^2$ is a measure of the fluctuations in the Larmor frequency resulting from the fluctuations in the surrounding magnetic field, and τ_c is their correlation time. The magnitude of these fluctuations can be tens of kHz due to dipolar interactions with surrounding nuclei. Equation (III-16) shows that the duration of an NMR signal is inversely proportional to the correlation time of molecular motion, such that slower molecular motions result in decreased signal duration, a smaller number of measurable precessions, and therefore an increased linewidth.

In this section it is shown that the presence of colloidal silica in solution with DAR-type peptides has dramatic effects on the solution ^{1}H NMR spectra of these molecules. Examining the effects on different resonances supports the electrostatic model of adsorption presented above, and gives evidence for orientation-specific adsorption.

Experimental: Solution ^{1}H NMR Spectroscopy of Peptide/Colloid Suspensions

Solution ^{1}H NMR spectra were collected on a Varian Inova-500 spectrometer with an inverse-coil probe; for 1D spectra 64 transients were typically collected using presaturation of the DHO solvent peak. Peak intensities were referenced to a standard solution of TSP (Aldrich, 98 atom % D, δ = –0.063 ppm from TMS [107]) in 10 mM phosphate buffer (pH ≈ 8), contained in an internal capillary tube (Aldrich). The chemical shift of this standard is known to depend on pH, but this dependence is negligible above pH 7.0 [107]. Typical experiments used peptide concentrations of 1.3 mg ml^{-1}, and colloid concentrations of 1.3 wt % HS-40. Experiments were buffered with 5 mM phosphate (from $NaH_2PO_4 \cdot H_2O$, Na_2HPO_4, or Na_3PO_4). Adjustments to pH were made using small amounts of NaOD and DCl in D_2O.

Average peak positions ($\bar{\delta}$) for βH and D-αH were calculated from the spectral intensity $I(\delta)$ using the center-of-mass formula

$$\bar{\delta} = \frac{\int_{\delta_{min}}^{\delta_{max}} I(\delta) \times \delta \times d\delta}{\int_{\delta_{min}}^{\delta_{max}} I(\delta) d\delta}$$

(III-17)

Integration limits δ_{min} and δ_{max} were held constant for any given peak in solution, but varied when necessary for adsorbed peaks with larger peak shifts. A-αH and R-αH multiplets overlap in 1D spectra; separated peaks were calculated from the average positions of the individual αH/NH cross peaks observed in TOCSY spectra in solution.

NMR spin-lattice (T_1) and spin-spin (T_2) relaxation times were measured using the inversion-recovery and CPMG sequences, respectively [154]. Samples contained 150 μM 4DAR5 in 10 mM sodium phosphate (pH 9) with concentrations of colloidal silica between 0 and 0.5 wt%. Exponential fits were determined by minimizing the sum of squared residuals using the solver contained in a commercial software package (Microsoft Excel); care was taken to ensure that the parameters presented represent global minima.

Results

The solution ^{1}H NMR spectra of peptides combined in solution with anionic colloidal silica reveal dramatic changes in the intensity of the signals. In the spectrum of 4DAR5 in D_2O solution with Ludox HS, certain signals disappear, while the remaining resonances are broadened (Figure III-13). The observed behavior can be explained by adsorption of the peptides to the colloidal particles. The rotation of these particles is slow relative to the tumbling of a peptide in solution, and so adsorption increases the motional correlation times of the peptide protons, leading to short T_2 values and signal broadening. The T_1 and T_2 values of the R-δ resonance of 4DAR5 as a function of silica concentration are shown in Figure III-14. Although a decrease is evident in both parameters as a function of increasing silica concentration, this decrease is more dramatic for T_2 than for T_1. In addition, since T_2 is much smaller than T_1, the linewidth is limited by T_2 and not T_1. At greater silica concentrations the peak decays too rapidly to be measured (within 16 ms).

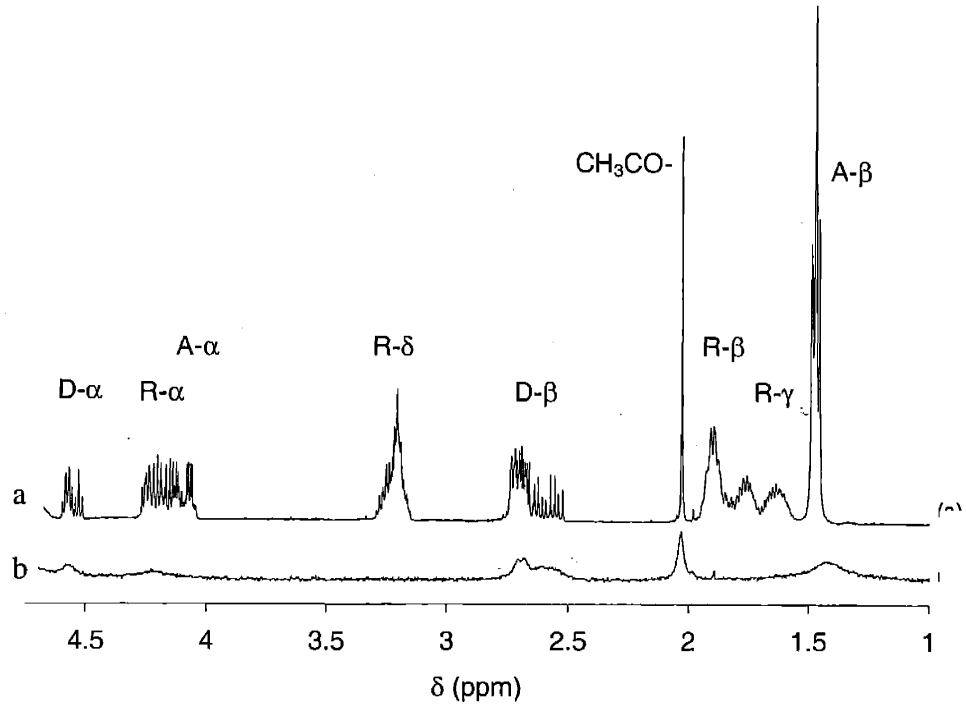

Figure III-13. **Effect of adsorption on the ^{1}H NMR spectrum of 4DAR5: (a) in solution, pH 8.4; (b) adsorbed to Ludox HS, pH 9.0.**

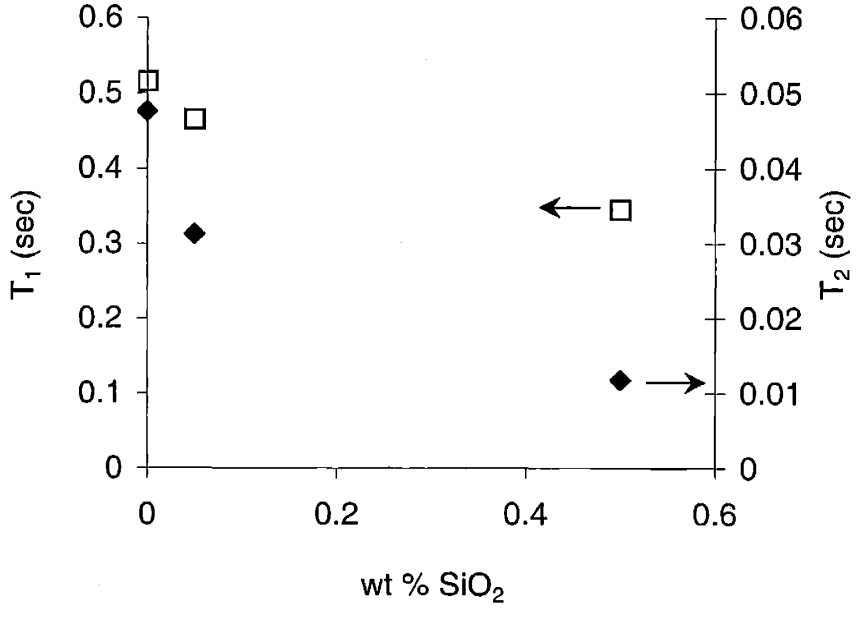

Figure III-14. **Effect of adsorption on the ^{1}H NMR relaxation time constants of the R-δ resonance: (□, left axis) spin-lattice relaxation time T_1 obtained from the inversion-recovery pulse sequence; (◆, right axis) spin-spin relaxation time T_2 obtained from the CPMG pulse sequence. Time constants were extracted from exponential fits found by minimizing the sum of residuals.**

Approximating the tumbling rate of peptides in water at room temperature in picoseconds as numerically equal to their molecular weight [154], and taking 4DAR5 (MW = 1500 g mol^{-1}) as an example, these molecules tumble on a timescale of approximately 1.5 ns. In contrast, tumbling of colloidal particles of radius R in solution of viscosity η occurs on a timescale given by [158]

$$\tau_t = \frac{4\pi\eta R^2}{3k_B T}$$

(III-18)

For 12 nm diameter Ludox HS silica particles in water at 25 °C, this timescale is 200 ns, which is two orders of magnitude slower than the peptide molecules.

Considering typical T_2 values for peptides in solution of ~0.5 sec (Figure III-14), this estimate indicates that NMR signals from nuclei moving on the timescale of a colloidal particle will be severely broadened. Indeed, no resonances are observed from a suspension of 21 nm diameter polystyrene particles (data not shown).

The protons of the arginine residues, which are electrostatically attracted to the anionic silica surface, are most strongly affected by adsorption. At silica concentrations above approximately 1 wt%, these resonances disappear completely from the ^{1}H NMR spectrum. This disappearance results from extreme signal broadening due to interaction with the slowly-rotating colloidal particles. Based on this interpretation of the NMR spectrum of adsorbed molecules, the arginine segment is immobilized at the surface. By contrast, the protons of the aspartate segment, which is repelled from the negatively-charged surface, retain significant signal intensity. Adsorption of the peptide decreases the intensity of these signals relative to the spectrum in solution, but does not eliminate them entirely. This indicates that the aspartate side chains retain local mobility, which allows the signals from these groups to be observed. Therefore, this segment is not immobilized at the surface, but instead, extends away from the substrate surface into solution. Adsorbed peptides are oriented on the silica surface by the electrostatic interactions between the surface charge and the dipolar charge distribution within the peptide. In studies of amphiphilic polymers adsorbed to colloidal substrates, an analogous effect of ^{1}H NMR signal intensities was observed, except that immobilization resulted from hydrophobic interactions [159,160].

The protons of the uncharged alanine residues retain less signal intensity than those of aspartate. These nuclei must be immobilized more effectively than aspartate, due to their proximity to the arginine segment, but the presence of detectable signals reveals that alanine residues retain some mobility. As discussed previously (Section III.6), the electrostatic interactions between the aspartate terminus of the peptide and the silica surface result in a driving force that favors separation of the N-terminus from the surface. This driving force overwhelms favorable van der Waals interactions between the alanine residues and the silica surface, and leads to a separation of these residues from the surface. Alanine residues are closer to the surface than the aspartate residues, but not directly adjacent to the surface.

The extent of the selective loss of ^{1}H NMR signal intensity resulting from adsorption varies among the DAR-type peptides studied here (Figure III-15). Arginine resonances are absent from the spectra of both adsorbed 5DAR4 and adsorbed 2DAR8, but the remaining alanine and aspartate resonances of 5DAR4 are broader and less intense than those of 2DAR8. 5DAR4 may be immobilized more effectively than 2DAR8 due to the greater number of cationic side chains in this peptide.

When adsorption conditions are varied to induce desorption, for example by decreasing the pH or reducing the amount of silica in solution, signals from non-adsorbed peptide are not observed. Figure III-16 is typical of this phenomenon. In this figure, the NMR spectra of samples with appreciable populations of peptide in solution, as suggested by sedimentation data, do not display NMR signals typical of free peptides in solution. This experiment was confirmed using 4DAYAR5: measurement of the solution NMR spectra revealed no peaks characteristic of non-adsorbed peptide, but sedimentation of silica particles and adsorbed peptide by centrifugation removed less than half of the total peptide in the sample (data not shown).[8]

[8] One alternative explanation for this phenomenon would be the presence of large numbers of ultrafine silica particles too small to be sedimented. Such particles would need to be at least 9 nm in diameter to avoid being removed by ultrafiltration, but could not be much larger since larger particles would be detected by UV absorbance spectroscopy. No such particles exist, as confirmed by both transmission FTIR of sedimented samples and TEM of a dried suspension (Section III.2).

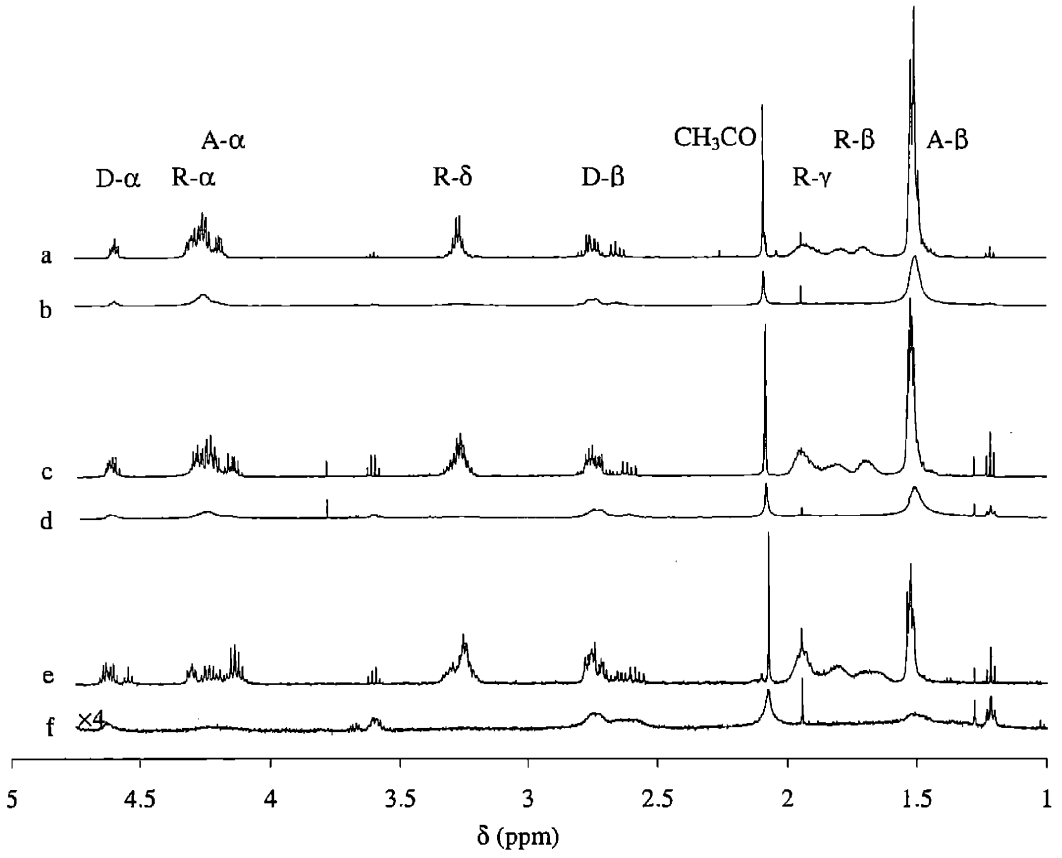

Figure III-15. Effect of adsorption on the ^{1}H NMR spectra of peptides of various residue compositions: 2DAR8 (a) in solution, (b) adsorbed to Ludox HS; 3DAR6 (c) in solution, (d) adsorbed to Ludox HS; 5DAR4 (e) in solution, (f) adsorbed to Ludox HS. Assignment of non-peptide resonances: 1.94 ppm: CH_3CN, introduced during synthesis; 1.2, 3.6 ppm: diethyl ether introduced during synthesis.

This observation suggests that the kinetics of peptide adsorption are sufficiently rapid such that all peptide molecules in the sample are equivalent on the timescale of the NMR experiment. All of the molecules in the sample have the same fast spin-spin relaxation rate (shorter T_2), even though only a fraction of the molecules are adsorbed at any given time. NMR spectra and adsorption isotherms thus reflect different, and complementary aspects of the adsorption process. Adsorption isotherms reflect the fraction of peptide adsorbed at any given time, but NMR spectra reflect the fraction of peptide which interacts with the surface on the timescale of the NMR experiment (within the relaxation time, about 50 ms). The lack of sharp signals indicate that this fraction is essentially 100% for the samples in

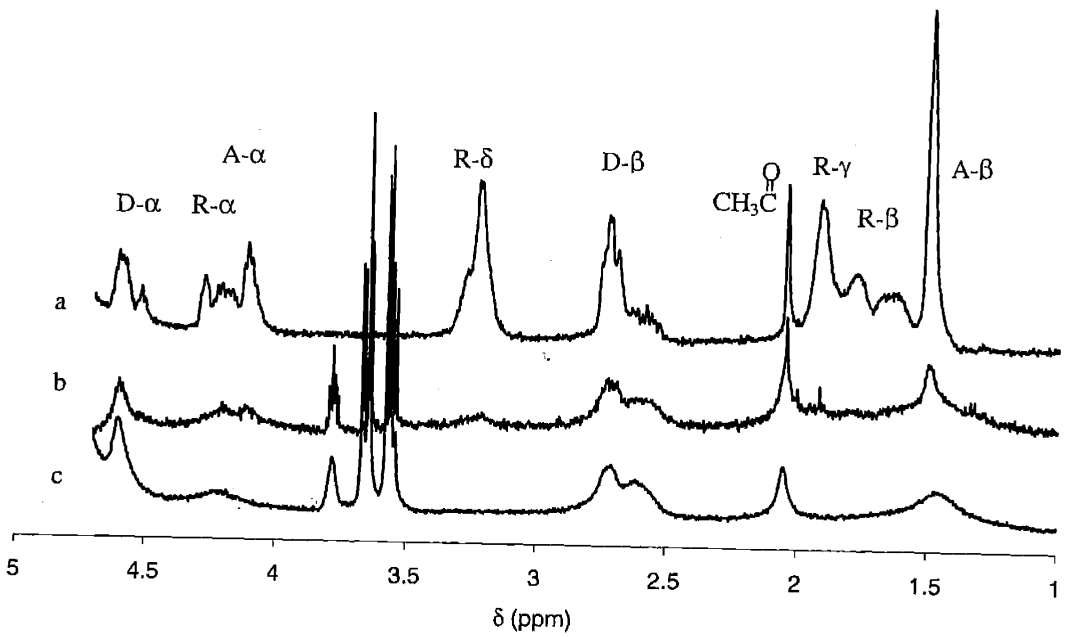

Figure III-16. Dependence of 5DAR4 ^{1}H NMR spectrum on Ludox HS concentration: (a) 700 μM 5DAR4 free in solution; (b) 700 μM 5DAR4, 0.5 wt% Ludox HS, approx. 30% of molecules adsorbed; (c) 700 μM 5DAR4, 4.5 wt% Ludox HS, approx. 90% of molecules adsorbed. The extents of adsorption are calculated from the adsorption isotherm in Figure III-8. Assignment of non-peptide resonances: 3.5-3.8 ppm: impurity from Ludox HS.

Figure III-16(b,c). The importance of dynamics in controlling the relaxation rate is illustrated by the fact that NMR spectra of solutions containing peptides with a net charge (for example, 4^+DAR4 and 4AAR4) and Ludox HS display no proton resonances. Adsorption removes all the motions of such peptides which are necessary to produce a signal under the conditions of solution NMR.

NMR signals reflect a trend in the mobility of adsorbed peptide molecules which is opposite to the fraction of adsorbed peptide. As shown in Figure III-17, decreased pH leads to a lower fraction of adsorbed molecules, but also leads to a dramatically decreased NMR signal strength. This may be a result of the greater α-helicity of adsorbed molecules at lower pH. Although fewer molecules are adsorbed at any one time at neutral pH, all the molecules in the sample still interact with the surface on the NMR timescale, and these interactions result in more rapid relaxation at neutral pH than at basic pH. The increased α-helicity in adsorbed molecules at pH 7 constrains the aspartate residues in a fixed orientation relative to the arginine residues at the surface. The aspartate residues are therefore more effectively

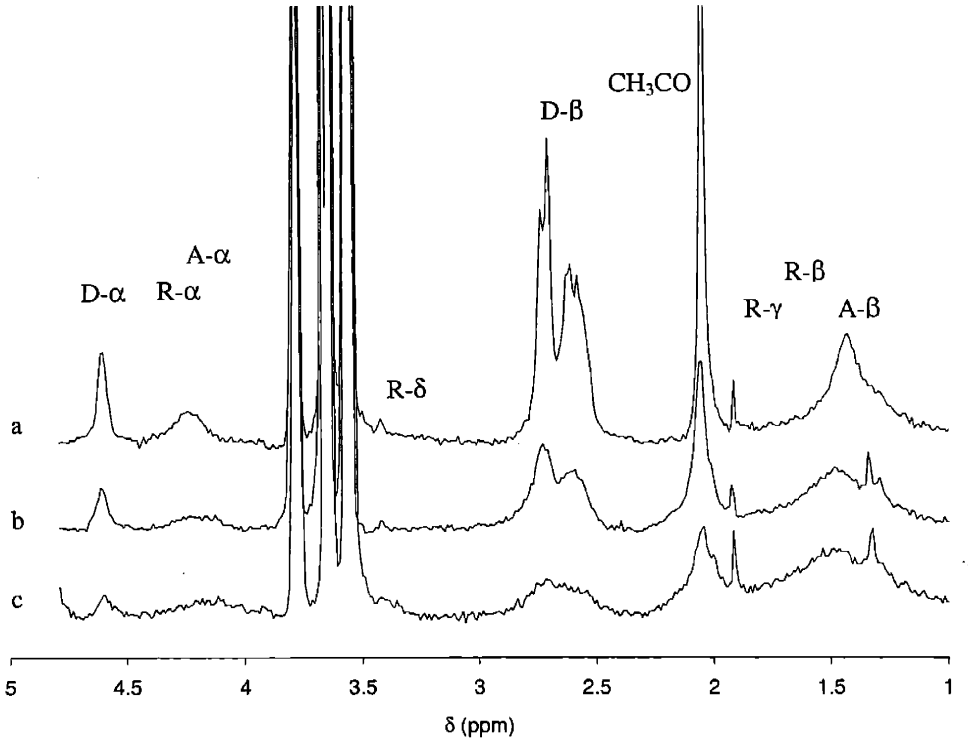

Figure III-17. Dependence of 5DAR4 ^{1}H NMR spectrum on pH in solution with Ludox HS colloidal silica: (a) 500 μM 5DAR4, 5.3 wt% Ludox HS, pH 9.15, approx. 90% of molecules adsorbed; (b) pH 7.80 (c) pH 7.01. Assignment of non-peptide resonances: 3.5-3.8 ppm: impurity from Ludox HS; 1.94 ppm: CH_3CN, introduced during synthesis.

immobilized at neutral pH than at basic pH because the adsorbed molecules are more rigid. This leads to a more rapid relaxation of ^{1}H signals from the aspartate residues in adsorbed molecules at neutral pH than at basic pH. This situation is shown schematically in Figure III-18.

Examining the alanine and aspartate peaks which remain in the NMR spectra at high silica concentrations, where the amount of non-adsorbed peptide is negligible, reveals shifts in the conformationally-sensitive αH and βH signals. Different conformationally-sensitive signals from the same residue type (for example, those for αH and βH) display different peak shifts (Δδ) upon adsorption, as tabulated in Table III-VI. The functional relation between the dihedral angles ϕ and ψ and the chemical shift of αH peaks has been established [161]; upfield chemical shifts are strongly correlated with population of α-helical conformers. In contrast, the conformational sensitivity of βH signals is not well understood. Therefore, changes in the αH signals upon adsorption are assumed to more accurately reflect the residue-

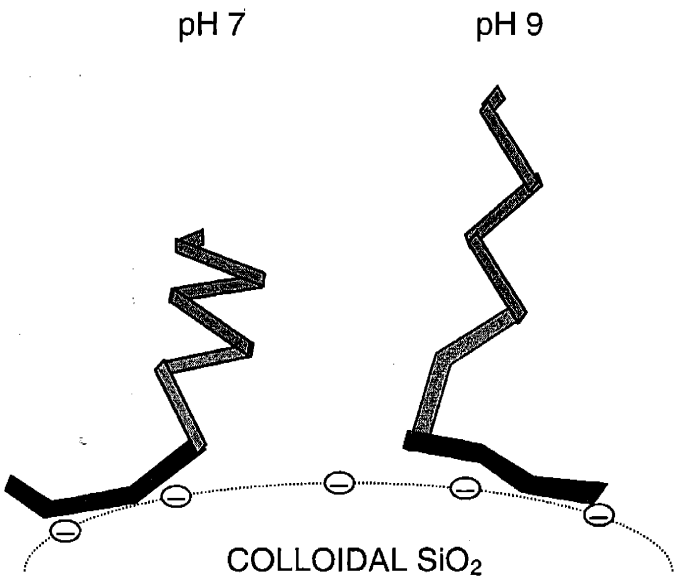

Figure III-18. Schematic diagram of the effect of surface charge on adsorbed peptides. The arginine segment is drawn adjacent to the surface, while the alanine and aspartate segments extend into solution. The alanine and aspartate segments are more α-helical at pH 7 (left) than at pH 9 (right).

Table III-VI. Conformationally-sensitive peak shifts in ^{1}H NMR spectra of 4DAR5. *Ideal values* are taken from [115], restated to reflect referencing to TMS (δ = 0 ppm). The literature values were originally referenced to 2,2-dimethyl-2-silapentane-5-sulfonic acid (DSS; δ = -0.048 ppm from TMS [107]). *Solution* and *Adsorbed* peak shifts were calculated from NMR spectra collected at pH 7.5 and 9, respectively, using center-of-mass integration or averaging of TOCSY cross peaks as described in the experimental section. No significant pH dependence was found in the quoted peaks in the pH range of interest. $f_{\alpha H}$ values were calculated from equation (III-19). The *Overall* α-helicity of 4DAR5 in solution estimated by NMR was calculated from the residue-weighted average of the three α-helicity values for the individual segments.

	Ideal values		*Measured in Solution*		*Measured Adsorbed to Ludox HS*			
Segment	$(\delta_{\alpha H})_{coil}$	$(\delta_{\alpha H})_{helix}$	$\delta_{\alpha H}$	$f_{\alpha H}$	$\delta_{\alpha H}$	$\Delta\delta_{\alpha H}$	$f_{\alpha H}$	$\Delta\delta_{\beta H}$
D	4.58	4.40	4.51	0.39	4.53	0.02	0.28	-0.11
A	4.15	4.00	4.08	0.47	4.18	0.07	-0.20	-0.05
R	4.27	3.94	4.14	0.39	—	—	—	—
			Overall:	0.42				

dependent reduction of α-helicity occurring upon adsorption. Changes in the βH peak shifts may contain complimentary conformational information, but their examination is beyond the scope of this work.

For the purposes of this calculation, a simple linear relation is assumed between changes in the αH peak shift observed for any particular residue in the peptide upon adsorption, and changes in the average degree to which this residue populates α-helical

conformers. Since NMR peak shifts and CD signal intensities arise from different physical mechanisms, the relation between α-helicity and αH peak shifts is not likely to be strictly linear; nevertheless, this assumption has previously been shown to provide high correlations between helicitiy values calculated from NMR and CD data for peptides in solution [162]. Peak shifts representing idealized random-coil and α-helical αH shifts are taken from [115] and tabulated in Table III-VI.

Peak shifts characteristic of α-helical and random-coil conformations are used to calculate the normalized quantities $f_{\alpha H}$ which suggest a measurement of residue-specific fractional α-helicity:

$$f_{\alpha H} = \frac{\delta_{\alpha H} - (\delta_{\alpha H})_{coil}}{(\delta_{\alpha H})_{helix} - (\delta_{\alpha H})_{coil}} \quad \textbf{(III-19)}$$

To the extent that this linear approximation captures the functional relationship between αH peak shifts and the population of helical conformers, changes in the quantity $f_{\alpha H}$ upon adsorption reflect losses of α-helicity within individual segments of the adsorbed peptide. As shown in Table III-VI, these changes are much greater for the A-αH signal than for the D-αH signal. For aspartate residues in adsorbed peptide, the value $f_{\alpha H} = 0.28$ reflects an estimate from the NMR measurement of an average of 28% α-helicity in these residues. In contrast, the negative value for alanine represents a complete loss of α-helicity by alanine residues.

α-Helicity measurements obtained from CD and NMR spectroscopy appear to be fairly well-correlated. The overall α-helicity of 4DAR5 is estimated from NMR by the weighted average of the $f_{\alpha H}$ measurements from each segment [162]. This value is 42% (Table III-VI), which is relatively close to the measurement of f_{Hel} (50%) from CD, listed in Table II-II. Therefore, the weighted average of the available $f_{\alpha H}$ measurements for adsorbed molecules is combined with the α-helicity of adsorbed molecules measured by CD to estimate the helicity remaining in the (invisible) arginine terminus. Adsorbed 4DAR5 molecules retain $\varphi_{Hel}^{ads} = 20\%$ of their α-helicity relative to their α-helicity in solution (Figure III-12), so the fractional α-helicity of adsorbed 4DAR5 molecules is calculated from $f_{Hel}^{ads} = \varphi_{Hel}^{ads} f_{Hel}^{free} = 0.2 \times 0.5 = 10\%$. Therefore the weighted average of the α-helicity in the

individual segments, aspartate (28%), alanine (0%), and arginine (unknown), should be equal to the value of α-helicity for the entire molecule obtained from CD (10% ± 2%, where the uncertainty represents the difference between the NMR and CD measurements in solution). This leads to an estimate of the arginine α-helicity of between 0% and 10%, consistent with a near-complete loss of α-helicity in this segment.

Combining the residue-specific α-helicity measurements by NMR with measurements of the overall α-helicity of the molecule thus indicates a near-complete loss of α-helicity in the adsorbed, NMR-silent arginine terminus. α-Helicity is most strongly destabilized in the segment closest to the surface, and mostly retained in the segment furthest removed from the surface. Unwinding probably occurs in the region of the α-helical peptide that is adjacent to the substrate surface, to maximize the favorable electrostatic interactions between the peptide and the charged substrate surface. A similar effect has been observed in the N-terminal fragment of statherin adsorbed to hydroxyapatite, studied by solid-state ^{13}C NMR [47]. The loss of α-helicity in the segment that extends away from the substrate surface is likely to result from the driving force to maximize the distance between the negatively charged aspartate terminus and the surface [115].

Conclusions

For the α-helical peptides studied, ^{1}H NMR spectroscopy shows that, even in the absence of a net charge on the peptide, adsorption occurs with orientational specificity, based on favorable electrostatic interactions between the adsorbing end of the peptide and the silica surface. Combined with data from CD spectroscopy, the segment-specific conformational information from NMR shows that the partial loss of peptide α-helicity in adsorbed molecules propagates from the adsorbed peptide terminus to the unadsorbed terminus.

8. Electrostatic Model of Peptide Adsorption

Enthalpy

The strong dependence of K_{eq} on pH leads to the hypothesis that electrostatic interactions are responsible for peptide adsorption. In this section, the enthalpy arising from electrostatic interactions between the screened surface charge of silica and the dipolar charge distribution on 4DAYAR5 is estimated, in order to determine whether this enthalpic term alone can account for the observed enthalpy of adsorption.

Since the electrostatic contribution to the enthalpy of adsorption (ΔH_{ads}^{el}) is a state function, it can be imagined to arise from two subprocesses: conformation change in the absence of an external field, which contributes an enthalpy ($\Delta H_{ads}^{el,conf}$), and positioning of the new conformation in an external field, which contributes an enthalpy ($\Delta H_{ads}^{el,pos}$). The former leads to contributions from the decrease in α-helicity, as well as to increased separation between the average locations of positive and negative charge. The latter component contains the stabilization arising from positioning of the positively-charged arginine side chains closer than the negatively-charged aspartate side chains to the silica surface:

$$\Delta H_{ads}^{el} = \Delta H_{ads}^{el,conf} + \Delta H_{ads}^{el,pos} = N\Delta f_{Hel}\Delta H_h + \frac{n_T k_C e^2}{\varepsilon}\left[\ell_{ads}^{-1} - \ell_{free}^{-1}\right] + n_T e(\Psi_C - \Psi_N) \qquad \textbf{(III-20)}$$

where N is the number of residues in the peptide, Δf_{Hel} is the change in the fractional α-helicity measured by CD (about 30% for 4DAYAR5), ΔH_h is the enthalpy of α-helix formation (≈1 kcal mol^{-1} per residue [95]), n_T is the number of unit charges at each terminus (four for 4DAYAR5), k_C is the Coulomb constant, e is the unit charge, ε is the relative dielectric constant of water (78 at room temperature), ℓ_{ads} and ℓ_{free} are the separations between the average locations (defined below) of negative and positive charge on the peptide N- and C-termini in the adsorbed and non-adsorbed conformations respectively, and Ψ_C and Ψ_N are the electrical potentials at the average location of the C- and N-terminal charges.[9] The first term ($N\Delta f_{Hel}\Delta H_h$) can immediately be calculated to be 16 kJ mol^{-1}. Further modeling of the

[9] In this work, the surface potential is written as Ψ to distinguish it from the dihedral angle ψ.

enthalpy of adsorption requires (i) an estimate of the geometry of conformation change in the peptide, and (ii) knowledge of the distance-dependence of the potential near the charged silica surface.

The average separation of positive and negative charges is dictated by the primary and secondary structures of the peptide, and is modulated by side chain conformations. Residues 1–4 of 4DAYAR5 have positively-charged side chains, and thus the average localization of positive charge is between residues 2 and 3. Similarly, the average localization of negative charge is between residues 11 and 12. Thus, the average localization of positive and negative charge is separated by 9 residues. Idealized models of the α-helix [9] have a 0.15 nm translation per residue along the α-helix axis. Thus using the separation given by this ideal α-helix, $\ell_{free} \approx (0.15\ \text{nm} \times 9) = 1.4\ \text{nm}$.

Conformational changes are shown to occur upon adsorption in Section III.6, and are modeled in more detail in Chapter IV.2; for now it is noted that the fully-extended β-strand form with a translation of 0.34 nm per residue represents an upper limit for the separation of the N- and C-termini. Clearly this upper limit is not obtained, since the CD spectra of peptides on the silica surface show no evidence of this conformation, so that ($\ell_{ads} < (3.4\ \text{Å} \times 9) = 3.1\ \text{nm}$). However, this upper limit is sufficient to show that the term $\frac{n_T k_C e^2}{\varepsilon}\left[\ell_{ads}^{-1} - \ell_{free}^{-1}\right]$ in Equation (III-20) is less than 3 kJ mol^{-1}.

The electrical potential Ψ as a function of distance from the silica surface may be modeled at several levels of approximation. The surface charge σ_0 (0.54 nm^{-2} ≡ 8.7 μC cm^{-2} measured at pH 9 in Section III.2) is used to calculate the surface potential Ψ_0 according to nonlinear Poisson-Boltzmann theory [163,164]

$$\sigma_0 = \left(\frac{2n_0 \varepsilon kT}{\pi}\right)^{1/2} \sinh\left(\frac{ze\Psi_0}{kT}\right) \qquad \textbf{(III-21)}$$

where Ψ_0 is the potential at the surface, n_0 is the number density of counterions in the bulk, and z is their valence. This leads to a surface potential $\Psi_0 = -140$ mV, which decreases rapidly in magnitude as a function of distance in the near-surface area due to screening by tightly-bound counterions in the Stern layer, as well as by the more diffuse charge in the

electrical double layer. Distance-dependent screening effects control the difference between Ψ_C and Ψ_N, which lead to adsorption, and thus are discussed in detail here.

In the diffuse layer, the potential is screened by the diffuse charges in the electrical double layer. The screening length is the Debye length ℓ_D given by the Guoy-Chapman model

$$\ell_D = \left(\frac{4\pi e^2}{\varepsilon kT} \sum_i n_i z_i^2 \right)^{-1/2} \qquad \text{(III-22)}$$

where n_i is the concentration of the ith ion species of valence z_i. For 10 mM borate buffer ($pK_a = 9$) the ionic strength is 0.01 mM and $\ell_D = 3$ nm. The screening produces the measured zeta potential at the shear plane (Ψ_ζ = -38 mV), which is generally considered to be no more than three solvent diameters, or approximately 1 nm from the surface [165]. A diagram of the estimated potential as a function of distance from the surface, which is only valid outside the Stern layer, is shown in Figure III-19(a).

The primary evidence for the presence of adsorbed ions in the Stern layer is that the experimentally-measured zeta potential is only 30% of the surface potential calculated from Equation (III-21) and, as shown in Figure III-19(a), screening from counterions in the diffuse layer is not sufficient to account for this difference. Specifically-adsorbed ions, which lose their hydrating water molecules upon adsorption, reside within the Stern layer on the inner Helmholtz plane (IHP), while nonspecifically-adsorbed ions reside on the outer Helmholtz plane (OHP). The potential within the Stern layer is approximated as a linearly-decreasing function of the local counterion population, modified by ion-dependent interactions with the surface as mentioned in Chapter II.1. Estimates of the actual width of these layers based on hydrated and nonhydrated ionic diameters [165] place the IHP at 0.1–0.2 nm, and the OHP at 0.6 nm.[10] The occupancy of the Stern layer and the resulting changes to the double-layer potential can be calculated [163,164]; sample plots are shown in Figure III-19(b).

[10] The OHP is close to but always within the "slip plane," at which Ψ is equal to the ζ-potential [164].

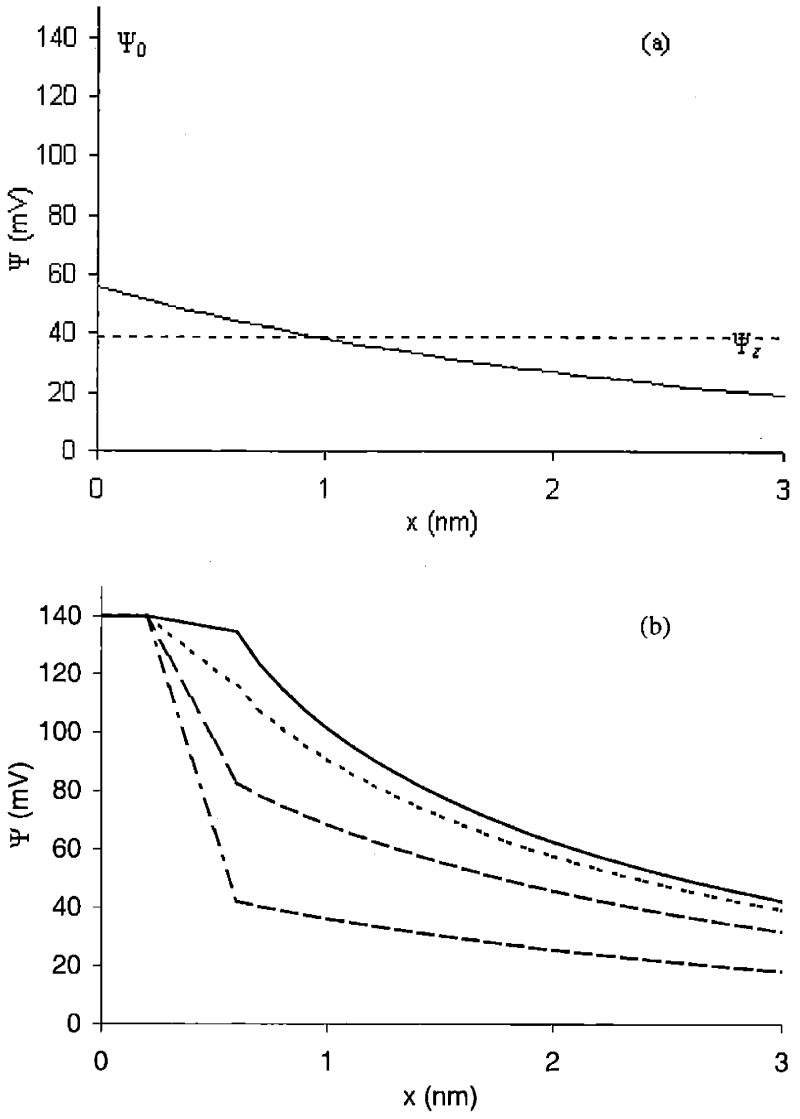

Figure III-19. Models of the potential in the electric double layer as a function of distance from the silica surface. (a) Guoy-Chapman model of the double-layer potential outside the Stern layer. The zeta potential of SiO_2 was imposed at 1 nm (diameter of 3 water molecules). (b) Stern layer corrections to the double-layer potential. Potentials were calculated assuming a Stern layer capacity of 0.2 μC m^{-2} and a specific adsorption potential of (——) 0 mV; (- - -) 40 mV; (— —) 60 mV; (— -) 70 mV [166].

In Section III.7, peptides were shown to be oriented on the surface with aspartate side chains at the N-terminus extending away from the surface into solution. These orientational effects, combined with the observation that aspartate side chains retain significant mobility by ^1H solution NMR, indicate that aspartate side chains are present in the diffuse layer, not the

Stern layer. The magnitude of the potential (Ψ_N) experienced by these side chains therefore cannot be greater than the measured zeta potential, ($-\Psi_N \leq -\Psi_\zeta$). The contour length of the peptide limits the separation which these side chains may obtain with respect to the negatively-charged surface, such that the lower bound for $-\Psi_N$ is the potential at a distance from the surface corresponding to the maximum charge separation derived above, ($-\Psi_N \geq -\Psi(\ell_{ads})$, where $\Psi(\ell_{ads}) = -19$ mV). Confinement of Ψ_N to this range is sufficient for the purposes of this approximation.

The final parameter needed for Equation (III-20), Ψ_C, depends strongly on the location of arginine side chains and requires care in its estimation. Arginine side chains are observed by solution ^{1}H NMR to be immobilized at the surface, and therefore must be in the Stern layer; the observation that the combination of a peptide solution with a suspension of anionic colloid at the same pH leads to a decrease in pH supports the idea that arginine side chains are strongly adsorbed in the Stern layer, where they may displace counterions such as Na^+ or H_3O^+. Since the electric field next to an infinite, flat, charged surface (a reasonable approximation on the lengthscale of the Stern layer, even for a 12 nm particle) is constant, the maximum potential to which these side chains may be subjected is the full surface potential in the absence of screening ($\Psi_0 = -140$ mV).

Population of the Stern layer by counterions as well as by peptide side chains could screen the side chains, thus decreasing the effective potential (Ψ_C). However, this is not likely to be significant if the effective ion sizes of the screening counterions and the adsorbed immonium groups of the arginine side chains are similar (that is, if the arginine side chains reside in the same plane as other counterions). If this is the case, then to the extent that steric hindrance prevents sodium from adsorbing specifically in the same location as a peptide molecule, the screening counterions are in fact the adsorbed immonium groups. The actual potential Ψ_C experienced by the arginine side chains is thus strongly distance dependent, with an upper limit of 140 mV. Combining this value with the above range of Ψ_N gives an estimate for the term $n_T e(\Psi_C - \Psi_N)$ in Equation (III-20) of -37 – -47 kJ mol^{-1}.

Calculation of the total electrostatic enthalpy of adsorption therefore results in a value of -23 – -33 kJ mol^{-1}, somewhat greater than the measured enthalpy of adsorption, -17 kJ mol^{-1}. As mentioned above, the arginine side chains are probably extremely close to

the surface, but some separation could arise due to steric effects from the peptide backbone and hydrating water, so they may not experience the full charge due to screening. In addition, image effects due to the large difference between the relative dielectric constants of water (ε_{H_2O} = 78) and silica (ε_{SiO_2} = 5) become important at small separations and would tend to decrease the electrostatic driving force for adsorption.[11] At this level of analysis, the electrostatic interactions between the dipolar charge distribution of the peptide and the screened silica surface charge are more than sufficient to account for the measured enthalpy of adsorption. The accuracy of this estimate would be increased most effectively by additional information on both the location of arginine side chains and the importance of image effects.

Entropy

Because the measured entropy of adsorption depends strongly on the assumptions necessary for data interpretation, a detailed model is not developed here. Instead, the measured value for the entropy of adsorption is discussed in the context of the observed conformation changes, and possible additional factors are described.

Equation (III-10) can be used to relate the entropy of adsorption measured in Chapter III.4 (ΔS_{ads} = 14.6 J mol^{-1} K^{-1} = 4.4 kJ mol^{-1} at room temperature) to the conformational changes of the peptide that are associated with adsorption. In the context of Equation (III-10), it was noted that the difference in entropy between the α-helix and random-coil states is approximately 3.5 kJ mol^{-1} at 25 °C. Therefore, the measured entropy of adsorption corresponds to a complete loss of α-helicity (in favor of a completely disordered structure) of 4.4/3.5 = 1.3 residues. For comparison, in Chapter III.6 it was shown that at pH 9 adsorption is associated with a loss of 75% of the original α-helicity of the peptide. Since the peptide 4DAYAR5 is 25% α-helical at 25 °C (Table II-II), the decrease in fractional α-helicity observed by CD corresponds to 2.4 residues (0.75 × 0.25 × 13) by CD. Therefore, the conformational changes observed by CD are more than sufficient to account for the measured entropy of adsorption.

[11] Image forces repel electrostatic charges from a region of decreased dielectric constant, since it is energetically favorable for the electric field produced by the charge to occupy the region of higher dielectric constant [167].

As mentioned previously, several processes including surface dehydration and ion displacement could influence the measured entropy of adsorption, leading to differences between the values obtained from adsorption isotherms and CD spectroscopy. The conformational changes observed do not represent a transition between perfectly ordered and disordered states. CD spectroscopy appears to indicate a transition between imperfect α-helices, and coiled structures which are not completely random. The difference in isodichroic points observed for the helix–coil transition arising from thermal destabilization and adsorption indicates that the two endpoints of these transitions are not equivalent, and therefore the adsorbed conformation possesses less entropy than the true random-coil structure. This would tend to decrease even further the entropy which can be accounted for by conformational changes. Overall, the measured positive entropy of adsorption is consistent with the observed loss of α-helicity of adsorbed molecules, representing a shift in the average peptide conformation such that the population of α-helical conformers is decreased, combined with additional factors which act to decrease the entropy of adsorption.

9. Conclusions

A model system has been developed for studying the adsorption of structured molecules and the resulting changes in conformation. Adsorption isotherms were measured in detail for one particular peptide, 4DAYAR5, which possesses a tyrosine chromophore that facilitates quantitative analysis. Adsorption of this peptide to two sizes of amorphous colloidal silica between pH 7 and 9 is reversible, and follows idealized models (Langmuir or Frumkin fits) up to equilibrium solution concentrations of approximately 800 μM. Adsorption increases strongly with pH, which controls the surface charge of the amorphous silica. Determination of the temperature dependence of the equilibrium constant for adsorption allowed the derivation of the enthalpy associated with this process. This value was consistent with estimates of the electrostatic energy of the interaction between the charged surface and the dipolar electrostatic charge distribution on the peptides, although quantitative modeling was not possible due to the sensitivity of such calculations on the exact position of arginine side chains in the near-surface layers, which are not known with precision. Adsorption isotherms for other peptides depend on sequence in a relatively predicable way:

the equilibrium constant is strongly correlated with the number of charges on the peptide termini, and it increases substantially when a net charge is added to the molecule.

Circular dichroism showed that adsorbed molecules lose partial α-helicity. Not surprisingly, the fraction of α-helicity retained by adsorbed molecules was strongly correlated with the charge on the peptide termini. Interestingly, no significant correlation was observed between the fraction of α-helicity retained by adsorbed molecules and the fractional α-helicity of molecules in solution. In other words, the extent of α-helicity of a peptide in solution was not a good predictor of the extent to which this conformation was destabilized upon adsorption. The loss of α-helicity of 4DAYAR5 observed upon adsorption is consistent with the measured positive entropy of adsorption, although other processes appear to contribute to the observed entropy of adsorption.

Solution ^{1}H NMR showed that positively-charged arginine side chains at the peptide N-terminus interact directly with the negatively-charged colloidal silica surface, while negatively-charged aspartate side chains at the C-terminus are repelled from the surface. Analysis of conformationally-sensitive Hα peak shifts for the segments of peptide which remain visible by ^{1}H solution NMR upon adsorption indicate little change in fractional α-helicity for the non-adsorbed aspartate terminus, but a significant decrease in the α-helicity of the intervening alanine segment. Although NMR signals from the segment that is in direct contact with the surface are not visible, a combination of the signals observed by NMR with the overall α-helicity measured by CD indicates that the adsorbed arginine terminus undergoes a near-complete loss of α-helicity, consistent with the proposal [7] that destabilization of an α-helix due to interaction with the surface propagates from the adsorbed terminus into the non-adsorbed portions of the molecule.

The estimated length of the peptide is longer than estimates of the distance between the surface and the shear layer. In this case it appears that the shear layer, at which the zeta potential associated with electrokinetic phenomena is measured, coincides roughly with the boundary between molecules or groups that are visible in ^{1}H solution NMR. Molecules within the shear plane, which are considered to move with the surface, are immobilized on the NMR time scale since the rotational correlation time of the colloidal particle is relatively large on this timescale. The arginine residues are located within this shear plane, in the Stern layer,

but the aspartate residues and at least some of the alanine residues are located outside it. Taken together, this is an exceptionally detailed picture that provides a basis for modeling the factors that drive adsorption and conformational change.

Chapter IV. Functionality of Adsorbed Peptides

1. Introduction

Preserving the functionality of adsorbed biomolecules remains an important challenge. For example, immobilization of naturally-occurring enzymes at an interface can result in decreased catalytic activity relative to the solution state [43], while conformational changes of adsorbed proteins can modulate blood compatibility of biomaterials [6]. Biological functionality of adsorbed molecules thus may have important ramifications for the efficiency of a device or for the health of an organism. For naturally-occurring molecules, biological functionality can be defined as the ability to participate in the interactions of the native state. Such interactions are often easily observed, for example by measurement of catalytic activity of adsorbed molecules, but the detailed basis for the loss of functionality is often obscured by the complexity of natural proteins.

The model system developed in previous chapters enables detailed studies of the processes of adsorption and conformation change for synthetic α-helical peptides. The purpose of this chapter is to use the information derived from these studies to gain insight into the biological functionality of adsorbed molecules. The biological activities of natural peptides often arise from their secondary structures. This is the case in the disruption of cell membranes by peptide antibiotics or toxins [168], and aggregation of the amyloid-β peptide into plaques associated with Alzheimer's disease [169]. Other peptides interact specifically with surfaces; for example, fish antifreeze glycopeptides inhibit the formation of ice by preferential adsorption to certain crystal planes [170]. These systems demonstrate that peptides may possess biological functionality in a variety of contexts, and that a general understanding of the relation between structural perturbations and the biological functionality of adsorbed molecules has applications in diverse areas.

For the synthetic peptides studied here, which have no native role in biological systems, an expanded definition of functionality is necessary. Peptide functionality, in general, is the ability to participate in specific interactions with other biomolecules; the specificity of an interaction is measured by its dependence on the peptide sequence and conformation. The α-helicity of adsorbed DAR-type peptides is an important component of

their functionality, since adsorbed peptides could form specific complexes with engineered enzymes (which would be highly sequence- and conformation-specific). Thus an understanding of the balance of interactions that lead to conformational change in adsorbed peptides would provide a model system for studying biological functionality of adsorbed molecules. In Section IV.2, measurements of the α-helicity remaining in adsorbed molecules as a function of pH and temperature are presented. The vulnerability of the α-helicity of adsorbed molecules to an additional mechanism of destabilization is examined, and the relationship between the coiled conformations on the surface and at elevated temperature is addressed.

Adsorbed peptides can also participate in enzyme-catalyzed chemical reactions such as proteolysis (amide bond cleavage). The rate of proteolysis is highly enzyme- and peptide-dependent, and is dominated by cleavage at preferred sites along the peptide backbone, as dictated by the sequence. Thus, the rate of proteolysis and the distribution of products formed is also a measure of the functionality of adsorbed peptide molecules. Section IV.3 presents a study of the rate of proteolysis of adsorbed peptide, focusing on differences in the interactions between peptides and other biomolecules in the solution and adsorbed states.

2. Conformational Properties of α-Helices at the Silica-Water Interface

Introduction

Studies of protein unfolding transitions have frequently made use of both chemical and thermal denaturation [171,172]. Addition of urea or guanidine hydrochloride to solutions of protein, or an increase in temperature, typically cause a discrete unfolding transition that is signaled by a relatively sudden change in CD intensity, fluorescence, or heat capacity. Limited concentrations of chemical denaturant, insufficient to induce the unfolding transition at lower temperatures, reduce the temperature at which the transition occurs. Typically, a simple thermodynamic model is assumed for the free energy of the system (for example, a two-state unfolding transition and a linear dependence of the free energy of this transition on denaturant concentration). Fitting the observed transitions to this model then provides values

for the enthalpy and entropy of the phase transition, as well as its dependence on solvent concentration.

The discrete two-state unfolding transition typically observed for proteins arises from the interdependence of the interactions that stabilize the folded conformation [10]. The conformation of α-helical peptides, though lacking a cooperative transition, is dictated by many of the same enthalpic and entropic factors which are responsible for the folded structures of proteins. These include hydrogen bonding among backbone and side chain groups, which tend to stabilize α-helix formation, as well as the natural tendency toward a disordered conformation, which disfavors α-helicity. Thus the temperature dependence of the helix–coil transition of peptides can give insights into the thermodynamics of α-helix formation that are relevant to protein folding, but models for this transition for peptides must account for the large number of conformations available to the peptide along the folding pathway.

Classical models of helix–coil transitions [101,102] allow each residue to reside in either enthalpically-favored α-helix or entropically-favored coil states. The relative energies of these two states depends on the states of neighboring residues. α-Helical states are disfavored if the adjoining residues are coiled; cooperative α-helix formation, by a series of neighboring residues, is therefore favored. These basic models correctly predict several properties of peptides, including the tendency of α-helicity to decrease with temperature, to increase with peptide length, and to be concentrated in the center of the peptide relative to the termini. Similar to treatments of protein unfolding transitions, fitting these models to the helix–coil transition as a function of temperature and chemical denaturant provides thermodynamic parameters for conformational change, which are interpreted in this case as single-residue quantities [173]. Many modifications have been made to these basic models [97]; of interest here will be those that account for sequence dependence [174] and for interactions with components of the solvent that can stabilize or destabilize α-helicity [102,103,175]. The ability of classical helix–coil models to capture the basic features of the helix–coil transition in solution, combined with their amenability to modifications to account for more peptide-specific features, makes them an attractive framework for use in modeling the conformational change of peptides adsorbed to silica surfaces.

In this section, CD measurements of the α-helicity of adsorbed cationic peptides are presented as a function of temperature and pH. These cationic peptides are adsorbed completely, even at intermediate pH and elevated temperature; they provide a reliable measure of the response of the peptide conformation to destabilization by both adsorption and elevated temperatures. Interesting trends are found in the temperature dependence of the α-helicity of adsorbed molecules as a function of pH, since the pH controls the surface charge and therefore influences the strength of the intermolecular electrostatic interactions between the surface and adsorbed peptide. The balance of intermolecular and intramolecular interactions that contribute to α-helicity is examined using a statistical model of the helix-coil transition for adsorbed molecules. This model incorporates modifications to the Lifson-Roig theory to introduce residue-specific interactions with the surface.

Theory

Two well-characterized [176] statistical models for the helix–coil transition in solution are commonly used. Models such as that of Zimm and Bragg [173], which count the number of α-helical hydrogen bonds, define conformation according to the hydrogen-bonded (α-helical) and non-bonded (coil) states of the backbone peptide groups, and assign statistical weights to the α-helix and coil states. These statistical weights are controlled by the enthalpy and entropy of α-helix formation. The Lifson-Roig model [177], on the other hand, bases these statistical weights on conformational integrals. The two models are equivalent [176], both capturing the localization of α-helicity at the center of peptides and the dependence of α-helicity on temperature.

Either model can be modified for application to adsorbed peptides with defined sequence; the modified model described in this work combines desired features from both models. Amino acid side chains interact with the surface differently according to their charge, so the relative statistical weights of the α-helix and coil states should be associated with the α-carbon, as in the Lifson-Roig model, not with one or the other of its adjoining peptide groups, as in the Zimm-Bragg model. Otherwise, a conceptual problem arises in associating the enthalpy and entropy of α-helix formation, which are a function of the amino

acid side chain, with the peptide group, which is the same from residue to residue. In the Lifson-Roig model, these thermodynamic parameters are related to the conformational properties of the α-carbon via conformational integrals over all the accessible values of the dihedral angles (ϕ and ψ). This is not convenient in the present work, because these conformational integrals require a model for the enthalpy and entropy of α-helix formation as a function of the dihedral angles. Such detailed information is not currently available for adsorbed molecules. Instead of deriving the statistical weight of the α-helix and coil states from conformational integrals over all the accessible values of the dihedral angles, it is desirable to associate the thermodynamic parameters with the α-helix and coil states as a whole, since the fractional population of α-helix states can be calculated directly from the measured CD spectrum using Equation (II-2). Discretization of residue conformations into distinct α-helix and coil states is a feature of the Zimm-Bragg model, but not of the Lifson-Roig model.

A statistical model in which the enthalpy and entropy of α-helix formation are considered to be a function of the conformational properties of the α-carbons (not the peptide groups), but considers only discrete α-helix and coil states (instead of conformational integrals over all accessible dihedral angles), can be formulated by considering an α-carbon i to be α-helical if the carbonyl group of residue i–2 forms a hydrogen bond with the amide proton of residue i+2. This definition is plausible since the ability to form the hydrogen bond in question is intimately associated with the conformation of this α-carbon. It is also mostly a matter of convenience, merely embodying a conceptual basis for the assumptions of both the Zimm-Bragg and Lifson-Roig models. Following the methodology and notation of the Lifson-Roig theory [173] as modified by Baldwin and coworkers to include residue-specific α-helix-forming [95] and capping [84,174] propensities, the conformation of an idealized DAR-type peptide with N residues is written as a sequence of states of the peptide groups with side chain types i; h_i designates the hydrogen-bonded (α-helical) state and c_i designates the non-bonded (coil) state. Since the experimental data was collected for 4^+DAR4, where the N-terminal acetyl and C-terminal amide caps contribute possible hydrogen-bonding partners, one arbitrary sample conformation for this peptide is given for illustrative purposes:

$$c_{Ac}\, c_D\, c_D\, c_D\, h_D\, h_A\, h_A\, h_A\, h_A\, h_R\, h_R\, c_R\, c_R\, c_R\, c_{Am} \qquad \textbf{(IV-1)}$$

The statistical weight of each conformation in the molecular partition function depends on the relative statistical weights assigned to the α-helix (h_i) and coil (c_i) states of each residue; these terms are calculated from energetic parameters that embody the physical assumptions of the model:

- The reference state is the coil state *in solution*. Thus the contribution to the molecular partition function from residue i in the local conformation $c_{i-1}\, c_i\, c_{i+1}$, is denoted as β_i and is normalized (without loss of generality) to a value of 1 in the coil state in solution.
- Peptide α-helices are based on hydrogen bonding between peptide groups that are separated by three positions. The statistical weight of the α-helical state is denoted w_i if the adjacent residues are hydrogen bonded, so that the local conformation is $h_{i-1}\, h_i\, h_{i+1}$. The parameter w_i is calculated from the free energy of α-helix formation (ΔG_h) according to the Boltzmann weighting [103]:

$$w_i = e^{-\Delta G_h / RT} \qquad \textbf{(IV-2)}$$

- If residues i-1 and/or i+1 are not hydrogen bonded, the statistical weight of the α-helical state is decreased to $v << 1$. This imposes an energetic penalty on interfaces between α-helix and coil states (i.e. local conformations $x_{i-1}\, h_i\, y_{i+2}$, where x or $y \neq h$), which is associated with the difficulty of imposing the necessary α-helical conformation on the adjacent unbonded residue.
- Residues in certain coiled conformations can provide "capping" interactions to adjacent residues that form an α-helix terminus, since these latter residues lack the α-helical hydrogen bond. The first three residues at the beginning (N-terminus) of an α-helix participate as hydrogen-bond donors from their backbone carbonyl groups to the backbone amide protons from residues in the α-helix, but their amide protons are not involved as hydrogen bond acceptors. Similarly, the end (C-terminus) of an α-helix has three residues that have hydrogen-bonded amide protons but lack hydrogen bonds involving their carbonyl groups. Certain side chain

types stabilize α-helix N-termini by providing hydrogen-bond acceptors for the adjacent backbone amide protons, while others stabilize α-helix C-termini by providing hydrogen-bond donors for backbone carbonyls. Thus the statistical weights of the coil conformations $x_{i-1}\,c_i\,h_{i+1}$ and $h_{i-1}\,c_i\,x_{i+1}$ (where x is c or h) are n and c, respectively.

The statistical weight of any given peptide conformation (such as the one given in Equation (IV-1)) is a sum of the contributions from individual residues. The contribution of any given residue i to the statistical weight depends on its neighbors according to the rules enumerated above. These rules are encoded in the matrix $\mathbf{I}_i$:

$$\mathbf{I}_i = \begin{array}{c} \\ h_{i-1}\,h_i \\ h_{i-1}\,c_i \\ c_{i-1}\,h_i \\ c_{i-1}\,c_i \end{array} \begin{array}{c} \begin{array}{cccc} h_i\,h_{i+1} & h_i\,c_{i+1} & c_i\,h_{i+1} & c_i\,c_{i+1} \end{array} \\ \begin{bmatrix} w_i & v & 0 & 0 \\ 0 & 0 & \sqrt{n_i c_i} & c_i \\ v & v & 0 & 0 \\ 0 & 0 & n_i & \beta_i \end{bmatrix} \end{array}$$

(IV-3)

Each entry $[\mathbf{I}_i]_{l,m}$ contains the contribution to the statistical weight from residue i given the local conformation corresponding to the row and column indices l and m. For example, $[\mathbf{I}_A]_{1,1} = w_A$ is the entry for an alanine residue in the interior of an α-helix, represented by the local conformation $h_{i-1}\,h_i\,h_{i+1}$; $[\mathbf{I}_D]_{4,3} = n_D$ is the entry for an aspartate residue forming the N-cap of an α-helix, represented by the local conformation $c_{i-1}\,c_i\,h_{i+1}$; $[\mathbf{I}_R]_{1,2} = v$ is the entry for an arginine residue forming the C-terminus of an α-helix, represented by the local conformation $h_{i-1}\,h_i\,c_{i+1}$; and $[\mathbf{I}_x]_{1,3} = 0$, since the local conformation $h_{i-1}\,h_i$ is inconsistent with the local conformation $c_i\,c_{i+1}$.

The statistical weight of any particular molecular conformation is the sum of the contributions from each of the residues. To calculate the molecular partition function, the statistical weights of every possible molecular conformation are summed simultaneously through matrix multiplication. As described in detail elsewhere [174,177], this sum is equal to

$$Z = \vec{u}^T \prod_{j=1}^{N} \mathbf{I}_j \, \vec{u}$$

(IV-4)

where $\vec{u} = [0\ 0\ 0\ \beta]^T$ can be considered to be the matrix representation of a capping group, which can only have a coil conformation.

To find the prevalance of any particular conformation in any particular residue i, the partition function is recalculated, constrained such that it includes only molecular conformations having the desired local conformation for residue i. For example, the probability that the local conformation of residue i is found from

$$p(h_{i-1}\, h_i\, h_{i+1}) = \frac{1}{Z}\vec{u}^T\left(\prod_{j=1}^{i-1} I_j\right)\begin{bmatrix} w_i & 0 & 0 & 0 \\ 0 & 0 & 0 & 0 \\ 0 & 0 & 0 & 0 \\ 0 & 0 & 0 & 0 \end{bmatrix}\left(\prod_{j=i+1}^{n} I_j\right)\vec{u}$$

(IV-5)

The matrix in square brackets has been substituted for $\mathbf{I}_i$. This restricts the sum to molecular conformations with the desired local conformation ($h_{i-1}\, h_i\, h_{i+1}$) by setting the statistical weight of all other local conformations (i.e., every matrix element except the one corresponding to $h_{i-1}\, h_i\, h_{i+1}$) to 0. The fractional α-helicity of any particular residue i is the normalized statistical weight of molecular conformations in which that residue is α-helical:

$$(f_{Hel})_i = \frac{1}{Z}\vec{u}^T\left(\prod_{j=1}^{i-1} I_j\right)\begin{bmatrix} w_i & v & 0 & 0 \\ 0 & 0 & 0 & 0 \\ v & v & 0 & 0 \\ 0 & 0 & 0 & 0 \end{bmatrix}\left(\prod_{j=i+1}^{n} I_j\right)\vec{u}$$

(IV-6)

The fractional α-helicity of a peptide is the average of the fractional α-helicities of its residues.

Within this framework, the values of w_i and v may be found by fitting the α-helicity of different peptides as a function of temperature to the helix–coil transition theory. This has been done by a variety of researchers [97], but there is no set of consensus values due to the fact that these parameters contain a dependence on sequence context which is unaccounted for in the theory. Development of an additional set of parameters based on the temperature dependence of α-helicity within the family of DAR-type peptides is a possibility, but would contribute little to the model of surface interactions and it is beyond the scope of this work. Instead, the values of w_i in this study will be those of Baldwin and coworkers [95] which were

Table IV-I. Parameters for prediction of α-helicity in solution: w = Lifson-Roig α-helix forming propensity (n/a: these values do not affect the calculation); ΔH_h = enthalpy of α-helix formation used to scale w with temperature, [a]Reference [95]; n = N-capping propensity, c = C-capping propensity, v^2 = α-helix nucleation constant, [b]Reference [84].

Residue	*Charge*	$w\ (0\ ^oC)^a$	$\Delta H_h\ (kcal\ mol^{-1})^a$	n^b	c^b	$v^{2\,b}$
Acetyl	none	n/a	1	12	1	0.0023
Aspartate	-	0.31	1	20	0	0.0023
Alanine	none	1.61	1	1	1	0.0023
Arginine	+	1.09	1	1.3	2.1	0.0023
Amide	none	n/a	1	1	1.3	0.0023

found for short synthetic alanine-based α-helical peptides, but with different sequences than those studied here. The temperature dependence of w_i is set by its identification as the equilibrium constant for α-helix formation, Equation (IV-2), combined with the value of $\Delta H_h = 1$ kcal mol^{-1}, which has been determined calorimetrically and is not strongly sensitive to residue type [95]. Based on these values a reasonable [178] entropic contribution to α-helix formation can be calculated (-11 J mol^{-1} K^{-1} for alanine). The final parameter needed for solution helix–coil transitions, v^2 was assigned a value of 0.0023, as was done in other studies [82,83]. Qualitatively similar results are obtained for a range of w_i and v parameters, provided the values chosen support the experimentally observed α-helix formation in solution. The parameters used to describe the helix–coil transition in solution are given in Table IV-I.

The values of β_i are not equal to 1 for adsorbed molecules due to the ability of residues to interact with the surface in the coiled state. Adsorption to a surface could, in general, lead to a variety of conformational changes about which very little is known. For the purposes of this model, it is assumed that adsorption provides reversible "binding" interactions between the surface and certain coiled states.[12] The new statistical weight of the coil state (relative to the statistical weight of the coil state in the absence of any surface interaction) is written

$$\beta = \sum_i \Omega_i e^{-\Delta H_i / RT} = \sum_i e^{-\Delta G_i / RT} \qquad \textbf{(IV-7)}$$

[12] If residues in helical states can also interact with the surface, the interaction modeled here is that of the coiled states relative to the helical states.

where each term in the sum represents a possible substate of the accessible coiled conformations, and $\sum_i \Omega_i = \Omega_c \equiv 1$. If $\beta > 1$ the α-helical conformations are destabilized by the interaction with the surface, and a decrease in α-helicity of the molecule as a whole results. A similar approximation has been used to model the increase in helicity of poly-β-benzyl-L-aspartate with increasing temperature, due to interactions between the sidechains and dichloroacetic acid in solution [175]. In the present work the form of β has been written to incorporate the proper behavior in the limit of weak surface interactions [179] ($\lim_{\Delta G_i \to 0} (\beta) = 1$).

As an example of the application of Equation (IV-7), the arginine residues of the molecule 4^+DAR4 are considered. These are attracted electrostatically to the colloidal silica surface, resulting in the orientation of the molecule on the surface such that the arginine residues at the C-terminus are apposed to the surface. In general, not all coil conformations necessarily participate in this interaction, so the statistical weight contains two terms:

$$\beta_R = \Omega_b e^{-\Delta H_b / RT} + (1 - \Omega_b) = 1 + \Omega_b (e^{-\Delta H_b / RT} - 1) \qquad \textbf{(IV-8)}$$

where the enthalpy (ΔH_b) is the electrostatic interaction between the ionic side chain and the negatively-charged surface (which is controlled by pH), and Ω_b is the number of conformations which are able to participate in this interaction (this value is assumed to be independent of pH).

Interactions between the other residues of the peptide and the surface are qualitatively different. As described in Chapter III for related peptides, the aspartate residues of the peptide N-terminus are repelled from the surface and reside in the diffuse layer. The potential gradient in the diffuse layer ($\partial\Psi/\partial z$) provides a driving force to maximize the separation of these residues from the surface. This driving force promotes conformations in the N-terminal aspartate residues, as well as in the intervening alanine residues at the center of the peptide, such that the projection of the peptide contour length is increased in the direction normal to the surface.[13] Correspondingly, this driving force disfavors other conformations which

[13] This set of favored conformations is likely to include the conformational space of β-strands; however, no evidence for this secondary structure is observed by CD.

decrease this distance. The number of conformations that are favored and disfavored by this driving force are represented by Ω_s and Ω_u, respectively, and the statistical weight of the aspartate and alanine coiled states is then found to be:

$$\beta_A = \Omega_s e^{-\Delta H_s / RT} + \Omega_u e^{+\Delta H_s / RT} = e^{+\Delta H_s / RT} - 2\Omega_s \sinh(\Delta H_s / RT)$$

(IV-9)

Here the enthalpy of the interaction (ΔH_s) that stabilizes "stretched" conformations in any particular residue is the electrostatic stabilization that results from translation of the ν charges between the N-terminus and the residue in question (inclusive) a distance δ in the direction normal to the surface. This distance is characteristic of the change in projection of the contour length of one residue along the normal to the surface:

$$\Delta H_s = \nu e N_A \delta \left(\frac{\partial \Psi}{\partial z} \right)_{z_N}$$

(IV-10)

where e is a unit charge, N_A is Avogadro's number, and the potential gradient ($\partial\Psi/\partial z$) is evaluated at the average position of the charged aspartate sidechains, z_N. Neither this distance nor the stretching length δ is known with certainty; however, the above equation can be used to find the dependence of the enthalpy ΔH_s on the pH. The gradient of the potential is related to the value of the potential through the equation [166]

$$\frac{e}{kT}\frac{\partial \Psi}{\partial z} = -2\kappa \sinh\left(\frac{e\Psi}{2kT} \right)$$

(IV-11)

For the range of interest ($\Psi \approx$ -40 mV), once the temperature-dependence of the dielectric constant is taken into account, the potential gradient is nearly independent of temperature, and its dependence on the potential is nearly linear. Therefore, as was the case for the arginine interaction, this enthalpy is assumed to be controlled by pH, while the entropy is assumed to be independent of pH.

The forms derived above for the statistical weights of the coil states of adsorbed molecules involve thermodynamic parameters for interactions with the surface. Parameters may either be modeled or fit from experimental data. These forms and parameters embody

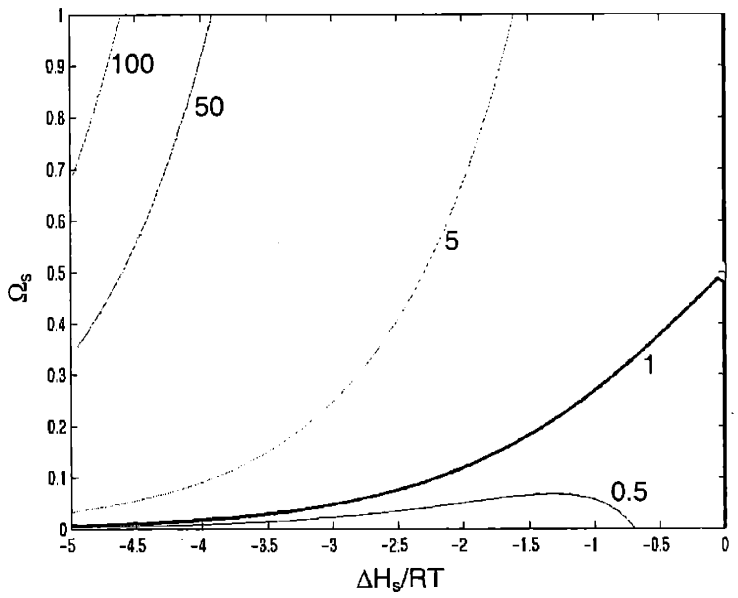

Figure IV-1. Contour plot of β_A calculated from Equation (IV-9). Values of the function β_A are indicated adjacent to the contour lines.

the physical assumptions of the model which, though simplified, capture the essential features of the adsorption process. They give insight into the interactions of individual residues with the surface, as well as the way in which these interactions translate into conformational changes in the molecule as a whole.

Although Equation (IV-9) accounts for enthalpically-favored "stretched" states, it is important to note that it can lead to values of β less than unity. This occurs for relatively small values of Ω_s and $-\Delta H_s$, which corresponds to a situation where the coil state on the surface is disfavored overall because of a relatively large number of states (Ω_u) that position negatively-charged residues closer to the surface than average coil conformations. Values of β_A are shown in Figure IV-1 as a function of the enthalpy and entropy of the stretched state. The bold contour line (with a contour value of 1) separates the sets of parameters which favor and disfavor the coil state relative to the situation in the non-adsorbed peptide. The region below this line represents the disfavored coil states described above, which are characterized by relatively weak surface interaction enthalpies, and small numbers of possible conformations (small Ω_s). The region above this line, with contour values greater than 1, represents stabilized coil states, which have surface interactions characterized by strongly negative enthalpies, and with a variety of possible conformations (large Ω_s).

Given the highly idealized nature of this model, the enthalpy and entropy values used to calculate β_i are regarded as effective parameters. Examining their effect on the helix–coil transition on the surface, as simulated by this statistical model, provides information on the energetics of the interaction between the peptide and the surface. It is important to note that the trends predicted by the model result from the functional forms derived above, and are qualitatively similar for a range of thermodynamic parameters representing realistic enthalpy and entropy values for interactions with the surface.

Experimental

CD spectra of the HPLC-purified peptide 4^{+}DAR4 in solution with colloidal silica purified as in Chapter III.2 were taken in 1 mm pathlength quartz cells (Starna) on an Aviv-220 spectrometer. Typical spectra were measured between 190 and 250 nm, at every 1 nm with at least 2 s averaging if no colloid was present, and 10 s averaging if colloid was present. Ludox HS concentrations were measured by drying a sample of known mass and measuring the mass of silica remaining.

Fractional α-helicity of molecules in solution (in the absence of any surface interaction) was predicted using the FORTRAN program written by other researchers and previously made available by anonymous ftp [174]. This program was modified to include the effects of temperature according to Equation (IV-2) as well as the forms of β specified in Equations (IV-8) and (IV-9). This modified program is shown in Appendix B, along with a sample calculation. Enthalpies were scaled linearly within the range between strong and weak surface interaction energies to simulate the effect of changing pH while the entropies were held constant.

Temperature Dependence of α-Helicity of Adsorbed Molecules

4DAYAR5 molecules in solution with colloidal silica gain α-helicity with increasing temperature (data not shown), but a large contribution of the observed increase of $-[\theta]_{222}$ is due to alteration of the adsorption equilibrium. Increased temperature leads to desorption of

molecules from the silica surface, as shown in the temperature-dependent adsorption isotherms presented in Chapter III.4 (Figure III-7). It is possible in principle to correct for this effect by determining the actual adsorbed amount as a function of temperature in samples used for CD measurements. However, this is impractical due to light scattering: the largest-diameter particles that can be used for precise CD measurements are Ludox TM (22 nm diameter), but such small particles cannot be sedimented effectively by centrifugation except in the high-speed Sorvall centrifuge, which cannot attain temperatures greater than 30 °C.

The use of 4^{+}DAR4 provides a way to determine the α-helicity of adsorbed molecules. Due to the net positive charge, it adsorbs more strongly to colloidal silica than 4DAYAR5, and it is adsorbed completely at silica concentrations of about 6 wt% at pH 7.37, as shown in Figure IV-2. Virtually all molecules in the samples with Ludox HS concentrations above 6 wt% are adsorbed, even at 90 °C, as indicated by the absence of a dependence of α-helicity on Ludox HS concentration above this value.

α-Helicity of these adsorbed molecules was measured as a function of increasing pH and temperature, as shown in Figure IV-3. At pH ≈ 7, the α-helicity of adsorbed molecules decreases with increasing temperature. In this regime, adsorption induces an additional destabilization of α-helicity beyond that caused by temperature. This behavior is typical of that observed for α-helical peptides in solution when α-helicity is destabilized by two simultaneous mechanisms, such as by a combination of elevated temperature and added chemical denaturant.

In contrast, at pH ≈ 8 the α-helicity of adsorbed molecules is nearly independent of temperature, and at pH ≥ 9 the α-helicity of adsorbed molecules *increases* with increasing temperature. These trends provide evidence for a temperature dependence of the intermolecular interactions between peptide and surface groups which offsets that of the intramolecular interactions that stabilize α-helicity of peptides in solution. The temperature dependence of α-helicity results from the competition between two temperature-dependent functions: the statistical weight of the α-helical state, whether free or adsorbed, tends to decrease with temperature, but at basic pH this is overwhelmed by the temperature dependence of the surface interaction, which decreases more strongly with temperature.

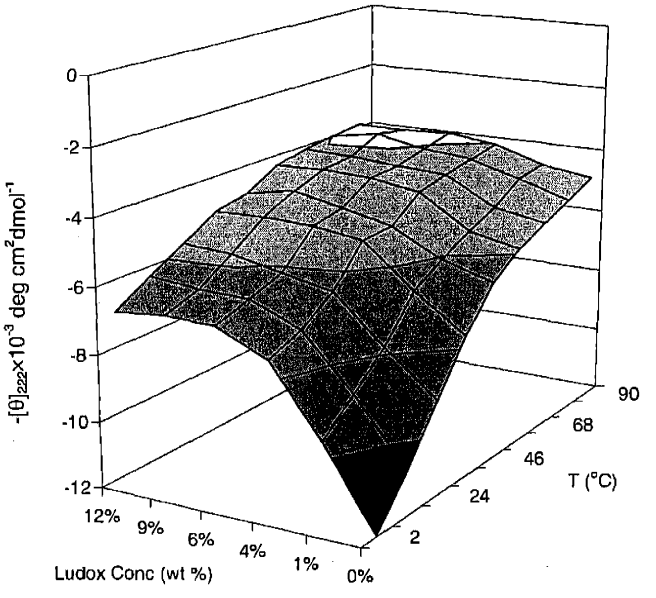

Figure IV-2. CD signal of 4⁺DAR4 ($[\theta]_{222}$) as a function of temperature and Ludox HS concentration. Adsorption conditions are at 76 μM peptide concentration and pH 7.37. Values are linear interpolations between nearest surrounding temperature points, averaged between ascending and descending temperature scans. Some hysteresis was observed between ascending and descending temperature scans. Roughness in the surface is completely accounted for by the signal to noise ratio of the data collection. Note that the separation between lower left axis labels and data points does not reflect their true pH values. α-Helicity is independent of Ludox HS concentration above 6 wt%, which indicates complete adsorption above this concentration.

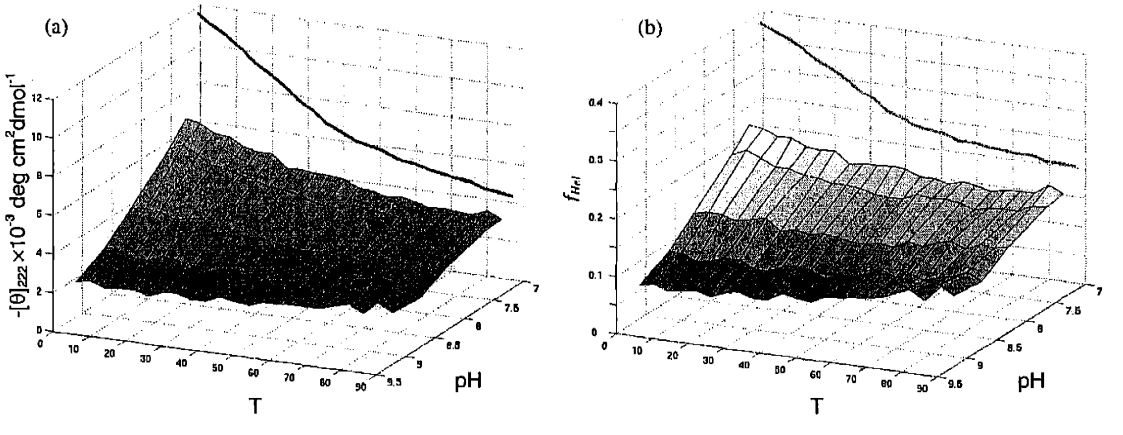

Figure IV-3. α-Helicity of adsorbed 4⁺DAR4 as a function of pH and temperature: (a) specific α-helicity, and (b) fractional α-helicity remaining in adsorbed 4⁺DAR4 molecules, calculated from the specific α-helicity using Equation (II-2).

The pH at which the change in the sign of the temperature dependence of α-helicity of adsorbed molecules occurs is not known exactly, since the coefficient of temperature in the denominator of Equation (II-2) is not known with precision. The value of

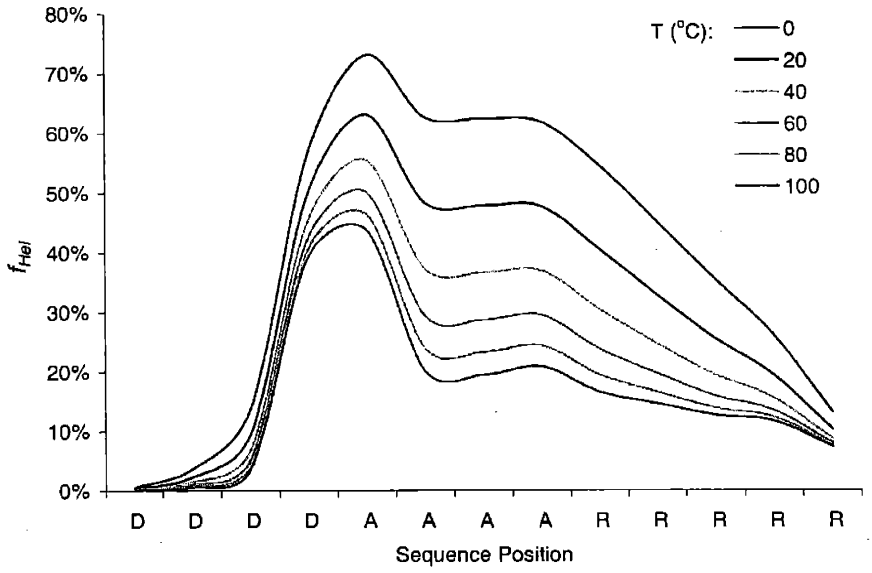

Figure IV-4. Estimates of average molecular conformation of 4^{+}DAR4 in solution produced by the sequence-dependent Lifson-Roig model with N- and C-capping. Parameters are given in Table IV-I.

100 deg cm^2 $dmol^{-1}$ T^{-1} has been used in this work, but different magnitudes for this coefficient have been reported [103]. The order of magnitude of this coefficient seems well-established, and the trends in α-helicity as a function of temperature shown in Figure IV-3(a) are modulated, but not qualitatively changed, by the value of this coefficient.

As noted in the introduction to this section, statistical models of the helix–coil transition in solution capture thermal destabilization of α-helicity, as well as the localization of α-helicity in the central residues of peptides. Therefore, the conformation of DAR-type peptides in solution may be estimated using the parameters given in Table IV-I and setting $\beta_i = 1$. Temperature-dependent results from this model are shown in Figure IV-4. The differential α-helix content at the termini is a result of the lower α-helix-forming propensity of aspartate relative to arginine ($w_D < w_R$); this ranking is common to nearly all reported sets of parameters, and is in agreement with the site-specific conformational measurements reported in Chapter II.4 for 4DAR5.

An enthalpically-favored, entropically-disfavored bound state destabilizes α-helicity of the arginine terminus. The favored coil state propagates into the rest of the peptide, leading to destabilized α-helicity of the alanine terminus as well. In the limit of strong binding ($\beta_R >> 1$), the statistical model of an adsorbed peptide with $\beta_A = \beta_D = 1$ is identical to that of a

Table IV-II. Thermodynamic parameters for residue interactions with the silica surface: ΔH_b, ΔS_b: enthalpy and entropy of arginine residue interactions with silica surface; ΔH_s, ΔS_s: enthalpy and entropy of alanine residue interactions with silica surface. Aspartate-surface interactions are found by scaling ΔH_s downward as per the discussion of Equation (IV-10).

Surface interaction energy	*Arginine interaction*		*Alanine, Aspartate interactions*	
	ΔH_b (kJ mol^{-1})	ΔS_b (J mol^{-1} K^{-1})	ΔH_s (kJ mol^{-1})	ΔS_s (J mol^{-1} K^{-1})
Weak	-3.3	-5.8	-1.3	-12.6
Strong	-10.0	-5.8	-4.2	-12.6

shorter peptide containing only the aspartate and alanine segments free in solution with the arginine segment removed. However, even in the limit of strong binding, an interaction with only the arginine terminus is insufficient to lead to the near-complete destabilization of α-helicity over the entire molecule which is observed for molecules adsorbed below room temperature at or above pH 9. This implies that the interactions of alanine and aspartate residues with the surface must be modeled, in order to capture the conformational behavior of the peptide.

Calculating β_A and β_D from equation (IV-9), thereby allowing alanine and aspartate residues to interact with the surface, leads to destabilization of α-helicity over the entire molecule under conditions of strong adsorption. Typical modeling parameters are tabulated in Table IV-II. These parameters lead to $\beta_A > 1$ for strong adsorption ($\Delta H_b = -10$ kJ mol^{-1}) at low temperature, as required to duplicate the near-complete α-helicity loss under these conditions, but at higher temperature and lower pH, β_A and β_D are between 0.8 and 1.0. In other words, this particular model allows the coil state of alanine and aspartate residues of an adsorbed molecule to be either favored or disfavored relative to the coil state in the absence of any surface interaction, and best captures the experimental behavior when both cases occur depending on pH and temperature. Estimates of α-helicity as a function of sequence position are shown in Figure IV-5. α-Helicity of adsorbed molecules is dominated by the alanine segment. Interestingly, this model predicts only minor loss of α-helicity from the aspartate segment at 20 °C, in agreement with the observation that the D-αH signal in ^{1}H NMR of adsorbed 4DAR5 did not shift significantly, indicating a relatively unperturbed conformation.

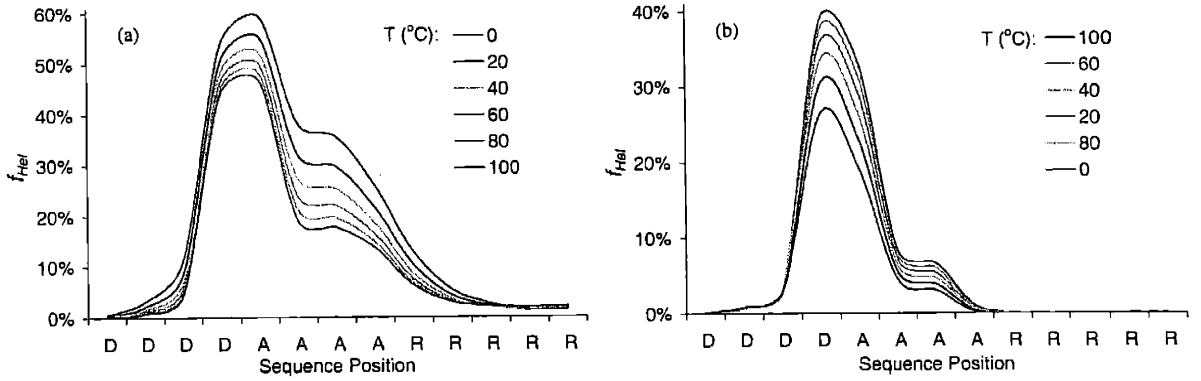

Figure IV-5. Estimates of the conformation of 4⁺DAR4 on the silica surface with energetic parameters corresponding to (a) weak adsorption; (b) strong adsorption. Parameters for the surface interaction energies are given in Table IV-II. Parameters for α-helix formation are the same as in Table IV-I.

The ability of this statistical model to reproduce the observed sign change in the temperature dependence of the fractional α-helicity ($\partial f_{Hel}^{Ads}/\partial T$), from negative values at intermediate adsorption affinity (neutral pH) to positive values at strong adsorption affinity (high pH), provides a stringent test of the extent to which the balance between intramolecular and intermolecular bonding is captured. In Figure IV-6, the dependence of the overall fractional α-helicity on temperature and surface interaction is plotted for the parameters used to describe the surface interaction (Table IV-II), allowing ΔH_b to range from weak to strong interactions. The resulting surface is very similar to the experimental results plotted in Figure IV-3(b). The values for the parameters chosen for "weak" adsorption approximate adsorption at neutral pH, while the parameters for "strong" adsorption approximate adsorption at basic pH.

The circumstances under which the statistical model can predict the inversion of temperature dependence can be evaluated analytically. The behavior of only one segment type is considered, and sequence heterogeneity is neglected. Although the perturbations to β are residue-dependent, the temperature dependence of the conformation of adsorbed peptide at strong surface interaction energies appears to be dominated by residues D4 – A8 (Figure IV-5). Therefore in the following discussion, the temperature dependence of w and β, in the forms of Equations (IV-2) and (IV-9), respectively, will be examined to find the range of parameters for which the temperature dependence of fractional α-helicity ($\partial f_{Hel}^{Ads}/\partial T$) can

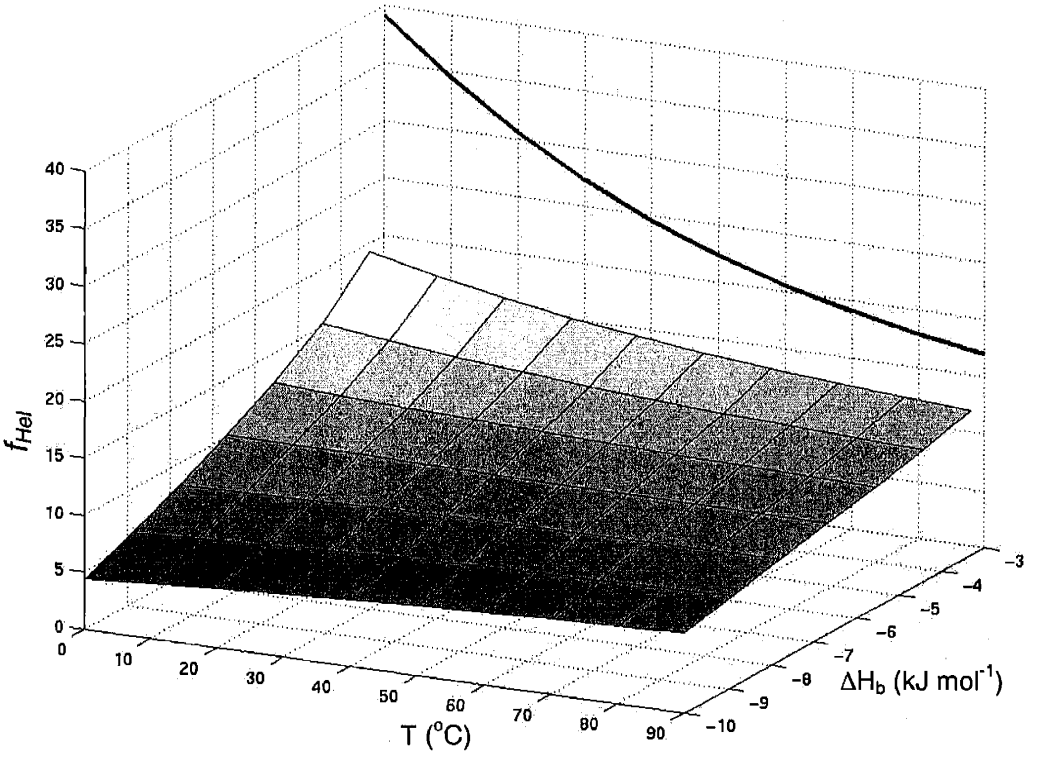

Figure IV-6. Fractional α-helicity for free (line) and adsorbed (surface) molecules as a function of temperature and ΔH_b ranging from weak to strong surface interactions.

change sign. For the parameters listed in Table IV-II, β and w are of the same order of magnitude. Since these quantities correspond to the statistical weights of the coil and α-helix states, respectively, an estimate of the dependence of α-helicity on temperature can be made by comparing the temperature dependence of these two quantities. More specifically, by neglecting cooperativity ($v \rightarrow 1$), finite α-helix length ($N \rightarrow \infty$), and capping effects ($n, c \rightarrow 1$), a greatly simplified equation for the fractional α-helicity [173] is produced:

$$\left(f_{Hel}^{Ads}\right)_{\substack{\sigma=1 \\ n,c=1 \\ N=\infty}} = \frac{w}{w+\beta} \qquad \textbf{(IV-12)}$$

Differentiation of this equation shows the condition for which the dependence of α-helicity on temperature can change from positive to negative:

$$\beta \frac{\partial w}{\partial T} - w \frac{\partial \beta}{\partial T} = 0$$

(IV-13)

The free energy of α-helix formation and its temperature dependence are independent of the strength of the surface interaction, so the dependence of α-helicity of adsorbed molecules on temperature is controlled by the terms β and $\partial\beta/\partial T$. The term $\partial\beta/\partial T$ is small and negative for the weak surface interaction energies (Table IV-II), but large and negative for the strong interaction energies. This leads to a change in sign of $\partial f_{Hel}^{Ads}/\partial T$ between weak and strong surface interaction energies. Therefore, in this simplified model, the observed temperature dependence of α-helicity of adsorbed molecules is shown to be determined by the relative importance of the temperature dependences of the α-helix and coil states.

The simplified treatment of the surface interaction terms for adsorbed molecules thus captures both the effects that adsorption has on conformation, and the temperature dependence of these effects. For a weak surface interaction energy, the temperature dependence of the α-helicity of adsorbed molecules is controlled by the enthalpy of α-helix formation, which represents the same factors that control the α-helicity of peptides in solution. In contrast, for a strong adsorption enthalpy, the intermolecular interactions between peptide and surface dominate the intramolecular bonding that stabilizes the α-helicity of peptides in solution. The interactions between peptide and surface become weaker at higher temperature, allowing adsorbed molecules to regain α-helicity. Taken together, the trends predicted by the model are in good qualitative agreement with the experimental results, and they support the view that the inversion of the dependence of α-helicity on temperature for adsorbed molecules is a result of the balance of temperature dependences of competing intramolecular and intermolecular interactions.

3. Proteolysis of Adsorbed Short α-Helical Peptides

Introduction

Many important classes of bioactive peptides, such as peptide hormones and the antifreeze glycopeptides, have functions that depend on their ability to participate in molecular recognition and specific binding. Nearly all biochemical reactions in which peptides and proteins participate, such as phosphorylation, glycosylation, and proteolysis, occur with a high degree of specificity. An understanding of the driving forces for adsorption and orientation of short α-helical peptides on silica surfaces is important, because adsorption may alter or eliminate the specific interactions upon which the biological functions of such molecules depend.

Proteolysis is an ideal model biochemical reaction for quantitative study of the effects of adsorption, since a wide variety of enzymes exist that exhibit well-characterized sequence specificity, thus giving a great deal of flexibility to experimental design. Adsorption of enzymes to colloidal particles is partly determined by the charge of the enzyme relative to the surface. Because adsorption may lead to changes in catalytic activity, the activity of an enzyme in the presence of colloidal particles depends on its charge and optimal pH range, both of which vary widely among enzymes. Thermolysin (34,600 g mol^{-1} [180]) is a protease isolated from a thermophilic bacterium, *Bacillus thermoproteolyticus*. Commonly used in detergents, it retains activity at temperatures up to 60 °C [181]. It is an endopeptidase (i.e., it favors cleavage at interior residues of a peptide chain) that is specific for bulky apolar side chains, particularly isoleucine, leucine (L), valine, phenylalanine (F), and, to a lesser extent, alanine (A) [181]. The isoelectric point of thermolysin is 4.45 [182], which implies a negative surface charge at pH 8. These features are all essential for selection of this enzyme for the model biochemical reaction of proteolysis of DAR-type peptides on surfaces. DAR-type peptides present a variety of A-A peptide linkages as possible cleavage sites for the enzyme, each of which may have a different relative activity depending on the conformation and orientation of the peptide on the surface. In addition, the enzyme is robust and repelled electrostatically from the silica surface, properties which minimizing adsorption and denaturation that could interfere with proteolysis.

Since complete adsorption of the peptide is essential for unambiguous interpretation of the results, the peptide 4AAR4 (Ac-AAAAAAAARRRR-Am) adsorbed to Ludox TM was selected, in order to maximize the amount of adsorbed peptide. This peptide is expected to adsorb via arginine side chains. However, this molecule may be less strongly oriented than aspartate-containing DAR-type peptides on the surface, due to the absence of strong electrostatic repulsion between the N-terminus and the surface.

Experimental

Thermolysin was obtained from Sigma (P1512, Protease Type X) and recrystallized from aqueous calcium acetate according to the published procedure [181]. Lyophilized enzyme was dissolved in the standard buffer for this reaction (10 mM $CaCl_2$, 10 mM tris buffer, pH 7.8) and the concentration was measured spectrophotometrically using a molar extinction coefficient of 66,300 M^{-1} cm^{-1} at 280 nm [181]. Adsorption of this enzyme to Snowtex ZL was evaluated at pH 8.0 by the isotherm techniques described previously.

The peptide 4AAR4 was purified by RP-HPLC and was dissolved in the standard buffer at two different concentrations, which were measured by CD spectroscopy. Ludox TM colloidal silica was purified using an Amicon filter as described in Chapter III.2, then suspended in the buffer. Small amounts of aqueous HCl and NaOH were used to adjust the pH.

Known amounts of the peptide, enzyme, and colloid solutions were combined and vortexed immediately. Samples were removed at intervals using a micropipette and were added to 0.2 N acetic acid to quench the reaction. The extent of reaction was measured using a ninhydrin assay [183] (Sigma), which undergoes a colorimetric ($\lambda_{max} = 560$ nm) redox reaction with primary amine groups but not with the tris buffer. Each peptide bond cleavage reaction produces a primary amine on the C-terminal fragment.

In a separate experiment, the extent of adsorption of 4AAR4 to Snowtex ZL in buffer was determined by combining known volumes of peptide and colloid solutions, centrifuging in the Sorvall centrifuge, and measuring the CD spectra of the resulting solutions.

Samples were prepared for MALDI-TOF mass spectrometry by pipetting quenched proteolysis solutions repeatedly through a ZipTip™ pipette tip (Millipore) loaded with C18

chromatography media, followed by rinsing with 5% aqueous acetonitrile. This treatment causes peptide fragments to adhere to the hydrophobic surface of the packing material in the tip. The tip was then rinsed with 50% aqueous acetonitrile to desorb the fragments, and the solution was subjected to MALDI-TOF analysis. Samples were analyzed by the Biopolymers Laboratory in the Center for Cancer Research at MIT in positive ion mode on a Sciex Model API 365 mass spectrometer.

Results

No adsorption of thermolysin to colloidal silica was detected by the standard method of UV difference spectra. This experiment provides assurance that interactions between the enzyme and surface are minimized, but it does not preclude very weak adsorption (i.e., below the signal to noise ratio of the experiment, approximately 5%) or time-dependent inactivation of the protein. The possibility of weak reversible protein adsorption will be discussed later in this section. No time-dependent inactivation was observed in the experiments described below.

Reaction conditions were selected such that peptides subject to proteolysis were dominated by those adsorbed to the surface. Three important conditions must be fulfilled for this to be the case: 4AAR4 must be predominantly adsorbed to the colloidal silica rather than in solution; the reaction rate must be controlled by the available peptide, and not limited by enzyme turnover kinetics; and the reactivity of the adsorbed peptide must not be eliminated by adsorption to the surface.

Fulfillment of the first condition was demonstrated for these experimental conditions using CD spectroscopy (Figure IV-7). No peptide is detectable in solution after removal of adsorbed peptide by centrifugation. This result was expected from calculations based on the adsorption isotherm measured previously and described in Chapter III. After analysis of the signal to noise ratio of the CD spectra, the extent of adsorption was calculated to be at least 98.7% for the highest peptide concentrations studied, and an even higher adsorbed percentage was obtained at lower peptide concentrations.

In order for the surface reaction to be dominant, it is also necessary for the enzyme turnover kinetics to be rapid relative to the available peptide concentration. If the turnover

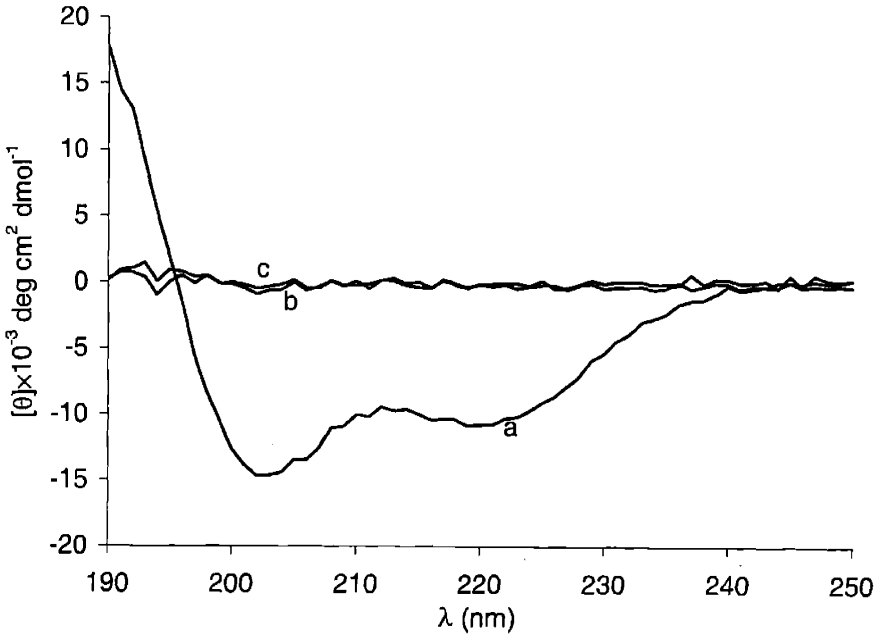

Figure IV-7. CD spectra of peptide and colloid samples in the proteolysis buffer (10 mM $CaCl_2$, 10 mM tris buffer, pH 7.8): (a) AAR, no colloid; (b) supernatant of 4AAR4 (329 μM (0.41 mg ml^{-1})) and Ludox TM (10 wt %) solution, after removal of colloid with adsorbed 4AAR4 by centrifugation; (c) supernatant of 4AAR4 (33 μM (0.04 mg ml^{-1})) and Ludox TM (10 wt %) solution, after removal of colloid with adsorbed 4AAR4 by centrifugation. No peptide is detected in the supernatant solutions within the uncertainty limit of CD. Further detail is given in the text.

rate is extremely slow, even a very small amount of peptide in solution could be sufficient to dominate the total reaction, if it is much more accessible to the enzyme than that on the surface. To determine the conditions for enzyme saturation, the mechanism of proteolysis of the peptide 4AAR4 (*AAR*) into N-terminal peptide fragments (*A*) and C-terminal peptide fragments (*AR*) catalyzed by a known concentration of thermolysin (*Th*) can be modeled as [184]:

$$Th + AAR \underset{k_{-1}}{\overset{k_1}{\rightleftarrows}} Th - AAR \xrightarrow{k_2} Th + A + AR$$

(IV-14)

This mechanism, combined with the steady-state approximation, leads to the kinetic expression

$$\left(\frac{d[AR]}{dt}\right)_{t=0} = \frac{k_2[Th][AAR]}{K_M + [AAR]}$$

(IV-15)

Here, k_2 and $K_M = (k_{-1} + k_2)/k_1$ are both enzyme- and substrate-specific constants. The value of k_2 is approximately 70 s^{-1} for one commonly-used substrate, N-furylacryloylglycyl-L-leucinamide (Fua-G-L-NH_2, G = glycine) [185]. Values of 1000 s^{-1} have been reported for hydrolysis of the F-L bond in tri- and tetrapeptides of the form X-F-L-A [184], where the identity of the first amino acid (X) was varied, and of the A-L bond in various tripeptides [186]. Values as low as 1.6 s^{-1} were reported for a set of tripeptides with an initial G residue [187]. Reported values of K_M also vary widely, but they are frequently on the order of 2.5 mM (for Fua-G-L-NH_2). Much lower values (0.08 mM) were reported for the tripeptides containing an initial G residue [187]. Because the work here is confined to $[AAR] << K_M$, only the ratio k_2/K_M is observable; this ratio is similar to the one for Fua-G-L-NH_2 (28 mM^{-1} s^{-1}).

Equation (IV-15) quantitatively defines the conditions for enzyme saturation. The enzyme is saturated only if $[AAR] >> K_M$. In this case the peptide proteolysis reaction displays zero-order kinetics, with a reaction rate $V_{max} = k_2[Th]$. In contrast, under the condition $[AAR] << K_M$, the reaction rate is $(k_2/K_M)[AAR][Th]$, and the quantity k_2/K_M is a pseudo-first-order rate constant for peptide proteolysis.

Thus for the surface reaction to be dominant in this situation (for which the vast majority of peptide is adsorbed), it is necessary that

$$[AAR]_{soln} << K_M \qquad \textbf{(IV-16)}$$

where $[AAR]_{soln}$ represents the concentration of peptide free in solution. Since, as described previously, no free peptide was detectable within experimental error for the samples studied in this work, Equation (IV-16) is fulfilled for even the smallest values of K_M quoted above (0.08 mM), as well as for the more typical values of K_M (2.5 mM) which, as mentioned above, are most likely to apply to this system.

Fulfillment of the third condition for dominance of the surface reaction (that adsorption does not eliminate peptide proteolysis) can be determined readily by the reaction rate over the course of the experiment, assuming the other two conditions above are fulfilled. In other words, given that there is only a small percentage of peptide free in solution, a solution-phase reaction that is controlled by peptide concentration (not by enzyme turnover kinetics) occurring in the presence of colloid would have a reaction rate on the order of this

same small percentage of the solution reaction rate. In contrast, in the presence of colloid, rapid proteolysis still occurred, as shown in Figure IV-8(a). Therefore, this reaction must be dominated by proteolysis of adsorbed peptide.

At the peptide concentration relevant to Figure IV-8, the reaction kinetics show remarkably little influence from the presence of colloidal silica, even for this strongly-adsorbing peptide. The initial velocity of the reactions were the same within error, and significant deviations between the two only occur after about 30 minutes, when the concentration of 4AAR4 has been greatly reduced. At lower initial peptide concentrations, the proteolysis rate is significantly reduced by the presence of colloidal silica, as shown in Figure IV-8(b). This data is of lower quality, due to the decreased peptide concentration. Nevertheless, the data show that the reaction rate in the presence of colloid is significantly slowed.

The trends shown in Figure IV-8(b) appear similar to those of a reaction in the absence (no Ludox TM) and presence (Ludox TM) of a reversible competitive inhibitor [188] to the enzyme activity. In the present case the inhibition could be caused by reversible association of thermolysin with colloidal particles. For the samples plotted in Figure IV-8(a) there is an average of more than six peptide molecules per colloidal particle, but for Figure IV-8(b) there is one-tenth this value, or less than one molecule per particle. Therefore it is useful to think of the competitive inhibition as coming from colloidal particles with no adsorbed peptide molecules. Although thermolysin does not adsorb to the Snowtex ZL surface in a detectable quantity, it is possible that weak surface interactions, not detected by the adsorption experiment, could lead to appreciable fractions of adsorbed enzyme, given the high concentration of high-surface-area Ludox TM particles used for proteolysis experiments. Alternatively, thermolysin molecules could populate the near-surface area solely through random thermal motion, which could explain the trends in Figure IV-8(b); the goal of the following discussion is to establish that this hypothesis provides a satisfactory explanation of this data.

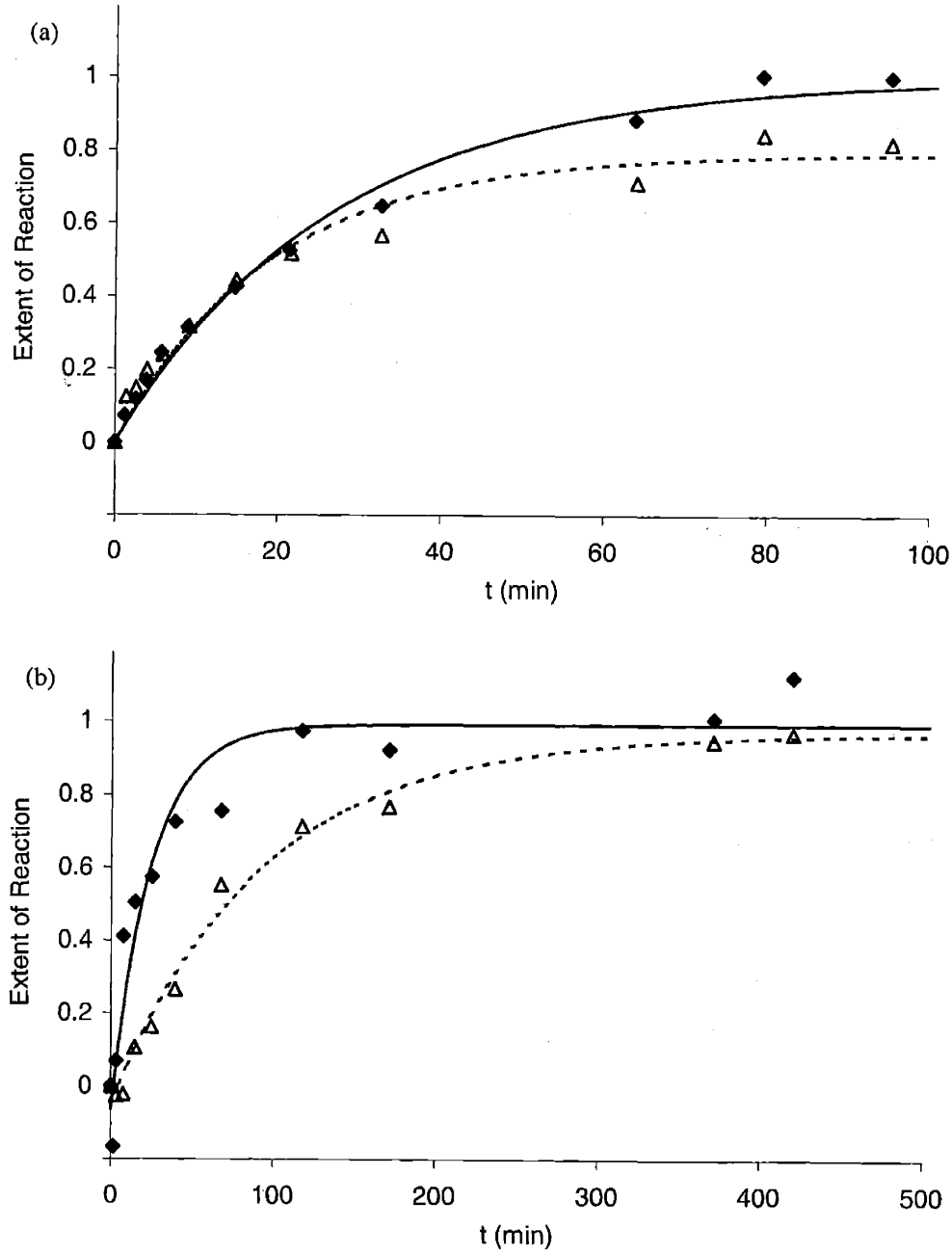

Figure IV-8. Kinetics of proteolysis of 4AAR4 by thermolysin. (a) Time dependence of 4AAR4 proteolysis at 0.55 mg ml^{-1} (370 μM) peptide concentration with (△) and without (◆) Ludox TM. Additional data points at 902 min (not shown) confirm the plateaus shown. (b) time-dependence of 4AAR4 proteolysis at 0.055 mg ml^{-1} (37 μM) peptide concentrations with (△) and without (◆) Ludox TM. Additional data points at 830 and 892 min (not shown) confirm the plateaus shown. Other reaction conditions: 11 wt% SiO_2 particles (Ludox TM), 0.019 mg ml^{-1} (0.55 μM) thermolysin, pH 7.8. Trendlines of the form $\left(1-e^{-t/\tau}\right)$ are shown only as guides, with values of the time constant (τ) of (a) 54 s for the data with Ludox TM (- - -), 75 s for the data without Ludox TM (—); (b) 16 s for the data with Ludox TM (- - -), 59 s for the data without Ludox TM (—).

Since the solution-phase proteolysis reaction follows Michaelis-Menten kinetics, this framework will be used to formalize and analyze this hypothesis. Although there is no evidence to support or refute the proposition that proteolysis of adsorbed peptides also follows Michaelis-Menten kinetics, it is instructive to consider the effects of adsorption on the reaction mechanism of Equation (IV-14). Modification of this mechanism to include strong adsorption of peptide, as well as competitive inhibition due to weak dsorption of protein (adsorbed molecules and surface-phase reaction rates are indicated by an asterisk), leads to the scheme

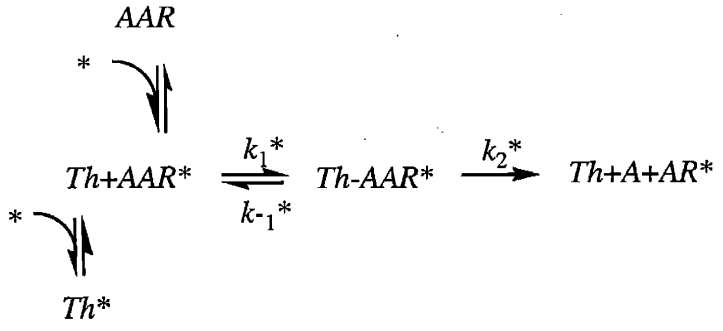

(IV-17)

Here, the double arrows denote an equilibirum, with the larger arrow indicating the favored interaction, and asterisks indicating that the interaction involves adsorption. Peptide adsorption is assumed to be essentially complete, so that the solution-phase reaction can be neglected. In addition, the competing adsorption of enzyme is to be interpreted as occurring only on particles with no adsorbed peptide; adsorption of the enzyme to particles with adsorbed peptide molecules is always identified with enzyme-peptide complex formation. This is an important assumption and can be restated as follows: no inhibition of proteolysis is observed from the presence of colloidal silica when the peptide concentration is high enough to provide multiple adsorbed peptide molecules for each particle; therefore interactions between the enzyme and areas of such particles not containing peptide are neglected. This could be due, for example, to the neutralization of surface charge by adsorbed peptide and the resulting enhancement of adsorption to these sites.

In order to make the above hypothesis plausible, it is still necessary to provide an explanation for the apparent equality between the proteolysis rate on the surface (k_2^*/K_M^*) and the corresponding value for the solution-phase reaction, (k_2/K_M). The parameter k_2 primarily reflects the energy of the transition state for formation of peptide fragments from the enzyme–

peptide complex. To a first approximation, the energy barrier to this transition state may not be significantly different in the adsorbed reaction. In contrast, the value of K_M could be changed by adsorption, but in this situation no evidence for such a change is apparent. In other words, the population of the enzyme–peptide complex is the same as in solution:

$$\frac{[ES]^*}{[E][S]^*} = \frac{[ES]}{[E][S]} \qquad \textbf{(IV-18)}$$

Alhough this is somewhat surprising, it is plausible because although the energy of an adsorbed 4AAR4 molecule is lower than that of the same molecule in solution (due to the electrostatic interactions that drive adsorption), to a first approximation the energy of the enzyme-peptide complex is lowered by this same amount. This leads to the same population of enzyme-peptide complexes, and therefore to the same overall reaction rate. Taken together, the hypothesis of competitive inhibition of peptide proteolysis provides one possible explanation for the trends in Figure IV-8.

Mass spectrometry of quenched samples from reactions at a peptide concentration of 0.055 mg ml^{-1}, with and without colloid, reveals the presence of two sets of fragments between 500 and 1700 g mol^{-1}. The first set corresponds to peptide fragments of the form H-A_nR_4-NH_2 which result from proteolysis of 4AAR4. Proteolysis by thermolysin resulted in n values between 1 and 3 for the reaction in solution, and between 1 and 5 for the reaction in the presence of colloid. As shown in Figure IV-9, the proteolysis site appears to be less specific for the reaction in the presence of colloid, and to be shifted toward the N-terminus. This is consistent with a preferred orientation of the peptide on the surface such that the positively-charged C-terminal arginine residues are apposed to the negatively-charged surface. Formation of the peptide-enzyme complex may be enhanced for N-terminal alanines because of its increased accessibility to thermolysin molecules in solution.

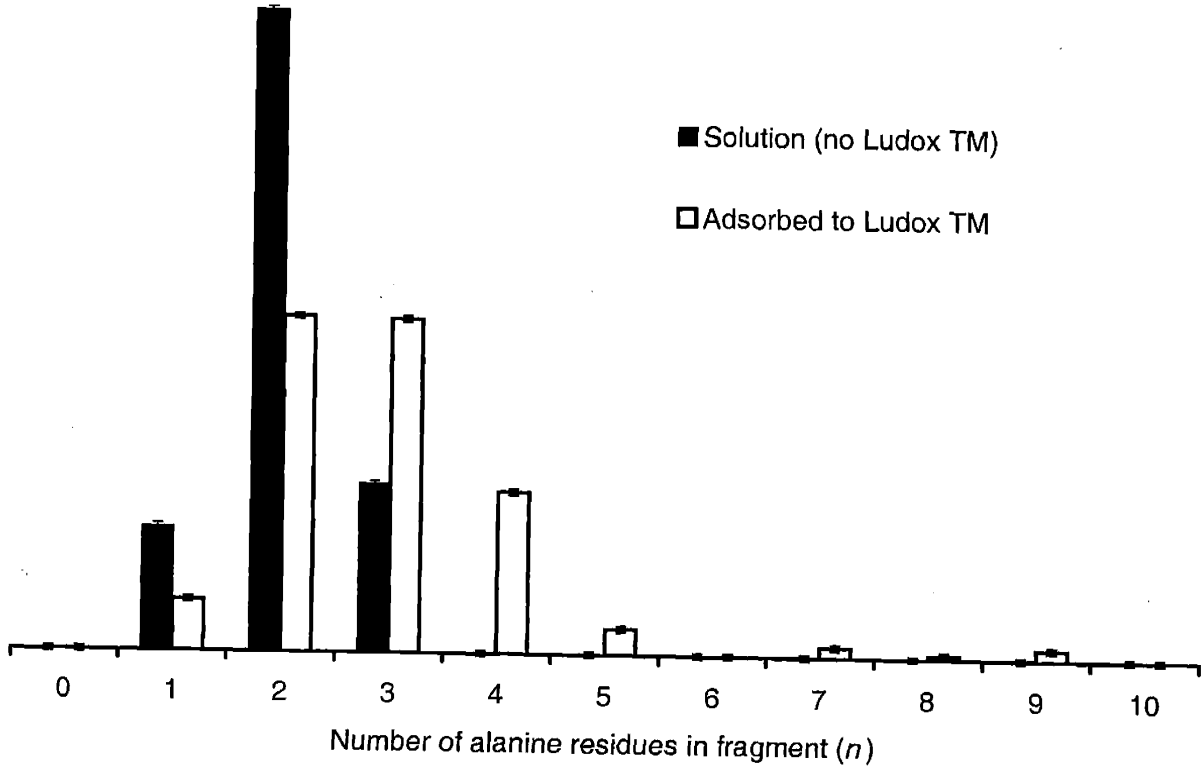

Figure IV-9. Mass spectrometry measurements of proteolysis products of the form H-A_n-R_4-Am (H represents an uncapped peptide N-terminus, a primary amine which is protonated in the tris buffer) from reaction in solution (■) and in the presence of Ludox TM (□). The intensity of the signal is plotted as a function of the parameter *n* characterizing the fragment. Mass spectrometry is not a quantitative technique due to varying ionization properties among molecules; however, it is assumed that the trends between reactions may be roughly compared since factors such as ionization properties should be the same for samples from both reactions. Error bars reflect the noise in the baseline only. Peak heights are normalized to give the same total sum of peak heights for both reactions.

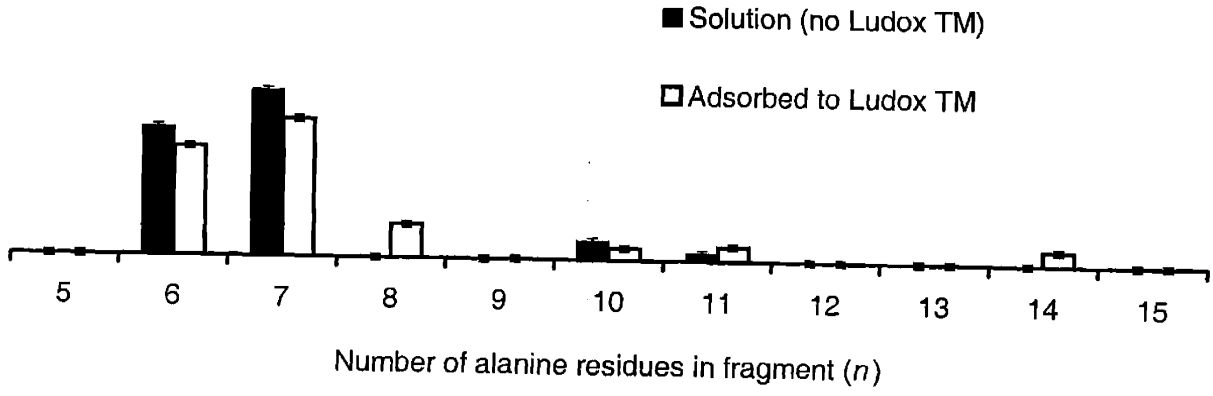

Figure IV-10. Mass spectrometry measurements of proteolysis products of the form Na·A_n-R_4-Am (sodium adducts). These peaks are from the same spectra as Figure IV-9, and peak heights are plotted with the same vertical scale. As in Figure IV-9, error bars reflect only baseline noise, and peak heights are normalized to give the same total sum of peak areas for both reactions.

A second set of peaks is detected, shown in Figure IV-10. These correspond to sodium adducts of $H\text{-}A_nR_4\text{-}NH_2$ fragments. For this set, n is primarily between 6 and 8, though small peaks are detected for n = 10, 11. These latter peaks likely result from multiple proteolysis events, but they are of relatively low intensities and do not reveal any significant difference between the solution-phase and surface reactions. The reversibility of proteolysis by thermolysin is well-established and in fact has applications in certain peptide syntheses, particularly where equilibrium favors the formation of an insoluble product with a larger molecular weight [180].

The detection of a relatively small quantity of fragments arising from multiple proteolysis events does not affect the main conclusions of this work. The samples studied were quenched at the endpoint of the initial proteolysis reaction of 4AAR4. Proteolysis or synthesis of these fragments is expected to be slow relative to proteolysis of 4AAR4. The peptide bonds of smaller fragments are less susceptible to proteolysis by an endoprotease. In addition, the synthesis of peptide bonds between the fragments from the first proteolysis reaction (of 4AAR4) can only result in reattachment of arginine-containing fragments to alanine-containing fragments, thus resulting in soluble peptides. This synthesis is not driven by insolubility of the product, and therefore is unlikely to be favored relative to proteolysis. Therefore, while the reversibility of proteolysis by thermolysin would likely lead to a complicated distribution of final peptide fragments at equilibrium, the attainment of this equilibrium is slow relative to the rate of the initial proteolysis event. As expected, the bulk of the peptide fragments observed by mass spectroscopy were produced by a single proteolysis event of 4AAR4. Investigation of the pathways by which additional fragments may be produced is beyond the scope of this work.

Conclusions

In this section, proteolysis of the peptide 4AAR4 by the enzyme thermolysin was investigated, for samples with and without Ludox TM. The extent of proteolysis was monitored colorimetrically, and samples were subsequently analyzed with mass spectrometry. Although adsorption of 4AAR4 to Ludox TM is reversible, the strong positive charge on the peptide leads to complete adsorption (98.7+ %) at the peptide and particle concentrations

used. Given this data, it was shown that the proteolysis reaction in the presence of Ludox TM is dominated by adsorbed peptide. Nevertheless, for samples containing approximately six peptide molecules per particle, proteolysis proceeded at a rate equal to that in the absence of Ludox TM, within the uncertainty of the experiment. For samples containing less than one peptide molecule per particle, a significant decrease in the initial rate of proteolysis was observed. These trends provide evidence for competitive inhibition of the proteolysis reaction by particles without adsorbed peptide. Minor differences were observed in the distribution of peptide fragments produced by the proteolysis reaction in solution, and in the presence of Ludox TM. The distribution of proteolysis sites for adsorbed peptides was broadened, and shifted away from the positively-charged C-terminus, which adsorbs electrostatically to the negatively-charged silica surface. Adsorbed peptides thus retain a surprisingly high degree of functionality, as measured by the model biochemical reaction (proteolysis) in the present study.

4. Conclusions

In Section IV.1, a definition was presented for the functionality of adsorbed peptides: functionality is the ability to participate in specific interactions with other biomolecules. Section IV.2 presented detailed measurements and modeling of the α-helicity of adsorbed peptides and its dependence on pH and temperature. Conformation is one important aspect of the functionality of adsorbed molecules, crucial to molecular recognition as well as catalytic activity. This work showed that the strength of the electrostatic interactions between the surface and adsorbed peptide is controlled by pH through the resulting variations in surface charge. Adsorption acts to destabilize α-helicity at all temperatures studied, causing α-helicity losses in addition to those caused by thermal destabilization.

At high adsorption affinities (i.e., basic pH), increased temperature leads to an increase in α-helicity of adsorbed molecules. This phenomenon can be explained by a statistical model of α-helicity formulated using the detailed picture of the adsorption mechanism established in Chapter III. This model predicts the peptide α-helicity as a function of sequence position, and accounts for destabilization of α-helicity due to elevated

temperature as well as interactions between the silica surface and charged side chains. When electrostatic interactions between the surface and adsorbed peptide are sufficiently strong, the temperature dependence of the α-helicity of adsorbed molecules is controlled by the temperature dependence of these interactions. An increase in the α-helicity of adsorbed molecules with increased temperature is predicted by the model, similar to the dependence observed experimentally.

In Section IV.3, the rate of proteolysis of adsorbed peptide catalyzed by the enzyme thermolysin was studied. In this study, the model system of short α-helical peptides adsorbed to colloidal silica was extended by adding a catalytic enzyme, in order to assay the functionality of adsorbed peptides. Thermolysin was chosen in order to minimize adsorption of the enzyme to the surface, and to provide a range of possible proteolysis reactions within each adsorbed molecule. The rate of proteolysis was not significantly affected by peptide adsorption to colloidal silica when several peptide molecules were present in solution for each silica particle, but the rate was significantly decreased when less than one peptide molecule was present per particle. These trends were interpreted as evidence for competitive inhibition of the proteolysis reaction by reversible interactions between thermolysin molecules and peptide-free silica surfaces. Interpretation of the data in this way leads to the surprising result that the proteolysis of adsorbed molecules proceeds at largely the same rate as proteolysis in solution. More sophisticated kinetic studies would be required to verify this proposal; in particular, the comparison of the proteolysis rate of irreversibly-grafted peptides would be desirable to establish the importance of peptide desorption. The pattern of reaction products produced from adsorbed peptides shares basic features with that from the solution reaction, reflecting the specificity of the enzyme chosen; however, adsorption alters the relative availability of residues and therefore the distribution of reaction products obtained.

Chapter V. Effects of Surface Chemistry and Structure on Peptide Adsorption

1. Introduction

The technical importance of understanding protein and peptide adsorption arises from the potential for this process to be controlled though material selection and surface engineering. The model system developed in previous chapters provides a basis for studying the effects of surface properties on the adsorption and conformation change of short α-helical peptides. Systematic variations in the chemical composition and spatial arrangement of surface groups, using the surface of amorphous colloidal silica as a reference, are linked to changes in the amount of adsorbed peptide. Since adsorption of DAR-type peptides on this reference surface occurs in a well-defined orientation driven by electrostatic interactions, the mechanism by which surface properties influence adsorption can be studied in detail, and the relative importance of surface composition and nanoscale topology can be revealed. Exploring the effect of chemical functionality introduced into the surface structure suggests techniques for controlling the amount of adsorbed peptide.

Silica can be coated with a capping layer of alumina [126]. The resulting surface has an isoelectric point of pH 7-8, which allows the study of adsorption on a cationic surface at neutral and acidic pH. The changes in the conformation and orientation of adsorbed molecules relative to observations on colloidal silica result from the chemical properties of the alumina groups present on the surface, particularly the altered surface charge.

The effects of surface composition and nanoscale topology on adsorption of DAR-type peptides can be further elucidated by comparing the adsorption on colloidal silica to that on well-characterized colloidal zeolites. Zeolites are a family of microporous crystalline aluminosilicates of the general structural formula [189]

$$M_{x/n}[(AlO_2)_x(SiO_2)_y]\cdot wH_2O \qquad \textbf{(V-1)}$$

where M is a cation with charge $+n$. Zeolites include more than 70 distinct crystal structures [190]. The water-sorbing properties of zeolites have been known for hundreds of years, but new applications of these unique materials are constantly being found in a variety of fields, including ion-exchange and catalysis [191]. For example, colloidal zeolites have

been used as building blocks for nanoporous membranes [192-194]; and siliceous polymorphs have been studied as model surfaces for cytotoxicity [195].

Synthesis is accomplished by hydrothermal crystallization from an aluminosilicate gel, often in the presence of an organic structure-directing agent [196]. These cationic organic molecules are used under favorable synthesis conditions to select a particular crystal structure. Each material contains internal micropores (less than 2 nm in diameter [189]) with topological constraints dictated by the particular crystal structure. The internal surface area bounding this pore volume is a framework of tetrahedrally-coordinated silicon and aluminum atoms connected by oxygen bridges. Previous studies of zeolites such as sodalite (SOD), Linde Type A (LTA), and faujasite (FAU)[14] have revealed a large amount of information about the pore size, framework composition patterns or "zoning", and cation siting within these structures [197]. Such information is important to forming as clear a picture as possible of the near-surface structure and composition. FAU possesses 1.3 nm diameter FAU supercages accessed by 0.74 nm apertures [198], while the channels of LTA are 0.41 nm in diameter, and the 6-membered ring aperture of the sodalite β-cage (the truncated octahedron structure upon which SOD, LTA, and FAU structures are based) is 0.23 nm. In each of these crystal structures, there exists only one type of tetrahedral silicon or aluminum site. The distribution of aluminum among the tetrahedral sites in faujasite avoids formation of Al-O-Al bridges (Lowenstein's Rule), and Al-O-Si-O-Al bridges (Dempsey's Rule), but this tendency is modulated by crystallization kinetics [199,200]. Diagrams of relevant zeolite surfaces are shown in Figure V-1, along with a molecular model of the peptide 4DAYAR5 for comparison.

Aluminum in a tetrahedral site introduces a negative charge into the SiO_2 parent material, with charge neutrality of the material maintained by exchangeable extraframework cations. In frameworks that have sufficiently large pores, all or most of these internal cations are accessible to the bulk solvent and may be exchanged for other cations by incubation in concentrated solutions at elevated temperature. Hydrolysis, or hydronium ion exchange, is a

[14] In common usage, the three-letter abbreviation is a label for the crystal framework (the geometry of tetrahedral and bridging sites) and implies nothing about the composition of the material. In this work, materials for which only one composition was studied (FAU and LTA) will be designated by their structure code only, while the abbreviation for the sodalites will include an indication of their composition: SOD–∞ for siliceous sodalite, and SOD–*N* for aluminosilicates with *N* representing the gel Si/Al ratio.

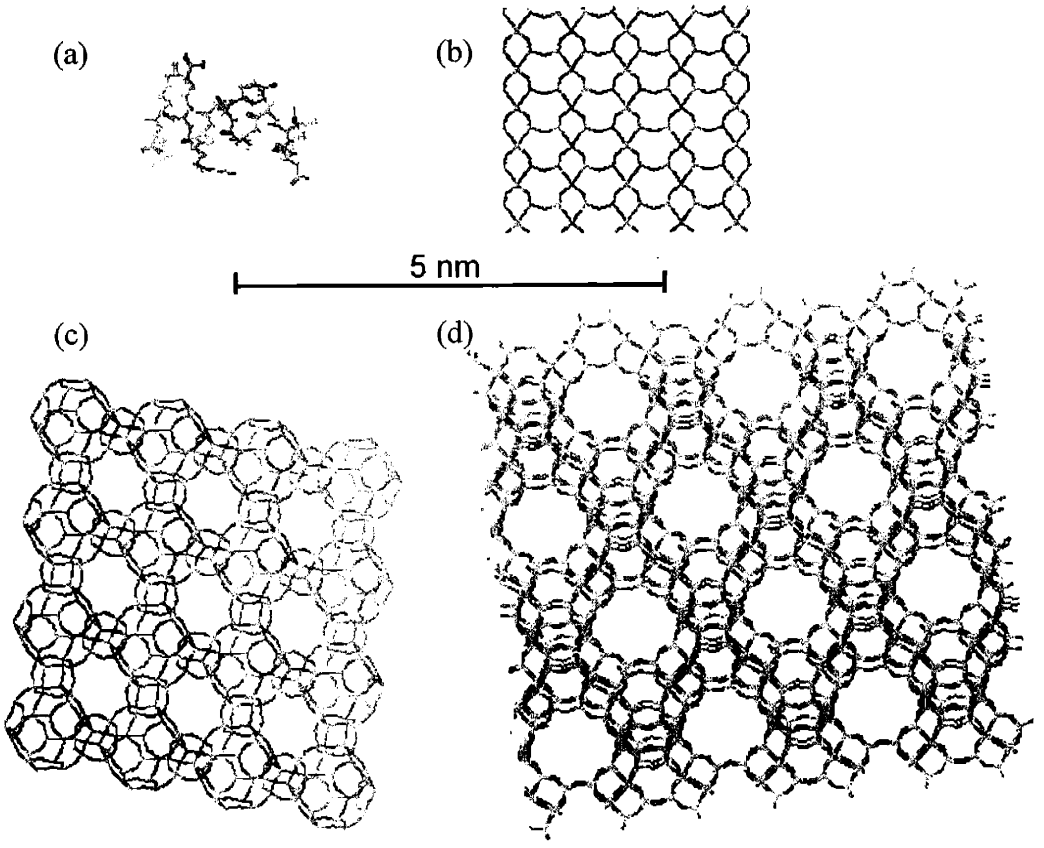

Figure V-1. Diagrams of zeolite surfaces in relation to the peptide: (a) 4DAYAR5; (b) SOD {110}; (c) LTA {100}; (d) FAU {111}. The scale bar is 5 nm for all the models shown. Surface models and the conformation of the peptide were produced using Cerius2.1 molecular modeling software (Accelrys). The conformation of the peptide, shown only for visualization of the relative dimensions, was estimated by starting with an ideal α-helical conformation ($\phi = -62^{\circ}$, $\psi = -41^{\circ}$), then performing energy minimization (UFF forcefield), molecular dynamics (50 ps, NPT mode), then a final energy minimization

special case of cation exchange; an example of the hydronium ion exchange of a sodium-containing zeolite (Z) is shown:

$$Na\text{-}Z + H_2O \leftrightarrows HZ + NaOH \qquad \textbf{(V-2)}$$

The hydronium ion exchange reaction per se is reversible and may be modeled by thermodynamic mass-action relations in the ionic strength range of interest [201]. However, low pH values can promote irreversible structural changes, including dissolution of silicon and aluminum species from the zeolite framework. The mass-action relations predict a dramatic increase in the hydronium ion exchange rate at acidic pH, which has been observed

by elemental analysis [201,202]. In this work, hydronium ion exchange was observed by the appearance of mobile tetramethylammonium (TMA) cations in solution ^{1}H NMR spectra.

The unique crystal structures and chemical compositions of these materials result in external surfaces which have been shown by AFM [203] and TEM [204] to exhibit nanoscale topology characteristic of the underlying crystal structure. This nanoscale topology has dimensions similar to those of small molecules, and therefore can provide unique sites for adsorbates [205]. Zeolite surfaces have well-defined silicon-oxygen bond lengths and angles imposed by the crystal structure, along with controlled amounts of tetrahedrally-coordinated framework aluminum sites and exchangeable cations. The maximum pore sizes of crystalline aluminosilicates to date are too small to admit proteins, or even short peptide chains; size exclusion experiments have only been demonstrated with mesoporous materials [206]. Adsorbed peptides are therefore confined to the external surface. Zeolites expand the range of surface topologies available for silica and aluminosilicate compositions, and allow testing of the effects of different surface topologies and compositions on the amount of adsorbed peptide.

This chapter contains measurements of the conformation and orientation of DAR-type peptides on cationic alumina-capped colloidal silica, and qualitative interpretation of these results using the model developed previously for anionic colloidal silica. The interpretation arises from the electrostatic model of adsorption, since the most important difference between these two surfaces is a change in the sign of the surface charge. Characterization of the zeolites discussed above is then described, with special attention to properties of the external surface. Adsorption isotherms of 4DAYAR5 on the zeolites are presented, and the differences from colloidal silica are interpreted in terms of the additional surface functionality introduced by crystallinity and tetrahedral alumina sites.

2. Experimental

Cationic alumina-capped colloidal silica (DuPont) was obtained from Aldrich in grade CL-30, which has a surface area of 230 $m^2 g^{-1}$ and a particle diameter of 12 nm (manufacturer's specifications). Peptide adsorption and conformation change was

characterized spectroscopically in a manner similar to the procedures outlined in Chapter III. The pH was controlled in the range 3.8 – 4.5 with 10 mM sodium acetate buffer for CD experiments in H_2O, or with perdeuterated sodium acetate buffer (Aldrich, 99+ atom % D) for NMR experiments in D_2O. 500 MHz ^1H solution NMR spectra were collected at pH* 4.5 and 25 °C with typical concentrations of 0.44 mg ml^{-1} (290 μM) 4DAR5 and 3.4 wt % Ludox CL. All spectra were referenced to TSP (δ = -0.063 ppm from TMS in $CDCl_3$ [107]) contained in an internal capillary (10 mM sodium phosphate, pH* 7.95) and were scaled using the integrated intensity of this peak. The DHO peak was removed by presaturation. The magnetic field was homogenized using automated gradient shimming. Typically 128 or 256 spectra were averaged. All spectra were baseline corrected and drift corrected using the Varian software.

Synthesis

Several compositions of sodalite in the sodium form were synthesized according to published procedures [207,208]. Silica (Cabosil M-5, Cabot), and sodium aluminate (EM Industries) were dissolved separately with sodium hydroxide (Mallinckrodt) in ethylene glycol (Aldrich). These solutions, with the gel compositions listed in Table V-I, were combined, aged for one day, then heated in Teflon-lined reactors (Parr Instrument Co.) for 5-14 days at 175 °C. These materials were not removed from solvent between synthesis and measurement of the adsorption isotherm.

Colloidal LTA and FAU were synthesized according to published procedures [209,210]. The resulting milky suspensions were centrifuged at 4000 g for 1-2 hours and the particles were resuspended in deionized water. The resulting stable colloidal solution was analyzed for surface composition and specific surface area. A portion of the sample was ion-exchanged in 1 M NaCl at 90 °C overnight in a closed reaction vessel. This procedure removed 88% of the TMA from the surface region of colloidal FAU, and 73% from the surface region of colloidal LTA, as measured by XPS. The exchanged material was used for adsorption isotherms. Since the solids were not dried, they were not exposed to atmospheric gases, which, on high-energy surfaces such as these, can quickly lead to a layer of adventitious material containing mainly hydrocarbons and other organics.

Table V-I. Gel composition, and assumed density (ρ), of materials used for adsorption isotherms. The sample name is based on the crystal structure and, for the variable-composition sodalites, contains an indication of the molar gel composition ratio Si/Al.

Sample	*Gel Composition*	*ρ (g/cm^3)*
Snowtex ZL		2.2
FAU	$10SiO_2 \cdot 2.3Al_2O_3 \cdot 5.7TMA_2O \cdot 0.06Na_2O \cdot 570H_2O$	1.9
LTA	$10SiO_2 \cdot 2.3Al_2O_3 \cdot 5.7TMA_2O \cdot 0.35Na_2O \cdot 570H_2O$	1.9
SOD–∞	$4\ SiO_2 \cdot 0.5\ Na_2O \cdot 40$ EG	2.0
SOD–20	$4\ SiO_2 \cdot 0.1\ Al_2O_3 \cdot 0.5\ Na_2O \cdot 40\ C_2H_4O_2$	2.0
SOD–5	$4\ SiO_2 \cdot 0.4\ Al_2O_3 \cdot 0.5\ Na_2O \cdot 40\ C_2H_4O_2$	2.0
SOD–2.5	$4\ SiO_2 \cdot 0.8\ Al_2O_3 \cdot 0.5\ Na_2O \cdot 40\ C_2H_4O_2$	2.0

Electron Microscopy

Slurries were dried at 66 °C to produce fine powders for SEM. These were spread without grinding on an adhesive carbon backing, gold-coated, and imaged with digital data acquisition at 5-10 kV (Hitachi S-530 SEM / Oxford Instruments).

Dilute suspensions for TEM were dried on 200 mesh Cu grids with carbon substrates (Ladd Research Industries Inc.) and analyzed at 200 kV (JEOL 200CX).

Surface Composition

Surface compositions were measured by X-ray photoelectron spectroscopy (XPS) using a Kratos AXIS system (Kratos Analytical) with a monochromatized Al Kα x-ray source. Dried powders were applied to adhesive carbon tape in a uniform layer, outgassed at high vacuum overnight, and analyzed.

Surface Area Measurement

Particle size distributions were calculated from centrifugal sedimentation analysis performed on a Horiba CAPA-700 (Horiba Instruments Inc.) according to the manufacturer's instructions. Slurries were diluted in H_2O to give an absorbance at 560 nm (A_{560}) of between 0.7 and 0.9. Particle diameters were measured between 0.03 and 0.9 μm in 0.03 μm increments during sedimentation at 5000 rpm (4500 rcf). The surface area was calculated from the particle size distribution using the instrumental programming. This calculation

requires values for the solid densities to be input (listed in Table V-I), but these values have little impact on the final result.

Adsorption of N_2 from a 30% N_2 / 70% He gas mixture was measured on all solids using a Quantasorb flow-through BET apparatus. Slurries were dried in air at 66 °C and the resulting solid pieces were ground with a small mortar and pestle set. The resulting fine powder was dried at 100 °C or 200 °C under flowing N_2/He and measured according to the manufacturer's instructions. Powders were maintained under the N_2/He mixture between drying and surface area measurement. Surface area was calculated using the single-point BET method.

Adsorption Isotherms

Adsorption isotherms were measured at pH 9 in 10 mM borate buffer according to the procedure described in Chapter III.3. Because of the low surface area of high-silica sodalites, isotherms on these materials were measured from extremely small spectral differences. Therefore great care was taken in the measurement of the concentration of the peptide solution. This sample was used as an internal standard in the isotherm, subject to the same dilution and centrifugation procedure as samples with solid. For the high-silica sodalites, which have large particle sizes and rapidly settle out of solution, the slurry was stirred rapidly using a magnetic mixer while aliquots of the suspension were withdrawn. Data points were analyzed using a simple difference method as well as spectral subtraction. Spectral subtraction increased the quality of the isotherms on high-silica sodalites relative to the simple difference method, but made little difference for the isotherms on other materials. The overall trends in the isotherm data were the same for the two methods. The results presented here are those obtained from spectral subtraction.

3. Results

Adsorption on Cationic Alumina-Capped Colloidal Silica

Titration of cationic, alumina-capped colloidal silica (Ludox CL) with KOH indicates a surface charge density of approximately 2.13 $AlOH_2^+$ groups per square nanometer, or approximately one $AlOH_2^+$ group per 0.5 nm^2, at pH 4.3.

Interpretation of spectroscopic results is complicated in this system due to protonation of aspartate side chains below pH 4.5. The change in net charge leads to a decrease in solution α-helicity (Figure II-8) and to shifts in the positions of the aspartate signals in the ^1H NMR spectrum. For this reason, comparisons are made with values of solution α-helicity at the same pH to minimize errors arising from this effect. The CD spectra of peptides in solution with the positively-charged alumina-capped surface at pH 4.5 indicate a loss of α-helicity analogous to that which occurs with the negatively-charged silica. The spectra have the same isodichroic point, as shown in Figure V-2.

NMR spectra of 4DAR5 combined with cationic alumina-capped silica display a dramatically different pattern of intensity changes than previously, shown in Figure V-3. Aspartate signals are selectively eliminated, as are those from the acetyl capping group. The arginine protons and, to a lesser extent, the alanine protons remain, but they have decreased in intensity and broadened relative to the solution spectra. The interpretation of such features of NMR spectra was developed in Chapter III.7. Application of these principles indicates that DAR-type peptides adsorb to positively-charged alumina in a specific orientation, opposite to that adopted on anionic silica. The negatively-charged N-terminal aspartate residues are immobilized on the surface and the C-terminus extends into solution, as would be expected based on electrostatic considerations.

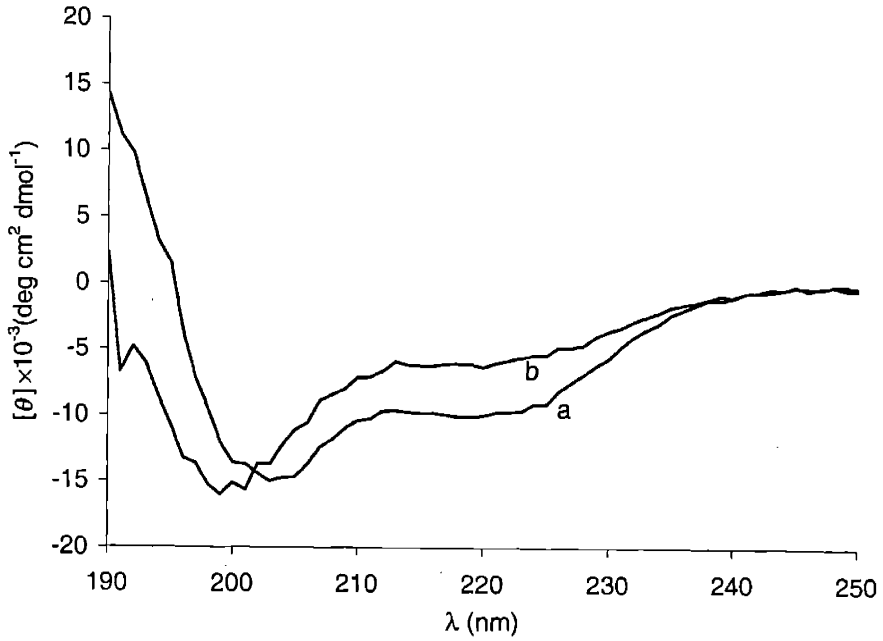

Figure V-2. Effect of adsorption to cationic alumina-capped colloidal silica on the peptide conformation at 25 °C: 5DAR4, 1.9 mg ml^{-1} (120 μM) (a) free in solution, pH 4; (b) in solution with Ludox CL (3 wt%), pH 3.84.

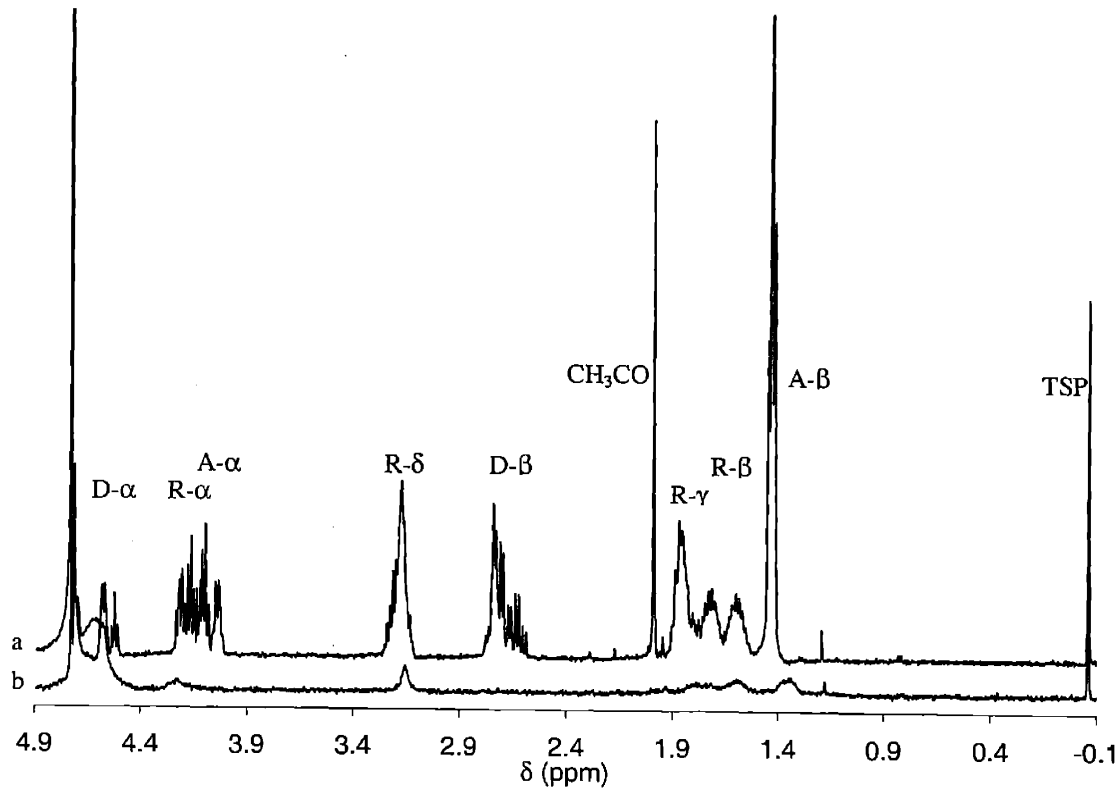

Figure V-3. 500 MHz ^{1}H solution NMR spectra of 4DAR5 in solution with cationic colloidal silica at 25 °C. (a) 4DAR5 (0.44 mg ml^{-1}, 290 μM) in 10 mM sodium acetate-d_3 buffer, pH* 4.5; (b) 4DAR5 (0.44 mg ml^{-1}, 290 μM), Ludox CL (3.4 wt% SiO_2), in 10 mM sodium acetate-d_3 buffer, pH* 4.5.

CD measurements show that adsorbed 4DAR5 loses 70% of its solution α-helicity under the conditions of Figure V-3. NMR peak shifts in the residues contributing to the spectrum are consistent with the loss of α-helicity observed by CD, particularly the downfield shift in the multiplet of alanine-α and arginine-α protons, and the upfield shift in the peak for alanine-β. Under these conditions, the former multiplet represents signals from both alanine and arginine α-protons, and the 1D solution spectra do not contain sufficient information to resolve these two groups. The entire peak is shifted with respect to its position in the solution spectrum, indicating that both the alanine and arginine segments undergo significant conformational change upon adsorption to the surface.

Zeolite Characterization

SEM shows that SOD–∞ particles (space group: *Im3m*) are highly faceted; a typical micrograph is shown in Figure V-4. Crystal habit is synthesis- and precursor-dependent. This particular sample possesses a predominantly rhombic dodecahedral morphology, expressed by approximately 70% of the particles in Figure V-4 (this value is also representative of micrographs containing a larger number of particles; this data is not shown). Axes of rotational symmetry possessed by these particles may be aligned with those of the underlying *m3m* point group to determine the crystal face expressed. Taking the crystallographic axes to be in the direction of the orthogonal four-fold axes of the *m3m* point group, the surfaces expressed are identified as the {110} crystal planes. The remaining particles have complex shapes for which the surfaces expressed are more difficult to identify. However, upon close inspection of Figure V-4, these more complicated particles appear to be based on modifications to the basic rhombic dodecahedron. At least half of the surface area of such particles corresponds to the basic morphology, while the remaining facets may be either new planes, or reoriented {110} planes. The SOD–∞ particles studied here thus express the {110} plane with at least 85% specificity, while the remaining facets are not readily identified. In samples with increasing aluminum contents the faceting is progressively less pronounced: facets of SOD–20 are on the order of 1 μm, while those of SOD–5 and

Figure V-4. SEM micrographs of synthetic sodalites: (a) SOD–∞, 20 μm scale bar; (b) SOD–20, 5 μm scale bar.

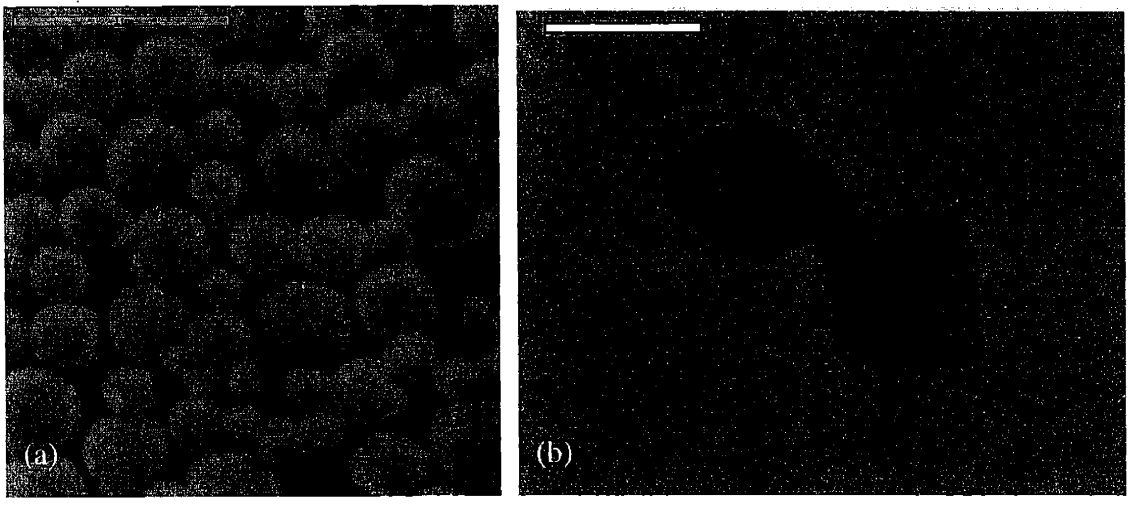

Figure V-5. Electron micrographs of synthetic large-pore zeolites: (a) SEM micrograph of colloidal LTA particles, 1 μm scale bar; (b) TEM micrograph of colloidal FAU particles, 0.06 μm scale bar.

SOD–2.5 are not visible with the resolution of the microscope. The particle size decreases and surface area increases as the alumina content is increased.

Large-pore zeolites synthesized here displayed two very different morphologies. SEM of colloidal LTA reveals nonfaceted particles (Figure V-5(a)) for which the crystal faces expressed, as well as their relative proportions, are not easily identifiable. TEM of colloidal FAU reveals highly symmetric and faceted octahedral particles (Figure V-5(b)), in agreement with previously published results [211]. As described above for SOD–∞, the symmetry of the FAU particles is an expression of the underlying point group and may be used to deduce the

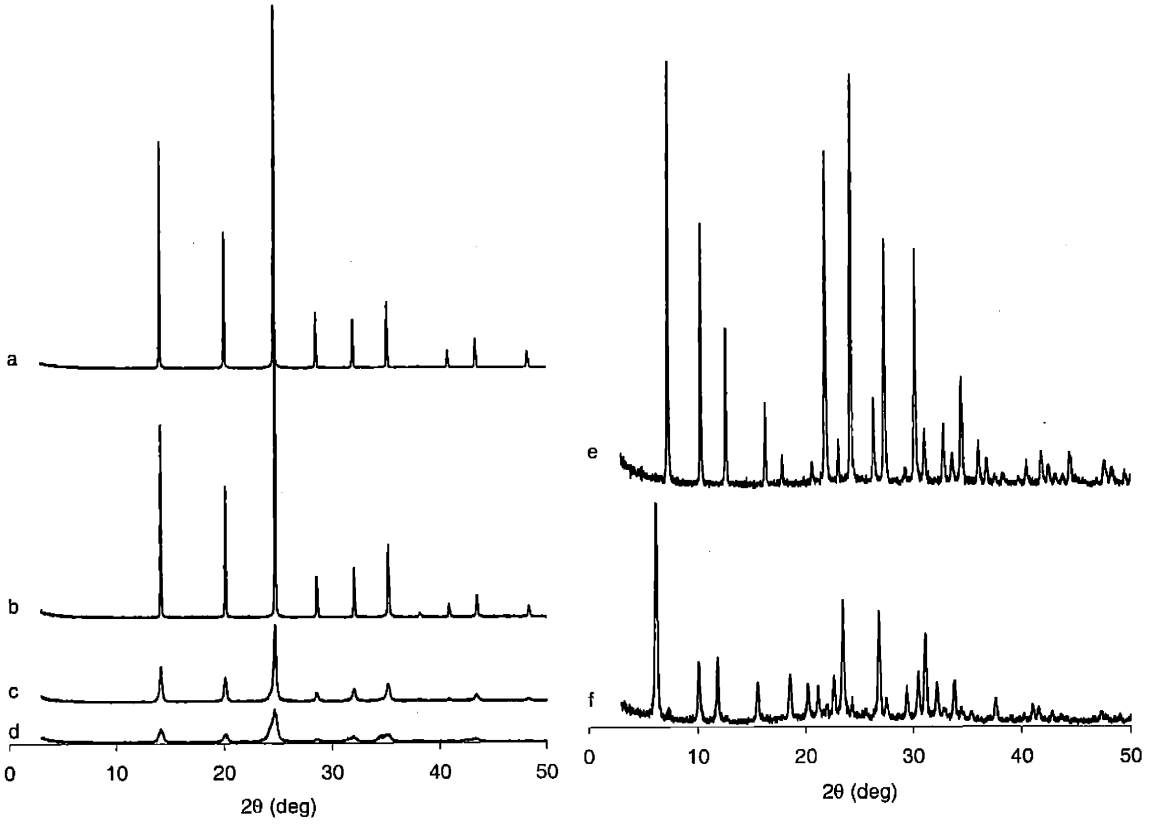

Figure V-6. XRD patterns of synthetic zeolites (a) SOD–∞; (b) SOD–20; (c) SOD–5; (d) SOD–2.5 (e) LTA; (f) FAU. Sodalites (left) are plotted with the same absolute scaling, offset for clarity, so that the peak magnitudes reflect the diffraction intensity. The same is true of the large-pore zeolites (right).

crystal face. Aligning the four-fold symmetry axes of octahedra with those of the *m3m* point group results in the identification of the FAU particle surfaces with the {111} crystal face.

Zeolite samples are highly crystalline, as shown for the XRD patterns for sodalite samples in Figure V-6(a-d), and for large-pore zeolites (FAU and LTA) in Figure V-6(e-f). Zeolites had different stabilities in aqueous solution; titration of dilute suspensions of SOD–∞ samples with HCl had no detectable effect on the XRD pattern, while the patterns of large-pore materials changed in a minor but systematic way as shown in Figure V-7. Hydronium ion exchange is known to occur with decreased pH, and to affect the structure of zeolites (as noted in the introduction). Therefore, hydronium ion exchange could be responsible for the changes in the XRD pattern with the addition of HCl.

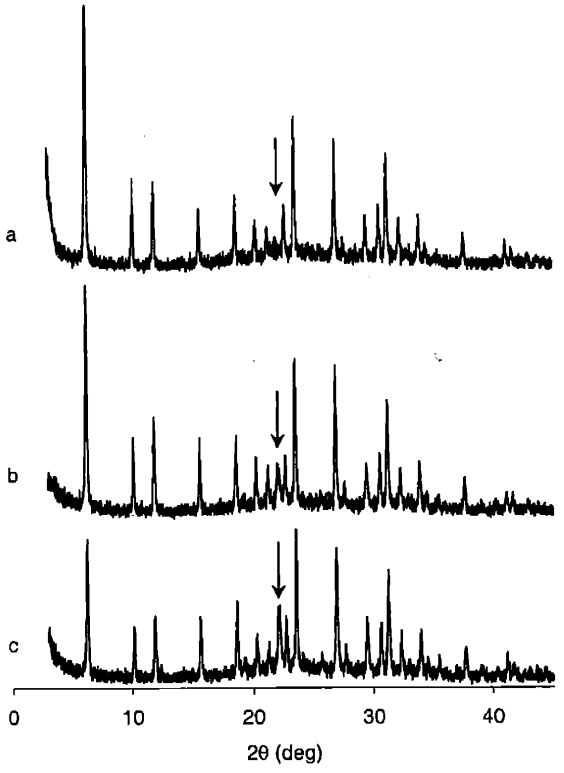

Figure V-7. Effect of pH on the structure of colloidal FAU: (a) pH 9; (b) pH 7; (c) pH 4. Particle suspensions were titrated with dilute HCl, then the particles were removed by centrifugation, dried, and measured. Patterns are plotted with the same absolute scaling, offset for clarity, so that the peak magnitudes reflect the diffraction intensity. The arrows highlight changing peak intensity at more acidic pH.

Powder samples are listed in Table V-II with surface compositions measured by XPS, and surface areas. Particle sizes measured by microscopy are consistent in all cases with those measured by centrifugal sedimentation. Particle size distributions measured from centrifugal sedimentation are listed as S_{geom}. The reproducibility of these measurements was tested for Snowtex ZL colloidal amorphous silica (74 nm particle diameter), and found to be within 10%. The dependence of the surface area measurement on the pH, ionic strength, and purity of the colloidal suspension was investigated and found to be within this reproducibility. Snowtex ZL is the only member of the set for which the surface area could be reliably measured by centrifugal sedimentation. The other particles, being crystalline, are nonspherical and could have nanoscale surface topology that leads to an increased external surface area.

Table V-II. Surface area of materials used for adsorption isotherms. Surface compositions were measured by XPS (M = Na + TMA). S_{geom} is the surface area based on the particle diameter. Values of S_{geom} marked with an asterisk were approximated using SEM while the other values were obtained from centrifugal sedimentation. S_{N_2} was obtained from N_2 adsorption.

Sample	*Surface Composition*	S_{geom}	S_{N_2} *(100 °C)*	S_{N_2} *(200 °C)*
Snowtex ZL	SiO_2	27.4	27	32
FAU	$Si_{0.66}Al_{0.33}M_{0.51}O_2$	25.6	86,108	355
LTA	$Si_{0.70}Al_{0.30}M_{0.44}O_2$	12.1	15	202
SOD–∞	$Si\ Na_{0.24}(C_2H_4O_2)_{0.17}O_2$	0.19*		0.14
SOD–20	$Si_{0.94}Al_{0.06}Na_{0.32}(C_2H_4O_2)_{0.17}O_2$	0.32*		0.28
SOD–5	$Si_{0.79}Al_{0.21}Na_{0.40}(C_2H_4O_2)_{0.17}O_2$	13.3		44
SOD–2.5	$Si_{0.75}Al_{0.25}Na_{0.45}(C_2H_4O_2)_{0.17}O_2$	18.0		98

For the relatively large SOD–∞ and SOD–20 particles, the surface area S_{geom} is calculated from the particle size distribution measured by SEM approximated by a spherical geometry for simplicity (this approximate value is only used for comparison to the value from N_2 adsorption).

An attempt was made to measure the external surface area of each material, by measuring the amount of stearic acid adsorbed from benzene or toluene [212,213]. However, results were highly variable for all materials studied here. In most cases, the surface areas predicted by the published value for monolayer coverage of stearic acid were far below the surface areas found from centrifugal sedimentation. The surface area found from centrifugal sedimentation represents a lower limit on the actual external surface area; therefore, formation of a complete monolayer was not observed. The results of this method are considered inaccurate and are not presented here.

S_{N_2} denotes surface area results from single-point BET. The measurement of Snowtex ZL surface area by N_2 adsorption is in agreement with the results from centrifugal sedimentation and is approximately equal to the value calculated from the manufacturer's specifications. This validates the BET technique for surfaces with low porosity, which includes the sodalite surfaces. However, the accuracy of the BET technique applied to large-pore zeolites is strongly preparation-dependent. Drying large-pore zeolites at 200 °C makes large amounts of internal surface area available to N_2 with corresponding increases in the measured surface area relative to the same powders dried at 100 °C. Some internal surface area may also be accessible in solids which are dried at only 100 °C, and cannot easily be

separated from the desired external surface area. The severity of this problem can be estimated by comparing the BET measurements (S_{N_2}) with the surface area based on particle size (S_{geom}): for LTA these two values are relatively close, indicating that the contribution to S_{N2} from internal surface area is small. However, for FAU the S_{N_2} value is much larger than S_{geom}; this difference likely arises from the contribution of internal surface area to S_{N_2} and is expected based on the larger pores of this material, which allow more efficient N_2 penetration.

Taken together, the above data present a challenging problem of determining the correct surface area by which to normalize peptide adsorption isotherms. Normalization is the limiting factor in accurate determination of the equilibrium constants (K_{eq}) for peptide adsorption on different surfaces. For the high-silica sodalite zeolites, the BET measurement appears to be sufficiently accurate. Due to the exceedingly small pore size associated with this structure, only the external surface is accessible for N_2 adsorption. SOD–∞ and SOD–20 have highly faceted surfaces. Separate AFM measurements (data not shown) indicate that these materials grow from the gel through a layer-growth mechanism, and therefore their external surfaces are likely to be nearly smooth on the molecular lengthscale, containing little nanoscale topology which would add to the measured surface area. Therefore, it is not surprising that the BET measurements for these solids are in reasonably good agreement with the external surface area visible by microscopy.

Although high-resolution micrographs are not available for the other sodalite materials, SOD–5 and SOD–2.5, the surfaces of these solids appear to be very rough based on the disagreement between the BET and centrifugal sedimentation measurements. This is not surprising given the dramatic increase in surface complexity of SOD–∞ relative to SOD–20, which is easily observed by SEM (Figure V-4). Although it is not clear that the surface area available to adsorbing peptides is the same as that available to N_2, the latter is probably a better indication than the value based only on particle size. Therefore, in the absence of reliable results from surfactant adsorption, the BET measurement is considered to provide the best practical normalization for peptide adsorption isotherms on sodalites.

The large-pore zeolites FAU and LTA have large amounts of internal surface area which are readily accessible to N_2. It appears that neither nanoscale topology nor internal surface area is important in determining the N_2 adsorption of LTA, as indicated by the

relatively close agreement between this measurement and the surface area based on external geometry. N_2 gas may be prevented from entering the pores of the LTA sample by TMA cations remaining after heating at 100 °C. By contrast, after heating at 200 °C, the surface area of LTA measured by N_2 adsorption has increased to a value (202 m^2 g^{-1}) which appears to be dominated by the internal surface area. For FAU, there is a large difference between the surface area values determined from N_2 adsorption and particle geometry, which could be due to either nanoscale topology, internal surface area, or both. In the absence of another reliable method for surface area determination, the values from centrifugal sedimentation are used for both of these powders, and direct comparison with the other isotherms, measured using BET, is avoided. This allows the isotherms on LTA and FAU to be compared as a test of crystal structure dependence, subject to the assumption that the contribution of nanoscale topology, which must increase the surface area, is similar for both solids.

Adsorption Isotherms

Adsorption isotherms of 4DAYAR5 on sodalite samples with a range of alumina contents are shown in Figure V-8. Fitting parameters for the isotherms shown are given in Table V-III. Comparison between isotherms of the same peptide (4DAYAR5) on different surfaces is used to deduce the effect of variations in surface composition and topology on the free energy of peptide adsorption. Analysis of adsorption isotherms allows the extraction of equilibrium constants, and free energies, for peptide adsorption. Determining the effect of crystal structures and chemical compositions on the free energy of peptide adsorption is an important first step in determining how different surfaces may control the adsorption mechanism.

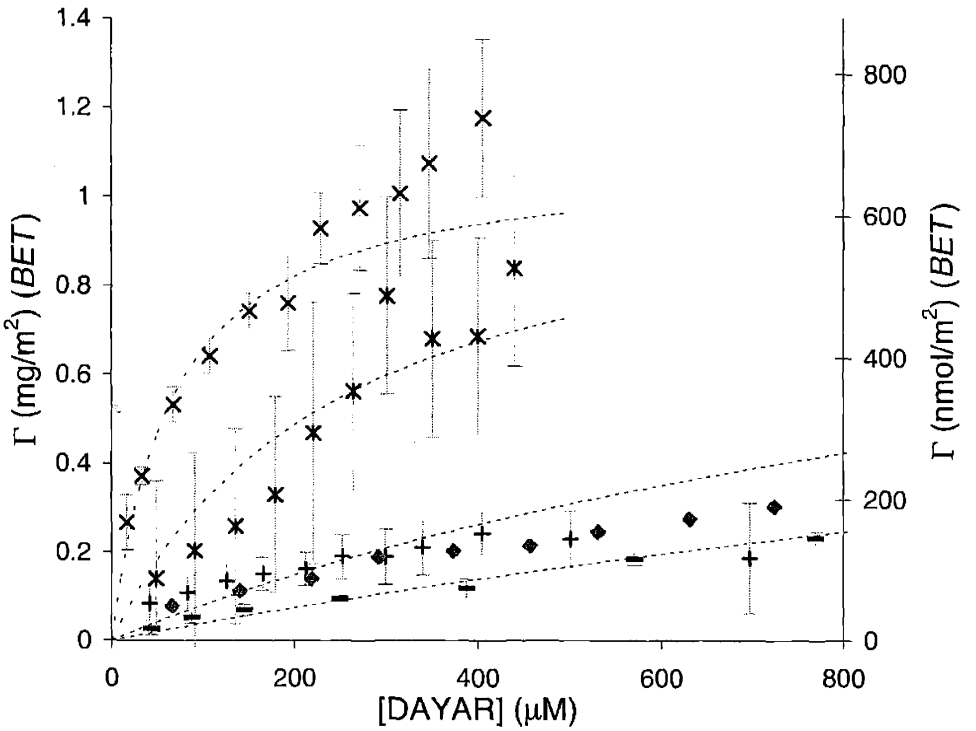

Figure V-8. Adsorption isotherms of 4DAYAR5 to synthetic sodalites at pH 9 in 10 mM sodium borate buffer: (×) SOD–20; (✳) SOD–∞; (+) SOD–5; (◆) Snowtex ZL shown here for comparison; (–) SOD–2.5. Fitting parameters are given in Table V-III.

Table V-III. Fitting parameters for adsorption isotherms of 4DAYAR5 on zeolites shown in Figures V-8 and V-9.

Solid	K_{eq} *(L/mol)*	Γ_{max} *(mg/m²)*	*Surface Area Normalization Used*
SOD–∞	4024	1.1	BET
SOD–20	15052	1.1	BET
SOD–5	790	1.1	BET
SOD–2.5	363	1.1	BET
FAU	1272	3.5	Centrifugal sedimentation
LTA	603	3.7	Centrifugal sedimentation

For the adsorption isotherm of 4DAYAR5 on SOD–∞, the data in the range available is dramatically different from that on amorphous colloidal silica. To a first approximation, these two surfaces have identical compositions, the main difference being the presence of one occluded non-exchangable ethylene glycol molecule per sodalite β-cage, which is isolated from the solvent and therefore not expected to influence the behavior of adsorbates. In

contrast, the surface topology on the nanometer lengthscale is quite different: while the Snowtex ZL is amorphous, the sodalite crystal structure imposes a fixed set of bond angles on the tetrahedral silica sites, as well as a periodicity on the surface silanol groups on the order of 1 nm (for perspective, a surface coverage of one 4DAYAR5 molecule per nm^2 is 2.6 mg m^{-2}). SEM indicates that a limited set of crystal planes is observed in this sample of SOD–∞. Therefore, these two isotherms provide a direct measurement of the effect of organizing surface silanol groups into a periodic array. The dramatic increase in adsorption on SOD–∞ indicates that, on average, the free energy of adsorption of 4DAYAR5 on the crystal faces expressed by this sample is much greater than that on amorphous colloidal silica. Although uncertainty in the specific surface area of SOD–∞ probed by adsorbed peptide is significant, twice as much peptide is adsorbed on SOD–∞ as on Snowtex ZL, well outside the uncertainty of the BET experiment. Thus, the increase in the amount of adsorbed peptide is significant relative to the uncertainty of this experiment.

Even in the relatively low concentration range available, the adsorption isotherm of 4DAYAR5 on SOD–∞ exceeds the apparent plateau value of 0.6 mg m^{-2} for this peptide on colloidal silica used in Chapter III.3. This could be partly due to error in the surface area used for normalization, but, as mentioned above, the uncertainty is not large enough to account for this difference. Larger amounts of 4DAYAR5 adsorbed on the SOD–∞ surface may be associated with a change in the configuration of adsorbed molecules to accommodate the greater packing density. The maximum observed coverages are about 60% of the close-packed monolayer density of 4DAYAR5 in an α-helical conformation (approximately 0.5 molecule nm^{-2}, estimated from Figure V-1). However, adsorption of 4DAYAR5 to the SOD–∞ surface may be associated with conformational changes analogous to those observed on the amorphous colloidal silica surface. Adsorption in a coiled conformation, with a specific orientation, may tend to increase the value for the close-packed monolayer density, but quantitative estimates of this effect would require more information on the conformation and orientation of adsorbed molecules than is currently available. In any case, the large free energy of adsorption appears to drive the formation of a relatively dense layer of 4DAYAR5 on the SOD–∞ surface. The increase in the equilibrium constant could be due to a changing surface potential. Although the zeta potential of SOD–∞ has not been measured, it has been

shown [214] that the surface charge of quartz is more negative than that of amophous silica. The siliceous sodalite polymorph may also have a more negative surface charge, which would lead to a greater amount of adsorbed peptide.

Surface composition has a strong effect on the free energy of adsorption of 4DAYAR5 on sodalite surfaces, as revealed by the alterations observed in the adsorption isotherm as aluminum is added to the framework. In the case of SOD–20, the presence of approximately one negatively-charged tetrahedral alumina site per 2 nm^2 (calculated from the measured surface composition, Si/Al = 16, and the density of tetrahedral sites on the {110} surface) results in an increase in the free energy of adsorption of approximately -3 kJ mol^{-1} calculated from the measured equilibrium constants, relative to the adsorption of this same peptide on SOD–∞. Using the electrostatic model of adsorption developed in the previous chapter to explain this effect, the aluminum sites may provide electrostatic stabilization to adsorbed peptides in addition to that which arises from the negative surface charge developed by deprotonation of surface silanol groups. The interaction between 4DAYAR5 and the high-silica sodalite aluminosilicate surface could not be detected by XPS: no peak shifts were observed for sodalite samples with peptide relative to sodalite samples with no peptide. Either the noncovalent peptide-surface interactions are not sufficiently strong to perturb the electronic binding energies of the framework aluminum, or the interactions are altered in the absence of solvent.

Further increases in the alumina content of the surface appear to have the opposite effect: for relatively aluminum-rich sodalite surfaces, the adsorption isotherms of 4DAYAR5 (normalized by the BET surface area) decrease to the level of amorphous colloidal silica. The adsorption isotherm for on SOD–5 (21% surface Al), is similar to that on Snowtex ZL, while that for 4DAYAR5 on SOD–2.5 (25% surface Al) is significantly lower. Aluminum sites of high-silica zeolites tend to maintain a greater Brønsted acidity than those of aluminum-rich zeolites [215]. Therefore, interactions between aluminum sites may lead to a decrease in the magnitude of the surface charge for the SOD–5 and SOD–2.5 surfaces. In addition, the high-aluminum sodalites may express different crystal faces; given the importance of surface structure observed for the siliceous surfaces, this could also account for the dramatic decrease in K_{eq}. In sum, the observed decrease of K_{eq} to below that observed for adsorption to colloidal silica is reasonable, but it cannot be attributed to any one surface characteristic. This

uncertainty is a result of the simultaneous changes in surface morphology and composition that arise during the synthesis of these materials.

The isotherms for adsorption of 4DAYAR5 to sodalites are consistent with a variety of possible values of Γ_{max}, but for clarity this parameter has been set to 1.1 mg m^{-2} so that they can be compared. The decrease in adsorption affinity with increasing aluminum is significant but its magnitude is uncertain due to the difficulty of choosing the correct surface area for normalization: if the isotherms on these solids are instead normalized using the S_{geom} values from centrifugal sedimentation (the lower limit of surface area), the same trend is maintained but its importance is greatly decreased so that the isotherms lie closer together.

Adsorption isotherms for 4DAYAR5 on large-pore zeolites (FAU and LTA) are shown in Figure V-9; fitting parameters are given in Table V-III. With similar surface compositions, these two surfaces provide additional tests of the effect of surface topology and composition on the free energy of peptide adsorption. 4DAYAR5 adsorbs to FAU more strongly than to LTA. This could be in part due to the slightly lower aluminum content of the FAU samples relative to LTA; in the sodalite samples, decreasing aluminum content was associated with increased adsorption affinity.

As noted previously, the surface area measurement used to normalize the isotherms on FAU and LTA is different from that used for the isotherms on sodalite and colloidal silica samples. Therefore, it is difficult to establish whether the high surface coverages observed in these isotherms are significant. However, normalization of the LTA isotherm by the BET value for surface area (which is ideally an upper limit on the external surface area) leads to greater amounts of adsorbed 4DAYAR5 on LTA than on SOD–2.5. Therefore, the available data indicate that LTA surfaces have a higher affinity for the peptide than do sodalites of similar composition. This is not likely to be solely due to surface potential; LTA has previously been shown to have a zeta potential of –43 mV [216], comparable to that of colloidal silica. Instead, the greater amount of adsorbed peptide may be due to the arrangement of surface groups in nanoscale pores on the surface, which may be large enough to admit part of the positively-charged peptide C-terminus. This would allow the side chains to optimize their interactions with surface groups more effectively than on surfaces which lack this structural feature.

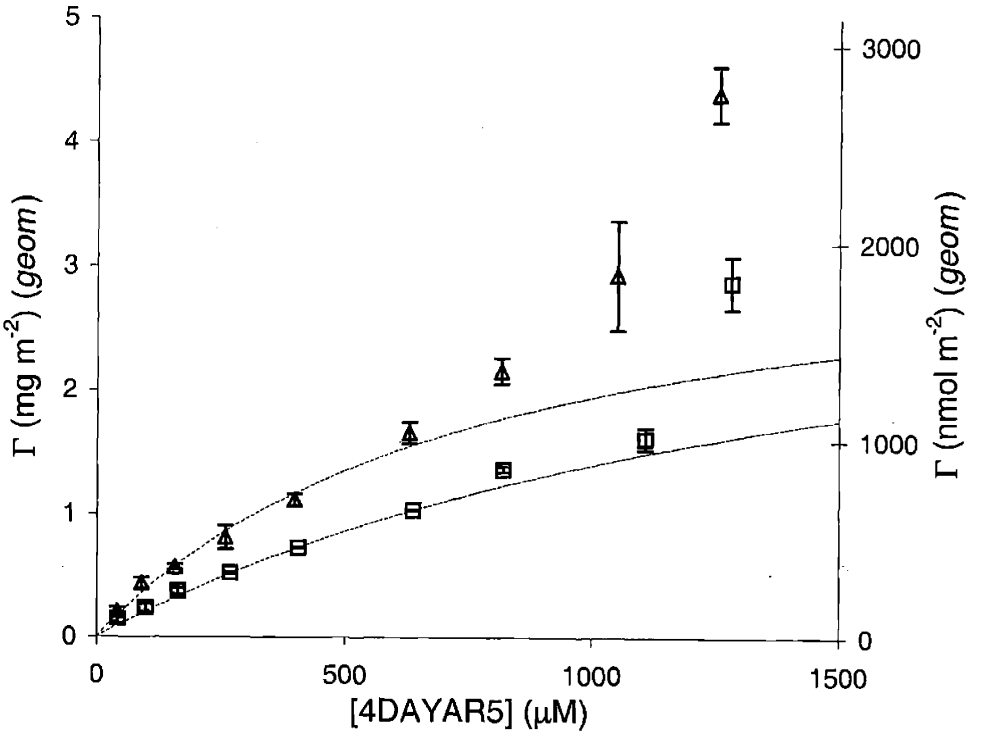

Figure V-9. Adsorption isotherms of 4DAYAR5 at pH 9 in 10 mM sodium borate buffer to large-pore synthetic zeolites: (△) colloidal FAU; (□) colloidal LTA. Fitting parameters are given in Table V-III.

The pH dependence of the adsorption of 4DAYAR5 to LTA displays significant differences from adsorption to Snowtex ZL. As colloidal suspensions of LTA are acidified, the amount of 4DAYAR5 adsorbed to these large-pore zeolites increases weakly with decreasing pH between 8.5 and 6, opposite from the behavior observed on amorphous or siliceous zeolite surfaces, as shown in Figure V-10. Both the sodium-exchanged and as-synthesized (TMA) forms of LTA display the same behavior. The effect is observable for FAU, but less pronounced.

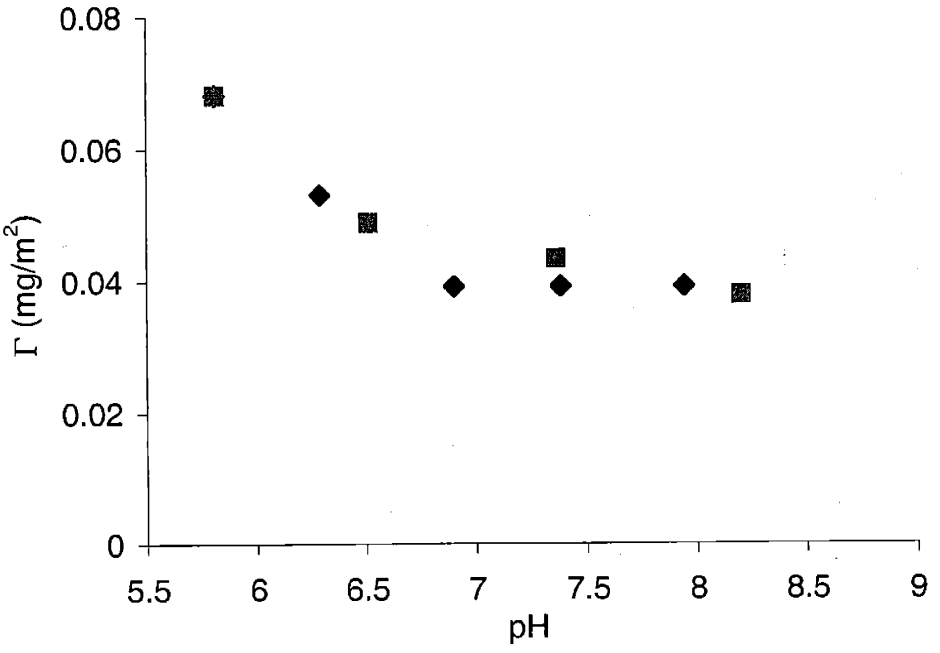

Figure V-10. Reversible changes in the adsorbed amount of 4DAYAR5 on colloidal FAU. Peptide was combined in solution with FAU particles, and the solution was titrated with dilute HCl (◆, decreasing pH) or NaOH (■, increasing pH). Aliquots were periodically taken, the particles with adsorbed peptide were separated by centrifugation, and the remaining peptide concentration was measured by UV absorbance.

As noted above, a decrease in pH to 6 leads to rapid hydronium ion exchange, in which the cations associated with the tetrahedral aluminum sites are replaced with protons. The effects of hydronium ion exchange on the solution ^{1}H NMR spectra of colloidal solutions of unexchanged FAU are shown in Figure V-11. No hydronium ion exchange is observed at pH 7 and above (though the observed material is TMA-exchanged, and differences in hydronium ion exchange for the sodium-exchanged material, which cannot be observed by ^{1}H solution NMR, cannot be excluded). No irreversible changes in peptide affinity occur with hydronium ion exchange; upon increasing the pH, the adsorbed peptide desorbs. Thus, the altered pH-dependence may arise from a competition between cationic species that interact with tetrahedral aluminum sites.

Among the variations studied here, surface composition and structure both have dramatic effects on the peptide adsorption equilibrium. Surface charge plays a large role in determining the orientation of the peptide on the surface, as evidenced by the reorientation of peptides on alumina-capped surfaces. Surface structure also appears to be important in determining the adsorption affinity, as evidenced by the dramatic increase in adsorption

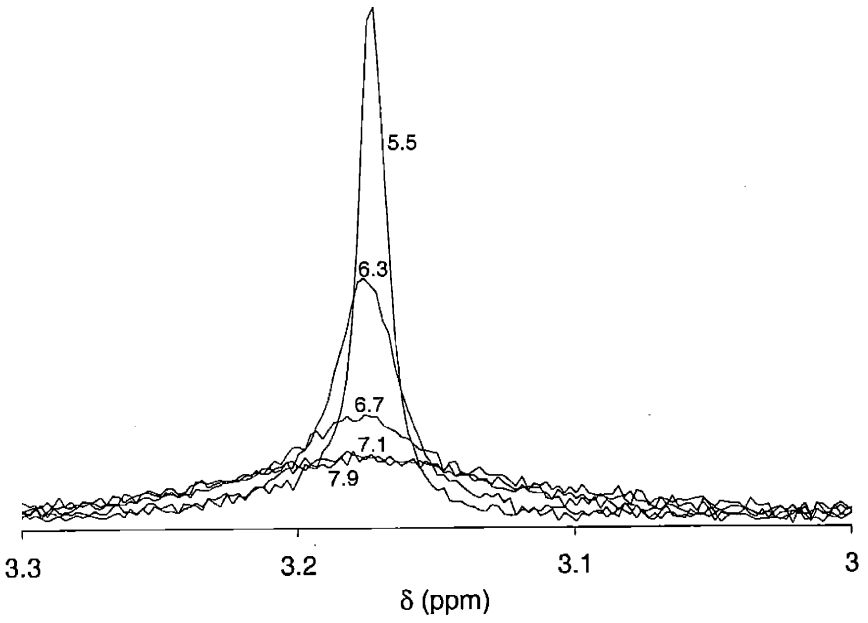

Figure V-11. Solution ^{1}H NMR signal of colloidal FAU suspensions at various pH values (shown alongside spectra). Particles were suspended in D_2O and titrated with dilute DCl. Spectra were normalized using the integrated peak intensity of TSP in a capillary tube.

observed on a siliceous sodalite surface, as well as the large difference between nonporous (sodalite) and large-pore (FAU and LTA) aluminosilicate surfaces. In what follows, the reasons for these dependences will be explored by considering the energetics of adsorption in this system.

In Chapter III, the electrostatic component of the free energy of adsorption was estimated by modeling the potentials at which charged peptide side chains were positioned, treating these charges as equivalent. In order to avoid this assumption, the individual contributions to the free energy of adsorption from each residue may be considered to arise from the electrostatic, noncovalent bonding of identical side chains to a variable arrangement of surface groups, offset by the energetic penalty associated with the conformation changes necessary to localize side chains at the surface, given the connectivity of the peptide and the spatial arrangement of surface functional groups.

For flexible molecules and a relatively high density of surface groups, wide variations in the arrangement of surface functional groups are possible without altering the number of noncovalent, electrostatic interactions between the peptide and the charged surface. Favorable contacts with the readily-available surface groups are made by every residue that

has the correct charge. The view that these molecules are flexible on the surface is supported by the fact that adsorption affinity to amorphous colloidal SiO_2 increases dramatically and monotonically with the number of terminal charges, indicating that a charge at any position along the terminus is able to contribute significantly to the free energy of adsorption. The density of oxide surface groups is mainly a function of the bond length; this is not varied significantly on any of the surfaces studied. Since adsorbing peptides are flexible enough to allow the maximum number of interactions with nearly any arrangement of functional groups, the number of these interactions is determined by the sequence of the peptide. These interactions, however, require conformational changes in the adsorbing terminus: α-helicity is lost and side chains are localized at the surface. Therefore, adsorption will be favored when the conformational preferences of the adsorbate are complementary to the spatial arrangement of surface groups.

Within the adsorbed terminus of the peptides, the residues that interact electrostatically with the charged surface are identical (arginine), while the ability of the zeolite surfaces to form these interactions is a function of both surface composition and crystal structure. The latter dependence is due to the effect of crystal structure on nanoscale topology, bond angles, and, therefore, surface charge. The mechanism by which the adsorption affinity of peptide is affected by the crystallinity of a siliceous material, even for materials with no accessible pore volume such as sodalite, thus involves the effects of crystallinity both on nanoscale topology, and on the overall surface charge.

Imposing a crystal structure with relatively large pores can have even more dramatic effects, as was observed in FAU and LTA. As discussed above, these peptides are flexible and likely make the same number of residue–surface contacts with large-pore aluminosilicates as with sodalite. Chemically and energetically, these contacts are probably comparable to those formed with the aluminum-rich sodalite surfaces, so the apparent increase in the amount of peptide adsorbed to LTA relative to sodalite samples of similar compositions probably results from reduced energetic penalties of forming these contacts. This leads to the conclusion that microporous topologies result in higher adsorbed amounts than non-porous surfaces because they allow molecules to adsorb in more energetically favorable conformations. It is not clear whether these conformations are therefore similar to the solution conformations; quantitative α-helicity measurements of DAR-type peptides on

colloidal LTA and FAU surfaces were difficult due to scattering from these larger particles. The conformation of DAR-type peptides on zeolite surfaces is therefore an interesting area for future work.

Specific interactions are associated with large binding constants, as well as a unique conformation and orientation. Thus the interactions studied here do not represent specific binding, because they lack a large binding constant, as well as the necessary uniqueness in conformation. It is interesting to consider how specificity could be studied within this model system. Binding constants are emergent functions associated with large numbers of contacts formed by the interaction. Adding several charged residues to the DAR-type peptides would boost the binding constant into the range of specific interactions. However, in order to impart specificity to the interaction between peptides and oxide surfaces, it would be necessary to restrict the formation of the maximum number of contacts to one unique conformation. DAR-type peptides contain an unusual, artificial sequence, and are likely to interact with surfaces in a nonspecific fashion, since the residues which contribute to the favorable free energy of adsorption are identical, and therefore can interact with the surface in a large number of different configurations. Specificity could be studied within this model system by selecting a surface with high symmetry and a variety of chemical functionalities (such as the colloidal FAU particles studied here). On sufficiently small particles, the orientation and conformation of adsorbing peptides for the surface selected could be studied using the techniques here, thus restricting the interaction to a relatively small number of possible geometries. With the help of molecular modeling, the sequence of the adsorbing terminus of the peptide could be engineered to match the surface functionality. Though these experiments are beyond the scope of this work, they demonstrate the potential for studying a variety of types of interactions within this model system.

4. Conclusions

Adsorption of DAR-type peptides to a cationic alumina surface occurs in a specific orientation, opposite to that adopted on anionic silica, and is associated with a similar degree of α-helicity loss. This finding is consistent with the electrostatic model of adsorption and

demonstrates that the polarity of surface charge controls the orientation and dictates which functional groups on the adsorbed molecule interact with the surface.

The use of zeolites expands the available range of surface topology and composition in a systematic way, enabling separate study of the effects of these two surface properties on adsorbed molecules. When normalized for surface area, the differences between these adsorption isotherms were significant. This is not surprising, given the importance of surface composition to the adsorption and desorption of model proteins [8]. Measurement of the adsorption isotherm of 4DAYAR5 on the highly-faceted SOD–∞ at pH 9 allowed direct comparison with the isotherm on amorphous colloidal silica, and therefore isolated the effect of imposing uniform topology and bond angles on the silica surface via the underlying crystal structure. The effect was to dramatically increase the adsorbed amount. Because the surface potential varies among silica polymorphs, the difference in the amount of adsorbed peptide could be due to a change in zeta potential.

This adsorbed amount was increased further by incorporating a relatively small amount of aluminum into the crystal structure, which introduces a negative charge. Since the importance of electrostatic forces in peptide adsorption were established in Chapter III, it is not surprising that incorporation of negatively-charged sites increased adsorption. Crystallite habit and particle size changed simultaneously with the incorporation of aluminum, and therefore some effects due to a change in surface nanoscale topology cannot be ruled out. Incorporation of greater amounts of aluminum into the crystal structure led to a decrease in the amount of adsorbed peptide. Progressive changes in the nature of surface groups as a function of surface composition may be associated with a decreased acidity of aluminum sites, as well as a gradual decrease in surface charge.

Two large-pore zeolites, FAU and LTA, having high-quality crystal structures with different pore sizes, provided another direct probe of the influence of crystal structure on peptide adsorption. These two materials were synthesized through nearly identical hydrothermal processes differing only in the addition of sodium chloride and incubation times. The particle size and morphology of the samples were significantly different, while their surface aluminum content was similar to within 10%. Interestingly, surface topology did not appear to affect adsorption; the differences in adsorption affinity followed the trend expected for the difference in aluminum contents without displaying additional effects.

Although it was difficult to normalize the surface areas of these materials available for peptide adsorption, the available data indicates that the amount of peptide adsorbed on these materials is significantly larger than that on sodalites of similar composition. The presence of nanoscale topology may admit peptide termini and provide for more effective optimization of contacts, leading to a more negative free energy of adsorption.

Chapter VI. Conclusions

The model system developed in this work provides a picture of the adsorption and conformation change of DAR-type peptides on amorphous anionic colloidal silica, a comparatively simple model surface. Adsorbed peptides were investigated using adsorption isotherms, as well as CD and NMR spectroscopy. These results, combined with the dependence of the adsorption process on peptide sequence, demonstrated the importance of electrostatics in driving adsorption and conformation change. The functionality of peptides adsorbed to the silica surface was evaluated by characterization of the α-helicity retained as a function of adsorption conditions, and by the behavior of the adsorbed molecules as a substrate for a model biological reaction. Finally, the substrate dependence of adsorption was examined, starting with cationic, alumina-capped colloidal silica, another comparatively simple model surface. The principles derived from the model oxide surfaces were applied to interpret adsorption isotherms of 4DAYAR5 on a carefully chosen set of model surfaces containing systematic variations in surface chemistry and topology. In this section, the results of this study regarding loss of structural order, adsorption specificity, and reversibility are discussed in the context of important questions in protein adsorption, conformation change, and surface functionality. Possible applications of the systematic variations in surfaces are discussed. Finally, these results are contextualized in how they influence the most important end result of immobilization at an interface, biological functionality.

In contrast to protein adsorption, peptide adsorption is reversible. Increasing the number of peptide residues providing favorable electrostatic interactions with the surface in the range studied here (between two and five residues) increases the adsorption affinity of the peptide but does not lead to irreversible adsorption. Therefore it is interesting to consider briefly what would be required to cause irreversible adsorption of these molecules; that is, to use the model system developed here to investigate the minimum criteria for irreversible adsorption. Irreversibility of protein adsorption is thought to arise from the formation of a large number of interactions with the surface, which results in a large decrease in the free energy of adsorbed molecules relative to the solution state [18]. A simple, two-state model provides a sufficient explanation for high-affinity isotherms, which are observed for a variety of macromolecules including proteins, hydrophobic surfactants, and polyelectrolytes. The

presence of significant differences between ascending and descending adsorption isotherms (hysteresis) observed for many protein-surface systems is likely due to the presence of multiple adsorbed states, some of which are responsible for irreversible adsorption, combined with strong interactions among adsorbed molecules. For example, a protein that displays adsorption hysteresis is likely to be present either in a variety of adsorbed states, in which case the observed desorption is from reversibly-adsorbed states, or in a relatively uniform, metastable adsorbed layer, the structure of which represents only one of a large variety of possible structures. The characteristics of the adsorbed layer which is formed may depend on adsorption conditions such as the amount of protein in solution relative to the available surface area [145]. Alternative structures may be differentiated by, for example, the strength of the interactions among adsorbed molecules. Desorption may then allow the structure of the adsorbed layer to change in a kinetically-controlled way such that the remaining molecules become irreversibly adsorbed, leading to the observed hysteretic behavior. Thus, mechanisms are conceivable whereby irreversibility arises either from the number of protein–surface contacts formed, or from the conformational states available to the protein upon adsorption. In this context, it is noted that gross conformational changes are not required to provide irreversibility with respect to dilution. For example, lysozyme adsorbs irreversibly to colloidal silica, but the change in secondary structure associated with irreversible adsorption is strongly dependent on the surface coverage. Although conformational changes are observed in the presence of excess surface, minimal conformational changes are observed in a fully-saturated surface layer [42]. Therefore, the adsorbed proteins establish a large number of favorable interactions, either with each other or with the surface, with minimal conformation changes observed by CD. Understanding these more complex features of protein adsorption continues to be a fascinating challenge, and holds great opportunity for novel approaches.

The peptides studied here lack any mechanism for irreversible adsorption. The energy barrier to desorption is so low that desorption occurs without any observable delay; in other words, none of the adsorbed states are irreversible. Peptides are apparently not capable of forming sufficiently strong intramolecular interactions to provide an observable kinetic barrier to desorption. Irreversible adsorption of DAR-type peptides would thus require a larger number of intermolecular interactions with the surface, or sufficiently strong interactions

among adsorbed molecules to hinder desorption. The threshold of irreversibility and its dependence on adsorbate structure would be an interesting topic for future study.

In this model system, adsorption is associated with a loss of α-helical structure. The loss of ordered secondary structure is a ubiquitous feature of protein adsorption processes [39], and is commonly posited to contribute to the free energy of adsorption [18]. Therefore it is interesting to consider the extent to which loss of order is a general feature of the adsorption of conformationally-ordered molecules. This question is likely to become more important as attempts are made in the future to imbue immobilized molecules with novel conformations and functionalities. There are systems in which adsorbed molecules have a higher degree of conformational order, such as proteins adsorbed to fluorocarbon surfaces [43,44]. Adsorption leads to a reoptimization of conformation; adsorption environments that reinforce the intramolecular interactions giving rise to order in protein and peptide structures can lead to an increase in ordered secondary structure in adsorbed molecules. Nevertheless, this work provides a case study of why loss of order is a relatively common feature of protein adsorption: simple surfaces introduce nonspecific fields such as electrical fields or planes of hydrophobic contacts which exert nonspecific forces on molecules, and nonspecific forces seldom act to increase order in molecules that are already highly ordered.

Adsorption was shown to lead to different coil conformations than thermal destabilization, as shown by the altered isodichroic point observed in CD studies of the helix-coil transition on the surface. This is in agreement with the finding that forced unfolding by AFM occurs through different intermediates than thermal destabilization [58] and indicates that, although concepts from protein folding in solution are frequently useful in analyzing conformational changes that occur upon adsorption, they must be applied with care. For example, although the development of the molten-globule mechanism for protein folding in solution has implications for understanding structural changes in adsorbed proteins, it is important to remember that molecules on a surface need not necessarily pass through the same intermediate states of structure loss. Because different coil states may arise from different mechanisms of structural perturbation, it is not surprising that adsorption to silica results in α-helicity losses, even at elevated temperatures where α-helicity is partially destabilized in solution. Understanding and controlling reversible conformational changes of

structured molecules at interfaces is important in surface engineering applications, and therefore it is interesting to note that the structural perturbations arising from adsorption could lead to novel conformations, and perhaps novel functionalities, not accessible from chemical or thermal methods in solution.

The specificity of the adsorbed conformation is a separate question from the average conformation change in adsorbed molecules, and it has important implications for the function of adsorbed molecules. However, this work does not provide direct measurement of the distribution of conformations of molecules in solution or adsorbed, and the treatment of specificity is therefore limited to a set of general predictions. Visualization of this question is aided by consideration of the general features of the free energy landscape of the molecule, which is a complicated function of the dihedral angles that parameterize the molecular conformation. Adsorbed molecules preferentially populate conformers that correspond to the global minimum of the energy landscape. In contrast to the issue of a loss or gain of ordered conformation, which deal with the position of the global minimum, the question of specificity may be conceived of as whether it appears as a shallow basin or deep well. Shallow basins correspond to nonspecific adsorption in a large number of conformations with nearly equivalent free energies. In contrast, deep wells are associated with specific conformations. In this work, the specificity of the adsorbed conformation can best be visualized from the statistical model developed for adsorbed 4^{+}DAR4. The stretched substates of the coiled conformational space defined in Chapter IV.2 were less populated at weak surface interaction strengths, corresponding to adsorption at neutral pH. This was manifested in relatively low values for β_A. In contrast, when surface interactions were strong, these states were more populated, and the values of β_A increased. This is a special case of the more general observation that highly-specific conformations are poised at a balance between large competing forces, which lead to narrow wells in the energy landscape. Therefore, as the adsorption affinity increases and larger forces are exerted on adsorbed molecules, the distribution of conformations of adsorbed peptides is expected to narrow, and the specificity of the adsorbed conformation increases.

Solution ^{1}H NMR has been used to provide information on the adsorption of surfactants, both by directly examining the mobility of adsorbed surfactants [159,160] and by examining changes in the relaxation rate of solvent molecules that results from changes in the

structure of the adsorbed layer [217]. In combination with CD spectroscopy, NMR was especially useful in this system, in providing both orientational and conformational information. The dramatically different picture of the adsorbed amount which this technique gives relative to that found from sedimentation has not previously been noted. As discussed in Chapter III.7, sedimentation measures the fraction of molecules adsorbed at any given time, while NMR is a cumulative measure of interactions with the surface, and the signal intensity retained reduces to the free fraction only in the limit of slow kinetics relative to the NMR timescale. The importance of kinetics is further evidenced by the complete disappearance of all resonances of peptides with a net charge, such as 4^{+}DAR4. These considerations have important implications for utilization of NMR in future adsorption studies: for systems with slow adsorption kinetics relative to the NMR timescale, solution NMR provides information about the adsorbed fraction. However, for systems that have rapid adsorption kinetics relative to the NMR timescale, in which all molecules are spectroscopically equivalent, NMR provides information about the relative relaxation rates of different portions of the molecule, and therefore on their relative mobilities. The possibility of using NMR to explore on/off kinetics in systems in which these rates are on the order of the NMR timescale also deserves consideration in future work.

Enzymatic cleavage of peptide bonds indicated that adsorption can significantly decrease the availability of molecules for this model biochemical reaction, but that even under conditions of complete adsorption, molecules can be rapidly cleaved. The distribution of reaction products is shifted from the solution reaction, but retains the general features of the original distribution. One desired insight from such studies is how information on the driving forces for adsorption and conformational change can be used to understand the implications of this process for biological functionality. In this system, the driving forces for the adsorption process were in many ways distinct from the features that influence biological functionality. For example, although orientation of adsorbed molecules, not surprisingly, appeared to be important, the rate of the reaction appeared to be controlled more by kinetic factors such as diffusion of enzyme and peptide molecules. An understanding of the conformation and orientation of adsorbed molecules may thus be a necessary, but not sufficient condition for a predictive understanding of biological functionality.

Systematic variations of surface composition and structure are essential to draw clear conclusions regarding the forces exerted on adsorbed proteins and peptides by surfaces. This work showed that direct hydrothermal synthesis of zeolites is a powerful way to systematically expand the range of available surface properties. Understanding the adsorption mechanism for one surface was important in interpreting experimental data from other surfaces, but it was clear that each surface introduced unique challenges and required additional interpretation. Crystal surface topology, in the absence of significant differences in composition, can influence the free energy of adsorption of short α-helical peptides for both siliceous and aluminosilicate surfaces. Changes in surface composition can dramatically alter the adsorbed amount and its dependence on pH. Understanding and predicting how such factors might affect the adsorption behavior of proteins could lead to progress on important questions such as the polymorph-dependent toxicity of silica particles [195,218].

This work has provided a model system in which questions regarding adsorption and conformation change can be asked and answered. The study of protein conformation on surfaces is expected to advance alongside the constant progress in solution folding studies. An important component of this progress is reduction of complex issues to questions which can be answered experimentally in a well-characterized system. Although a predictive theory of protein adsorption and conformation change may be far off, model systems such as this one should help to clarify the important mechanisms behind this process, and provide insight into technological problems.

Appendix A. Procedure for Determining Fractional α-Helicity of Adsorbed Molecules

In this section it is shown explicitly how the experimentally-measured CD signals containing contributions from molecules both in solution and adsorbed were interpreted to find the CD signal of adsorbed molecules. In this analysis, CD samples may have arbitrary (but known) concentrations of colloid and peptide. Important assumptions, explained in more detail in the text, are that

- CD signals are additive
- changes in CD spectra of adsorbed molecules are due to conformation changes and not to the proximity of the oxide surface
- the measured CD signal $[\theta]_{222} = \begin{cases} 0 \text{ for completely nonhelical molecules} \\ ([\theta]_{222})_{free} \text{ for non-adsorbed molecules} \end{cases}$
- the adsorbed amount is a function only of the concentration of peptide in solution at equilibrium, and is not perturbed by the sedimentation process used to measure the isotherm

Given these assumptions, along with the adsorbed amount $\Gamma(c)$, the value of $[\theta]_{222}$ can be determined for adsorbed molecules in the following way.

First, the CD data are used to create two plots on the same set of axes as the actual adsorption isotherm; each plot has one data point for each CD sample. The first plot is the total concentration of peptide in the CD samples before adsorption c_{tot}. Since adsorption is neglected, their ordinate $\Gamma(c)$ is null and they all lie on the abscissa. The second plot is the apparent adsorption "isotherm" calculated from the change in CD signal assuming that all adsorbed molecules are completely coiled; the coordinates of these data points (c_{CD}, $\Gamma_{CD}(c)$) are given by:

$$c_{CD} = \frac{\theta_{222}^{meas}}{\theta_{222}^{free}} c_{tot}$$

$$\Gamma_{CD} = \left(1 - \frac{\theta_{222}^{meas}}{\theta_{222}^{free}}\right) \frac{c_{tot}}{S} \qquad \textbf{(A-1)}$$

where S is the concentration of surface area in that particular CD sample (in m^2 ml^{-1}) and the measured CD signal need not necessarily be normalized. An example of this is shown in

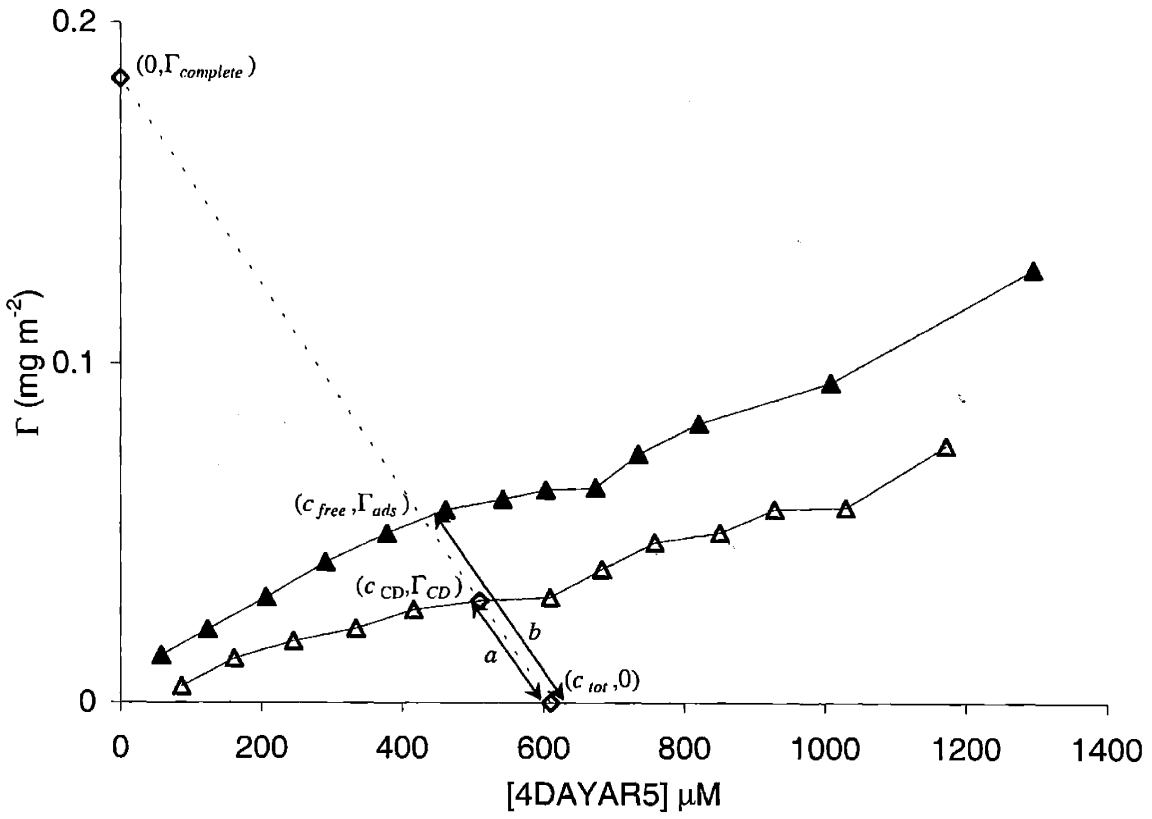

Figure A-1. Plot of adsorption isotherm (▲), CD data points (△), and variables pertaining to one particular CD data point (-◇-) discussed in the text. Only one c_{tot} point is shown.

Figure A-1. If adsorbed molecules are completely coiled, the data points of the apparent adsorption "isotherm" from CD will lie on the adsorption isotherm $\Gamma(c)$. However, if the α-helicity of the adsorbed molecules is between 0 and $(-[\theta]_{222})_{free}$, their difference from the adsorption isotherm is quantitatively related to the amount of α-helicity retained by adsorbed molecules.

The quantitative relation between the plots in Figure A-1 and the fractional α-helicity in adsorbed molecules can be derived. A CD sample has a known total concentration of peptide (c_{tot}), which must be the sum of the adsorbed amount and the solution concentration:

$$c + S \times \Gamma(c) = c_{tot} \qquad \textbf{(A-2)}$$

This equation defines a line on Figure A-1 which passes through both the data points plotted above for a particular CD sample. The intersection of this straight line with the adsorption

isotherm occurs at coordinates (c_{free}, Γ_{ads}), where c_{free} is the amount of peptide free in solution and Γ_{ads} is the adsorbed amount at equilibrium. The intersection of this same straight line with the ordinate (0, $\Gamma_{complete}$) gives the surface coverage in the case of complete adsorption where $\Gamma_{complete} = c_{tot}/S$.

The equation $X^{ads} = \Gamma_{ads} / \Gamma_{complete}$ holds by definition. Therefore using Equations (III-12) and (A-1) the fraction of α-helicity lost by adsorbed molecules relative to their solution α-helicity is given by:

$$\varphi_{Loss}^{ads} = 1 - \varphi_{Hel}^{ads} = \frac{1}{X^{ads}}\left(1 - \frac{\theta_{222}^{meas}}{\theta_{222}^{free}}\right) = \frac{\Gamma_{complete}}{\Gamma_{ads}}\left(\frac{\Gamma_{CD} S}{c_{tot}}\right) = \Gamma_{CD}/\Gamma_{ads}$$

(A- 3)

Using the property of similar triangles, this is equivalent to the fraction *a*/*b* of the "tie line" connecting the data points (c_{tot},0) and (Γ_{ads},c_{free}). The quantity X^{ads} can be read off this same line as *b*/*c*.

Appendix B. Source Code and Sample Calculations for the Helix–Coil Transition of Peptides on the Silica Surface

1. Introduction

In this section, calculations are shown for the model of the helix–coil transition on the charged silica surface developed in Chapter IV.2, in order to demonstrate how this model was implemented. As described in the text, these calculations were made by modifying a research code obtained by anonymous ftp (web address: ftp://cmgm.stanford.edu/pub/caphelix). In Section 2, operation of this code to obtain theoretical values for α-helicity of peptides in solution is described. Modifications are described which incorporate the dependence of α-helicity on temperature as in equation (IV-2). In Section 3, modifications are described which incorporated the values of β according to the model in Equations (IV-8) and (IV-9). Finally, Section 4 lists the source code itself.

2. Solution Calculations

The program `caphelix` prompts the user for the names of files containing the peptide sequence and residue-specific parameters for α-helix formation, then reads the desired information in from these files. These files are listed in Scheme B-1 and Scheme B-2 respectively. The program then outputs:

- the value of the partition function
- the α-helicity as a function of sequence position
- the overall α-helicity of the molecule.

A sample output file is shown in Scheme B-3. These values can be explicitly reconstructed as follows. The value of the partition function is calculated from equation (IV-4), which for the sequence of the peptide 4^{+}DAR4 is:

```
Sequence: DAR4+
15
 1   X
 2   D
 3   D
 4   D
 5   D
 6   A
 7   A
 8   A
 9   A
10   R
11   R
12   R
13   R
14   R
15   Z
```

Scheme B-1. Sequence file.

```
helix parameter library
 26
 1   ALA  A    1.61, 0.0023, 1.0, 1.0
 2   GLU  B    0.00, 0.0000, 1.0, 1.0
 3   CYS  C    0.00, 0.0000, 1.0, 1.0
 4   ASP- D    0.31, 0.0023, 20.0, 0.0
 5   GLU- E    0.00, 0.0000, 1.0, 1.0
 6   PHE  F    0.00, 0.0000, 1.0, 1.0
 7   GLY  G    0.00, 0.0000, 1.0, 1.0
 8   HIS+ H    0.00, 0.0000, 1.0, 1.0
 9   ILE  I    0.00, 0.0000, 1.0, 1.0
10   HIS  J    0.00, 0.0000, 1.0, 1.0
11   LYS+ K    0.00, 0.0000, 1.0, 1.01
12   LEU  L    0.00, 0.0000, 1.0, 1.00
13   MET  M    0.00, 0.0000, 1.0, 1.0
14   ASN  N    0.00, 0.0000, 1.0, 1.0
15   ASP  O    0.00, 0.0000, 1.0, 1.0
16   PRO  P    0.00, 0.0000, 1.0, 1.0
17   GLN  Q    0.00, 0.0000, 1.0, 1.0
18   ARG+ R    1.09, 0.0023, 1.3, 2.1
19   SER  S    0.00, 0.0000, 1.0, 1.0
20   THR  T    0.00, 0.0000, 1.0, 1.0
21   LYS  U    0.00, 0.0000, 1.0, 1.0
22   VAL  V    0.00, 0.0000, 1.0, 1.0
23   TRP  W    0.00, 0.0000, 1.0, 1.0
24   ACE  X    1.00, 0.0023, 12.0, 1.0
25   TYR  Y    0.00, 0.0000, 1.0, 1.0
26   AMD  Z    1.00, 0.0023, 1.0, 1.3
```

Scheme B-2. α-Helix parameter file.

$$Z = [0\ 0\ 0\ 1]\mathbf{I}_D^4\,\mathbf{I}_A^4\,\mathbf{I}_R^5\begin{bmatrix}0\\0\\0\\1\end{bmatrix} \qquad \textbf{(B-1)}$$

Using the form of **I** found in Equation (IV-3) and the parameters in Table IV-I this can easily be shown to be 16.299, as listed in Scheme B-3. The fractional α-helicity of an individual residue is the probability of a local conformation $x_{i-1}\,h_i\,y_{i+1}$ where x and y can be either c or h. This value is calculated from Equation (IV-6) for an arbitrary residue i. As an arbitrary example, this value can be found for the N-terminal alanine residue (adjacent to the aspartate segment, $i = 6$)

$$(f_{Hel})_5 = \frac{1}{Z}[0\ 0\ 0\ 1]\mathbf{I}_D^4\begin{bmatrix}w_A & v & 0 & 0\\ 0 & 0 & 0 & 0\\ v & v & 0 & 0\\ 0 & 0 & 0 & 0\end{bmatrix}\mathbf{I}_A^3\,\mathbf{I}_R^5\begin{bmatrix}0\\0\\0\\1\end{bmatrix} \qquad \textbf{(B-2)}$$

This value is 0.7299. The same value can be extracted from Scheme B-3 by adding the `helix prob` (probability of this residue having a statistical weight of w_A; the value

```
  ----- Input -----

Sequence data file: DAR4p.seq
Sequence: DAR4+

 N =  15

Helix Parameter Library: helix.lib
helix parameter library

Naa in library =   26

  ----- Output -----

Z =  0.16299E+02

                helix      nuclei      n cap      c cap
                prob       prob        prob       prob

      1     X    0.0000     0.0000     0.0057     0.0000
      2     D    0.0000     0.0057     0.0308     0.0000
      3     D    0.0057     0.0308     0.0995     0.0000
      4     D    0.0366     0.0995     0.4293     0.0000
      5     D    0.1277     0.4377     0.3011     0.0000
      6     A    0.4208     0.3091     0.0166     0.1309
      7     A    0.5871     0.0396     0.0209     0.1213
      8     A    0.5725     0.0509     0.0344     0.0270
      9     A    0.5056     0.1126     0.0326     0.0390
     10     R    0.4000     0.1460     0.0423     0.1030
     11     R    0.2952     0.1556     0.0491     0.1364
     12     R    0.1905     0.1634     0.0602     0.1454
     13     R    0.0783     0.1816     0.0473     0.1559
     14     R    0.0000     0.1312     0.0000     0.1797
     15     Z    0.0000     0.0000     0.0000     0.1312

% stabilized helix (w) =  29.273116

% helix (v or w) =  39.105384

# helix =   0.931829
```

Scheme B-3. Output file from the original source code `caphelix.f`. The peptide sequence file `DAR4p.seq` and parameter library `helix.lib` are as listed in Scheme B-1 and Scheme B-2 respectively.

0.4208 can also be calculated from (IV-5)) and `nuclei prob` (probability of this residue having a statistical weight of $v = 0.3091$) probabilities for this residue.

Finally, to calculate the fractional α-helicity of the overall molecule, the fractional α-helicities of each residue are summed and divided by N where N is the number of residues, not including capping groups. Capping groups are assumed not to contribute to the fractional α-helicity measured by CD and therefore are not included in the normalization. This can be easily verified using the values in Scheme B-3.

The fractional α-helicities output by the code are functions of the values of w_i, v_i, n_i, c_i, and β_i for each residue i. The temperature dependence of α-helicity is incorporated by

varying these parameters as a function of temperature. The model developed in Chapter IV.2 assumes that only w_i varies with temperature. The code was modified to scale the parameters w_i for a new value of temperature according to Equation (IV-2). These is done in loop 22, boxed in the source code listed (Section IV). For simplicity, the way in which the desired temperature is specified is described in the next section, since it is related closely to the specification of surface interaction parameters.

3. Surface Calculations

The studies of peptide–surface interactions in Chapter IV.2 presented two types of information from the statistical model: the peptide α-helicity as a function of sequence position, and also the overall α-helicity for an array of specified values of ΔH_s and T, for comparison with experimental data. The α-helicity as a function of sequence position is taken from output files such as the one shown in Scheme B-3. The lines specifying the thermodynamic parameters and the resulting values of β are loops 21 and 23-25. The incorporation of β into the calculation is boxed as well.

The arrayed α-helicity values as a function of ΔH_s and T could be extracted from individual runs of the program, but for convenience the source code was modified to perform α-helicity calculations for an entire matrix. Therefore the remaining modifications are to create these arrays, store the α-helicity values in them after each calculation, and finally to output these values in a format suitable for a surface plot.

4. Source Code

The relevant source code files are listed in this section. The first file is the header file containing variable declarations. The end of this file is denoted by a solid line, and this is followed by the main source code. Lines of code added in this work are boxed.

```
*  caphelix.h
*
*  Code implementing the original Lifson-Roig model written by John Schellman
```

```
*  and modified by Hong Qian, University of Oregon, Eugene, OR.
*
*  Modifications to include capping as described in  Biochemistry 33, pp3396.
*  added by Carol Rohl and Tanja Kortemme, Stanford University, Stanford,
*  CA 94305.
*
*       1994 Biochemistry 33: 3396.
*
*      Determination of Free Energies of N-Capping in alpha-Helices
*      by Modification of the Lifson-Roig Helix-Coil Theory to Include
*      N- and C-Capping
*
*     by Andrew J. Doig,
*        Avijit Chakrabartty,
*        Tod M. Klingler and
*        Robert L. Baldwin
*
*     Department of Biochemistry
*     Stanford Univerisity Medical Center
*     Stanford, California  94305-5307
*-----------------------------------------------------------------------
*
        INTEGER         N,              ! the # of residues in the sequence
     .                  Numseq(500)     ! sequence in numerical integer

        REAL*8          perhel,          ! % of helix (v+w)
     .                  perw,           ! % of w
     .                  segment,        ! # of helix segment
     .                  Z,              ! the partition function
     .                  HP(500),        ! the % of helix in each residue
     .                  NP(500),        ! nucleate probability in each residue
     .                  ncapp(500),     ! ncap probability of each residue
     .                  ccapp(500),     ! ccap probability of each residue
     .                  sigma(30),      ! nucleation factor, Zimm's notation
     .                  sval(30),       ! s values
     .                  v(30),          ! square root sigma, Lifson's notation
     .                  ncap(30),       ! n cap parameter, C-D modification
     .                  ccap(30),       ! c cap parameter, C-D modification
c
c Mike Read 1/3/02
c Modification to add beta, the relative statistical weight of the coil state
c
     .                  beta(30),       ! coil relative statistical weight
     .                  sval2(30),
     .                  FHel(10,10),    ! helicities
     .                  temps(10),      ! desired temperatures
     .                  energs(10),     ! desired energies
     .                  betas(6,10,10),
     .                  VL(4),          ! left end vector, Dirac's "bra"
     .                  VR(4),          ! right end vector, Dirac's "ket"
     .                  D(4,4),        ! derivitive of WM respect to v
     .                  WM(4,4)         ! working matrix

        COMMON/HELIXi/  N, Numseq
        common/helixr1/ perhel, perw, segment, Z, HP, NP, ncapp, ccapp
        common/helixr2/ sigma, sval, v, ncap, ccap, VL, VR, D, WM
        common/mike/    beta,betas,fHel,temps,energs,sval2
```

```
*
*  Code implementing the original Lifson-Roig model written by John Schellman
*  and modified by Hong Qian, University of Oregon, Eugene, OR.
*
*  Modifications to include capping as described in  Biochemistry 33, pp3396.
*  added by Carol Rohl and Tanja Kortemme, Stanford University, Stanford,
*  CA 94305.
*
*       1994 Biochemistry 33: 3396.
```

```
*
*      Determination of Free Energies of N-Capping in alpha-Helices
*      by Modification of the Lifson-Roig Helix-Coil Theory to Include
*      N- and C-Capping
*
*     by Andrew J. Doig,
*        Avijit Chakrabartty,
*        Tod M. Klingler and
*        Robert L. Baldwin
*
*     Department of Biochemistry
*     Stanford Univerisity Medical Center
*     Stanford, California  94305-5307
*
* Modifications to include temperature-dependence and surface interactions
* by Mike Read
*
*-----------------------------------------------------------------------
C
C       Filename: caphelix.f
C -------------------------------------------------------------------------

C       This program is for calculating the helix content of a polypeptide
C       with an arbitrary sequence.  A sequence file input which contains
C       single letter representation is required.  This sequence is
C       converted into a numerical representtion, according to the
C       definition in the sigma-s parameter library.  Then subroutine
C       HELIX is called.

C --- varibles declearations ---------------------------------------------

        IMPLICIT DOUBLE PRECISION (A-H, O-Z)

        include "caphelix.h"

        CHARACTER*1     Lseq(500)       ! sequence in single character

        CHARACTER*40    filename        ! filename

        CHARACTER*80    LBtitl,         ! title in the library
     .                  Ltitle          ! title in the sequence file

        CHARACTER*4     aacode(30)      ! 3letter amino acid from library
        INTEGER         Naa             ! the # of residues in the library

        REAL*8          Heltot,         ! total helix
     .                  sp              ! spur function sp(U,V)

C-----------------------------------------------------------------

        DATA            zero/0.0d0/,
     .                  one/1.0d0/
C--- input inquire -----------------------------------------------------

5       write (6,*)
        write (6,'('' Enter the sequence file_'', $)')
        read  (5,'(A40)') filename
        open  (unit=8, status='old', file=filename, err=9999)
        write (6,*)
        write (6,'('' Reading the sequence data...'', A40)') filename

        read  (8, '(A80)') ltitle               ! read in comments
        read  (8, '(I)') N                      ! # of residues

        DO 10 I = 1, N
               read (8,'(5X,A1)') LSEQ(I)
10      continue

        close (unit=8)

C -----print out sequence ----------------------------
```

```
      open  (unit=9, status='unknown', file='hcontent.rep')

      write (9,*)
      write (9,*) '  ----- Input -----'
      write (9,*)
      write (9,*) 'Sequence data file: ', filename
       write (9,'(1x, A80, /, ''  N = '', I3)') ltitle, N

C ----- read in sigma-s library ----------------------------

15    write (6,*)
      write (6,'('' Enter the helix parameter library
     . (Default:helix.lib)_'', $)')

      read  (5, '(A40)') filename
      open  (unit=8, status='old', file=filename,
     .        defaultfile='helix.lib', err=9998)

      write (6, '(/, '' Loading the helix parameter library'', A40)') filename

      read (8, '(A80)') LBtitl
      read (8, '(I)') Naa

      DO 11 i = 1, Naa
             read (8, '(5x, A4, 6X,4F)')
     .             aacode(i), SVAL(i), sigma(i), ncap(i), ccap(i)
              sval2(i)=sval(i)
11    continue

      close (unit=8)
```

```
c
c Mike Read 1/3/02
c Modifications to recalculate values of w at an arbitrary temperature
c  and to specify beta
c
      beta(1)=1
      beta(15)=1
      do 20 itemp = 1, 10
        do 21 ienerg = 1, 10
          temps(itemp) = 10.*(itemp-1.)
          temp=temps(itemp)
          energs(ienerg) = -10000.*(ienerg-1.)/9.
          RT=8.314*(temp+273.15)
          Omegab=.5
          DeltaHb=energs(ienerg)
          Omegas=.22
          DeltaHs=-4235.66*(ienerg-1.)/9.
```

```
          do 22 i = 1, Naa
                  sval(i)=sval2(i)*exp(4184./8.314*(1./(temp+273.15)
     .             -1./273.15))
22        continue
```

```
          do 23 i = 2, 5
                  beta(i)=exp(DeltaHs/RT*(i-1.)/4.)
     .             -2*Omegas*sinh(DeltaHs/RT*(i-1.)/4.)
                  betas(i-1,itemp,ienerg)=beta(i)
23        continue
          do 24 i = 6, 9
                  beta(i)=exp(DeltaHs/RT)-2*Omegas*sinh(DeltaHs/RT)
                  betas(5,itemp,ienerg)=beta(i)
24        continue
          do 25 i = 10,14
                  beta(i)=1.+Omegab*(exp(-DeltaHb/RT)-1.)
                  betas(6,itemp,ienerg)=beta(i)
25        continue
```

```
C----Print out library to screen----------------------
```

```
c       write(6,'(/, '' aa        w          v          n          c''
c     .       , /)')
c       do 111 i=1, 26
c
c
c              write(6, '(a4, 2x, f10.4, f10.4,
c     .        f10.4, f10.4, f10.4)')
c     .        aacode(i), sval(i), sigma(i), ncap(i), ccap(i), beta(i)
c111    continue
c
c
C -----print out sigma-s library ------------------------------------
c
c      write (9,*)
c      write (9,*) 'Helix Parameter Library: ', filename
c       write (9,'(1X, A80, /, '' Naa in library = '', I4)')
c     .        LBtitl, Naa
c
C ----- calculation start ----------------------------------------

          do 50 i = 1, N
50           Numseq(i) = ichar(Lseq(i)) - 64

C                    convert one letter code to library order code, where
C                    A-Z corresponding to 1-26.  Lower case character
C                    should not be used.

          DO 60 i = 1, 26
60           v(i) = DSQRT(sigma(i))        ! convert sigma to v


          call vectset              ! set constants in end vectors

          call helix
           FHel(itemp,ienerg)=perhel
21       continue
20      continue

        write(10,990) (energs(i),i=1,10)
        write(11,991) (((betas(i,j,k),i=1,6),j=1,10),k=1,10)
        do 26 i = 1, 10
          write(10,990) temps(i),(FHel(i,j),j=1,10)
26      continue

990   format (11(2x,E))
991   format (6(2x,E))

       write (9,*)
       write (9,*) '  ----- Output -----'

       WRITE (9,'(/,'' Z = '', E12.5,/)') Z
       WRITE (9,'(12X, ''    helix     nuclei     n cap     c cap'')')
       WRITE (9,'(12X, ''    prob      prob       prob      prob '',/)')


       DO 7 i = 1, N
          WRITE (9, '(5X, I3, 4X, A, F10.4, F10.4, F10.4, F10.4)')
     .        i, char(numseq(i)+64), HP(i), NP(i), ncapp(i), ccapp(i)
7      continue

       WRITE (9,'(/, '' % stabilized helix (w) = '', F10.6)') perw
       WRITE (9,'(/, '' % helix (v or w) = '', F10.6)') perhel
       WRITE (9,'(/, '' # helix = '', F10.6)') segment

       WRITE (6,*)
       WRITE (6,*) 'A summary report is in hcontent.rep'
       WRITE (6,*)
999    stop

9998   write (6, '(/, '' File not found!'')')
       goto 15
```

```
9999    write (6, '(/, '' File not found!'')')
        goto 5
        end
*-----------------------------------------------------------------------
*-----------------------------------------------------------------------

        SUBROUTINE HELIX

        IMPLICIT DOUBLE PRECISION (A-H, O-Z)

        include "caphelix.h"


        REAL*8          Heltot,         ! total helix
     .                  sp,             ! spur function sp(U,V)
     .                   VT(4),                 ! working vector
     .                   Vtemp(4)       ! temporary working vector

C ----- start loop over residues ----------------------------------------

        call VEQ(VL,VT)                 ! set working vector equal to left end vector
        do 3 k = 2, N-1
                call MATSET(k)
                call VXM(VT,WM,VTEMP)
                call VEQ(VTEMP,VT)
3       continue

        Z = SP(VT,VR)

C -----start loop over residues to evaluate dlnZ/dlnW -------------

        do 1 i = 1, 4
                 do 1 j = 1, 4
1                        D(i,j) = 0.0

        DO 2 i = 2, N-1
                call VEQ(VL,VT)
                DO 4 k = 2,N-1
                        CALL MATSET(k)
                        IF(k.EQ.i)
     .                   THEN
                                D(1,1) = WM(1,1)
                                call VXM(VT,D,VTEMP)    ! can be improved, since
                                call VEQ(VTEMP,VT)      ! there are many zeros
                        ELSE                            ! in DW.
                                call VXM(VT,WM,VTEMP)
                                call VEQ(VTEMP,VT)
                        ENDIF
4               continue
                HP(i) = SP(VT,VR)/Z
2       continue

        Heltot = 0.0
        do 6 i = 3, N-2
                heltot = Heltot + HP(i)
6       continue
        perw = 100.0*Heltot/(N-4)

C -----start loop over residues to evaluate dlnZ/dlnv -------------


        do 313 i = 1, 4
                 do 313 j = 1, 4
313                       D(i,j) = 0.0

        DO 222 i = 2, N-1
                 call VEQ(VL,VT)
                 DO 444 k = 2,N-1
                          CALL MATSET(k)
                          IF(k.EQ.i)
     .                    THEN
```

```
                                D(1,2) = WM(1,2)        ! this calculation
                                D(3,1) = WM(3,1)        !
                                D(3,2) = WM(3,2)        !
                                call VXM(VT,D,VTEMP)    ! can be improved,
                                call VEQ(VTEMP,VT)       ! there are many zeros
                        ELSE                             ! in DW.
                                call VXM(VT,WM,VTEMP)
                                call VEQ(VTEMP,VT)
                        ENDIF
444             continue
                NP(i) = SP(VT,VR)/Z
222     continue

        Segment = 0.0
        do 66 i = 2, N-1
                segment = segment + NP(i)
66      continue
       perhel = 100.0 *(heltot + segment)/(N-2)
        Segment = segment/2.0

C -------------------dlnZ/dlnn--------------------------------------
        call VEQ(VL,VT)
        VT(4) = 0.0                             ! the derivitive of VL

        DO 51 k = 2,N-1
                CALL MATSET(k)
                call VXM(VT,WM,VTEMP)
                call VEQ(VTEMP,VT)
51      continue
        ncapp(1) = SP(VT,VR)/Z


        do 44 i = 1, 4
                do 44 j = 1, 4
44                      D(i,j) = 0.0

        DO 52 i = 2, N-1
                call VEQ(VL,VT)
                DO 54 k = 2,N-1
                        CALL MATSET(k)
                        IF(k.EQ.i)
                          THEN
                                D(4,3) = WM(4,3)
                                  D(2,3) = WM(2,3) / 2.0    ! n*d(sqrt(nc))/dn =
C                                                                   sqrt(nc)/2
                                call VXM(VT,D,VTEMP)
                                call VEQ(VTEMP,VT)
                        ELSE
                                call VXM(VT,WM,VTEMP)
                                call VEQ(VTEMP,VT)
                        ENDIF
54              continue
                ncapp(i) = SP(VT,VR)/Z
52      continue

        ncapp(N) = 0.0

C ---------------------dlnZ/dlnc---------------------------------------
        ccapp(1) = 0.0


        do 515 i = 1, 4
                do 515 j = 1, 4
515                     D(i,j) = 0.0

        DO 77 i = 2, N-1
                call VEQ(VL,VT)
                DO 78 k = 2,N-1
                        CALL MATSET(k)
                        IF(k.EQ.i)
                        THEN
```

```
                                D(2,4) = WM(2,4)
                                D(2,3) = WM(2,3) / 2.0   ! c*d(sqrt(nc))/dc =
C                                                           sqrt(nc)/2
                                call VXM(VT,D,VTEMP)
                                call VEQ(VTEMP,VT)
                        ELSE
                                call VXM(VT,WM,VTEMP)
                                call VEQ(VTEMP,VT)
                        ENDIF
78                continue
                  ccapp(i) = SP(VT,VR)/Z
77          continue

            call VEQ(VL,VT)
            DO 555 k = 2,N-1
                   CALL MATSET(k)
                   call VXM(VT,WM,VTEMP)
                   call VEQ(VTEMP,VT)
555         continue

            call VEQ(VR,VTEMP)                  !derivative vector for VR
            VTEMP(4) = 0.0

            ccapp(N) = SP(VT,VTEMP)/Z

            return
            end

C ^^^^^^^^^^^^^^^^^^^^^^^^^^^^^^^^^^^^^^^^^^^^^^^^^^^^^^^^^^^^^^^^^^^^^^
            SUBROUTINE VECTSET

C           define end vectors VL, VR

            IMPLICIT DOUBLE PRECISION (A-H, O-Z)

            include "caphelix.h"

            CHARACTER*1     an

            REAL*8          vv,
     .                      cc,
     .                       nn

C-----------------------------------------------------------------------


c           write (6, '(/, ''Want to specify for end residues
c         . (Default:N)_'', $)')
c           read  (5, '(A1)') an
            an='n'
            nn = 0.0
            if ((an .eq. 'y') .or. (an .eq. 'Y'))
     .      then
                   write (6, '(/, '' Enter the left end ncap for '', A1,
     .                        '' (Default:'', F7.5, '')_'', $)')
     .                        char(Numseq(1)+64), v(Numseq(1))
                   read  (5, '(F)') nn
            endif
            if (nn .eq. 0.0) then
                   nn = ncap(NUMSEQ(1))
             endif

C           write (9,*)
C           write (9,*) 'Left end residue (', char(Numseq(1)+64),
C         .                  ') v = ', vv

            VL(1) = 0.0                 ! VL = (0,0,n,1)
            VL(2) = 0.0
            VL(3) = nn
            VL(4) = 1.0
```

```
      cc = 0.0
      if ((an .eq. 'y') .or. (an .eq. 'Y'))
     . then
            write (6, '(/, '' Enter the right end ccap for '', A1,
     .                  '' (Default:'', F7.5, '')_'', $)')
     .                 char(Numseq(N)+64), v(Numseq(N))
            read  (5, '(F)') cc
      endif
      if (cc .eq. 0.0) then
            cc = ccap(NUMSEQ(N))
      endif

C     write (9,*)
C     write (9,*) 'Right end residue (', char(Numseq(N)+64),
C    .            ') v = ', vv

      VR(1) = 0.0                    ! VR = (0,c,0,1)
      VR(2) = cc
      VR(3) = 0.0
      VR(4) = 1.0

      return
      end

C ^^^^^^^^^^^^^^^^^^^^^^^^^^^^^^^^^^^^^^^^^^^^^^^^^^^^^^^^^^^^^^^^^^^^^^^^^^^^^^^^
      SUBROUTINE MATSET(k)

C     define transition matrices WM

      IMPLICIT DOUBLE PRECISION (A-H, O-Z)

      include "caphelix.h"

      INTEGER        k              ! the kth residue in peptide

      REAL*8         vv,
     .               cc,
     .               nn

C-----------------------------------------------------------------------

      WM(1,1) = SVAL(NUMSEQ(k))
      vv = V(NUMSEQ(k))
      nn = ncap(NUMSEQ(k))
      cc = ccap(NUMSEQ(k))
c
c Mike Read 1/3/02
c Modification to change 1 to beta
c
      bb = beta(k)
      WM(1,2) = vv
      WM(1,3) = 0.0
      WM(1,4) = 0.0
      WM(2,1) = 0.0                  !       [w v 0        0]
      WM(2,2) = 0.0                  ! WM = |0 0 sqr(nc) c|
      WM(2,3) = dsqrt(nn*cc)         !       |v v 0        0|
      WM(2,4) = cc
      WM(3,1) = vv                   !       [0 0 n        1]
      WM(3,2) = vv
      WM(3,3) = 0.0
      WM(3,4) = 0.0
      WM(4,1) = 0.0
      WM(4,2) = 0.0
      WM(4,3) = nn
      WM(4,4) = bb

      return
      end
```

```
C ^^^^^^^^^^^^^^^^^^^^^^^^^^^^^^^^^^^^^^^^^^^^^^^^^^^^^^^^^^^^^^^^^^^^^^^^
      SUBROUTINE VXM(U,A,V)

C     This routine calculates V, the product of left end vector U
C     and matrix M.  <V| = <U|A| is a vecter itself.

      IMPLICIT DOUBLE PRECISION (A-H, O-Z)

      REAL*8          A(4,4), U(4), V(4)

      do 10 i =1, 4
10          V(i) = 0.0
      do 20 i =  1,4
            do 20 j = 1, 4
                  V(i) = U(j)*A(j,i) + V(i)
20    continue
      return
      end

C ^^^^^^^^^^^^^^^^^^^^^^^^^^^^^^^^^^^^^^^^^^^^^^^^^^^^^^^^^^^^^^^^^^^^^^^^
      REAL*8 FUNCTION sp(U,V)

C     This function calculates the spur (inner product) of two vectors
C     U and V.
C       sp(U,V) = <U|V> = U(1)V(1) + U(2)V(2) + U(3)V(3) + U(4)V(4).

      IMPLICIT DOUBLE PRECISION (A-H, O-Z)

      REAL*8          U(4), V(4)

      sp = 0.0
      do 10 i = 1, 4
10          sp =U(i)*V(i) + sp
      return
      end

C ^^^^^^^^^^^^^^^^^^^^^^^^^^^^^^^^^^^^^^^^^^^^^^^^^^^^^^^^^^^^^^^^^^^^^^^^
      SUBROUTINE VEQ(U,V)

C     This subroutine set vector V = vector U.

      IMPLICIT DOUBLE PRECISION (A-H, O-Z)

      REAL*8          U(4), V(4)

      do 1 i = 1, 4
1           V(i) = U(i)
      return
      end
```

References

1. Hirata, I., Morimoto, Y., Murakami, Y., Iwata, H., Kitano, E., Kitamura, H. & Ikada, Y. (2000). Study of complement activation on well-defined surfaces using surface plasmon resonance. *Coll. Surf. B* **18**, 285-292.
2. Palecek, S. P., Loftus, J. C., Ginsberg, M. H., Lauffenburger, D. A. & Horwitz, A. F. (1997). Integrin-ligand binding properties govern cell migration speed through cell-substratum adhesiveness. *Nature* **385**, 537-540.
3. Mann, S. (1996). Biomineralization and biomimetic materials chemistry. In *Biomimetic materials chemistry* (Mann, S., ed.). VCH Publishers Inc., New York.
4. Weiner, S., Veis, A., Beniash, E., Arad, T., Dillon, J. W., Sabsay, B. & Siddiqui, F. (1999). Peritubular dentin formation: crystal organization and the macromolecular constituents in human teeth. *J. Struct. Biol.* **126**, 27-41.
5. Ratner, B. D. (1993). New ideas in biomaterials science – a path to engineered biomaterials. *J. Biomed. Mater. Res.* **27**, 837-850.
6. Sevastianov, V. I. (1991). Interrelation of protein adsorption and blood compatibility of biomaterials. In *High performance biomaterials* (Szycher, M., ed.). Technomic Publishing Co., Inc., Lancaster.
7. Burkett, S. L. & Read, M. J. (2001). Adsorption-induced conformational changes of alpha-helical peptides. *Langmuir* **17**, 5059-5065.
8. Read, M., Mayes, A. M. & Burkett, S. L. (1999). Control and characterization of protein adsorption on ceramic surfaces. In *Mineralization in Natural and Synthetic Biomaterials* (Li, P., Calvert, P., Levy, R. J., Kokubo, T. & Scheid, C. R., eds.), Vol. 599. Materials Research Society, Boston, MA.
9. Creighton, T. E. (1993). *Proteins: structures and molecular properties.* 2 edit, W. H. Freeman and Company, New York.
10. Creighton, T. E. (1990). Protein folding. *Biochem. J.* **270**, 1-16.
11. Lim, W. A. & Sauer, R. T. (1991). The role of internal packing interactions in determining the structure and stability of a protein. *J. Mol. Biol.* **219**, 359-376.
12. Privalov, P. L. (1989). Thermodynamic problems of protein structure. *Annu. Rev. Biophys. Chem.* **18**, 47-69.
13. Parthasarathy, R., Chaturvedi, S. & Go, K. (1996). Design of alpha-helical peptides: their role in protein folding and molecular biology. *Prog. Biophys. Molec. Biol.* **64**, 1-54.
14. Ramirez-Alvarado, M., Blanco, F. J., Niemann, H. & Serrano, L. (1997). Role of beta-turn residues in beta-hairpin formation and stability in designed peptides. *J. Mol. Biol.* **273**, 898-912.
15. Perczel, A. & Hollosi, M. (1996). Turns. In *Circular dichroism and the conformational analysis of biomolecules* (Fasman, G. D., ed.). Plenum Press, New York.
16. Andrews, M. J. I. & Tabor, A. B. (1999). Forming stable helical peptides using natural and artificial amino acids. *Tetrahedron* **55**, 11711-11743.
17. Brant, D. A. & Flory, P. J. (1965). The configuration of random polypeptide chains. II. Theory. *J. Am. Chem. Soc.* **87**, 2791-2800.
18. Haynes, C. A. & Norde, W. (1994). Globular proteins at solid/liquid interfaces. *Coll. Surf. B: Biointerf.* **2**, 517-566.

19. Hlady, V. & Buijs, J. (1996). Protein adsorption on solid surfaces. *Curr. Opin. Biotech.* 7, 72-77.
20. Norde, W. & Lyklema, J. (1991). Why proteins prefer interfaces. *J. Biomater. Sci. Polymer. Edn.* **2**, 183-202.
21. Norde, W. (1986). Adsorption of proteins from solution at the solid-liquid interface. *Adv. Coll. Int. Sci.* **25**, 267-340.
22. Macritchie, F. (1978). Proteins at interfaces. In *Advances in protein chemistry* (Anfinsen, C. B., Edsall, J. T. & Richards, eds.), pp. 283-325. Academic press, New York.
23. Brash, J. L. & Horbett, T. A., Eds. (1986). Proteins at Interfaces. Vol. 343. ACS Symposium Series. Washington, DC: Americal Chemical Society.
24. Malmsten, M., Burns, N. & Veide, A. (1998). Electrostatic and hydrophobic effects of oligopeptide insertions on protein adsorption. *J. Coll. Int. Sci.* **204**, 104-111.
25. Arai, T. & Norde, W. (1990). The behavior of some model proteins at solid-liquid interfaces: 1. Adsorption from single-protein solutions. *Coll. Surf.* **51**, 1-15.
26. Duncan, M., Gilbert, M., Lee, J. & Warchol, M. (1994). Development and comparison of experimental assays to study protein/peptide adsorption onto surfaces. *J. Coll. Int. Sci.* **165**, 341-345.
27. Welle, A., Grunze, M. & Tur, D. (1998). Plasma protein adsorption and platelet adhesion on poly[bis(trifluoroethoxy) phosphazene] and reference material surfaces. *J. Coll. Int. Sci.* **197**, 263-274.
28. Fair, B. D. & Jamieson, A. M. (1980). Studies of protein adsorption on polystyrene latex surfaces. *J. Coll. Int. Sci.* **77**, 525-534.
29. Luo, Q. & Andrade, J. D. (1998). Cooperative adsorption of proteins onto hydroxyapatite. *J. Coll. Int. Sci.* **200**, 104-113.
30. Rapoza, R. J. & Horbett, T. A. (1990). Postadsorptive transitions in fibrinogen: influence of polymer properties. *J. Biomed. Mater. Res.* **24**, 1263-1287.
31. Elwing, H., Welin, S., Askendal, A., Nilsson, U. & Lundstrom, I. (1987). A wettability gradient method for studies of macromolecular interactions at the liquid/solid interface. *J. Coll. Int. Sci.* **119**, 203-210.
32. Lee, J. H. & Lee, H. B. (1998). Platelet adhesion onto wettability gradient surfaces in the absence and presence of plasma proteins. *J. Biomed. Mater. Res.* **41**, 304-311.
33. Galisteo, F. & Norde, W. (1995). Protein adsorption at the AgI-water interface. *J. Coll. Int. Sci.* **172**, 502-509.
34. Sarkar, D. & Chattoraj, D. K. (1996). Kinetics of desorption of proteins from the surface of protein-coated alumina by various desorbing reagents. *J. Coll. Int. Sci.* **178**, 606-613.
35. McGuire, J., Wahlgren, M. C. & Arnebrant, T. (1995). Structural stability effects on the adsorption and dodecyltrimethylammoniom bromide-mediated elutability of bacteriophage T4 lysozyme at silica surfaces. *J. Coll. Int. Sci.* **170**, 182-192.
36. Wahlgren, M. & Arnebrant, T. (1997). Removal of T4 lysozyme from silicon oxide surfaces by sodium dodecyl sulfate: a comparison between wild type protein and a mutant with lower thermal stability. *Langmuir* **13**, 8-13.
37. Woody, R. W. (1996). Theory of circular dichroism of proteins. In *Circular dichrosim and the conformational analysis of biomolecules* (Fasman, G. D., ed.), pp. 25-67. Plenum Press, New York.

38. Vermeer, A. W. P. & Norde, W. (2000). CD spectroscopy of proteins adsorbed at flat hydrophilic quartz and hydrophobic teflon surfaces. *J. Coll. Int. Sci.* **225**, 394-397.
39. Kondo, A., Oku, S. & Higashitani, K. (1991). Structural changes in protein molecules adsorbed on ultrafine silica particles. *J. Coll. Int. Sci.* **143**, 214-221.
40. Billsten, P., Wahlgren, M., Arnebrant, T., McGuire, J. & Elwing, H. (1995). Structural changes of T4 lysozyme upon adsorption to silica nanoparticles measured by circular dichroism. *J. Coll. Int. Sci.* **175**, 77-82.
41. Kondo, A. & Mihara, J. (1996). Comparison of adsorption and conformation of hemoglobin and myoglobin on various inorganic ultrafine particles. *J. Coll. Int. Sci.* **177**, 214-221.
42. Norde, W. & Favier, J. P. (1992). Structure of adsorbed and desorbed proteins. *Coll. Surf.* **64**, 87-93.
43. Zoungrana, T., Findenegg, G. H. & Norde, W. (1997). Structure, stability, and activity of adsorbed enzymes. *J. Coll. Int. Sci.* **190**, 437-448.
44. Maste, M. C. L., Norde, W. & Visser, A. J. W. G. (1997). Adsorption-induced conformational changes in the serine proteinase savinase: a tryptophan fluorescence and circular dichroism study. *J. Coll. Int. Sci.* **196**, 224-230.
45. Rienstra, C. M., Hohwy, M., Hong, M. & Griffin, R. G. (2000). 2D and 3D ^{15}N-^{13}C-^{13}C NMR chemical shift correlation spectroscopy of solids: assignment of MAS spectra of peptides. *J. Am. Chem. Soc.* **122**, 10979-10990.
46. Long, J. R., Dindot, J. L., Zebroski, H., Kiihne, S., Clark, R. H., Campbell, A. A., Stayton, P. S. & Drobny, G. P. (1998). A peptide that inhibits hydroxyapatite growth is in an extended conformation on the crystal surface. *Proc. Natl. Acad. Sci. USA* **95**, 12083-12087.
47. Shaw, W. J., Long, J. R., Dindot, J. L., Campbell, A. A., Stayton, P. S. & Drobny, G. P. (2000). Determination of statherin N-terminal peptide conformation on hydroxyapatite crystals. *J. Am. Chem. Soc.* **122**, 1709-1716.
48. Nagadome, H., Kawano, K. & Terada, Y. (1993). Identification of the adsorbing site of lysozyme onto the hydroxyapatite surface using hydrogen-exchange and ^{1}H NMR. *FEBS Letters* **317**, 128-130.
49. Robeson, J. L. & Tilton, R. D. (1996). Spontaneous reconfiguration of adsorbed lysozyme layers observed by TIRF with a pH-sensitive fluorophore. *Langmuir* **12**, 1996.
50. Edmiston, P. L., Lee, J. E., Cheng, S.-S. & Saavedra, S. S. (1997). Molecular orientation distributions in protein films. 1. Cytochrome c adsorbed to substrates of variable surface chemistry. *J. Am. Chem. Soc.* **119**, 560-570.
51. Jakobsen, R. J. & Strand, S. W. (1993). Biological applications of attenuated total reflection (ATR) spectroscopy. In *Internal reflection spectroscopy: theory and applications* (Francis M. Mirabella, J., ed.). Marcel Dekker, Inc., New York.
52. Chittur, K. K. (1998). FTIR-ATR for protein adsorption to biomaterial surfaces. *Biomaterials* **19**, 357-369.
53. Bentaleb, A., Abele, A., Haikel, Y., Schaaf, P. & Voegel, J. C. (1998). FTIR-ATR and radiolabeling study of the adsorption of ribonuclease A onto hydrophilic surfaces: correlation between the exchange rate and the interfacial denaturation. *Langmuir* **14**, 6493-6500.

54. Lenk, T. J., Horbett, T. A., Ratner, B. D. & Chittur, K. K. (1991). Infrared spectroscopic studies of time-dependent changes in fibrinogen adsorbed to polyurethanes. *Langmuir* **7**, 1755-1764.
55. Miura, Y., Kimura, S., Imanishi, Y. & Umemura, J. (1999). Oriented helical peptide layer on the carboxylate-terminated alkanethiol immobilized on a gold surface. *Langmuir* **15**, 1155-1160.
56. Roddick-Lanzilotta, A. D. & McQuillan, A. J. (1999). An in situ infrared spectroscopic investigation of lysine peptide and polylysine adsorption to TiO_2 from aqueous solutions. *J. Coll. Int. Sci.* **217**, 194-202.
57. Jackson, M. & Mantsch, H. H. (1995). The use and misuse of FTIR spectroscopy in the determination of protein structure. *Crit. Rev. Biochem. Mol. Biol.* **30**, 95-120.
58. Paci, E. & Karplus, M. (2000). Unfolding proteins by external forces and temperature: the importance of topology and energetics. *Proc. Natl. Acad. Sci. USA* **97**, 6521-6526.
59. Carrion-Vazquez, M., Oberhauser, A. F., Fowler, S. B., Marszalek, P. E., Broedel, S. E., Clarke, J. & Fernandez, J. M. (1999). Mechanical and chemical unfolding of a single protein: a comparison. *Proc. Natl. Acad. Sci. USA* **96**, 3694-3699.
60. Ostuni, E., Yan, L. & Whitesides, G. M. (1999). The interaction of proteins and cells with self-assembled monolayers of alkanethiolates on gold and silver. *Coll. Surf. B* **15**, 3-30.
61. Patel, N., Bhandari, R., Shakesheff, K., Cannizzaro, S., Davies, M., Langer, R., Roberts, C., Tendler, S. & Williams, P. (2000). Printing patterns of biospecifically-adsorbed protein. *J. Biomater. Sci. Polym. Ed.* **11**, 319-331.
62. Lantz, M. A., Jarvis, S. P., Tokumoto, H., Martynski, T., Kusumi, T., Nakamura, C. & Miyake, J. (1999). Stretching the alpha-helix: a direct measure of the hydrogen-bond energy of a single peptide molecule. *Chemical physics letters* **315**, 61-68.
63. Haggerty, L. & Lenhoff, A. M. (1993). Analysis of ordered arrays of adsorbed lysozyme by scanning tunneling microscopy. *Biophys. J.* **64**, 886-895.
64. Ruzgas, T., Csoregi, E., Emneus, J., Gorton, L. & Marko-Varga, G. (1996). Peroxidase-modified electrodes: fundamentals and applications. *Analytica Chimica Acta* **330**, 123-138.
65. Benson, D. E., Conrad, D. W., Lorimier, R. M. d., Trammell, S. A. & Hellinga, H. W. (2001). Design of bioelectronic interfaces by exploiting hinge-bending motions in proteins. *Science* **293**, 1641-1644.
66. Chen, T., Barton, S. C., Binyamin, G., Gao, Z., Zhang, Y., Kim, H.-H. & Heller, A. (2001). A miniature biofuel cell. *J. Am. Chem. Soc.* **123**, 8630-8631.
67. Scouten, W. H., Luong, J. H. T. & Brown, R. S. (1995). Enzyme or protein immobilization techniques for applications in biosensor design. *Trends Biotech.* **13**, 178-185.
68. Wu, C.-W., Lee, J.-G. & Lee, W.-C. (1998). Protein and enzyme immobilization on non-porous microspheres of polystyrene. *Biotech. Appl. Biochem.* **27**, 225-230.
69. Thomson, N. H., Smith, B. L., Almqvist, N., Schmitt, L., Kashlev, M., Kool, E. T. & Hansma, P. K. (1999). Oriented, active *Escherichia coli* RNA polymerase: an atomic force microscope study. *Biophys. J.* **76**, 1024-1033.

70. Peula, J. M., Hidalgo-Alvarez, R. & Nieves, F. J. d. l. (1998). Covalent binding of proteins to acetal-functionalized latexes. I. Physics and chemical adsorption and electrokinetic characterization. *J. Coll. Int. Sci.* **201**, 132-138.
71. Patel, N., Davies, M. C., Hartshorne, M., Heaton, R. J., Roberts, C. J., Tendler, S. J. B. & Williams, P. M. (1997). Immobilization of protein molecules onto homogeneous and mixed carboxylate-terminated self-assembled monolayers. *Langmuir* **13**, 6485-6490.
72. Johnsson, B., Lofas, S., Lindquist, G., Edstrom, A., Hillgren, R. M. M. & Hansson, A. (1996). Comparison of methods for immobilization to carboxymethyl dextran sensor surfaces by analysis of the specific activity of monoclonal antibodies. *J. Mol. Recognit.* **8**, 125-131.
73. Mansfeld, J. & Ulbrich-Hofmann, R. (2000). Site-specific and random immobilization of thermolysin-like proteases reflected in the thermal inactivation kinetics. *Biotechnol. Appl. Biochem.* **32**, 189-195.
74. Swindells, M. B., MacArthur, M. W. & Thornton, J. M. (1995). Intrinsic phi, psi propensities of amino acids, derived from the coil regions of known structures. *Nat. Struct. Biol.* **2**, 596-603.
75. Pauling, L., Corey, R. B. & Branson, H. R. (1951). The structure of proteins: two hydrogen-bonded helical configurations of the polypeptide chain. *Proc. Natl. Acad. Sci.* **37**, 205-210.
76. Aurora, R. & Rose, G. D. (1998). Helix capping. *Protein Science* **7**, 21-38.
77. Chen, Y. H., Yang, J. T. & Chau, K. H. (1974). Determination of helix and beta-form of proteins in aqueous solution by circular dichroism. *Biochemistry* **13**, 3350-3359.
78. Schellman, J. A. & Oriel, P. (1962). Origin of the cotton effect of helical polypeptides. *J. Chem. Phys.* **37**, 2114-2124.
79. Manning, M. C. & Woody, R. W. (1991). Theoretical CD studies of polypeptide helices – examination of important electronic and geometric factors. *Biopolymers* **31**, 569-586.
80. Besley, N. A. & Hirst, J. D. (1999). Theoretical studies toward quantitative protein circular dichroism calculations. *J. Am. Chem. Soc.* **121**, 9636-9644.
81. Richardson, J. S. & Richardson, D. C. (1988). Amino acid preferences for specific locations at the ends of alpha helices. *Science* **240**, 1648-1652.
82. Gans, P. J., Lyu, P. C., Manning, M. C., Woody, R. W. & Kallenbach, N. R. (1991). The helix-coil transition in heterogenous peptides with specific side-chain interactions: theory and comparison with CD spectral data. *Biopolymers* **31**, 1605-1614.
83. Scholtz, J. M., Qian, H., York, E. J., Stewart, J. M. & Baldwin, R. L. (1991). Parameters of helix-coil transition theory for alanine-based peptides of varying chain lengths in water. *Biopolymers* **31**, 1463-1470.
84. Doig, A. J. & Baldwin, R. L. (1995). N- and C-capping preferences for all 20 amino acids in alpha-helical peptides. *Protein Science* **4**, 1325-1336.
85. Agou, F., Yang, Y., Gesquiere, J.-C., Waller, J.-P. & Guittet, E. (1995). Polyanion-induced alpha-helical structure of a synthetic 23-residue peptide representing the lysine-rich segment of the N-terminal extension of yeast cytoplasmic aspartyl-tRNA synthetase. *Biochemistry* **34**, 569-576.

86. Collawn, J. F. & Paterson, Y. (1990). Stabilization of helical structure in two 17-residue amphipathic analogues of the C-terminal peptide of cytochrome c. *Biopolymers* **29**, 1289-1296.
87. Bolin, K. A., Pitkeathly, M., Miranker, A., Smith, L. J. & Dobson, C. M. (1996). Insight into a random coil conformation and an isolated helix: structural and dynamical characterisation of the C-helix peptide from hen lysozyme. *J. Mol. Biol.* **261**, 443-453.
88. Shoemaker, K. R., Kim, P. S., York, E. J., Stewart, J. M. & Baldwin, R. L. (1987). Tests of the helix dipole model for stabilization of alpha-helices. *Nature* **326**, 563.
89. Marqusee, S. & Baldwin, R. L. (1987). The role of intrahelical ion-pairs in alpha-helix formation by synthetic peptides. *Proc. Natl. Acad. Sci. USA* **84**, 8898-8902.
90. Sandberg, W. S. & Terwilliger, T. C. (1989). Influence of interior packing and hydrophobicity on the stability of a protein. *Science* **245**, 54-57.
91. Dill, K. A. (1990). Dominant forces in protein folding. *Biochemistry* **29**, 7133-7155.
92. Smith, P. K., Krohn, R. I., Hermanson, G. T., Mallia, A. K., Gartner, F. H., Provenzano, M. D., Fujimoto, E. K., Goeke, N. M., Olson, B. J. & Klenk, D. C. (1985). Measurement of protein using bicinchoninic acid. *Anal. Biochem.* **150**, 76-85.
93. Zhang, S. (1999). *Personal Communication.*
94. Rao, V., Altman, M. & Zhang, S. (2001). Behavior of resilient dipolar alpha-helical peptides. *Protein Science* **In Press**, .
95. Baldwin, R. L. (1995). Alpha-helix formation by peptides of defined sequence. *Biophys. Chem.* **55**, 127-135.
96. Padmanabhan, S., York, E. J., Stewart, J. M. & Baldwin, R. L. (1996). Helix propensities of basic amino acids increase with the length of the side-chain. *J. Mol. Biol.* **257**, 726-734.
97. Kallenbach, N. R., Lyu, P. & Zhou, H. (1996). CD spectroscopy and the helix–coil transition in peptides and polypeptides. In *Theory of Circular Dichroism of Proteins* (Fasman, G. D., ed.), pp. 201-257. Plenum Press, New York.
98. Chakrabartty, A., Kortemme, T., Padmanabhan, S. & Baldwin, R. L. (1993). Aromatic side-chain contribution to far-ultraviolet circular dichroism of helical peptides and its effect on measurement of helix propensities. *Biochemistry* **32**, 5560-5565.
99. Chakrabartty, A., Kortemme, T. & Baldwin, R. L. (1994). Helix propensities of the amino acids measured in alanine-based peptides without helix-stabilizing side-chain interactions. *Protein Sci.* **3**, 843- 852.
100. Silva, R. A. G. D., Kubelka, J., Bour, P., Decatur, S. M. & Keiderling, T. A. (2000). Site-specific conformational determination in termal unfolding studies of helical peptides using vibrational circular dichroism with isotopic substitution. *Proc. Natl. Acad. Sci. USA* **97**, 8318-8323.
101. Smith, J. S. & Scholtz, J. M. (1996). Guanidine hydrochloride unfolding of peptide helices: separation of denaturant and salt effects. *Biochemistry* **35**, 7292.
102. Scholtz, J. M., Barrick, D., York, E. J., Stewart, J. M. & Baldwin, R. L. (1995). Urea unfolding of peptide helices as a model for interpreting protein unfolding. *Proc. Natl. Acad. Sci. USA* **92**, 185-189.
103. Luo, P. & Baldwin, R. L. (1997). Mechanism of helix induction by trifluoroethanol: a framework for extrapolating the helix-forming properties of peptides from trifluoroethanol/water mixtures back to water. *Biochemistry* **36**, 8413-8421.

104. Pardi, A., Billeter, M. & Wuthrich, K. (1984). Calibration of the angular dependence of the amide proton-Calpha proton coupling constants, $^3J_{HN\alpha}$, in a globular protein. *J. Mol. Biol.* **180**, 741-751.
105. Liff, M. I., Lyu, P. C. & Kallenbach, N. R. (1991). Analysis of asymmetry in the distribution of helical residues in peptides by ^{1}H NMR. *J. Am. Chem. Soc.* **113**, 1014-10119.
106. Schwarzinger, S. & al, e. (2001). Sequence-dependent correction of random-coil NMR chemical shifts. *J. Am. Chem. Soc.* **123**, 2970-2978.
107. Wishart, D. S. & Sykes, B. D. (1994). Chemical shifts as a tool for structure determination. In *Methods in Enzymology*, Vol. 239, pp. 366. Academic Press, Inc.
108. Pedersen, T. G., Thomsen, N. K., Andersen, K. V., Madsen, J. C. & Poulsen, F. M. (1993). Determination of the rate constants k_1 and k_2 of the Linderstrom-Lang model for protein amide hydrogen exchange. *J. Mol. Biol.* **230**, 651-660.
109. Radford, S. E., Buck, M., Topping, K. D., Dobson, C. M. & Evans, P. A. (1992). Hydrogen exchange in native and denatured states of hen egg-white lysozyme. *Proteins: Structure, Function, and Genetics* **14**, 237-248.
110. Rohl, C. A., Scholtz, J. M., York, E. J., Stewart, J. M. & Baldwin, R. L. (1992). Kinetics of amide proton exchange in helical peptides of varying chain lengths. Interpretation by the Lifson-Roig equation. *Biochemistry* **31**, 1263-1269.
111. Rohl, C. A. & Baldwin, R. L. (1997). Comparison of NH exchange and circular dichroism as techniques for measuring the parameters of the helix-coil transition in peptides. *Biochemistry* **36**, 8435-8442.
112. Rohl, C. A. & Baldwin, R. L. (1994). Exchange kinetics of individual amide protons in 15N-labeled helical peptides measured by isotope-edited NMR. *Biochemistry* **33**, 7760.
113. Wuthrich, K. (1986). *NMR of proteins and nucleic acids*, John Wiley & Sons, New York.
114. Wishart, D. S. & Case, D. A. (2001). Use of chemical shifts in macromolecular structure determination. In *Methods in Enzymology*, Vol. 338, pp. 3. Academic Press Inc.
115. Wishart, D. S., Sykes, B. D. & Richards, F. M. (1991). Relationship between nuclear magnetic resonance chemical shift and protein secondary structure. *J. Mol. Biol.* **222**, 311-333.
116. Toniolo, C., Polese, A., Formaggio, F., Crisma, M. & Kamphuis, J. (1996). Circular dichroism spectrum of a peptide 3_{10}-helix. *J. Am. Chem. Soc.* **118**, 2744-2745.
117. Karle, I. L. & Balaram, P. (1990). Structural characteristics of alpha-helical peptide molecules containing Aib residues. *Biochemistry* **29**, 6747-6756.
118. Merutka, G., Morikis, D., Bruschweiler, R. & Wright, P. E. (1993). NMR evidence for multiple conformations in a highly helical model peptide. *Biochemistry* **32**, 13089.
119. Bradley, E. K., Thomason, J. F., Cohen, F. E., Kosen, P. A. & Kuntz, I. D. (1990). Studies of synthetic helical peptides using circular dichroism and nuclear magnetic resonance. *J. Mol. Biol.* **215**, 607-622.
120. Wright, P. E., Dyson, H. J. & Lerner, R. A. (1988). Conformation of peptide fragments of proteins in aqueous solution: implications for initiation of protein folding. *Biochemistry* **27**, 7167-7175.

121. John J. Osterhout, J., Baldwin, R. L., York, E. J., Stewart, J. M., Dyson, H. J. & Wright, P. E. (1989). 1H NMR studies of the solution conformations of an analogue of the C-peptide of ribonuclease A. *Biochemistry* **28**, 7059-7064.
122. Millhauser, G. L. (1995). Views of helical peptides: a proposal for the position of 3_{10}-helix along the thermodynamic folding pathway. *Biochemistry* **34**, 3873-3877.
123. Mayo, K. H., Haseman, J., Young, H. C. & Mayo, J. W. (2000). Structure-function relationships in novel peptide dodecamers with broad-spectrum bactericidal and endotoxin-neutralizing activities. *Biochemical journal* **349**, 717-728.
124. Avbelj, F., Luo, P. & Baldwin, R. L. (2000). Energetics of the interaction between water and the helical peptide group and its role in determining helix propensities. *Proc. Natl. Acad. Sci. USA* **97**, 10786-10791.
125. Scholtz, J. M. & Baldwin, R. L. (1992). The mechanism of alpha-helix formation by peptides. *Annual review of biophysics and biomolecular structure* **21**, 95-118.
126. Iler, R. K. (1979). *The chemistry of silica*, John Wiley and Sons, New York.
127. Tadros & Lyklema. (1968). Adsorption of potential-determining ions at the silica-aqueous electrolyte interface and the role of some cations. *J. Electroanal. Chem.* **17**, 267.
128. Weast, R. C., Ed. (1984). CRC handbook of chemistry and physics. 65 edit. Boca Raton, FA: CRC Press, Inc.
129. Atkins, P. (1994). *Physical chemistry*. 5 edit, W. H. Freeman and Co., New York.
130. Lin, S.-Y., McKeigue, K. & Maldarelli, C. (1991). Diffusion-limited interpretation of the induction period in the relaxation in surface tension due to the adsorption of straight chain, small polar group surfactants: theory and experiment. *Langmuir* **7**, 1055-1066.
131. Minton, A. P. (1999). Adsorption of globular proteins on locally planar surfaces. II. Models for the effect of multiple adsorbate conformations on adsorption equilibria and kinetics. *Biophys. J.* **76**, 176-187.
132. Lundstrom, I. (1985). Models of protein adsorption on solid surfaces. *Prog. Coll. Polymer Sci.* **70**, 76-82.
133. Talbot, J., Tarjus, G., Tassel, P. R. v. & Viot, P. (2000). From car parking to protein adsorption: an overview of sequential adsorption processes. *Coll. Surf. A Physicochem. Eng. Aspects* **165**, 287-324.
134. Soderquist, M. E. & Walton, A. G. (1980). Structural changes in proteins adsorbed on polymer surfaces. *J. Coll. Int. Sci.* **75**, 386-397.
135. Bentaleb, A., Haikel, Y., Voegel, J. C. & Schaaf, P. (1998). Kinetics of the homogenous exchange of alpha-lactalbumin adsorbed on titanium oxide surface. *J. Biomed. Mater. Res.* **40**, 449-457.
136. Andrade, J. D. (1985). Principles of protein adsorption. In *Surface and interfacial aspects of biomedical polymers* (Andrade, J. D., ed.), pp. 1-80. Plenum Press, New York.
137. Casson, B. D. & Bain, C. D. (1999). Unequivocal evidence for a liquid-gas phase transition in monolayers of decanol adsorbed at the air/water interface. *J. Am. Chem. Soc.* **121**, 2615-2616.
138. Fainerman, V. B., Lucassen-Reynders, E. H. & Miller, R. (1998). Adsorption of surfactants and proteins at fluid interfaces. *Coll. Surf. A Physicochem. Eng. Aspects* **143**, 141-165.

139. Gileade, E., Kirowa-Eisner, E. & Penciner, J. (1975). *Interfacial electrochemistry*, Addison-Wesley, Reading, MA.
140. Fasman, G. D., Ed. (1975). Handbook of biochemistry and molecular biology. 3 edit. Vol. A1. Cleveland: CRC Press.
141. Brownlee, K. A. (1960). *Statistical theory and methodology in science and engineering*. 1 edit, John Wiley & Sons, Inc., New York.
142. Popov, A. & Borisova, T. (2001). Adsorption of dicarbollylcobaltate (III) anion at the water/1,2-dichloroethane interface. Influence of counterions' nature. *J. Coll. Int. Sci.* **236**, 20-27.
143. Quan, C., Khoe, G. & Bagster, D. (2001). Adsorption of sodium lauryl sulfate onto arsenic-bearing ferrihydrite. *Water Res.* **35**, 478-484.
144. Shafei, G. M. S. E., Moussa, N. A. & Philip, C. A. (2000). Association of molybdenum ionic species with alumina surface. *J. Coll. Int. Sci.* **228**, 105-113.
145. Haynes, C. A. & Norde, W. (1995). Structures and stabilities of adsorbed proteins. *J. Coll. Int. Sci.* **169**, 313-328.
146. Norde, W. & Lyklema, J. (1979). Thermodynamics of protein adsorption. *J. Coll. Int. Sci.* **71**, 350-365.
147. Miranda, P. B. & Shen, Y. R. (1999). Liquid interfaces: a study by sum-frequency vibrational spectroscopy. *J. Phys. Chem. B* **103**, 3292-3307.
148. Lee, S.-W. & Laibinis, P. E. (1998). Protein-resistant coatings for glass and metal oxide surfaces derived from oligo(ethylene glycol)-terminated alkyltrichlorosilanes. *Biomaterials* **19**, 1669-1675.
149. Waddell, T. G., Leyden, D. E. & DeBello, M. T. (1981). The nature of organosilane to silca-surface bonding. *J. Am. Chem. Soc.* **103**, 5303-5307.
150. Tian, M., Lee, W.-K., Bothwell, M. K. & McGuire, J. (1998). Structural stability effects on adsorption of bacteriophage T4 lysozyme to colloidal silica. *J. Coll. Int. Sci.* **200**, 146-154.
151. Karlsson, M., Martensson, L.-G., Johsson, B.-H. & Carlsson, U. (2000). Adsorption of human carbonic anhydrase II variants to silica nanoparticles occur stepwise: binding is followed by successive conformational changes to a molten-globule-like state. *Langmuir* **16**, 8470-8479.
152. Kondo, A. & Fukuda, H. (1998). Effects of adsorption conditions on kinetics of protein adsorption and conformational changes at ultrafine silica particles. *J. Coll. Int. Sci.* **198**, 34-41.
153. Mason, R. D., Lind, D. A. & Marchal, W. G. (1999). *Statistical techniques in business and economics*. 10 edit, Irwin McGraw-Hill, New York.
154. Hore, P. J. (1995). *Nuclear magnetic resonance*, Oxford University Press, New York.
155. Fyfe, C. A. (1983). *Solid state NMR for chemists*, C.F.C. Press, Ontario.
156. Delpuech, J.-J. (1995). Introduction: dynamic phenomena in NMR. In *Dynamics of solutions and fluid mixtures by NMR* (Delpuech, J.-J., ed.), pp. 357. John Wiley and Sons, New York.
157. Slichter, C. P. (1990). *Principles of magnetic resonance*. 3 edit, Springer-Verlag, New York.
158. Lindman, B., Olsson, U. & Soderman, O. (1995). Surfactant solutions: aggregation phenomena and microheterogeneity. In *Dynamics of solutions and fluid mixtures by NMR* (Delpuech, J.-J., ed.), pp. 357. John Wiley and Sons, New York.

159. Haggerty, J. F. & Roberts, J. E. (1995). ^{1}H-NMR studies of nonionic surfactant adsorption onto colloidal particles. *J. Appl. Polymer Sci.* **58**, 271-278.
160. Colombie, D., Landfester, K., Sudol, E. D. & El-Aasser, M. S. (1998). Determination of the adsorption isotherm of the nonionic surfactant Triton X-405 on polystyrene latex particles using 1H NMR. *J. Coll. Int. Sci.* **202**, 554-557.
161. Beger, R. D. & Bolton, P. H. (1997). Protein phi and psi dihedral restraints determined from multidimensional hypersurface correlations of backbone chemical shifts and their use in the determination of protein tertiary structures. *J. Biomol. NMR* **10**, 129-142.
162. Lee, M. S. & Cao, B. (1996). Nuclear magnetic resonance chemical shift: comparison of estimated secondary structures in peptides by nuclear magnetic resonance and circular dichroism. *Protein engineering* **9**, 15-25.
163. Usui, S. (1984). Electrical double layer. In *Electrical Phenomena at Interfaces* (Kitahara, A. & Watanabe, A., eds.), pp. 15-46. Marcel Dekker, Inc., New York.
164. Davies, J. T. & Rideal, E. K. (1963). *Interfacial Phenomena.* 2 edit, Academic Press, New York.
165. Attard, P., Antelmi, D. & Larson, I. (2000). Comparison of the zeta potential with the diffuse layer potential from charge titration. *Langmuir* **16**, 1542-1552.
166. Adamson, A. W. & Gast, A. P. (1997). *Physical chemistry of surfaces*, John Wiley & Sons, Inc., New York.
167. Jackson, J. D. (1999). *Classical electrodynamics.* 3 edit, Wiley, New York.
168. Dathe, M. & Wieprecht, T. (1999). Structural features of helical antimicrobial peptides: their potential to modulate activity on model membranes and biological cells. *Biochim. et Biophys. Acta* **1462**, 71-87.
169. Soto, C., Castano, E. M., Frangione, B. & Inestrosa, N. C. (1995). The alpha-helical to beta-strand transition in the amino-terminal fragment of the amyloid beta-peptide modulates amyloid formation. *J. Biol. Chem.* **270**, 3063-3067.
170. Knight, C. A., Driggers, E. & DeVries, A. L. (1993). Adsorption at ice of fish antifreeze glycopeptides 7 and 8. *Biophys. J.* **64**, 252-259.
171. Kuhlman, B. & Raleigh, D. P. (1998). Global analysis of the thermal and chemical denaturation of the N-terminal domain of the ribosomal protein L9 in H_2O and D_2O. Determination of the thermodynamic parameters, ΔH°, ΔS°, and ΔC_p°, and evaluation of solvent isotope effects. *Protein Sci.* **7**, 2405-2412.
172. Ibarra-Molero, B., Makhatadze, G. I. & Matthews, C. R. (2001). Mapping the energy surface for the folding reaction of the coiled-coil peptide GCN4-p1. *Biochemistry* **40**, 719-731.
173. Zimm, B. H. & Bragg, J. K. (1959). Theory of the phase transition between helix and random coil in polypeptide chains. *J. Chem. Phys.* **31**, 526-535.
174. Doig, A. J., Chakrabartty, A., Klingler, T. M. & Baldwin, R. L. (1994). Determination of free energies of N-capping in alpha-helices by modification of the Lifson-Roig helix–coil theory to include N- and C-capping. *Biochemistry* **33**, 3396-3403.
175. Dupre, D. B. (1990). Multiple helix-coil transitions. *Biopolymers* **30**, 1051-1060.
176. Qian, H. & Schellman, J. A. (1992). Helix-coil theories: a comparative study for finite length polypeptides. *J. Phys. Chem.* **96**, 3987-3993.
177. Lifson, S. & Roig, A. (1961). On the theory of helix-coil transition in polypeptides. *J. Chem. Phys.* **34**, 1963-1974.

178. Pace, C. N. & Scholtz, J. M. (1998). A helix propensity scale based on experimental studies of peptides and proteins. *Biophys. J.* **75**, 422-427.
179. Schellman, J. A. (1987). Selective binding and solvent denaturation. *Biopolymers* **26**, 549-559.
180. Wayne, S. I. & Fruton, J. S. (1983). Thermolysin-catalyzed peptide bond synthesis. *Proc. Natl. Acad. Sci. USA* **80**, 3241.
181. Matsubara, H. (1970). Purification and assay of thermolysin. *Meth. Enzymol.* **19**, 642-651.
182. Glendening, T. (2000). *Personal Communication.*
183. Moore, S. (1968). Amino acid analysis: aqueous dimethyl sulfoxide as solvent for the ninhydrin reaction. *J. Biol. Chem.* **243**, 6281-6283.
184. Morgan, G. & Fruton, J. S. (1978). Kinetics of the action of thermolysin on peptide substrates. *Biochemistry* **17**, 3562-3568.
185. Khan, S. M. & Darnall, D. W. (1978). The hydrolysis of 3-(2-furylacryloyl)-glycyl-L-leucine amide by thermolysin. *Anal. Biochem.* **86**, 332-336.
186. Indig, F. E., Ben-Meir, D., Spungin, A. & Blumberg, S. (1989). Investigation of neutral endopeptidases (EC 3.4.24.11) and of neutral proteinases (EC 3.4.24.4) using a new sensitive two-stage enzymatic reaction. *FEBS Letters* **255**, 237-240.
187. Yang, J. J. & Wart, H. E. V. (1994). Kinetics of hydrolysis of dansyl peptide substrates by thermolysin: analysis of fluorescence changes and determination of steady-state kinetic parameters. *Biochemistry* **33**, 6508-6515.
188. Garrett, R. H. & Grisham, C. M. (1995). *Biochemistry*, Saunders College Publishing, New York.
189. Satterfield, C. N. (1996). *Heterogenous catalysis in industrial practice*, McGraw-Hill, New York.
190. Flanigen, E. M. (2001). Zeolites and molecular sieves: an historical perspective. In *Introduction to zeolite science and practice* 2 edit. (Bekkum, H. v., Flanigen, E. M., Jacobs, P. A. & Jansen, J. C., eds.), Vol. 137, pp. 11. Elsevier, New York.
191. Maesen, T. & Marcus, B. (2001). The zeolite scene – an overview. In *Introduction to zeolite science and practice* 2 edit. (Bekkum, H. v., Flanigen, E. M., Jacobs, P. A. & Jansen, J. C., eds.), Vol. 137, pp. 1. Elsevier, New York.
192. Lovallo, M. C. & Tsapatsis, M. (1996). Nanocrystalline zeolites. In *Advanced catalysts and nanostructured materials: Modern synthetic methods* (Moser, W. R., ed.). Academic Press Inc., New York.
193. Ha, K., Lee, Y. J. & Lee, H. J. (2000). Facile assembly of zeolite monolayers on glass, silica, alumina, and other zeolites using 3-halopropylsilyl reagents as covalent linkers. *Adv. Mater.* **12**, 1114.
194. Choi, S. Y., Lee, Y. J. & Park, Y. S. (2000). Monolayer assembly of zeolite crystals on glass with fullerene as the covalent linker. *J. Am. Chem. Soc.* **122**, 5201.
195. Fenoglio, I., Croce, A., DiRenzo, F., Tiozzo, R. & Fubini, B. (2000). Pure-silica zeolites (porosils) as model solids for the evaluation of the physicochemical features determining silica toxicity to macrophages. *Chem. Res. Toxicol.* **13**, 489-500.
196. Dyer, A. (1988). *An introduction to zeolite molecular sieves*, John Wiley & sons, New York.
197. Townsend, R. P., Ed. (1979). The properties and applications of zeolites. Vol. 33. Special Publication. London: The Chemical Society.

198. Feijen, E. J. P., Vadder, K. D., Bosschaerts, M. H., Lievens, J. L., Martens, J. A., Grobet, P. J. & Jacobs, P. A. (1994). Role of 18-crown-6 and 15-crown-5 ethers in the crystallization of polytype faujasite zeolites. *J. Am. Chem. Soc.* **116**, 2950-2957.
199. Melchior, M. T., Vaughan, D. E. W. & Pictroski, C. F. (1995). Local environment fine-structure in the ^{29}Si NMR spectra of faujasite zeolites. *J. Phys. Chem.* **99**, 6128.
200. Feijen, E. J. P., Lievens, J. L., Martens, J. A., Grobet, P. J. & Jacobs, P. A. (1996). Silicon and aluminum ordering in frameworks of FAU and EMT aluminosilicate zeolites crystallized in the presence of crown ethers. *J. Phys. Chem.* **100**, 4970-4975.
201. Harjula, R., Lehto, J., Pothuis, J. H., Dyer, A. & Townsend, R. P. (1993). Ion exchange in zeolites part 2: Hydrolysis and dissolution of zeolites. *J. Chem. Soc. Faraday Trans.* **89**, 971-976.
202. Marinsky, J. A. (1995). Gibbs-Donnan-Based Interpretations of the hydrolysis behavior of zeolites. *Ind. Eng. Chem. Res.* **34**, 2898-2909.
203. Weisenhorn, A. L., MacDougall, J. E., Gould, S. A. C., Cox, S. D., Wise, W. S., Massie, J., Maivald, P., Elings, V. B., Stucky, G. D. & Hansma, P. K. (1990). Imaging and manipulating molecules on a zeolite surface with an atomic force microscope. *Science* **247**, 1330-1333.
204. Alfredsson, V., Ohsuna, T., Terasaki, O. & Bovin, J.-O. (1993). Investigation of the surface structure of the zeolites FAU and EMT by high-resolution transmission electron microscopy. *Angew. Chem. Int. Ed. Engl.* **32**, 1210-1213.
205. Hirano, T., Li, W., Abrams, L., Krusic, P. J., Ottaviani, M. F. & Turro, N. J. (2000). Supramolecular steric effects as the means of making reactive carbon radicals persistent. Quantitative characterization of the external surface of MFI zeolites through a persistent radical probe and a Langmuir adsorption isotherm. *J. Org. Chem.* **65**, 1319-1330.
206. Han, Y. J., Stucky, G. D. & Butler, A. (1999). Mesoporous silicate sequestration and release of proteins. *J. Am. Chem. Soc.* **121**, 9897-9898.
207. Hong, S. B., Camblor, M. A. & Davis, M. E. (1997). Host-guest interactions in pure-silica and aluminosilicate sodalites containing ethylene glycol as a guest molecule. *J. Am. Chem. Soc.* **119**, 761-770.
208. Hong, S. B. & Camblor, M. A. (1997). SiO^- defects in as-synthesized pure-silica and aluminosilicate sodalites. *Chem. Mater.* **9**, 1999-2003.
209. Mintova, S., Olson, N., Valtchev, V. & Bein, T. (1999). Mechanism of zeolite A nanocrystal growth from colloids at room temperature. *Science* **283**, 958.
210. Mintova, S. & Valtchev, V. (1999). Synthesis of nanosized FAU-type zeolite. *Stud. Surf. Sci. Catal.* **125**, 141.
211. Zhu, G., Qiu, S., Yu, J., Sakamoto, Y., Xiao, F., Xu, R. & Terasaki, O. (1998). Synthesis and characterization of high-quality zeolite LTA and FAU single nanocrystals. *Chem. Mater.* **10**, 1483.
212. Hirst, W. & Lancaster, J. K. (1951). Effect of water on the interaction between stearic acid and fine powders. *Trans. Faraday Soc.* **47**, 318.
213. Orr, C. & Dallavalle, J. M. (1960). *Fine particle measurement: size, surface, and pore volume*, The Macmillan Company, New York.
214. Herrera-Urbina, R. & Fuerstenau, D. W. (1995). The effect of Pb(II) species, pH and dissolved carbonate on the zeta potential at the quartz/aqueous solution interface. *Coll. Surf. A* **98**, 25-33.

215. Farneth, W. E. & Gorte, R. J. (1995). Methods for characterizing zeolite acidity. *Chem. Rev.* **95**, 615-635.
216. Boudreau, L. C., Kuck, J. A. & Tsapatsis, M. (1999). Deposition of oriented zeolite A films: in situ and secondary growth. *J. Membrane Sci.* **152**, 41-59.
217. Shin, Y. W., Roberts, J. E. & Santore, M. (2001). The influence of charge variation on the adsorbed configuration of a model cationic oligomer onto colloidal silica. *J. Coll. Int. Sci.* **244**, 190-199.
218. Fubini, B. & Wallace, W. E. (2000). Modulation of silica pathogenicity by surface processes. In *Adsorption on silica surfaces* (Papirer, E., ed.). Marcel Dekker, Inc., New York.